LOAN DOCUMENT

PHOTOGRAPH THIS SHEET

DTIC ACCESSION NUMBER

LEVEL

INVENTORY

D

RIA - 81 - U1098

DOCUMENT IDENTIFICATION

21 OCT 1981

DISTRIBUTION STATEMENT A

Approved for public release;
Distribution Unlimited

DISTRIBUTION STATEMENT

ACCESSION FOR

NTIS	GRAM	
DTIC	TRAC	
UNANNOUNCED		
JUSTIFICATION		

BY

DISTRIBUTION/

AVAILABILITY CODES

| DISTRIBUTION | AVAILABILITY AND/OR SPECIAL | |

A-1

DISTRIBUTION STAMP

DATE ACCESSIONED

DATE RETURNED

19960904 100

DATE RECEIVED IN DTIC

REGISTERED OR CERTIFIED NUMBER

**H
A
N
D
L
E

W
I
T
H

C
A
R
E**

PHOTOGRAPH THIS SHEET AND RETURN TO DTIC-FDAC

DTIC FORM 70A
JUN 90

DOCUMENT PROCESSING SHEET

PREVIOUS EDITIONS MAY BE USED UNTIL
STOCK IS EXHAUSTED.

LOAN DOCUMENT

AMSAA

ARMY
MATERIEL
SYSTEMS
ANALYSIS
ACTIVITY

PROCEEDINGS
THIRD MEETING OF THE COORDINATING GROUP
ON
MODERN CONTROL THEORY
PART I

20-21 OCTOBER 1981
US ARMY MISSILE COMMAND
REDSTONE ARSENAL, AL 35989

DTIC QUALITY INSPECTED 5

U S ARMY MATERIEL SYSTEMS ANALYSIS ACTIVITY
ABERDEEN PROVING GROUND, MARYLAND 21005

DISCLAIMER NOTICE

THIS DOCUMENT IS BEST QUALITY AVAILABLE. THE COPY FURNISHED TO DTIC CONTAINED A SIGNIFICANT NUMBER OF PAGES WHICH DO NOT REPRODUCE LEGIBLY.

REPORT DOCUMENTATION PAGE		READ INSTRUCTIONS BEFORE COMPLETING FORM
1. REPORT NUMBER	2. GOVT ACCESSION NO.	3. RECIPIENT'S CATALOG NUMBER
4. TITLE *(and Subtitle)* Proceedings of the Third Meeting of the Coordinating Group on Modern Control Theory (20-21 Oct 1981) US Army Missile Command, Redstone Arsenal, AL 35989		5. TYPE OF REPORT & PERIOD COVERED Conference
		6. PERFORMING ORG. REPORT NUMBER
7. AUTHOR*(s)* H. Cohen (Chairman)		8. CONTRACT OR GRANT NUMBER*(s)*
9. PERFORMING ORGANIZATION NAME AND ADDRESS Director US Army Materiel Systems Analysis Activity Aberdeen Proving Ground, MD 21005		10. PROGRAM ELEMENT, PROJECT, TASK AREA & WORK UNIT NUMBERS DA Project No. 1R665706M541
11. CONTROLLING OFFICE NAME AND ADDRESS Director US Army Materiel Systems Analysis Activity ATTN: DRXSY-MP, Aberdeen Proving Ground, MD 21005		12. REPORT DATE November 1981
		13. NUMBER OF PAGES 285
14. MONITORING AGENCY NAME & ADDRESS*(if different from Controlling Office)* Cdr, US Army Materiel Development & Readiness Cmd, 5001 Eisenhower Avenue, Alexandria, VA 22333		15. SECURITY CLASS. *(of this report)* UNCLASSIFIED
		15a. DECLASSIFICATION/DOWNGRADING SCHEDULE

16. DISTRIBUTION STATEMENT *(of this Report)*

Approved for public release; distribution unlimited

17. DISTRIBUTION STATEMENT *(of the abstract entered in Block 20, if different from Report)*

18. SUPPLEMENTARY NOTES

19. KEY WORDS *(Continue on reverse side if necessary and identify by block number)*

Control Theory, Kalman Filtering, Man-Model, Maneuvering Target, Fire Control, Missile Guidance and Control

20. ABSTRACT *(Continue on reverse side if necessary and identify by block number)*

Report documents paper presented at third meeting of the coordinating group on modern control theory with emphasis on military weapon systems.

TABLE OF CONTENTS

Title	Page

THIRD MEETING

COORDINATING GROUP ON MODERN CONTROL THEORY

20-21 OCTOBER 1981

US ARMY MISSILE COMMAND
Redstone Arsenal, AL 35989

AGENDA

TUESDAY, 20 OCTOBER 1981

SESSION I: Control Theory & Applications   (Chairman - Dr. William C. Kelly)
           I/Simulation

WELCOMING STATEMENT -

0900 -   Analysis of Tank Fire Control Systems by Optimal Control Theory
          by Jonathan Korn, Sol W. Gully, David L. Kleinman
               ALPHATECH, Inc.
               3 New England Executive Park
               Burlington, Massachusetts 01803
          Hal Burke
               US Army Materiel Systems Analysis Activity
               Aberdeen Proving Ground, MD 21005

0930 -   General Structured Discrete-Time Observers
          by R. R. Beck
               US Army Tank-Automotive Command Research & Development Center
               Tank-Automotive Concepts Laboratory
               Warren, Michigan 48090
          K. C. Cheok and N. K. Loh
               Center for Robotics and Advanced Automation School of
                 Engineering
               Oakland University
               Rochester, Michigan 48063

1000 -   On The Design of Predictors for Fire Control Systems
          by James E. Leathrum
               US Army Materiel Systems Analysis Activity
               Aberdeen Proving Ground, MD 21005

1030 -   Microprocessor Implementation of an Adaptive Second Order
          Tracking/Prediction Algorithm for Tank Fire Control
          by P. T. Yip
               US Army Armaments Research & Development Command
               Fire Control & Small Caliber Weapons Systems Laboratory
               Dover, NJ 07801

1100 -   On The Credibility of Models
          by Naim A. Kheir
               School of Science and Engineering
               The University of Alabama in Huntsville
               Huntsville, AL 35899

1130 -   Armored Combat Vehicle Technology Evaluation Using the HITPRO/
          DELACC Simulation Methodology (Confidential)
          by J. Groff, Rosemary Mirabelle, Steven A. Carchedi
               US Army Materiel Systems Analysis Activity
               Aberdeen Proving Ground, MD 21005

SESSION II: Control Theory & Applications   (Chairman - Herbert E. Cohen)
             II/Simulation

1300 -   A Linear Nonlinear Control Problem
          by Leon Kotin
               Center for Tactical Computer Systems
               US Army Communications-Electronics Command
               Fort Monmouth, NJ 07703

1330 -   Application of Modern Estimation and Control Techniques to the
          GLAADS Test Vehicle
          by D. P. Glasson
               The Analytic Sciences Corporation
               Reading, Massachusetts 01867
           B. L. Shulman
               US Army ARRADCOM
               Dover, New Jersey 07801

1400 -   On Designing Robust Predictors Using Finite State MARKOV Chains
          by W. Dziwak & S. A. Goodman
               US Army Armament Research & Development Command
               Dover, NJ 07801
           E. B. Pate & M. Mintz
               Department of Systems Engineering
               University of Pennsylvania
               Philadelphia, PA 19104

1430 -   Robust Kalman Filtering
          by Dr. G. A. Hewer
               RF Anti-Air Branch
               Weapons Synthesis Division
               Naval Weapons Center
               China Lake, California 93555

1500 - A Case Study of Modern Direct Digital Autopilot Design
by George B. Doane III, Sherman M. Seltzer, & H. Eugene Worley
Control Dynamics Company
Huntsville, AL 35801

1530 - Robust Missile Guidance
by D. O. Molnar
The Boeing Aerospace Company
Guidance and Navigation Technology Group
P. O. Box 3999
Seattle, Washington 98124

WEDNESDAY, 21 OCTOBER 1981

SESSION III: Control Theory & Applications (Chairman - Dr. Harold Pastrick)
III/Simulation

0900 - A New Class of Guidance Laws for Air-to-Air Missiles
by Joseph N. Craig, Roger L. Barron, and Francis J. Cook
Adaptronics, Inc.
McLean, Virginia 22102

0930 - Estimating Time-To-Go For Use in Advanced Guidance Laws
by CPT Tom L. Riggs, USAF
Department of Astronautics and Computer Science
United States Air Force Academy, Colorado 80840

1000 - Microprocessor-Based Optimal Controllers for a Helicopter Turret
Control System
by N. Coleman, E. Carroll, and R. Johnson
US Army Armament Research and Development Command
Dover, New Jersey 07801
N. K. Loh
Center for Robotics and Advanced Automation
School of Engineering
Oakland University
Rochester, Michigan 48063

1030 - Discrete-Time Disturbance-Accommodating Control Theory: The
Disturbance-Utilization Mode
by C. D. Johnson
Professor of Electrical Engineering
Electrical Engineering Department
The University of Alabama in Huntsville
Huntsville, AL 35899

iii

DISCUSSION AND SUMMARY

The third meeting of the Coordinating Group on Modern Control Theory was characterized by the broad range of subject matter, including tank-helicopter fire control and their microprocessor implementation, tactical missile guidance and control, disturbance accommodation control, prediction-estimation design and theory, Martin robustification of Kalman filters for heavy tailed non-gaussian disturbances in monopulse radar tracking systems, credibility of computer models, time-to-go algorithms for advanced guidance laws and stability analysis for power systems.

Considerable interest was shown in the experience to date on the micro-processor implementation of the fire control algorithms carried out by members of the US Army Armament Research and Development Command. The work of Professor C. D. Johnson on disturbance accommodation control and applied by Dr. William Kelly of the US Army Missile Command and Norman Coleman of US Army Armament Research and Development Command clearly have broad applications to current fire control activities in the Army. A very high degree of interest was demonstrated by the concerns of Professor Naim Kheir of the University of Alabama in Huntsville in his paper on credibility of computer models. The Technical Committee on Model Credibility of the Society of Computer Simulation have proposed adapting several measures to quantify how well a model matches the performance of reality being modeled. The Theil inequality coefficient (TIC) was recommended for missile systems validation. Different measures of credibility were proposed for a wide range of problems.

The work of Professor James Leathrum of Clemson University in developing a design methodology for predictors in fire control systems and the work of Professor Nan Loh on generalized observers should prove to be significant contributions to Army activities in improving weapon system effectiveness. The results of ALPHATECH on disturbed recticle sight clearly demonstrate that first order lead angle prediction is ineffective against manuevering targets and that the disturbed rectile exhibited a significantly worse pointing performance than the stabilized sight.

Joe Craig of Adaptronics, Inc., provided promising results on trainable adaptive learning network (ALN) guidance lines which are computationally simple, uses only passive observables and can be realized using current microprocessor capabilities. The paper by Captain Tom Riggs of the Air Force Academy demonstrated that the time-to-go algorithm which uses range over range rate for estimating time-to-go severely limited missile performance and that the best performing algorithm is the simple closed form algorithm that forces the command missile axial acceleration to be equal to the actual missile axial acceleration.

The work done by TASC and University of Pennsylvania on air defense fire control (GLAADS) concluded that Markov chains predictors offer noise immunity over AR or ARIMA models and that modern control techniques in design of AAA fire control provided improvements in the performance and stabilization of the weapon system.

Work currently being pursued by the Naval Weapon Center at China Lake on the application of robust statistics to monopulse radar trackers is exciting and has the potential of significant improved performance in the presence of heavy tailed non-gaussian noise.

Overall, the Chairman was pleased by the free exchange of information and the strong interaction of participants. The Chairman at the close of the meeting announced that the fourth meeting of the Coordinating Group on Modern Control Theory will be held during the week of 25 October 1982 at Oakland University. Rochester, Michigan.

HERBERT E. COHEN
Chairman

DOCUMENTATION

These proceedings have been produced in two parts to assure rapid distribution of this document. Part I is unclassified while Part II is Confidential.

ACKNOWLEDGEMENT

The Chairman would like to take this opportunity to thank Dr. William C. Kelly and James A. McLean of the Guidance and Control Directorate, US Army Missile Laboratory for providing the facilities for holding this meeting and to Dr. Harold Pastrick of Control Dynamics Company for his support while he was affiliated with the US Army Missile Command and his active participation in these proceedings.

Next page is blank

SESSION I: CONTROL THEORY & APPLICATIONS I/SIMULATION

20 OCT 1981

(MORNING)

THIRD MEETING OF THE COORDINATING

GROUP ON MODERN CONTROL THEORY

HOSTED BY: US ARMY MISSILE COMMAND

ANALYSIS OF TANK FIRE CONTROL SYSTEMS
BY OPTIMAL CONTROL THEORY*

By
Jonathan Korn
Sol W. Gully
David L. Kleinman
ALPHATECH, Inc.,
3 New England Executive Park
Burlington, Massachusetts   01803
and
Hal Burke
U.S. Army Materiel Systems Analysis Activity
Aberdeen Proving Ground, Maryland   21005

INTRODUCTION

The primary purpose of a fire control system (FCS) is to track and control the firing at a moving (and possibly maneuvering) target. Often, it is desired to include a gun leading mechanism in the FCS in order to compensate for the fired projectile's time-of-flight toward the moving target. Recently, a research effort in which several fire control system designs were analyzed, was reported in (1). The control designs, all of which include (first order) lead-angle prediction capability, consisted of both disturbed reticle (DR), and stabilized sight-director systems (SS). Two major attributes distinguish a DR from a director-type SS system:
1. The lead predictor is included in the DR's visual loop, and
2. A gun-to-recticle crossfeed path exists in the DR system; thus, coupling the gun dynamics into the visual loop. The director type system, on the other hand, is disengaged from both predictor and gun dynamics.

Since the human operator is an integral part of the FCS, it is necessary that any performance analysis (tracking and gun-pointing in particular) be approached with appropriate gunner modeling. In this paper, the performance of two representative generic fire control systems, a disturbed reticle and a stabilized sight-director, is analyzed. The tool through which these systems are analyzed is the well known Optimal Control Model (OCM), (2)-(3). The OCM is a nomative performance-oriented model of the human operator engaged in a control task. In the case at hand, it is a gunner performing a tracking task.

First, the dynamical properties of the two FC systems are dis-
cussed. A brief overview of the gunner's (optimal control) model
follows, and the performance measures employed in the analysis
are introduced. The frequency-and time-domain modeling approach,
and the ensuing modeling results are then discussed.

DESCRIPTION OF THE FIRE CONTROL SYSTEMS

The modeling effort is initiated by selecting representative
generic FC systems for the disturbed reticle and the stabilized
sight-director designs. In the following, the basic characteris-
tics of these systems are described. We begin with the disturbed
reticle design.

DISBURBED RETICLE (DR) SYSTEM

The purpose of a tank fire control system is to accomplish the
functions of tracking, target-coordinate estimation and predic-
tion, and gun pointing. In a disturbed reticle design, these
functions are intermixed in a complex dynamic interaction of the
gunner, sight, and gun turret. The idea of a disturbed reticle
fire control system is to automate the computation of the correct
lead for a constant velocity target.

The physical behavior the the DR system is the following. The
gunner, seated in the turret, rotates with the gun. He observes
the target and reticle through his sight, and commands the rota-
tion of the gun with a hand control to keep the reticle on the
target. In constant velocity tracking, the rate of rotation of
the gun is proportional to the displacement of the hand controls.
Thus the hand control displacement should ideally be proportional
to the target angular rate, $\dot{\theta}_T$, if the gunner is successfully
keeping the reticle on the target.

The mechanical hand control position is transferred to an elec-
trical output, u, which in turn acts as an input to the reticle
and turret subsystem. The turret servo should ideally cause the
gun to lead the target by an angle $\lambda_c = T\dot{\theta}_T$, where T is the pro-
jectile time-of-flight. This will insure that it is possible to
hit a target moving with a constant angular rate. In the ideal
case of steady-state tracking of a constant angular velocity
target, the gunner does not perceive the lead but simply keeps the
reticle on the target.

The disturbed reticle design considered is mechanized with a turret
servo, a hand control filter, a reticle (sight) servo and a cross-
feed. The hardware required to implement the disturbed reticle
concept is shown in Fig. 1. The reticle is projected in the
gunner's line of sight by a movable beam splitter and mirror. In
addition, light from a light-emitting diode (LED) is reflected

3

off this mirror into an optical sensor to provide a position reference signal for the mirror servo. Since the lead screw positions the photosensor array, the (uncompensated) input to the mirror servo is proportional to the lead screw angle, θ_{LS}. However, this input is modified by combining it with a signal from an electronic crossfeed. The resulting signal is used to command the mirror servo which will null on the LED and position the reticle in the gunner's line of sight. The lead screw tachometer output and the command serve as inputs to simultaneously position the gun at angle θ_G.

The functional block diagram representing this design (DR) is shown in Fig. 2. The command u is applied to both the lead screw and gun turret servomechanisms. The lead screw servo is a position servo which deflects the optical sensor an amount Tu with respect to the gun. The deflection is proportional to the rotation $\dot{\theta}_{LS}$ of the lead screw and is measured by a potentiometer. A tachometer is used for stabilization and to develop a lead command to the gun rate servo.

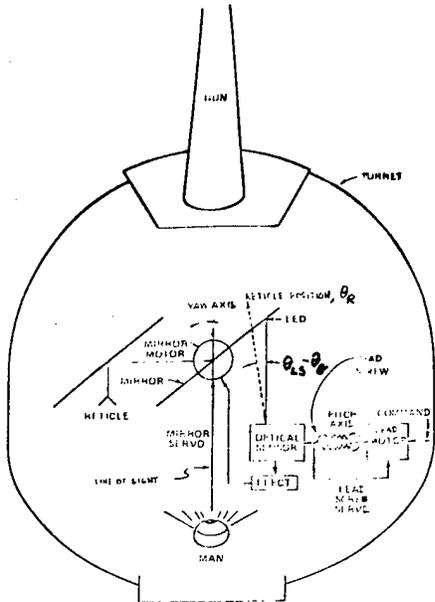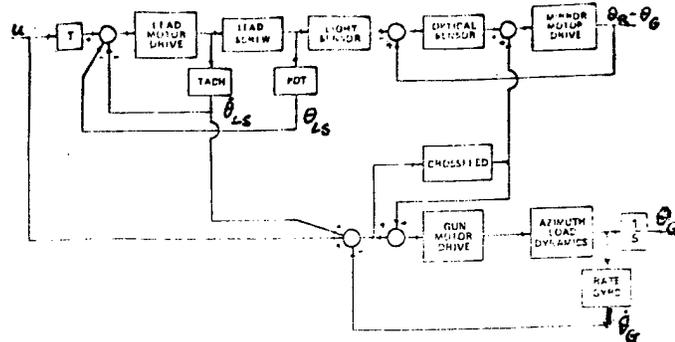Fig. 1. Physical Configuration, Disturbed Reticle Design (DR).

Fig. 2. Functional Diagram, Disturbed Reticle Design (DR).

The optical sensor picks up the deflected light angle and drives the mirror servo until the LED light is maximum. The mirror and gun servos also respond to the crossfeed compensation. The gun servo is rate compensated by gyro feedback. It is commanded by u and the crossfeed network.

4

The crossfeed network is central to the three individual servos in two ways. First, it is an integral part of the gun servo compensation network, and second, it provides crossfeeds to the mirror servo loop to slow the mirror when the gun servo cannot keep up with its command. This is seen by the following argument: when the gun servo error is large, indicating gun lag, the crossfeed signal is maximum and slows the mirror due to the negative sign. This tends to diminish the nominal lead Tu. A simplified state variable model (closed-loop) of the DR design is shown in Fig. 3.
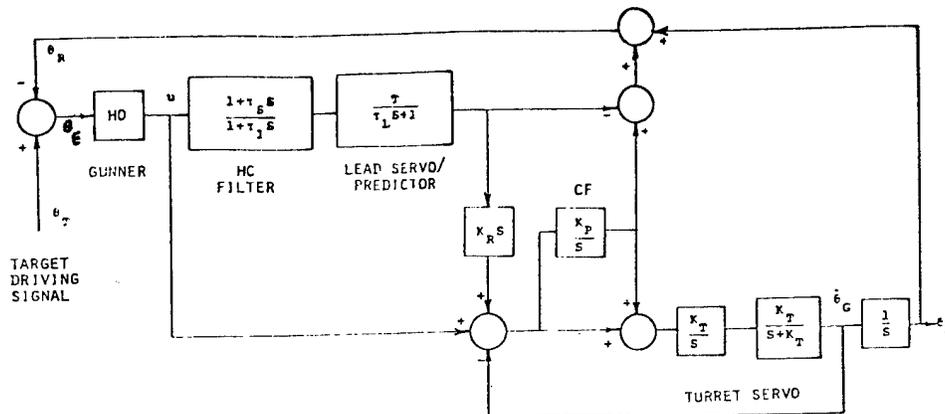
Fig. 3. Disturbed Reticle Design, State Variable Model.

In this representation we include the gunner in the control loop. Note that the (fast) optical sensor/mirror motor drive dynamics, as well as the system's inherent nonlinearities (1), are neglegted in the state space model and in the subsequent analysis. The pertinent state variables are defined as follows: θ_T = target commanded angle; θ_R = gunner's reticle (sight) angle; $\theta_E = \theta_T - \theta_R$ = tracking error; u $\triangleq$ gunner's control signal; θ_G = gun angle. Some of the characteristics of this configuration are summarized below.

1. The dynamics of the lead servomachanism are parameterized by its time constant, τ_L = .01 sec. The prediction time assumed is T=2 sec.
2. We explicitly include a lead servo tachometer gain K_R for a sensitivity analysis option as illustrated in the sequel. Nominally, K_R = 1.
3. The crossfeed gain is taken as K_p = 1.1, following (1).
4. We assume a second-order dynamics for the gun turret as shown in Fig. 3. The turret servo gain is K_T=10, resulting in a natural frequency of $\omega_T = K_T$=10 rad/sec and a damping ratio of ζ=0.5.
5. The hand-control (lag-lead) filter is designed to resolve the disparity between the fast sight dynamics and the slow gun turret dynamics, and its function is to lower the lead-servo bandwidth.

5

In the analysis that follows, the lag time-constant τ_I=1 sec, and the lead time-constant τ_S=0.1 sec.*

The gunner responding to the tracking error stimulus, generates the control command u which drives the gun turret and the reticle. Since the reticle angle θ_R is subtracted from the target signal θ_T, the human, in effect, controls the system defined by the transfer function $T_{DR}(s)$, viz.,

$$T_{DR}(s) = \frac{\theta_R(s)}{u(s)} = \frac{a_5 s^5 + a_4 s^4 + a_3 s^3 + a_2 s^2 + a_1 s + a_0 s}{s(s^3 + K_T s^2 + K_T^2 s + K_p K_T^2)(\tau_I s + 1)(\tau_L s + 1)} \quad (1)$$

where the a_i coefficients are function of the system parameters (5). Substitution of the appropriate parameter values yields the pole locations at 0, -100, -1, -1.23, -4.4 + j8.4 and zero locations at -.94, -1.39, -42.72, -3.6± j7.1. A Bode plot of $T_{DR}(s)$ is given in Fig. 4 (the transfer function pertaining to the SS system, $T_{SS}(s)$, is also shown, and will be discussed in the subsequent section).
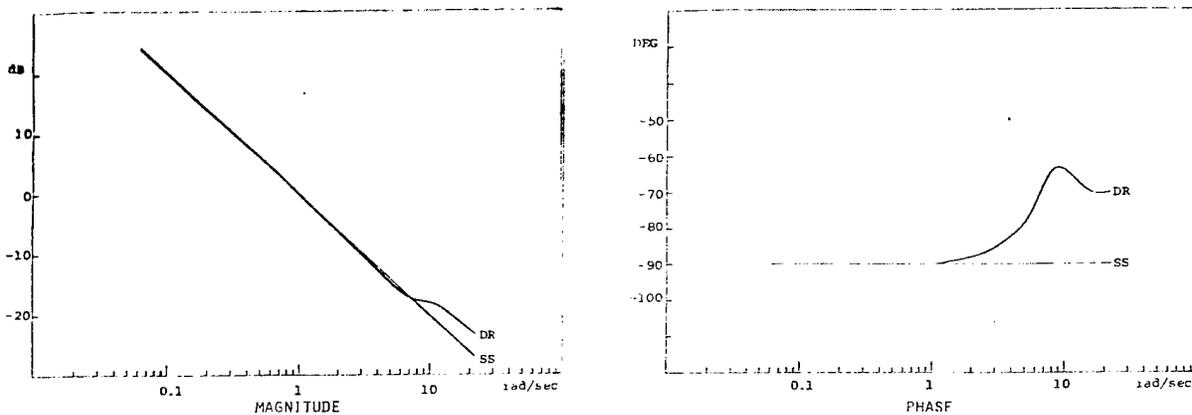
Fig. 4. Controlled Element Dynamics $\theta_R(s)/u(s)$.

It may be noted that the DR system has characteristics that closely approximate a rate-system, throughout the entire frequency range. This is not surprising, since the system's poles and zeros (other than the pole at the origin) which lie within the gunner's response range, essentially cancel each other. We see, therefore, that the direct effect of introducing the hand-control filter is to reduce the bandwidth of the gunner-controlled element such that it approximates a K/s-like system. Such a rate-system is a very desirable (easy) system for manual control. One must realize,

---

*This is an actual XM-1 Chrysler design (4).

6

however, that this system represents only the visual-loop dynamics. It will be shown in the sequel that the gun-pointing dynamics result in a totally unsatisfactory pointing performance.

STABILIZED-SIGHT DIRECTOR

The director type system structure is not as complex as the DR's, as the turret dynamics do not affect the gunner's visual loop. The physical components of a generic stabilized sight-director fire control system are illustrated in Fig. 5. Instead of the three servos that comprise the disturbed reticle system the stabilized sight employs two. The system uses a rate integrating gyroscope on the sight to provide an inertial reference in the azimuth axis. The azimuth sight gyro enables the effect of the gun turret rotation to be removed from the dynamics of the sight. This inertially stabilizes the sight so that it is independent of turret motion. As a consequence, the performance of the sight loop will be limited only by the ability of the human operator to track a target since the sight servo is several orders of magnitude faster than the operator response. In the subsequent analysis, the fast sight servo dynamics are neglected.

As indicated, the SS system consists of a two servo loops, one driving the sight and the other driving the turret. These two loops are each independently stabilized, both by rate integrating gyros. The command from the sight servo loop to the gun servo subsystem is used to pass target position information which is used in computing the correct angle to point the gun. The coupling from the gun servo to the sight servo loops locally references the sight servo to the gun and is due to the fact that the sight motor moves relative to the turret.

Fig.5. Physical Configuration, Stabilized Sight.

Fig. 6. Block Diagram, Stabilized Sight.

7

A (linear) block diagram of the SS system is given in Fig. 6. As shown in the figure the dynamic coupling of the turret motion to the sight director is immediately removed by the gyro. The gunner applies a signal to the gun sight servo. This signal is combined with sight position and rate feedback and used to drive the sight servo motor. In this figure θ_R represents the inertial angle of the reticle measured by a rate integrating gyro and θ_G represents the inertial angle in which the gun is poiting. Note that there is no need to lead the reticle since the sight is independent of the gun angle; thus the sight angle and the reticle angle, θ_R, are the same.

The lead angle computed by the system corresponds to $T\dot{\theta}_R$ which when added to θ_R is the correct angle the gun should aim to hit a constant velocity target. This signal is used to command the gun servo lead. Angular position information from the rate integrating gyros on the sight and gun are commanded as the difference between the sign and gun angles. The lead command will null itself when $\theta_R - \theta_G = T\dot{\theta}_R$.

Since we analyze in this paper the stabilized sight-director concept, and not an existing system, we may choose arbitrary dynamics for the visual loop. The appropriate choice is a rate system, $1/s$, so that any comparison between the SS and the DR systems will be meaningful. A simplified block diagram of such a system is shown in Fig. 7.

Fig. 7. Stabilized Sight-Director System.

Here, the gunner's controlled element dynamics are simply

$$T_{SS}(s) = \frac{1}{s} , \tag{2}$$

(see Fig. 4), and the gun turret servo is represented by a second-order underdamped system with characteristics similar to the DR's.

Thusfar, we have established the dynamics of the two generic FC systems, the performance of which we wish to analyze. In the following section we give a brief overview of the OCM, the main analytical tool which is employed in the analysis.

8

The Optimal Control Model (OCM) is well documented in the literature (2)-(3). A brief overview follows. Fig. 8 shows the structure of the OCM. The sight dynamics, $T_{DR}(s)$ or $T_{SS}(s)$, as well as any other pertinent system states are represented in state space form

$$\dot{x}(t) = Ax(t)+bu(t)+Ew(t)+Fz(t) \qquad (3)$$

$$y(t) = Cx(t)+du(t)$$

where $w(t)$ is a white-Gaussian disturbance with intensity W and $z(t)$ is a deterministic target trajectory. The displayed information $y(t)$ consists of tracking error $\theta_E(t)$ and error-rate $\dot{\theta}_E(t)$, and may include other auxiliary variables and their rate of change.
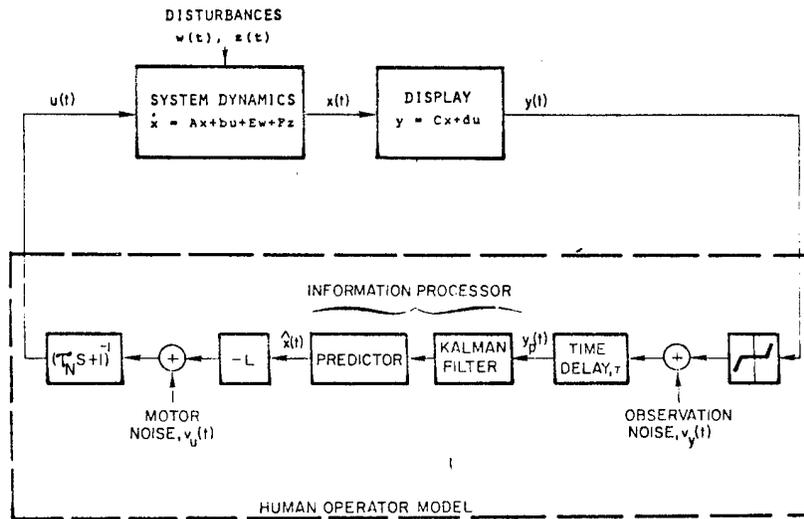

Fig. 8. Optimal Control Model of Gunner Response.

The visual assumption in the OCM is that the human perceives a delayed and noisy replica of $y(t)$, viz.,

$$y_p(t) = y(t-\tau) + v_y(t-\tau) \qquad (4)$$

where the white-Gaussian observation noise $v_{yi}(t)$ of the i-th indicator has covariance intensity

$$V_{yi}(t) = \pi\rho_{yi} E\left\{y_i^2(t)\right\} \qquad (5)$$

In these equations τ is the pilot's lumped time-delay, and ρ_{yi} is the observation noise/signal ratio of $y_i(t)$.

Given $y_p(t)$, the operator estimates the system state $\hat{x}(t-\tau)$ and predicts the current state $\hat{x}(t)$. He then develops an optimal control strategy by minimizing the quadratic cost functional

$$J(u) = E\left\{y'(t)Q_y y(t)+q_r \dot{u}^2(t)\right\} \tag{6}$$

where Q_y = diag (q_{yi}) are the relative weightings on the observations and q_r is the control-rate weighting*. Usually, the tracking error weighting coefficient, q_E, is non-zero, since the objective is to minimize the observed error. This strategy results in the optimal control gains, L, arising from the pertinent steady-state Riccati equation. With the inclusion of a motor noise, $v_u(t)$, in the pilot's control, the optimal control, $u(t)$, obeys the equation

$$\tau_N \dot{u}+u=L\hat{x}+v_u(t)=u_c(t)+v_u(t) \tag{7}$$

The parameter τ_N can be interpreted as a "neuro-motor" time constant. Usually, τ_N is specified and q_r is adjusted accordingly, as there is a one-to-one correspondence between the two.

The motor noise $v_u(t)$ is assumed to be white and Gaussian with intensity that scales with the covariance of $u(t)$,

$$V_u(t) = \pi\rho_u \text{ cov } [u(t)] \quad . \tag{8}$$

The coefficient ρ_u represents the motor-noise/signal ratio.

Modeling efforts utilizing the OCM can be approached in either of two ways:
1. steady-state mode, or
2. time-varying (nonstationary) mode.
In the steady-state mode $z(t)=0$, and the target input is modeled by a stationary colored noise. The usual practice is to let the disturbance $w(t)$ be a white-Gaussian noise, and to augment the system with the dynamics of a noise shaping filter that characterizes the driving noise. The stationary approach is most suitable for frequency domain analysis of human response. The model equations are represented in the frequency domain, so that various performance measures can be extracted. The model outputs include any of several possible transfer functions associated with the human, with the vehicle, or with the overall closed-loop system. In addition, the performance scores (tracking error RMS values) may be predicted.

---

*It is assumed that the human seeks a control strategy that would minimize control-rate rather than control.

In the time-varying case, the target's profile is deterministic, i.e., $z(t) \neq 0$ and $w(t)=0$. This modeling technique usually involves a comparison of experimental data time-histories (first- and second-order statistics) with the model-predicted ones. It is required, therefore, to develop the process mean and covariance propagation equations which arise from the non-random component $z(t)$ that drives the system. These equations, as well as the frequency domain equations, have been thoroughly documented in the literature, e.g. (2)-(3). Next, we analyze the control performance of the two gunner/FC systems. The analysis is performed in both frequency- and time-domain by employing the appropriate OCM techniques.

FREQUENCY-DOMAIN PERFORMANCE ANALYSIS

In this section we develop the frequency domain model for target tracking. First the statistical properties of the maneuvering target are determined. Next we obtain the overall system state space representation, which includes the target, the sight, and the gun dynamics. Finally we define frequency domain measures (metrics) for the fire control system performance evaluation and comparison.

TARGET EXCITATION SIGNAL

It is assumed that the target is an enemy tank that maneuvers towards the gunner in an avoidance path. It is also assumed that the target range is large enough to be taken as constant. Therefore, the only target-related variable of interest is the target's lateral displacement, or equivalently, the target's sight angle, $\theta_T(t)$. We assume that the target angle, $\theta_T(t)$, is a second-order Markov process driven by white Gaussian noise, $w(t)$, with an intensity of W. This assumption is practical and sufficient for our modeling effort. The noise-coloring process is assumed to be a butterworth filter with bandwidth $\omega_n = 0.5$ rad/sec. We obtain, therefore, the differential equation for target motion,

$$\ddot{\theta}_T(t) + 2\zeta\omega_n \dot{\theta}_T(t) + \omega_n^2 \theta_T(t) = \omega_n^2 w(t) \qquad (9)$$

where $\zeta = 1/\sqrt{2}$, and the resulting target signal power spectral density is

$$\Phi_T(\omega) = \frac{\omega_n^4 W}{\omega^4 + \omega_n^4} \qquad (10)$$

The appropriate target signal power value is selected as

$$E\left\{\theta_T^2(t)\right\} = \theta_{T,rms}^2 = 16 \text{ mrad}^2 \qquad (11)$$

11

i.e., $\dot{\theta}_{T,rms}$ = 4 mrad. This selection dictates the power of $\dot{\theta}_{T,rms}$, and it can be shown that for a butterworth filter,

$$\dot{\theta}_{T,rms} = \omega_n \theta_{T,rms} \quad . \tag{12}$$

Therefore, since ω_n = 0.5 rad/sec, we obtain $\dot{\theta}_{T,rms}$=2 mrad/sec. If we further assume that the (~constant) range, R=2000 meters, we obtain an equivalent target RMS lateral displacement and velocity ($R\theta_{T,rms}$ and $R\dot{\theta}_{T,rms}$,respectively) of 8 meters and 4 meters/second, respectively. These displacement, velocity, range, and bandwith values compare well with the Hardison tracking test simulations reported in (4). (Actually, any one of these four parameters is determined by the other three.)

MODEL DEVELOPMENT

The OCM structure requires a state-space form of the controlled element/target dynamics. Table 1 defines the state variables for the DR and SS systems.

TABLE 1. STATE VARIABLES FOR THE DR and SS SYSTEMS

	x_1	x_2	x_3	x_4	x_5	x_6	x_7	x_8
DR	θ_T	$\dot{\theta}_T$	Lead Servo Angle	HC Filter Signal	θ_G	$\dot{\theta}_G$	Input Signal to Turret Servo to LPF	θ_R
SS	θ_T	$\dot{\theta}_T$	θ_R	θ_G	$\dot{\theta}_G$	--	--	--

One may notice that $x_4=\theta_G$ and $x_5=\dot{\theta}_G$ in the SS system are unobservable states. They are included so that predictions can be made of the gun motion.

The displayed information in all systems is, of course, the tracking error, $\theta_E(t)$, but the gunner extracts rate information, $\dot{\theta}_E(t)$, as well. The observation set is, therefore, $y'=[\theta_E \ \dot{\theta}_E]$. The state equations for the two systems can now be easily derived, and are given elsewhere (5). The system parameter values are listed in a previous section. For the gunner we select the OCM nominal parameter values: ρ_u=-25db; $\rho_{y1}=\rho_{y2}$=-20db; τ_N=.15 sec; τ=.2 sec. The cost functional used is

$$J(u) = E\left\{\theta_E^2(t) + q_r\dot{u}^2(t)\right\} \tag{13}$$

where q_r is uniquely determined by the neuromotor time constant, τ_N.

FREQUENCY DOMAIN MEASURES

The following frequency domain metrics are used in the performance analysis.

1. Gunner Describing Function, H(s)(magnitude and phase) — This transfer function conceivably can be calculated from field (or simulation) data. It is defined, relative to the given input disturbance, $w(s)*$, as the ratio of the transfer function between input u and noise w to the transfer function between output θ_E and noise w. Thus, assuming negative feedback

$$H(s) = -\frac{u(s)/w(s)}{\theta_E(s)/w(s)} \quad , \tag{14}$$

or conceptually,

$$H(s) = -\frac{u(s)}{\theta_E(s)} \tag{15}$$

2. Circulatory Transfer Function, O(s) (from θ_E back to θ_E signal) — This is a rather complex, but quite important transfer function. For single indicator/display system it is equal to the single-axis $Y_p Y_c$ (human-vehicle open-loop) found in the early man-machine literature (6). For multiloop systems it is equivalent to an "outer-loop" describing function. It is defined as follows. In the closed-loop system we open the loop at a given indicator containing position information and rate information ($\theta_E, \dot{\theta}_E$ in the case at hand). The loop transfer function, starting at the indicator θ_E, going through the human, the vehicle (slight/gun) and ending at $\dot{\theta}_E$ is O(s). Quantities such as gain and phase margins, as well as loop bandwidth are obtained.

In the context of this stability metric, we investigate the robustness of the disturbed reticle system to sight tachometer, K_R, failures(in the stabilized sight-director the predictor sub-system is out of the visual loop, and, therefore, failures of the tachometer have no effect on the loop stability). The underlying assumption in this analysis is that the gunner cannot adapt instantaneously to sudden failures in the sight tachometer, and his describing function, H(s), remains tuned to the old system, for which $K_R=1$. We then compute O(s) which is comprised now of the "old" gunner model and the "new" (degraded) system.

3. RMS values (scores) of the tracking error, $\theta_E(t)$ — This metric is a measure of the gunner's <u>tracking</u> performance. We do not analyze the <u>pointing</u> performance of the FC systems in the frequency

---

* We recognize that w(t) does not strictly have Laplace transform. This is not a problem since it "falls out" in the compution of H(s).

domain, since it involves signals at different times (the pointing error is defined as $\theta_T(t+T) - \theta_G(t)$, where T is the projectile's time-of-flight; also see subsequent section), and the OCM steady-state analysis can treat events at time t only. The pointing performance is addressed in the subsequent time-domain analysis.

FREQUENCY DOMAIN MODELING RESULTS

The modeling results are summarized in Figures 9 through 11. These results are discussed below.

1. Gunner Transfer Function — Figure 9 shows the magnitude and phase of H(s) for the two FC systems. The difference between the DR and the SS are relatively minor, as the visual loop dynamics in the two systems are almost identical (see Fig. 4). What is displayed in Fig. 9 is a typical human operator transfer function controlling a rate-like system.
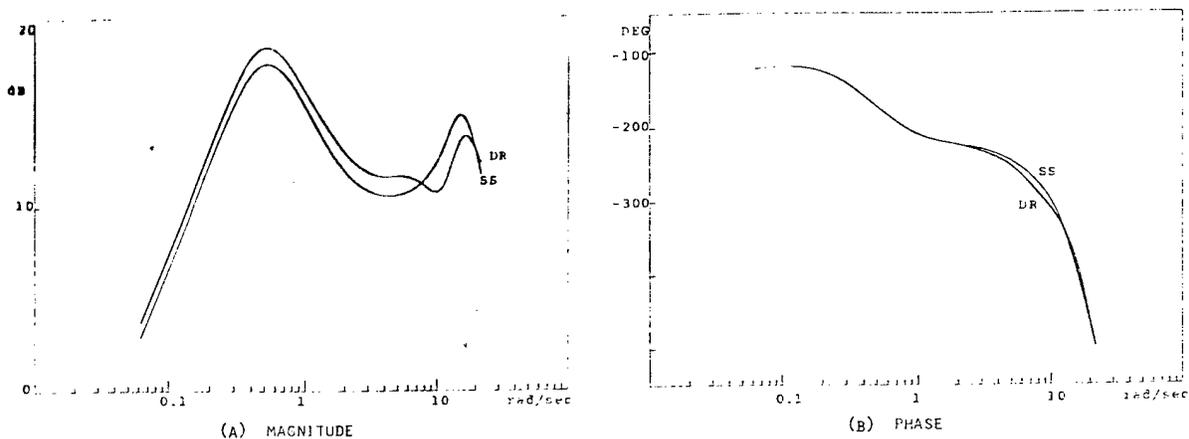

Fig. 9. Gunner Transfer Function, H(s).

2. Open-Loop Transfer Function — First we examine the loop (circulatory) transfer function, O(s), for the two FCs under nominal conditions. It was found that both DR and SS systems resulted in similar O(s) transfer functions in the nominal case. For that reason, only the DR's circulatory transfer function is shown in Fig. 10. The O(s) function for the SS can be assumed to be the same. The gain and phase margins are comparable (6-7 dB and 40°, respectively). Next we assume that the sight tachometer gain in the DR system is abruptly halved, i.e., K_R=.5. The resulting open-loop transfer function changes dramatically as evidenced by Fig. 11. It is clear that if the gunner fails to adapt to the new conditions (which is assumed to be the case under normal circumstances) the closed-loop DR system becomes unstable. In the stabilized sight-director, on the other hand, such danger is nonexistent, since the lead prediction loop is disengaged from the sight dynamics. The only effect of a

14

tachometer failure in the SS system is a degraded pointing performance, while all stability margins are maintained at their original levels.
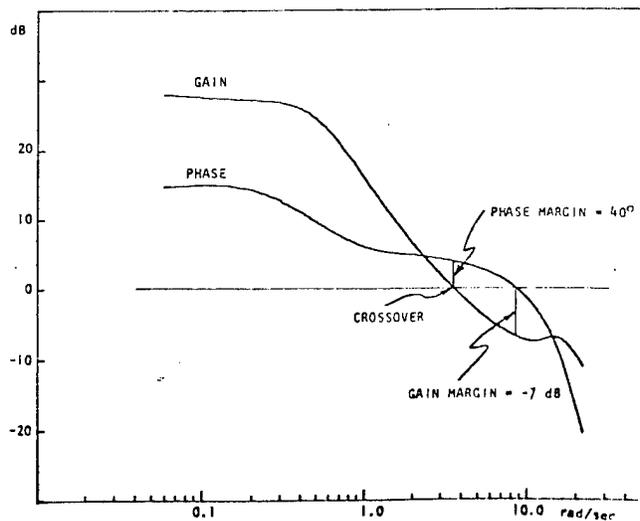

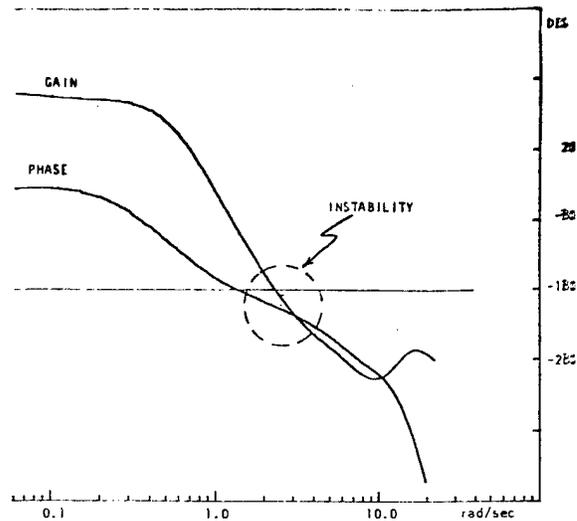Fig. 10. DR Gunner-Vehicle Open-Loop Transfer Function, $K_R=1$

Fig. 11. DR Gunner-Vehicle Open-Loop Transfer Function, $K_R=0.5$

3. RMS of Tracking Error (Scores) — The OCM predicted scores for the DR and the SS systems, given the hypotesized target dynamics, are 0.50 and 0.53 mrads, respectively. These scores are of the same order as those reported in (4). Thus, the difference in the tracking performance between the two systems is insignificant. This result could be expected since both systems have almost identical visual loop dynamics.

Next we analyze the FC system's performance in the time-domain, where more significant differences are uncovered.

TIME-DOMAIN PERFORMANCE ANALYSIS

TARGET MANEUVER

In contrast to the frequencey domain analysis, the target trajectory now is assumed to be "deterministic". In order to expose the differences between the two FCs and to evaluate their lead prediction capabilities, it was required to design a target maneuver with appreciable acceleration levels. We assume a target which maneuvers toward the gunner at an approximate range of R=750 meters. The maneuver begins at t=1 sec and ends at t=13 sec, at which point the target continues its movement with a constant velocity. The assumed trajectory is shown in Fig. 12.

15

Following (1), we assume a generalized Poisson-like tangential and radial target accelerations. Since the range assumed is effectively "constant", the gunner tracks only the target's lateral motion. Therefore, the only relevant quantity for the modeling effort is the target (resultant) lateral acceleration, $z(t)$. This acceleration is expressed in mrad/sec^2 and its profile is shown in Fig. 13. A more detailed description of this target intentional maneuver is given in (5).
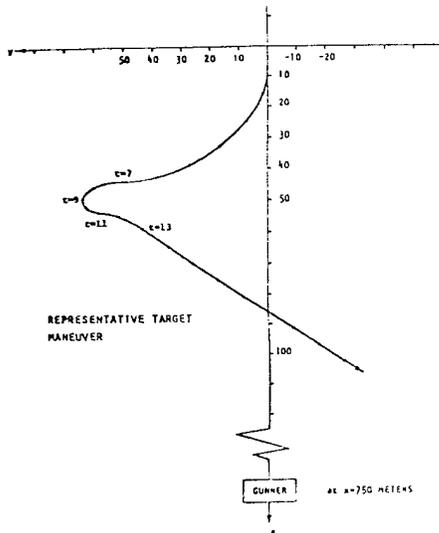
Fig. 12. Representative Target Trajectory.
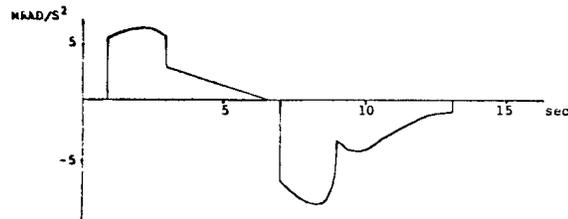
Fig. 13. Resultant Lateral Acceleration.

MODEL DEVELOPMENT

The DR and the SS systems are of course unchanged, and we use the states variables which were defined previously. The state equations are unchanged except for the target dynamics (first and second state variables), which are now

$$\dot{x}_1 = x_2, \quad \dot{x}_2 = z(t) \tag{16}$$

The z(t) component is modeled in the OCM's Kalman Filter (Fig. 8) as a "pseudo" white-noise with the intensity

$$W_d(t) = 2\tau_c z^2(t) , \tag{17}$$

where $\tau_c = 1$ sec, and is interpreted as the correlation time of the z(t) process. All OCM parameters as well as the cost functional J(u) (13) remain unchanged.

TIME-DOMAIN MEASURES

Applying the target driving acceleration, $z(t)$, the ensemble mean and covariance equations of the closed-loop system are propagated.

16

It is possible, then, to obtain time-histories (first and second order ensemble statistics) of the various signals in the control loop. In the present analysis we compare the following time-histories, obtained for the two FC systems.

1. Tracking Error, $\theta_E(t)$ — Based upon the similarity of the tracking loop dynamics, and the frequency-domain results, no significant differences are expected in tracking performance.

2. "First-order" gun pointing error, $\theta_{TG}^1(t)$ — This quantity is defined as

$$\theta_{TG}^1(t) = \theta_T(t) + T\dot{\theta}_T(t) - \theta_G(t) \quad . \tag{18}$$

Usually, one is interested in the tracking error, $\theta_E(t)$, statistics, as this is a fundamental measure in any tracking performance modeling effort. In the case at hand, we are also concerned with the evaluation of the dynamic properties of the two FC systems. The quantity $\theta_{TG}^1(t)$ is an excellent metric for such evaluation for the following reason: If we replaced the turret-servo second-order dynamics with a unity gain (i.e., $K_T \to \infty$), and if we assumed that the gunner tracks perfectly (i.e., $\theta_E(t) \equiv 0$), then, for constant velocity targets, $\theta_G(t) = \theta_T(t) + T\dot{\theta}_T(t)$, simply because of the fact that a first-order lead predictor is employed in each of the FC systems. Therefore, by evaluating the "first-order" pointing-error, $\theta_{TG}^1(t)$, we eliminate the pointing errors which are introduced by the inability of the first-order predictor to account for maneuvering (accelerating) targets. The signal $\theta_{TG}^1(t)$ merely reflects the effect of the tracking error on the gun output, and, more importantly it is a measure of the dynamic response of the FC systems at hand.

3. Total gun-pointing error, $\theta_{TG}(t)$ — This angle is defined as

$$\theta_{TG}(t) = \theta_T(t+T) - \theta_G(t) \quad , \tag{19}$$

and it reflects the total pointing error between the target at T(=2 sec) ahead and the present gun pointing angle. This quantity is a measure of the predictor's performance rather than the FC system's. In this sense, the statistical analysis of $\theta_{TG}(t)$ is a prelude to any future research effort on improving lead-angle prediction mechanisms.

MODELING RESULTS

The modeling results are summarized in Figs. 14 through 16.

1. Figure 14 shows the tracking error statistics for the two systems. Shown are (a) ensemble mean, $\theta_E(t)$, and (b) ensemble standard deviation, $\sigma_E(t)$. As expected, large transients are evident in the vicinity of $t \simeq 2$ sec and $t \simeq 8$ sec, as the largest acceleration peaks occur at these times. The error mean and variance values are comparable to the results reported in (4). No significant differences in tracking performance are detected between the SS

and the DR systems, because of the similarity of the visual-loop dynamics. Any conclusions from these results, however, may be misleading as now shown.

2. Figure 15 shows the "first order" pointing error results. It is clear that the DR system (which represents the actual Chrysler design) exhibits the largest pointing error mean, while its standard deviation $\sigma_{TG}^{1}(t)$, is actually the smallest. The physical interpretation of this result is that the DR's gun response is sluggish and exhibits a remarkably small variability by filtering out high frequency variations. Since the tracking error (θ_E) for the DR is actually the smallest, it is clear that the DR's unsatisfactory pointing performance is due to its sluggish dynamics, induced by the hand control filter. It is unfortunate that good tracking performance has been achieved at the expense of poor pointing performance.
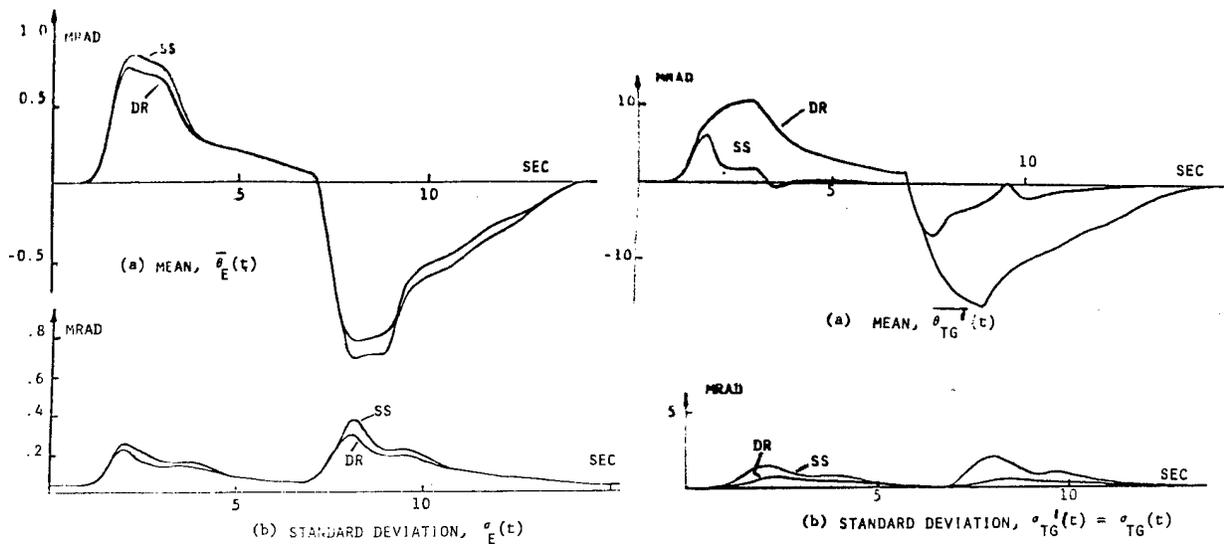

Fig. 14 Tracking Error Ensemble Statistics

Fig. 15 "First-Order" Gun Pointing Error Statistics

3. Figure 16 shows the ensemble statistics of the actual pointing angle $\theta_{TG}(t)$. The standard deviation, $\sigma_{TG}(t)$, is not shown since it is the same as in Fig. 15.
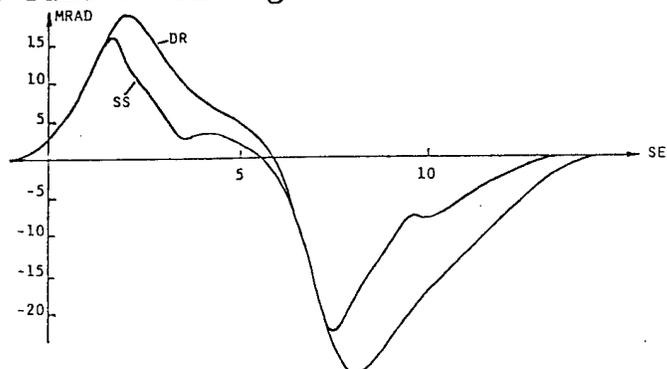

Fig. 16 Total Pointing Error Ensemble Mean

18

Two observations are quite obvious:
1. The pointing error and covariance levels are extremely large (over 20 mrad at one point) and reflect the failure of the first-order lead predictor to handle accelerating targets.
2. The DR exhibits a significantly worse pointing performance than the SS. The larger and longer persisting errors in the DR system are accorded to the sluggish gun response, which results from the introduction of the hand-control filter.

CONCLUSIONS

This paper documents partial results of a research effort to develop analytical techniques for evaluating tank fire control systems, and to apply the techniques to evaluate existing (disturbed reticle) and proposed (stabilized sight-director) fire control system mechanizations. The technique through which the two FC systems are analyzed is the Optimal Control Model (OCM) of human response. This modeling approach includes the gunner in the closed-loop, i.e., it considers the gunner-operator as an integral part of the FCS. The modeling results uncover some of the weaknesses of the disturbed reticle system. In particular, it is shown that under certain conditions the DR becomes dynamically unstable and, in general, its gun-pointing performance is unsatisfactory. In addition, it is shown that first-order lead-angle prediction is inappropriate in engagements involving maneuvering targets. Thus, a higher order predictor is necessary. This, however, is a subject of future research efforts.

REFERENCES

1. Gully, S.W. and N.R. Sandel, "Research on Fire Control Concepts for Maneuvering Targets," TARADCOM TR-12511.
2. Kleinman, D.L., S. Baron and W.H. Levison,"A Control Theoretic Approach to Manned-Vehicle Systems Analysis," IEEE Trans. on Auto. Control, Vol. AC-16, No. 6, 1971.
3. Kleinman, D.L. and S. Baron, "Manned Vehicle Systems Analysis by Means of Modern Control Theory," NASA CR-1753, June 1971.
4. Chrysler Corporation, "Evasive Target Lead Error Study Using the XM1 Fire Control System Simulator," Report No. XTR 8112-1, November 1979.
5. ALPHATECH, Inc., "Fire Control Concepts for Maneuvering Targets," work in progress.
6. McRuer, D.T., D. Graham, E. Krendel, and W. Riesner, Jr., "Human Pilot Dynamics in Compensatory Systems," Air Force Flight Dynamics Laboratory, Report AFFDL-TR-65-15, 1965.

GENERAL STRUCTURED DISCRETE-TIME OBSERVERS

R. R. Beck
U. S. Army Tank-Automotive Command
Research and Development Center
Tank-Automotive Concepts Laboratory
Warren, Michigan 48090

K. C. Cheok and N. K. Loh
Center for Robotics and Advanced Automation
School of Engineering
Oakland University
Rochester, Michigan 48063

ABSTRACT

A class of general structured discrete-time deterministic observers is developed. The one-step predicting or Luenberger observers and a class of current-update observers may be obtained from this class of general structured observers. Interesting relationships and important properties among various full-order observers are established. Optimal discrete-time observers are then developed, and it is shown that these optimal observers are structually and numerically equivalent to various forms of Kalman-Bucy filters.

1. INTRODUCTION

As is well known, the development and applications of filters and observers for stochastic and deterministic systems have dominated the literature for almost two decades, [1-20]. Among the most well-known techniques for estimating the state of a system are the stochastic Kalman-Bucy filters [1-4] and the deterministic Luenberger observers [5-8]. It is also well known [10,13,14] that an equivalence between the one-step predicting Kalman-Bucy filter and the full-order Luenberger observer can be established for a certain choice of observer gain. However, relationship between the various forms of Kalman-Bucy filters and other possible forms of deterministic observers which may provide additional insight into observer theory are obscure.

The main purpose of this paper is two fold. The first objective is to present a class of general structured discrete-time deterministic observers. The one-step predicting or Luenberger observers [5-8] and a class of current-update observers may be obtained from this class of general structured observers. Interesting properties among various forms of observers are established and it is shown that the one-step predicting or Luenberger observers and the current-update observers may be related via a set of time-update and measurement-update equations. The second objective is to develop a set of optimal gains for the class of general structured observers. The optimal gains are then used to establish a useful relationship between the optimal deterministic observers and the various forms of Kalman-Bucy filters.

The organization of the paper is as follows. Section 2 of the paper presents the development of the class of general structured discrete-time deterministic observers. Section 3 describes the relationship among various forms of full-order discrete-time deterministic observers. Optimal deterministic observers are derived in Section 4 using the notion of gradient matrices [21-24]. In Section 5, a useful equivalence between optimal full-order observers and the steady-state or time-invariant Kalman-Bucy filters is established. Throughout the paper, the notation, $z(i|j)$, will be used to denote the value of z of a dynamical equation at the discrete instant of time i updated by utilizing the measurements up to the instant of time j.

2. DISCRETE-TIME DETERMINISTIC OBSERVERS

Consider a deterministic dynamical system described by

$$x(k+1) = Ax(k) + Bu(k) , \quad x(0) = x_0, \tag{1a}$$

$$y(k) = Cx(k), \tag{1b}$$

where $x(k) \epsilon R^n$, $u(k) \epsilon R^r$, $y(k) \epsilon R^m$, $x_0 \epsilon R^n$ is arbitrary, and A, B, C are constant matrices of compatible dimensions. With no loss of generality, it is assumed that $\text{rank}[C] = m$. In general, $m < n$ so that the complete state $x(k)$ cannot be uniquely determined from the output relation (1b) alone. However, subject to the observability or detectability of (1), an estimate of $x(k)$ can be generated using an observer.

In this section, the development of a general class of discrete-time deterministic observers is investigated. Hence consider a general class of systems having the following structure:

$$z(k+1|k+1) = Fz(k|k) + Gy(k+1) + \tilde{G}y(k) + Hu(k), \tag{2a}$$

$$z(0|0) = z_0, \tag{2b}$$

$$x(k|k) = Pz(k|k) + Vy(k), \tag{2c}$$

where $z(k|k) \epsilon R^q$ with q being the dimension to be determined, z_0 is an arbitrary initial condition, F, G, $\tilde{G}$, H, P, and V are dimensionally compatible constant matrices to be determined, $\text{rank}[P] = q$, and $x(k|k) \epsilon R^n$ is the output of (2).

<u>Definition 1:</u> System (2) is said to be a <u>general structured observer</u> for (1) if

$$\lim_{k \to \infty} [x(k|k) - x(k)] = 0. \tag{3}$$

Define estimation error vectors as

$$e_z(k|k) \triangleq z(k|k) - Tx(k), \tag{4a}$$

$$e_x(k|k) \triangleq x(k|k) - x(k), \tag{4b}$$

where $T \in R^{q \times n}$ is to be determined; and whereby

$$\lim_{k \to \infty} e_z(k|k) = 0, \tag{5a}$$

$$\lim_{k \to \infty} e_x(k|k) = 0, \tag{5b}$$

imply that $z(k|k)$ estimates $Tx(k)$ and $x(k|k)$ estimates $x(k)$.

From (1), (2) and (4), it is straightforward to show that

$$e_z(k+1|k+1) = Fe_z(k|k) + (FT+GCA+\tilde{G}C-TA)x(k)+(H-TB+GCB)u(k), \tag{6a}$$

$$e_z(0|0) = z(0) - Tx(0), \tag{6b}$$

$$e_x(k|k) = Pe_z(k|k) + (PT+VC-I_n)x(k). \tag{6c}$$

The following theorem governs the existence of a general structured observer given by (2).

<u>Theorem 1:</u> Suppose (1) is completely observable and completely reachable. Then (2) is a general structured observer for (1) if and only if the following conditions are satisfied:

(a) $|\lambda_i[F]| < 1, \quad i = 1, \ldots, n,$ (7)

(b) $FT + \tilde{G}C + GCA = TA,$ (8)

(c) $H = TB - GCB,$ (9)

(d) $PT + VC = I_n,$ (10)

where $\lambda_i[\cdot]$ denotes the i-th eigenvalue of $[\cdot]$.

23

Proof: See Appendix A.

Remark 1: If (1) is completely observable and stabilizable but not completely reachable, then (7)-(10) in Theorem 1 are only a set of sufficient conditions for the existence of observer (2). This conclusion follows from the proof of Theorem 1 where condition (b) may not be always necessary when (1) is only stabilizable. ▲

In the sequel, two subclasses of the general structurea observers given by (2) are described, namely, the current-update observer and the one-step predicting[1] or Luenberger observer [5-8]. A current-update observer takes the form

$$z(k+1|k+1) = Fz(k|k) + Gy(k+1) + Hu(k), \qquad (11a)$$

$$z(0|0) = z_0, \qquad (11b)$$

$$x(k|k) = Pz(k|k) + Vy(k), \qquad (11c)$$

where (11) stems from (2) with $\tilde{G} = 0$. The term "current update" is usea to stress the fact that the most current measurement $y(k+1)$ is utilized for updating the state $z(k|k)$ of the dynamical equation (11a). The following corollary follows from Theorem 1.

Corollary 1: Suppose (1) is completely observable and reachable. Then (11) is a current-update observer for (1) if and only if

(a) $|\lambda_i[F]| < 1$, $i = 1,\ldots, n$, \qquad (12)

(b) $FT + GCA = TA$, \qquad (13)

(c) $H = TB - GCB$, \qquad (14)

(d) $PT + VC = I_n$. \qquad (15)

▲

On the other hand, setting $G = 0$ in (2) yields the one-step predicting or Luenberger observers, having the form [5-8],

$$z(k+1|k) = Fz(k|k-1) + \tilde{G}y(k) + Hu(k), \qquad (16a)$$

$$z(0|-1) = \bar{z}_0, \qquad (16b)$$

$$x(k|k-1) = Pz(k|k-1) + Vy(k), \qquad (16c)$$

---

[1] See Remark 3.

24

where the notations $z(k+1|k)$ and $x(k+1|k)$ are used to emphasis the fact that (16) is updated by a one-step previous measurement or that (16a) is a one-step prediction algorithm, and z_0 is an arbitrary initial condition. Similarly, Theorem 1 reduces to the following well known result [5-8] when $G = 0$.

Corollary 2: Suppose (1) is completely observable and reachable. Then (16) is a one-step predicting or Luenberger observer for (1) if and only if

(a) $\quad |\lambda_i[F]| < 1, \quad i = 1, \ldots, n,$ (17)

(b) $\quad FT + \tilde{G}C = TA,$ (18)

(c) $\quad H = TB,$ (19)

(d) $\quad PT + VC = I_n.$ (20)

▲

Remark 2: The matrices F and $\tilde{G}$ in (16a) may be shown to be given by

$$F = TAP + U_1 - (U_1 T + U_2 C) \begin{bmatrix} T \\ C \end{bmatrix}^{\#},$$ (21)

$$\tilde{G} = TAV + U_2 - (U_1 T + U_2 C) \begin{bmatrix} T \\ C \end{bmatrix}^{\#},$$ (22)

where $U_1 \in R^{q \times n}$ and $U_2 \in R^{q \times n}$ are arbitrary constant matrices and $[\cdot]^{\#}$ denotes the psendo-inverse [25,26] of $[\cdot]$.

▲

3. RELATIONSHIPS AMONG FULL-ORDER DISCRETE-TIME DETERMINISTIC OBSERVERS

In Section 2, the general structured observer described by (2), the current-update observer described by (11) and the one-step predicting or Luenberger observer described by (16) are all of order q where $q \leq n$. In this section, full-order general structured, current-update and one-step predicting or Luenberger observers with $q=n$ will be considered. The objective is to study the various interesting relationships and important properties of these full-order observers. Furthermore, the relationship between the full-order observers developed in this section and the Kalman-Bucy filter will be investigated in section 5, where it will be shown that a deterministic full-order observer can become a Kalman-Bucy filter under suitable conditions. The general structured observer described by (2) is therefore of fundamental and practical importance.

To proceed, let $T = I_n$, $P = I_n$ and $V = 0$, then Theorem 1 yields a full-order general structured observer of the form

$$x(k+1|k+1) = (A - \tilde{G}C - GCA)x(k|k) + Gy(k+1) + \tilde{G}y(k)$$

$$+ (B - GCB)u(k)$$

$$= Ax(k|k) + Bu(k) + G[y(k+1) - CAx(k|k) - CBu(k)]$$

$$+ \tilde{G}[y(k) - Cx(k|k)], \tag{23a}$$

$$x(0|0) = z_0. \tag{23b}$$

Setting $\tilde{G} = 0$ in (23) establishes a __full-order__ __current-update__ __observer__ (see also [18-20])

$$x(k+1|k+1) = (A - GCA)x(k|k) + Gy(k+1) + (B - GCB)u(k)$$

$$= Ax(k|k) + Bu(k) + G[y(k+1) - CAx(k|k) - CBu(k)], \tag{24a}$$

$$x(0|0) = z_0 ; \tag{24b}$$

while setting $G = 0$ in (23) results in a __full-order__ __one-step__ __predicting__ or __Luenberger__ __observer__ [5-7]

$$x(k+1|k) = (A - \tilde{G}C)x(k|k-1) + \tilde{G}y(k) + Bu(k)$$

$$= Ax(k|k-1) + Bu(k) + \tilde{G}[y(k) - Cx(k|k-1)], \tag{25a}$$

$$x(0|-1) = \bar{z}_0, \tag{25b}$$

where the notation $x(k+1|k)$ is used to emphasize that (25) is a one-step prediction algorithm.

__Remark 3:__ Equation (24) has the form of a Kalman-Bucy true filter while (25) has the form of a Kalman-Bucy one-step predicting filter, [1-4]; hence, the Luenberger observer described by (25) has also been referred to as a __one-step__ __predicting__ __observer__ in this paper. Also, it is observed that (24) and (25) can respectively be obtained from Corollaries 1 and 2 with $T=I_n$, $P=I_n$ and $V=0$. Furthermore, (25) can be derived from Remark 1 with $U_1=-U_2C$. ▲

Now the estimation errors associated with (23), (24) and (25) may be shown to be given by, respectively,

$$e_x(k+1|k+1) = (A - \tilde{G}C - GCA)e_x(k|k)$$

$$= A - \left\{ [\tilde{G} \mid G] \begin{bmatrix} C \\ CA \end{bmatrix} \right\} e_x(k\ k) , \tag{26a}$$

$$e_x(0|0) = x_0 - z_0 \; ; \tag{26b}$$

$$e_x(k+1|k+1) = (A - GCA)e_x(k|k), \tag{27a}$$

$$e_x(0|0) = x_0 - z_0; \tag{27b}$$

$$e_x(k+1|k) = (A - \tilde{G}C)e_x(k|k-1), \tag{28a}$$

$$e_x(0|-1) = x_0 - \bar{z}_0. \tag{28b}$$

Since it is desired that the estimation errors given by (26), (27) and (28) be made to approach the origin asymptotically, the gain matrices $\tilde{G}$ and G must be chosen such that $(A - \tilde{G}C - GCA)$, $(A - GCA)$, and $(A - \tilde{G}C)$ are asymptotically stable. It follows that the stabilities of the three matrices are closely related. The concept of observability and detectability [27-29] is useful and the following lemma is of importance.

Lemma 1:

(a-1) The pair $[A, C]$ is completely observable if and only if the pair $[A, (C'|A'C')']$ is completely observable. Furthermore, if the observability index of $[A, C]$ is n_0, then the observability index of $[A, (C'|A'C')']$ is n_0-1.

(a-2) The pair $[A, C]$ is completely detectable if and only if $[A, (C'|A'C')']$ is completely detectable.

(b-1) If A is nonsingular, then $[A, C]$ is completely observable if and only if $[A, CA]$ is completely observable.

(b-2) If A is singular and the pair $[A, C]$ is completely observable, then the pair $[A, CA]$ is completely detectable.

(b-3) If the pair $[A,C]$ is completely detectable, then the pair $[A,CA]$ is completely detectable. ▲

Hence it is clear from Lemma 1 that depending on the observability or detectability of the pair $[A,C]$, constant matrices $\tilde{G}$ and G can be found such that $|\lambda_i(A-\tilde{G}C-GCA)|<1$, $|\lambda_i(A-GCA)|<1$ and $|\lambda_i(A-\tilde{G}C)|<1$, for all $i=1,2,\ldots,n$.

A further useful relationship between the full-order current-update observer (24) and the one-step predicting or Luenberger observer (25) may be established via a pair of well known time-update and measurement-update equations [3]. Using the dynamics of system (1), a time-update or prediction algorithm may be defined as

$$\bar{x}(k+1|k) \triangleq Ax(k|k) + Bu(k), \tag{29a}$$

$$x(0|0) = z_0, \qquad (29b)$$

where $x(k+1|k)$ is a one-step predicted estimate. With this definition, the current-update observer (24) can be written as

$$x(k+1|k+1) = \bar{x}(k+1|k) + G[y(k+1) - C\bar{x}(k+1|k)], \qquad (30a)$$

$$\bar{x}(0|-1) = \bar{z}_o, \qquad (30b)$$

where (30) is a measurement-update equation [3]. Substituting (30) into (29) yields

$$\bar{x}(k+1|k) = A\bar{x}(k|k-1) + Bu(k) + AG[y(k) - C\bar{x}(k|k-1)], \qquad (31a)$$

$$\bar{x}(0|-1) = \bar{z}_o, \qquad (31b)$$

where (31) has the structure of the one-step predicting or Luenberger observer (25). It is clear that if the gain $\tilde{G}$ of (25) is chosen as

$$\tilde{G} = AG, \qquad (32)$$

then (25) and (31) describe the same estimate, i.e.,

$$\bar{x}(k|k-1) = x(k|k-1). \qquad (33)$$

Maintaining $\tilde{G} = AG$, it can be shown that[2]

$$\lambda_i[A - GCA] = \lambda_i[A - \tilde{G}C], \quad i=1,\ldots, n. \qquad (34)$$

It then follows that the stabilities and the convergence properties of the estimation errors of the full-order current-update and one-step predicting or Luenberger observers are equivalent. It is further remarked that the relationship $\tilde{G} = AG$ also turns out to be a natural consequence of a set of optimal gains for $\tilde{G}$ and G as will be pointed out in Section 5.

---

[2]Observe that $\lambda_i[MN] = \lambda_i[NM]$, where M and N are square matrices.

4. OPTIMAL DETERMINISTIC DISCRETE-TIME OBSERVERS

Constructions of optimal observer gains for the various full-order observers is given in this section. These optimal gains will be used in the next section to obtain a set of optimal deterministic observers which is structurally and numerically equivalent to a corresponding set of Kalman-Bucy filters. To achieve these objectives, an appropiate performance measure will be chosen.

Consider the estimation error equation given by (26) for the general structured observer, and consider the performance measure

$$
\begin{aligned}
J_1 &= \sum_{k=0}^{\infty} e_x'(k|k) W e_x(k|k) \\
&= \sum_{k=0}^{\infty} e_x'(0|0)(A - \tilde{G}C - GCA)'^k W (A - \tilde{G}C - GCA)^k e_x(0|0) \\
&\overset{\Delta}{=} e_x'(0|0) X e_x(0|0),
\end{aligned} \tag{35}
$$

where W is an nxn symmetric positive-definite weighting matrix, and X is an nxn symmetric matrix given by

$$
X = \sum_{k=0}^{\infty} (A - \tilde{G}C - GCA)'^k W (A - \tilde{G}C - GCA). \tag{36}
$$

It follows from Lemma 1 that if [A, C] is completely observable or completely detectable, then [A,(C'|A'C')'] is completely observable or completely detectable, respectively, so that there exist $\tilde{G}$ and G matrices such that $(A - \tilde{G}C - GCA)$ is asymptotically stable. The asymptotic stability of $(A - \tilde{G}C - GCA)$ ensures that X given by (36) exists and therefore J_1 is finite for finite $e_x(0|0)$. Furthermore, since W is positive-definite, it follows that X is positive-definite as may be seen from

$$
X = W + \sum_{k=1}^{\infty} (A - \tilde{G}C - GCA)'^k W (A - \tilde{G}C - GCA)^k. \tag{37}
$$

Also it can easily be shown that X satisfies

$$
X = (A - \tilde{G}C - GCA)' X (A - \tilde{G}C - GCA) + W. \tag{38}
$$

Now since J_1 given by (35) is explicitly dependent on the generally unknown initial estimation error $e_x(0|0)$, minimization of J_1 will give

rise to optimal gains which are dependent on the unknown initial condition $e_x(0|0)$. This difficulty may be alleviated by assuming that $e_x(0|0)$ is a random vector with arbitrary constant covariance given by

$$E[e_x(0|0)e_x'(0|0)] = Y, \tag{39}$$

where Y is an $n \times n$ positive-semidefinite matrix. An alternate performance measure is then given by

$$J_2 = tr[XY], \tag{40}$$

where $tr[\cdot]$ denotes the trace of $[\cdot]$. To accomplish the development of general structured observers which are structurally and numerically equivalent to the Kalman-Bucy filters, let the arbitrary covariance matrix Y be taken as

$$Y = Q + \tilde{G}R_1\tilde{G}' + GR_2G' - \tilde{G}N_1' - N_1\tilde{G}' - GN_2' - N_2G', \tag{41}$$

where Q is an $n \times n$ positive-semidefinite matrix, R_1 and R_2 are $m \times m$ positive-definite matrices and N_1 and N_2 are $n \times m$ matrices, to be assigned such that $Q_oQ_o' \triangleq Q - N_1R_1^{-1}N_1' - N_2R_2^{-1}N_2'$ is positive-semidefinite.

The constrained optimization problem posed by (38) and (40) may be reformulated as an unconstrained optimization problem by minimizing, with respect to $\tilde{G}$, G, X and Σ, the Lagrangian

$$J = tr\{XY + [(A - \tilde{G}C - GCA)'X(A - \tilde{G}C - GCA) + W - X]\Sigma'\} \tag{42}$$

where Σ is an $n \times n$ Lagrange multiplier matrix.

Using the notion of gradient matrices [21-24], the necessary conditions for an extremum are given by

$$\frac{\partial J}{\partial \tilde{G}} = 0 \quad , \quad \frac{\partial J}{\partial G} = 0 \quad , \quad \frac{\partial J}{\partial X} = 0 \quad \text{and} \quad \frac{\partial J}{\partial \Sigma} = 0 \quad . \tag{43}$$

The following lemma will be used to evaluate the gradient with respect to a symmetric matrix and the associated extremum conditions in (43).

Lemma 2: Consider

$$f = tr[AZ] \quad , \tag{44}$$

where A is an nxn arbitrary matrix and Z is an nxn symmetric matrix. Then [24]

$$\frac{\partial f}{\partial Z} = A + A' - \text{diag}[A] \quad , \tag{45}$$

where $\text{diag}[A] = \text{diag}\{a_{11}, a_{22}, \ldots, a_{nn}\}$, with a_{ii} being the diagonal elements of A. Furthermore, if A is also symmetric, then $\frac{\partial f}{\partial Z} = 0$ if and only if A=0. ▲

Assuming that X and Z are symmetric, evaluation of the gradient matrices in (43) yields

$$0 = 2X[\tilde{G}(C\Sigma C'+R_1) - A\Sigma C' + GCA\Sigma C'-\tilde{N}_1] \tag{46}$$

$$0 = 2X[G(CA\Sigma A'C+R_2) - A\Sigma A'C' + \tilde{G}C\Sigma A'C'-N_2] \tag{47}$$

$$0 = Y + (A-\tilde{G}C-GCA)\Sigma(A-\tilde{G}C-GCA)'-\Sigma, \tag{48}$$

$$0 = (A-\tilde{G}C-GCA)'X(A-\tilde{G}C-GCA) + W-X, \tag{49}$$

where Lemma 2 has been applied to obtain (48) and (49).

Remark 4: It is noted that in the literature, such as [16, 17, 21], little attempt has been made to explain the evaluation of gradients with respect to symmetric matrices, although, in general, correct results are given. ▲

The above results may be summarized in the form of a theorem (see also Lemma 1) as follows:

Theorem 2: Suppose (1) is completely observable or completely detectable. Let Q, R_1, R_2, N_1 and N_2 be the weighting matrices satisfying the conditions specified for (41). Then the optimal full-order general structured observer for (1) in the sense of minimizing the performance measure

$$J = \text{tr}[X(Q + \tilde{G}R_1\tilde{G}' + GR_2G' - \tilde{G}N_1' - N_1\tilde{G} - GN_2' - N_2G')] \tag{50}$$

subject to the algebraic constraint

$$X = (A - \tilde{G}C - GCA)' X (A - \tilde{G}C - GCA) + W, \tag{51}$$

is given by

$$x(k+1|k+1) = (A-\tilde{G}*C-G*CA) x(k|k) + G*y(k+1) + \tilde{G}*y(k) + (B-G*CB)u(k), \tag{52a}$$

$$x(0|0) = z_o, \tag{52b}$$

where W is asymmetric positive-definite weighting matrix, and

31

$$[\tilde{G}^* \mid G^*] = (A\Sigma C' + N_1 \mid A\Sigma A'C' + N_2)\left[\begin{bmatrix} C \\ CA \end{bmatrix} \Sigma (C' \mid A'C') + \begin{bmatrix} R_1 & 0 \\ 0 & R_2 \end{bmatrix}\right]^{-1} \tag{53}$$

with Σ being the symmetric positive-definite solution of the algebraic Riccati equation

$$\Sigma = A\Sigma A' + Q - (A\Sigma C' + N_1 \mid A\Sigma A'C' + N_2)\left[\begin{bmatrix} C \\ CA \end{bmatrix} \Sigma (C' \mid A'C') + \begin{bmatrix} R_1 & 0 \\ 0 & R_2 \end{bmatrix}\right]^{-1}\begin{bmatrix} (A\Sigma C' + N_1)' \\ (A\Sigma A'C' + N_2)' \end{bmatrix}.$$

$$\tag{54}$$

Furthermore, the asymptotic stability of $[A - \tilde{G}^*C - G^*CA]$ is guaranteed by the complete observability or detectability of the pair $[A, (C' \mid A'C')']$ and the complete reachability of the pair $[A, Q_o]$. ▲

The optimal gains for the current-update observer (24) and the one-step predicting or Luenberger observer (25) can be obtained in a similar procedure by setting either $\tilde{G}=0$ or $G=0$. The results are summarized below.

<u>Corollary 3</u>: Suppose system (1) is completely observable or completely detectable. Let $Q = Q_2$, N_2, and R_2 be as specified for (41) and let $\tilde{G}=0$ in (41). Then the optimal full-order current-update observer for (1), in the sense of minimizing the performance measure

$$J = tr[X(Q_2 + GR_2G' - GN_2' - N_2G')], \tag{55}$$

subject to the algebraic constraint

$$X = (A-GCA)' X (A-GCA) + W, \tag{56}$$

is given by

$$x(k+1|k+1) = (A-G^*CA)x(k|k) + (B-G^*CB)u(k) + G^*y(k+1),$$

$$= Ax(k|k) + Bu(k) + G^*[y(k+1) - CAx(k|k) - CBu(k)], \tag{57a}$$

$$x(0|0) = z_o, \tag{57b}$$

where W is a symmetric positive-definite weighting matrix, and

$$G^* = (A\Sigma A'C' + N_2)(CA\Sigma A'C' + R_2)^{-1}, \tag{58}$$

with Σ being the symmetric positive-definite solution of the algebraic Riccati equation

$$\Sigma = A\Sigma A' - (A\Sigma A'C'+N_2)(CA\Sigma A'C'+R_2)^{-1}(A\Sigma A'C' + N_2)' + Q_2. \tag{59}$$

Furthermore, the asymptotic stability of (A-G*CA) is guaranteed by the complete observability or detectability of the pair [A,CA] and the complete reachability of the pair $[A,Q_o]$. ▲

Corollary 4: Suppose (1) is completely observable or completely detectable. Let $Q = Q_1$, N_1 and R_1 be as specified for (41) and let G=0 in (41). Then the optimal full-order one-step predicting or Luenberger Observer for (1), in the sense of minimizing the performance measure,

$$J = tr[X(Q_1 + \tilde{G}R_1\tilde{G}' - \tilde{G}N_1' - N_1\tilde{G}')]. \tag{60}$$

subject to the algebraic constraint

$$X = (A-\tilde{G}C)' X (A-\tilde{G}C) + W, \tag{61}$$

is given by

$$x(k+1|k) = (A-\tilde{G}*C)x(k|k-1) + Bu(k) + \tilde{G}*y(k),$$

$$= A x(k|k-1) + Bu(k) + \tilde{G}*[y(k) - Cx(k|k-1)] , \tag{62a}$$

$$x(0|-1) = \bar{z}_o , \tag{62b}$$

where W is a symmetric positive-definite weighting matrix, and

$$\tilde{G}* = (A\tilde{\Sigma}C'+N_1)(C\tilde{\Sigma}C' + R_1)^{-1}, \tag{63}$$

with $\tilde{\Sigma}$ being the symmetric positive-definite solution of the algebraic Riccati equation

$$\tilde{\Sigma} = A\tilde{\Sigma}A' - (A\tilde{\Sigma}C'+N_1)(C\tilde{\Sigma}C'+R_1)^{-1}(A\tilde{\Sigma}C'+N_1)' + Q_1 . \tag{64}$$

Furthermore, the asymptotic stability of $[A-\tilde{G}*C]$ is guaranteed by the complete observability or detectability of the pair [A,C] and the complete reachability of the pair $[A,Q_o]$. ▲

33

The optimal observer gains basically depends on the solutions of the Riccati equations (54), (59) and (64). Numerous techniques for solving such equations are well known [30-33].

5. RELATIONSHIPS AMONG THE OPTIMAL FULL-ORDER OBSERVERS AND THE KALMAN-BUCY FILTERS

The objective of this section is to establish useful relationships among the optimal full-order observers developed in Section 4 and the various Kalman-Bucy filters.

Consider the system

$$x(k+1) = Ax(k) + Bu(k) + w(k) , \quad x(0) = x_o , \tag{65a}$$

with noisy measurements given by

$$y(k) = Cx(k) + v(k) , \tag{65b}$$

where $x(k)$, $u(k)$, $y(k)$, A, B and C are as given in (1), and $w(k)$ and $v(k)$ are independent zero-mean Gaussian white-noise vectors with covariances Q_w and R_v respectively.

A set of steady-state or time-invariant Kalman-Bucy filters are given by [3] :

True filter:

$$\hat{x}(k+1|k+1) = A\hat{x}(k|k) + Bu(k) + L[y(k+1) - CA\hat{x}(k|k) - CBu(k)] , \tag{66a}$$

$$\hat{x}(0|0) = z_o . \tag{66b}$$

One-Step predicting filter:

$$\hat{x}(k+1|k) = A\hat{x}(k|k-1) + Bu(k) + K[y(k) - C\hat{x}(k|k-1)] , \tag{67a}$$

$$\hat{x}(0|-1) = \bar{z}_o , \tag{67b}$$

where

$$L = \tilde{\Gamma}C'(C\tilde{\Gamma}C' + R_v)^{-1} , \tag{68}$$

$$K = A\tilde{\Gamma}C'(C\tilde{\Gamma}C'+R_v)^{-1} , \tag{69}$$

$$\tilde{\Gamma} = A\tilde{\Gamma}A' - A\tilde{\Gamma}C'(C\tilde{\Gamma}C'+R_v)^{-1}C\tilde{\Gamma}A' + Q_w, \tag{70}$$

where $\tilde{\Gamma}$ is the steady-state error covariance associated with the one-step predicting filter (67). Furthermore, the above filters (66) and (67) are related by the following equations [3]:

Measurement update:

$$\hat{x}(k+1|k+1) = \hat{x}(k+1|k) + L [y(k+1) - C\hat{x}(k+1|k)], \quad \hat{x}(0|-1)=\bar{z} , \tag{71}$$

$$\Gamma = \tilde{\Gamma} - \tilde{\Gamma}C'(C\tilde{\Gamma}C'+R_v)^{-1}C\tilde{\Gamma} . \tag{72}$$

Time-update:

$$\hat{x}(k+1|k) = A\hat{x}(k|k) + Bu(k), \quad \hat{x}(0|0)=z_o, \tag{73}$$

$$\tilde{\Gamma} = A\Gamma A' + Q_w , \tag{74}$$

where Γ is the steady-state error covariance associated with the true filter (66).

It remains to be verified that the above set of Kalman-Bucy filters can be derived from the results of Section 4. More specifically, the aim is to show that Corollaries 3 and 4 for the optimal deterministic observers can be equivalent to the steady-state true filter and one-step predicting filter. The measurement-update and time-update relationships for the filters and observers will also be established. It is easy to see that Corollary 4 gives rise to the one-step predicting filter if the weighting matrices $N_1=0$, $Q_1 =Q_w$ and $R_1=R_v$ are chosen for the performance measure (60), for then (63) and (64) reduce to, respectively,

$$\tilde{G}* = A\tilde{\Sigma}C'(C\tilde{\Sigma}C'+R_v)^{-1} \tag{75}$$

$$\tilde{\Sigma} = A\tilde{\Sigma}A' - A\tilde{\Sigma}C'(C\tilde{\Sigma}C'+R_w)^{-1}C\tilde{\Sigma}A' + Q_w, \tag{76}$$

which are structurally and numerically equivalent to (69) and (70), respectively, that is, $\tilde{G}* = K$ and $\tilde{\Sigma} = \tilde{\Gamma}$. On the other hand, if the weighting matrices

$Q_2 = Q_1 = Q_w$, $\qquad$ $N_2 = Q_w C'$ $\qquad$ and $\qquad$ $R_2 = CQ_w C' + R_v$ $\qquad$ are $\qquad$ chosen $\qquad$ for the performance measure (55) in Corollary 3, then (58) and (59) yield

$$G^* = (A\Sigma A' + Q_w)C'[C(A\Sigma A' + Q_w)C' + R_v]^{-1}, \tag{77}$$

$$\Sigma = (A\Sigma A' + Q_w) - (A\Sigma A'_w + Q_w)C'[C(A\Sigma A' + Q_w)C' + R_v]^{-1}C(A\Sigma A' + Q_w)'. \tag{78}$$

Denoting, with $Q_1 = Q_w$,

$$\hat{\Sigma} = A\Sigma A' + Q_w, \tag{79}$$

equations (77) and (78) become, respectively,

$$G^* = \hat{\Sigma}C'(C\hat{\Sigma}C' + R_v)^{-1}, \tag{80}$$

$$\Sigma = \hat{\Sigma} - \hat{\Sigma}C'(C\hat{\Sigma}C' + R_v)^{-1}C\hat{\Sigma}. \tag{81}$$

Substituting (81) into (79) results in

$$\hat{\Sigma} = A\hat{\Sigma}A' - A\hat{\Sigma}C'(C\hat{\Sigma}C' + R_v)^{-1}C\hat{\Sigma}A' + Q_w, \tag{82}$$

where it is seen from (70), (76) and (82) that $\hat{\Sigma} = \tilde{\Sigma} = \tilde{\Gamma}$. It follows from (68) and (80) that $G^* = L$. Furthermore, since (79) and (81) are identical to (74) and (72), respectively, it can be concluded that $\Sigma = \Gamma$. With $G^* = L$, the measurement-update equation (71) and the time-update equation (73) for the Kalman-Bucy filters are equivalent to the corresponding optimal measurement-update equation (30) with $G = G^*$, and the time-update equation (29). A complete equivalence between the optimal deterministic observers and the time-invariant Kalman-Bucy filters is thus established. Finally , it is interesting to note that the use of Corollary 4 and the relationship $\tilde{G} = AG$ in (32) can also be used to obtain the true filter (66) from the current-update observer (24).

CONCLUSIONS

The development of a class of deterministic general structured observers has been considered. From this class of general structured observers, the current-update observers and the one-step predicting or Luenberger observers can be derived. Interesting properties relating the full-order observers are pointed out. Optimal gains for these full-order observers are derived using an appropiate performance measure. It is shown that these optimal deterministic observers can be equivalent to, and hence may be as effective as, the steady-state or time-invariant Kalman-Bucy filters. The results of this paper have been extended to include reduced-order observers and time-optimal properties of the observers. The details will be given elsewhere.

APPENDIX A: Proof of Theorem 1: [see also [34]]

For sufficiency, it is clear that if (7)-(10) hold, then (6) reduces to

$$e_z(k+1|k+1) = Fe_z(k|k), \quad e_z(0) = e_{zo},$$

$$e_x(k|k) = Pe_z(k|k),$$

so that $e_z(k|k)$ approaches the origin asymptotically; since P is of full rank, $e_x(k)$ also approaches the origin asymptotically.

Conversely, suppose $e_z(k|k) = z(k|k) - Tx(k) \to 0$ and $e_x(k|k) \to 0$ as $k \to \infty$ for all $z(0)$, $x(0)$ and $u(k)$, $k = 0, 1,\dots$. Then setting $x(0) = 0$ and $u(k) = 0$ establishes the necessity for condition (a) in (6a). On the other hand, condition (c) must hold, for otherwise a $u(k)$ would always exist to drive $e_z(k|k)$ away from the origin. Likewise, unless condition (b) is satisfied, the reachability of (1) ensures that there would always exist a $x(k)$, driven by $u(k)$, which makes $e_z(k|k) \neq 0$ in (6a). Lastly, $e_z(k|k) \to 0$ and $e_x(k|k) \to 0$ as $k \to \infty$ yield $e_x(k|k) = [PT + VC - I_n]x(k) \to 0$ for arbitrary $x(k)$, thus establishing the necessity for condition (d). ▲

REFERENCES

[1]   R. E. Kalman, "A New Approach to Linear Filtering and Prediction Problems," _Journal of Basic Engineering, Trans. ASME_, Series D, Vol. 82, March 1960, pp. 35-45.

[2]   R. E. Kalman and R. S. Bucy, "New Results in Linear Filtering and Prediction Theory," _Journal Basic Engineering, Trans. ASME_, Series D, Vol. 83, March 1961, pp. 95-108.

[3]   B. D. O. Anderson and J. B. Moore, _Optimal Filtering_, Prentice-Hall, New Jersey, 1979.

[4]   Sage, A. P., and Melsa, J. L., _Estimation Theory with Application to Communications and Control_, McGraw-Hill, New York, 1971.

[5]   D. G. Luenberger, "Observing the State of a Linear System," _IEEE Trans. Mil. Electron._, Vol. MlL-8, April 1964, pp. 74-80.

[6]   D. G. Luenberger, "Observers for Multivariable Systems," _IEEE Trans. Automatic Contr._, Vol. AC-11, April 1966, pp. 190-197.

[7]   Luenberger, D. G., "An Introduction to Observers," _IEEE Trans. Automatic Control_, Vol. AC-16, Dec. 1971, pp. 596-602.

[8]   Gopinath, B., "On the Control of Linear Multiple Input-Output Systems," _Bell Syst. Tech. J._, Vol. 50, Mar. 1971, pp. 1063-1081.

[9]   Novak, L. M., "Optimal Observer Techniques for Linear Discrete-Time Systems," _Control and Dynamic Systems_, C. T. Leondes, Ed., Academic Press, New York, Vol. 9, 1973.

[10] Novak, L. M., "Discrete-Time Optimal Stochastic Observers," _Control and Dynamic Systems_, C. T. Leondes, Ed., Academic Press, New York, Vol. 12, 1976.

[11] Seborg, D. E., and Fisher, D. G., "Experience with Experimental Applications of Multivariable Computer Control," _Journal of Dynamic Systems, Measurement, and Control, Trans. ASME_, Vol. 101, June 1979, pp. 108-116.

[12] O'Riely, J., "On Linear Least-Square Estimators for Discrete-Time Stochastic Systems," _IEEE Trans. on Systems, Man, and Cybernetics_, Vol. SMC-10, No. 5, May 1980, pp. 276-279.

[13] Johnson, G. W., "A Deterministic Theory of Estimation in Control," _IEEE Trans. Automatic Control_, Vol. AC-14, Aug. 1969, pp. 380-384.

[14] Tse, E., and Athans, M., "Optimal Minimal-Order Observer-Estimator for Discrete Time-Varying Systems," _IEEE Trans. Automatic Control_, Vol. AC-15, Aug. 1970, pp. 416-426.

[15] Yuksel, Y. O. and Bongiorno, J. J. Jr., "Observers for Linear Multivariable Systems with Applications," IEEE Trans. Automatic Control, Vol. AC-16, Dec. 1971, pp. 603-613.

[16] Gourishanker, V., and Kudva, P., "Optimal Observers for the State Regulation of Linear Discrete-Time Plants," Int. J. Control, Vol. 26, No. 3, 1977, pp. 359-368.

[17] O'Riely, J., "Optimal Low-Order Feedback Controllers for Linear Discrete-Time Systems," Control and Dynamic Systems, C.T. Leondes, Ed., Academic Press, New York, Vol. 16, 1980.

[18] Willems, J. L., "Design of State Observers for Linear Discrete-Time Systems," Int. Journal. Systems Science, Vol. 11, No. 2, 1980, pp. 139-147.

[19] Willems, J. L., "Optimal State Reconstruction Algorithms for Linear Discrete-Time Systems,", Int. J. Control, Vol. 31, No. 3, 1980, pp. 495-506.

[20] Cheok, K. C., Loh, N. K., and Watanabe, K., "Design of a Class of Delayed-Measurement Observers," to be presented at the IFAC Symposium on Theory and Applications of Digital Control, January 5-7, 1982, India.

[21] Athans, M., "The Matrix Minimum Principle," Inform. Control, 1968, pp. 592-606.

[22] Athans, M., and Schweppe, F. C., "Gradient Matrices and Matrix Calculations," Lincoln Lab., M.I.T., Lexington, MA, TN 1965-63, 1965.

[23] Geering, H. P., "On Calculating Gradient matrices," IEEE Trans. Automatic Control, Vol. AC-21, Aug. 1976, pp. 615-616.

[24] Brewers, J. W., "The Gradient with Respect to a Symmetric Matrix," IEEE Trans. Automatic Control, Vol. AC-22, Apr. 1977, pp. 265-267.

[25] Rao, C. R., and Mitra, S. K., Generalized Inverse of Matrices and Its Application, John Wiley. New York, 1971.

[26] Strang, G., Linear Algebra and Its Applications, Academic Press, New York, 1976.

[27] Wonham, W. M., "On Pole Assignment in Multi-Input Controllable Linear Systems," IEEE Trans. Automatic Control, Vol. AC-12, 1967, pp. 660-665.

[28] Wonham, W. M., "On A Matrix Riccati Equation of Stochastic Control," SIAM J. Control, Vol. 6, No. 4, 1968, pp. 681-697.

[29] Kwakernaak, H., and Siran, R., Linear Optimal Control Systems, Wiley-Interscience, New York, 1972.

[30] Kortum, W., "Computational Techniques in Optimal State Estimation - A Tutorial Preview," _Journal of Dynamic Systems, Measurement and Control, Trans. ASME_, Vol. 101, June 1979, pp. 99-107.

[31] Durato, P., and Levis, A. H., "Optimal Linear Regulators: The Discrete-Time Case," _IEEE Trans. Autom. Control_, Vol. AC-16, Dec. 1971, pp. 613-620.

[32] Kon, B. C., _Digital Control System_, Hout, Rinehart and Winston, New York, 1980.

[33] Yasuda, K., and Hirai, K., "Upper and Lower bounds on the Solution of the Algebraic Riccati Equation," _IEEE Trans. Autom. Control_, Vol. AC-23, June 1979, pp. 483-487.

[34] Fortmann, T. E., and Williamson, D., "Design of Low-Order Observers for Linear Feedback Control Laws," _IEEE Trans. Autom. Control_, Vol. AC-17, June 1972, pp. 301-308.

Next page is blank.

ON THE DESIGN OF PREDICTORS FOR FIRE CONTROL SYSTEMS

James E. Leathrum
US Army Materiel Systems Analysis Activity
Aberdeen Proving Ground, Maryland 21005

BACKGROUND

The design of fire control systems has been characterized by a continuing controversy regarding the extent of estimation and prediction which should be mechanized. One extreme argues that the critical process is the tracking process which with current technology produces such large errors that a fire control system should not attempt to lead a maneuvering target. The other extreme argues that the methodology is at hand to deal with large observation errors and model identification. Thus, arbitrarily high order estimators and predictors should be implemented to produce a lead for engaging maneuvering targets.

Without taking an a priori position on the above issue, this report attempts to formalize some of the processes which may resolve the design problem. The problem is viewed as a trade-off between the errors incurred in propagating incorrect estimates through a predictor versus the errors incurred in failure to utilize an available estimate of a target state variable. The problem is similar to one which arises in numerical analysis wherein some situations "cancellation errors" may be larger than a computed result.

The design of predictors will be considered in the situation where the predictor exists in tandem with a Kalman estimator. This introduces no loss of generality, and yet, it is an acknowledgement of the current state -of-the-art. This structure does permit a presumption that state estimates and their variances are available for this analysis. The Kalman estimator would employ models of the form.

Target Model

$$X_{k+1} = \phi_k X_k + B_k U_k$$

Observation Model

$$Y_k = H_k X_k + V_k$$

The Kalman estimator would produce a sequence of estimates, $\hat{X}_k$, and variances of the estimation errors, P_k. If, at some time, it is necessary to predict ahead N steps without observations, the best, linear, unbiased estimator is

$$\hat{X}_{k+N} = \left(\prod_{i=0}^{N-1} \phi_{k+i} \right) \hat{X}_k$$

which would be approximated by

$$\hat{X}_{k+N} = (\phi_k)^N \hat{X}_k$$

The variance of the estimation error at k+N is obtained from the recussion

$$P_{k+1} = \phi_k P_k \phi_k + B_k Q_k B_k{}'$$

where $Q_k \equiv E(U_L U_k{}')$. Extrapolating this to k+N gives

$$P_{k+N} = \phi_k{}^N P_k (\phi_k{}^N) + \sum_{j=0}^{N-1} \phi_k{}^j B_{k+j} Q_{k+j} B'_{k+j} \phi_k{}^{j'}$$

which will be viewed as composed of

$$P_{k+N} = \left\{ \begin{array}{l} \text{Propagated variance} \\ \text{of the estimates} \end{array} \right\} + \left\{ \begin{array}{l} \text{Error variance} \\ \text{induced by} \\ \text{subsequent tar-} \\ \text{get motion} \end{array} \right\}$$

So far, this discussion seems to indicate that the design and analysis of the predictor of $\hat{X}_{k+N}$ is a closed issue and that the variances are left as a take-it-or-leave-it result. However, there is a choice to be made if one recognizes that the model is only one of a number of possible models. Furthermore, even if the models are correct, there may be a better, biased predictor. To formalize this notion, a predictor is defined as

$$\hat{X}_{k+N} = \phi^*{}_k \hat{X}_k$$

where $\phi^*{}_k$ is not necessarily $\phi_k{}^N$. The loss function of interest is the norm of the prediction error

$$\| E_p \| = \| \hat{X}_{k+N} - X_{k+N} \|$$

and the risk (which is to be minimized) will be

$$R(\phi^*) = E[\| E_p \|]$$

that is, we will seek that predictor algorithm, ϕ^*, which minimizes the expected norm of predictor error.

Although the problem just formulated is of interest in itself, there is an equally interesting dual. That is, given a maximum allowable risk, what predictor algorithm will lead to the best

overall estimator-predictor performance? Here, performance is viewed in terms of constraints placed upon sight technology and target agility. The least constraining design will be viewed as the best design.

FIRE CONTROL SYSTEMS AS A SPECIAL CASE

The problem definition stated in the previous section leaves a large number of parameters to be considered in the general case. To illustrate the utility of the approach, the subsequent discussion will be limited to situations which arise in the design of fire control systems. The following limitations will be presumed:

Only the positional component of the predictor error will be included in the loss function.

The model to be employed in the estimator is of the form

$$\phi_k = \begin{bmatrix} 1 & \Delta t & \Delta t^2/2 & \cdots \\ & 1 & \Delta t & \cdots \\ & \underline{0} & 1 & \cdot \\ & & & \cdot \\ & & & \cdot \end{bmatrix} \quad ; \quad B_k = \begin{bmatrix} \cdot \\ \cdot \\ \cdot \\ \cdot \\ \cdot \\ \Delta t^3/6 \\ \Delta t^2/2 \\ \Delta t \end{bmatrix}$$

$$H_k = \begin{bmatrix} 1 & 0 & 0 & \cdots & & 0 \end{bmatrix}$$

The prediction algorithm will be of the form

$$[\phi^*]_{\text{Position}} = \begin{bmatrix} 1 & \gamma_v t_f & \gamma_A t_f^2/2 & \cdots \end{bmatrix}$$

where $t_f = N\Delta t$, and the γ_V, γ_A, etc., are the optimization parameters.

The case of greatest interest in current applications is the one with a 3-dimensional state vector

$$\phi_k = \begin{bmatrix} 1 & \Delta t & \Delta t^2/2 \\ 0 & 1 & \Delta t \\ 0 & 0 & 1 \end{bmatrix} \quad ; \quad B = \begin{bmatrix} \Delta t^3/6 \\ \Delta t^2/2 \\ \Delta t \end{bmatrix}$$

$$H = \begin{bmatrix} 1 & 0 & 0 \end{bmatrix}$$

Here, the state vector is the position, velocity, and acceleration along a single axis of the target

$$X = \begin{bmatrix} x \\ v_x \\ a_x \end{bmatrix}$$

The prediction problem along each axis of the target can be treated independently for design purposes. In real-time, however, one would expect inherent coupling of the state equations along the respective axes. In other words, we will be generating up to three designs to be coupled together in a real-time implementation.

Concentrating upon a single coordinate axis, the loss function may be defined as

$$\epsilon_p{}^2 = (\hat{x} - x)^2{}_{k+N}$$

Here $\|\epsilon\|^2$ is used as a loss function for conciseness. In turn, the risk is

$$R(\phi^*) = E(\epsilon_p{}^2)$$

Using the definitions of $\hat{x}$ and x as well as the notation

$$T = [1 \ t_f \ t_f{}^2/2] = [\phi^N]_{position}$$
$$T^* = [1 \ \gamma_v t_f \ \gamma_A t_f{}^2/2] = [\phi^*]_{Position}$$

the risk condenses to

$$E(\epsilon_p{}^2) = T^* P_k T^{*\prime} + T^* Z_k (T^* - T)'$$
$$+ (T^* - T) Z'_k T^{*\prime}$$
$$+ (T^* - T) E(X_k X_k{}') (T^* - T)'$$
$$+ E(\epsilon^2{}_{TI})$$

where $Z_k = E[(\hat{X}_k - X_k) x'_k]$

and $E(\epsilon^2{}_{TI})$ = Variance of the target induced error

Thus, the risk is composed of terms which are interpreted as

$$E(\epsilon_p{}^2) = \text{Variance propagated from the estimation errors}$$

+ $\begin{cases} \text{Correlations between estimation errors and states} \\ \text{(2 terms)} \end{cases}$

+ $\begin{cases} \text{Mean squared magnitudes of the target states after} \\ \text{propagation} \end{cases}$

+ Error variances induced by subsequent target motion

Since the last term is not a function of the optimization parameters, it will be treated as a constant. The optimization involves a trade-off between the other terms. Thus, a new risk is formulated as the residual risk, $E(\varepsilon_R^2)$, due to the choice of the prediction algorithm.

$$E(\varepsilon_R^2) = E(\varepsilon_p^2) - E(\varepsilon^2_{TI})$$

In the first three terms of the risk equation, the filter parameters, P_k, Z_k, may be determined as ratios P_k/q and Z_k/q at steady state. These ratios, as well as r/q, are functions of a single bandwidth parameter, ω_v, for the target velocity.[1] (Note that $q \equiv E(U^2)$; $r \equiv E(V^2)$). After dividing the risk equation by q, and gathering terms, the dual optimization problem becomes one of maximizing.

$$r/E(\varepsilon_R^2) = \frac{K(\omega_V) \cdot N(S,t_f,\gamma_v,\gamma_A)}{D(\omega_V,t_f,\gamma_V,\gamma_A)}$$

$$S = E(XX')/E(\varepsilon_R^2)$$

$$N(S,t_f,\gamma_V,\gamma_A) = 1-[S_{33}(t^2_f/2)^2\ y^2 + S_{22}(t_f)^2 \cdot x^2$$
$$+ 2S_{23}\cdot(t_f^3/2)\cdot xy]$$

$$D(\omega_V,t_f,\gamma_V,\gamma_A) = T\ (P/q)T' - [(P_{33}/q)\cdot(t_f^2/2)^2 y^2$$
$$+ (P_{22}/q)(t_f)^2\cdot x^2 + 2(P_{23}/q)(t_f^3/2)\cdot xy]$$

where $x = 1-\gamma_V$ and $y = 1-\gamma_A$

$$K(\omega_V) = r/q$$

At the steady state design condition, the cross correlations, Z/q, are precisely the negative of the variance ratios, i.e.,

$$Z/q = -P/q$$

Given the target characteristics, specified in rough terms by S and ω_V, and the maximum allowable risk, the designer must choose γ_V and γ_A to maximize r. Maximizing r, in turn, maximizes q since q/r is a constant. Thus, the estimator-predictor combination is least constraining in respect to the sight technology and target agility.

The final form of the performance criterion is a rational function in x and y. Further direct analysis of the extrema of this

function is possible, but some preliminary insights may be possible by taking cross-sections of the contours with respect to coordinate planes. This corresponds to examining single variable perturbations about the standard first and second order predictors.

SOME SPECIAL PREDICTOR DESIGNS

Two interesting special cases offer some insight into the dual optimization of the predictor design. In each, one of the design parameters will be set to its natural value (i.e., $\iota = 1$).

$$r/E(\epsilon_R^2)\Big|_{y=0} = \frac{K(\omega_v)[1-S_{22}(t_f)^2 x^2]}{T(P/q)T' - (P_{22/q})(t_f)^2 x^2}$$

$$r/E(\epsilon_R^2)\Big|_{x=0} = \frac{K(\omega_v)[1-S_{33}(t_f^2/2)^2 y^2]}{T(P/q)T' - (P_{33/q})(t_f^2/2)^2 y^2}$$

Both of those functions are of the same general form, and both are symmetrical about the origin of the free variable (i.e., symmetrical about $\gamma=1$). The general form is

$$r/E(\epsilon_R^2) = C(\omega_v) \cdot \frac{[1-a(t_f,S)x^2]}{[1-b(t_f,\omega_v)x^2]}$$

where

$$C(\omega_v) = \frac{r/q}{T(P/q)T'}$$

$$a(t_f,S) = S_{ii} \cdot [t_f^{i-1}/(i-1)!]^2$$

$$b(t_f,\omega_v) = [(P_{ii}/q)/(T(P/q)T')]_f \cdot [t^{i-1}/(i-1)!]^2$$

This function is a ratio of parabolas whose shape is determined by the relative values of $a(t_f,S)$ and $b(t_f,\omega_v)$. Three shapes can occur as shown in Figure 1. The numerical values are taken from the next section. Thus, the offset, x, represents a typical velocity correction and y represents a typical acceleration collection.

ANALYSIS OF A NOMINAL CASE

As an example of the design process developed in the previous section, consider the case of a target described by

$$\omega_v = 0.15 \text{ hz} \quad \text{(velocity bandwidth)}$$

48

$$t_f = 1.5 \text{ sec} \quad \text{(time of flight)}$$

Referring to the estimator design procedure in Reference 1, the variance ratios are

$$
\begin{aligned}
(P/q)_{3,3} &= .106103 \\
"\quad{}_{2,3} &= .056289 \\
"\quad{}_{1,2} &= .015796 \\
"\quad{}_{1,3} &= .014217 \\
"\quad{}_{2,2} &= .044333 \\
"\quad{}_{1,1} &= .008765 \\
(r/q) &= .028993
\end{aligned}
$$

which, in turn, specifies

$$C(\omega_V) = \frac{r/q}{T(P/q)T'} = 0.0563$$

The optimization is done with respect to a maximum allowable risk which will be taken to be

$$E(\varepsilon_R{}^2) = (1.15)^2 m^2$$

The levels of the target state variables will be nominally assessed at

$$\sqrt{E(V^2)} = 2 \text{ m/sec}$$

$$\sqrt{E(A^2)} = 0.4 \text{ m/sec}^2$$

Utilizing the definitions in the previous sections

$$
\left.
\begin{aligned}
S_{22}(t_f{}^2) &= 6.80 \\
S_{33}(t_f{}^2/2)^2 &= .153
\end{aligned}
\right\} \quad a(t_f, S)
$$

$$
\left.
\begin{aligned}
(P_{22}/q)(t_f{}^2)/T(P/q)T' &= .199 \\
(P_{33}/q)(t_f{}^2/2)^2/T(P/q)T' &= .261
\end{aligned}
\right\} \quad b(t_f, \omega_V)
$$

The dimensionless optimal designs are characterized in each case by

$$a(t_f, \omega_V) > b(t, \omega_V) \text{ for } y=0$$

$$a(t_f, \omega_V) < b(t, \omega_V) \text{ for } x=0$$

Thus, the best value of γ_V is 1.0 while the worse value of γ_A is 1.0. One possible predictor is

$$T^* = [1 \quad t_f] \quad \text{(i.e., first order)}$$

That is, let $\gamma_V=1.0$ and $\gamma_A=0$. The performance is character-ized by

$$r/E(\varepsilon_R^2) = .0646$$

versus

$$r/E(\varepsilon_R^2) = C(\omega_V) = .0563$$

for the natural case of

$$T^* = [1 \quad t_f \quad t_f^2/2]$$

It must be noted that this is only one of a myriad of such results. This one is not surprising in light of the low level of accelera-

tion involved (i.e., $\sqrt{E(A^2)} = 0.4$ m/sec^2). Illustrating the rest of the design, note that

$$\sqrt{r} = \sqrt{0.0646} \cdot E(\varepsilon_R^2) = .292 \text{ meters}$$

$$\sqrt{q} = \sqrt{(r/q)^{-1}} \cdot r = 1.71 \text{ m/sec}^3$$

These are the maximum tolerable levels of observation error and target agility for the desired miss variance, $E(\varepsilon_R^2)$. Thus, not only is the optimal predictor algorithm found, but technolog-ical constraints are also available from the design.

UNREALIZABLE DESIGNS

It is evident from the general analysis of the optimal predictor designs, that some of the parameter values lead to negative values of $r/E(\varepsilon_R^2)$. One could argue that these are never cases of in-terest since they do not occur in the neighborhood of the natural parameters when a<b, and when a>b, the natural value is clearly optimal. Nonetheless, an interpretation of the results of when $r/E(\varepsilon_R^2)$ is negative is called for since the parameter values are realizable.

Since the desired risk, $E(\varepsilon_R^2)$, is asserted a priori, the case of negative $r/E(\varepsilon_R^2)$ corresponds to situations where that risk is not achievable by any r,q combination. This may arise because either the magnitudes of the states are too large, the risk is too small, the time of flight is too large, or the variance of the estimation errors is too large. Of all of these conditions, the time of flight is the most pervasive since it effects both the pole and zero placement. Thus, the whole structure of the optimal design as determined by the relative magnitude of $a(t_S,S)$ and $b(t_S,\omega_V)$ may be significantly altered by the time of flight (i.e., the distance to the target).

As an alternate approach to the analysis of propagated errors, the design of a predictor may be predicated upon some particular maneuver type. The maneuver type would then supplant the polynomial form which emerges from the Cartesian estimator. One very natural model for the subsequent motion of the target is the "steady turn" wherein the acceleration vector remains fixed with respect to the target, but it may, of course, rotate in an inertial frame. The predictor model is formulated as

$$
\begin{bmatrix} \dot{x} \\ \dot{y} \\ \dot{V} \\ \dot{A}_T \\ \dot{\theta} \\ \dot{A}_L \end{bmatrix} = \begin{bmatrix} 0 & 0 & \cos\theta & 0 & 0 & 0 \\ 0 & 0 & \sin\theta & 0 & 0 & 0 \\ 0 & 0 & 0 & 1 & 0 & 0 \\ 0 & 0 & 0 & 0 & 0 & 0 \\ 0 & 0 & 0 & 0 & 0 & \frac{1}{V} \\ 0 & 0 & 0 & 0 & 0 & 0 \end{bmatrix} \begin{bmatrix} x \\ y \\ V \\ A_T \\ \theta \\ A_L \end{bmatrix}
$$

where x and y are the target coordinates in an inertial frame, V is the total speed of the target, A_T and A_L are the longitudinal and lateral acceleration respectively, and θ is the orientation of the target motion (i.e., $V_x = V\cos\theta$).

Given fixed A_T and A_L, the V and θ components may be integrated over the time of flight.

$$V(t+t_f) = V(t) + A_T t_f$$

$$\theta(t+t_f) = \theta(t) + \frac{A_L}{A_T} \log (V(t+t_f)/V(t))$$

The positional integrals are approximated by "stepping" θ and V.

$$x(t+t_f) = x(t) + \sum_{i=0}^{N-1} (\cos\theta_i V_i)\Delta t + \frac{1}{2}\Delta t^2 \sum_{i=0}^{N-1} [\cos\theta_i(2i+1)]A_T$$

$$y(t+t_f) = y(t) + \sum_{i=0}^{N-1} (\cos\theta_i V_i)\Delta t + \frac{1}{2}\Delta t^2 \sum_{i=0}^{N-1} [\sin\theta_i(2i+1)]A_T$$

where $\qquad V_i = V(t) + A_T \Delta t$

$$\theta_i = \theta(t) + \frac{A_L}{A_T} \log (V_i/V(t))$$

$$N = t_f/\Delta t$$

This formula for $x(t+t_f)$ and $y(t+t_f)$ is a closed form predictor as it stands. Given the time, and computer resources, this could be the basis for a "steady turn" predictor.

A more efficient version of the predictor may be discerned by forcing the model to be circular in form (i.e., $A_T = 0$). This is the "coordinated turn." From this aproximation we get

$$V(t+t_f) = V(t) = V$$

$$\theta(t+t_f) = \theta(t) + \frac{A_L}{V} t_f = \theta(t) + \omega t_f$$

$$x(t+t_f) = x(t) + \frac{1}{N} \sum_{i=0}^{N-1} \cos\theta_i V t_f$$

$$y(t+t_f) = y(t) + \frac{1}{N} \sum_{i=0}^{N-1} \sin\theta_i V t_f$$

$$\theta_i = \theta(t)+i\omega\Delta t$$

Not only is this a simpler and more readily implemented predictor, but it is also beginning to show some of the same form as the "optimal" polynomial predictors.

In order to illustrate the similarity between the circular predictor and the polynomial predictors, the trigonometric terms will be expanded about the starting angle, $\theta_0=\theta(t)$.

$$\cos\theta_i = \cos\theta_0\cos(i\omega\Delta t)-\sin\theta_0\sin(i\omega\Delta t)$$

$$\sin\theta_i = \sin\theta_0\cos(i\omega\Delta t)+\cos\theta_0\sin(i\omega\Delta t)$$

then $$\cos(i\omega t) \approx 1-\frac{(i\omega\Delta t)^2}{2} + o[(i\omega\Delta t)^4]$$

$$\sin(i\omega\Delta t) = i\omega\Delta t - \frac{(i\omega\Delta t)^3}{6} + o[(i\omega\Delta t)5]$$

If the first two terms of the expansions are used, the prediction error due to truncation will be bounded by

$$|\epsilon| \le [(\omega t_f)^4/24]V t_f$$

52

Assuming that this bound is acceptable, the predicted position is further approximated by.

$$x(t+t_f) = x(t) + \gamma_v V_x t_f - \gamma_A \sin\theta_o A_L \cdot t_f^2/2$$

$$y(t+t_f) = y(t) + \gamma_v V_y t_f + \gamma_A \cos\theta_o A_L t_f^2/2$$

where

$$\gamma_v = \left[1 - \frac{\omega^2 t_f^2}{12} \frac{(2N-1)(N-1)}{N^2}\right]$$

$$\gamma_A = \frac{N-1}{N}\left[1 - \frac{\omega^2 t_f^2}{12} \frac{N-1}{N}\right]$$

which for large enough N is

$$\gamma_v \approx \left[1 - \frac{\omega^2 t_f^2}{6}\right]$$

$$\gamma_A \approx \left[1 - \frac{\omega^2 t_f^2}{12}\right]$$

Thus, in the final analysis, the coordinated turn provides another rationale for the choice of γ_v and γ_A. Together with the previous sections, it is now possible to compute the propagated errors for the circular predictor and compare them with the "optimal" forms.

OPTIMIZING SEVERAL PREDICTOR PARAMETERS.

The analysis of the previous section raises the immediate question of what performance can be achieved when several parameters are varied simultaneously. To illustrate that some interesting shifts in the points of optimability may occur, consider the situation where the velocities and accelerations are uncorrelated.

$$\frac{S_{23}}{\sqrt{S_{33}} \cdot \sqrt{S_{22}}} = 0$$

This is perhaps an extreme condition, but it is not too far from the condition observed in moving vehicles. Using the typical case discussed in Section 4, the covariance of the estimation errors is

$$\hat{P}_{23}/q = 0.0563$$

53

which substantiates the analysis of a two dimensional, joint optimization. The performance contours, in this case, show a slight degree of assymetry. The performance function is

$$\gamma / E(f_R{}^2) = \left(\frac{r/q}{T(P/q)T'} \right) \frac{1.-6.8x^2-.153y^2}{1-.199x^2-2(0.184)xy-.261y^2}$$

In the vicinity of x=0, y=1 (the best single parameter variants) the multi-parameter optimization involves a balancing of the

$$6.8x^2 \qquad \text{in the numerator}$$
$$\text{and} \qquad 2(0.184)x \qquad \text{in the denominator}$$

The value of x must be on the order of 10^{-3} in order to show an improvement in performance, and even then the improvement is infinitesimal.

Although the example being pursued here is only one of a number of cases of interest, this type of effect of P_{23} has been found to be quite characteristic. The numerator terms usually dominate the performance contour in the vicinity of the optimum. The extreme sensitivity of the performance in this region should be noted. The effect is even more accentuated at higher velocities and accelerations, and at longer times-of-flight. The phenomenon tends to suggest the need for over-design of the sighting mechanism to overcome these sensitivities.

For purposes of illustration, the coordinated turn, if used with the nominal conditions of Section 4, would lead to

$$\omega = \frac{\sqrt{E(A^2)}}{\sqrt{E(V^2)}} = .2 \text{ radian}$$

$$\omega t_f = 0.3 \text{ radian}$$

When used as a rationale for the selection of offset parameters, the γ_V and γ_A become

$$\gamma_V = 0.985$$

$$\gamma_A = 0.9925$$

which leads to performances that are barely distinguishable from the nominal second order case

$$r/E(\epsilon_R{}^2) = 0.0563$$

54

USING THE COORDINATED TURN MODEL TO REDUCE DESIGN SENSITIVITIES.

Given the results of the analysis for the nominal case in the previous section, the question of a strategy for reducing sensitivities arises. In order to illustrate an alternate approach to design, consider the nominal case

$$\omega_V = 0.05\text{hz (a lower frequency target)}$$

$$t_f = 3 \text{ sec}$$

and suppose that the velocity and acceleration are orthogonal (i.e., circular motion) with magnitudes

$$V = 120 \text{ m/sec}$$

$$A = 40 \text{ m/sec}^2$$

the required accuracy will be taken to be

$$E(\epsilon_p^2) = 25 \text{ m}^2.$$

Suppose prediction is to be done along the velocity vector. The first order predictor performance would be characterized by

$$r/E(\epsilon_R^2) = (.401) \frac{1-5184x^2}{1-.246x^2}$$

The undesirable sensitivity is evident in this case, and, thus, x must be kept very precisely at zero. The required sighting accuracy would be

$$r = 3.7 \text{ meters.}$$

If, however, the circular motion is taken to be the <u>nominal behavior</u>, then

$$\phi = \begin{bmatrix} 1 & (1-\dfrac{\omega^2 t_f^2}{6})t_f \\ 0 & 1 \end{bmatrix}$$

where $\quad \omega = A/V$

The predictor would be designed by selecting deviations from the nominal case, i.e.,

$$T^* = [1 \quad (1-\frac{\omega^2 t_F^2}{6}) \ t_f \gamma_V]$$

55

Where γ_v is the offset parameter with respect to the coordinated turn

In this case, the performance is characterized by

$$r/E(\epsilon_R^2) = (0.447) \cdot \frac{1-3600x^2}{1-.156x^2}$$

Not only is the sensitivity reduced, but the nominal performance is improved since

$$T(\hat{P}/q)T' = \hat{P}_{11}/q + 2(\hat{P}_{12}/q)(1-\frac{\omega^2t^2}{6})t_f$$

$$+ (\hat{P}_{22}/q)(1-\frac{\omega^2t^2}{6})^2t_f^2$$

The sighting accuracy can now be relaxed to

$$r = \sqrt{0.438} \cdot \sqrt{E(\epsilon_R^2)} = 3.31 \text{ meters}$$

The corresponding result for prediction along the acceleration vector are

$$r/E(\epsilon_R^2) = (0.401) \cdot \frac{1-1296x^2}{1-.145x^2}$$

for the nominally parabolic model, and

$$r/E(\epsilon_R^2) = (0.414) \frac{1-1089x^2}{1-0.125x^2}$$

for the coordinated turn model.

In the context of this work, the gross difference between the coordinated turn and the parabolic motion would be considered to be target induced error, ϵ_{TI}. It should be noted in passing, however, that such errors may be significant, i.e.

ϵ_{TI} = 60 meters along the velocity vector;

ϵ_{TI} = 15 meters along the acceleration vector, due to the inappropriate choice of predictor model for the current nominal case.

CONCLUSIONS AND RECOMMENDATIONS.

The results of the previous sections should be viewed as indicative of the potential screening power of a design methodology based upon propagated errors. Critical choices in predictor parameters are possible and performance characteristics are discernible.

Given the pervasive influence of the time of flight, t_f, on the results obtained herein, one must conjecture at this point about the real time features of the methodology. One could feed forward smoothed estimates V and A and compute the optimal γ_V and γ_A during an engagement. The potential gain from such a scheme is so great that it deserves some testing using a fire control simulator.

It is apparent that the major predictor design issues may vary greatly with the intensity of the target motion. For larger leads, the importance of the correct modeled nominal motion cannot be overemphasized. From one model to the next there may be significant differences in sensitivity and propagated error as well. In any case, for large leads, there is seldom an opportunity to use other than the natural values of γ_V and γ_A.

On the other hand, for less intense motion, situations may arise where propagated error completely dominates a correction. Whole terms may drop out of the predictor as a result. Here, however, the differences between nominal models is not so significant.

REFERENCES

1. Leathrum, J. F., "A Design Methodology for Estimates and Pre-dictors in Fire Control Systems," AMSAA Technical Report No. 315, Dec 1980
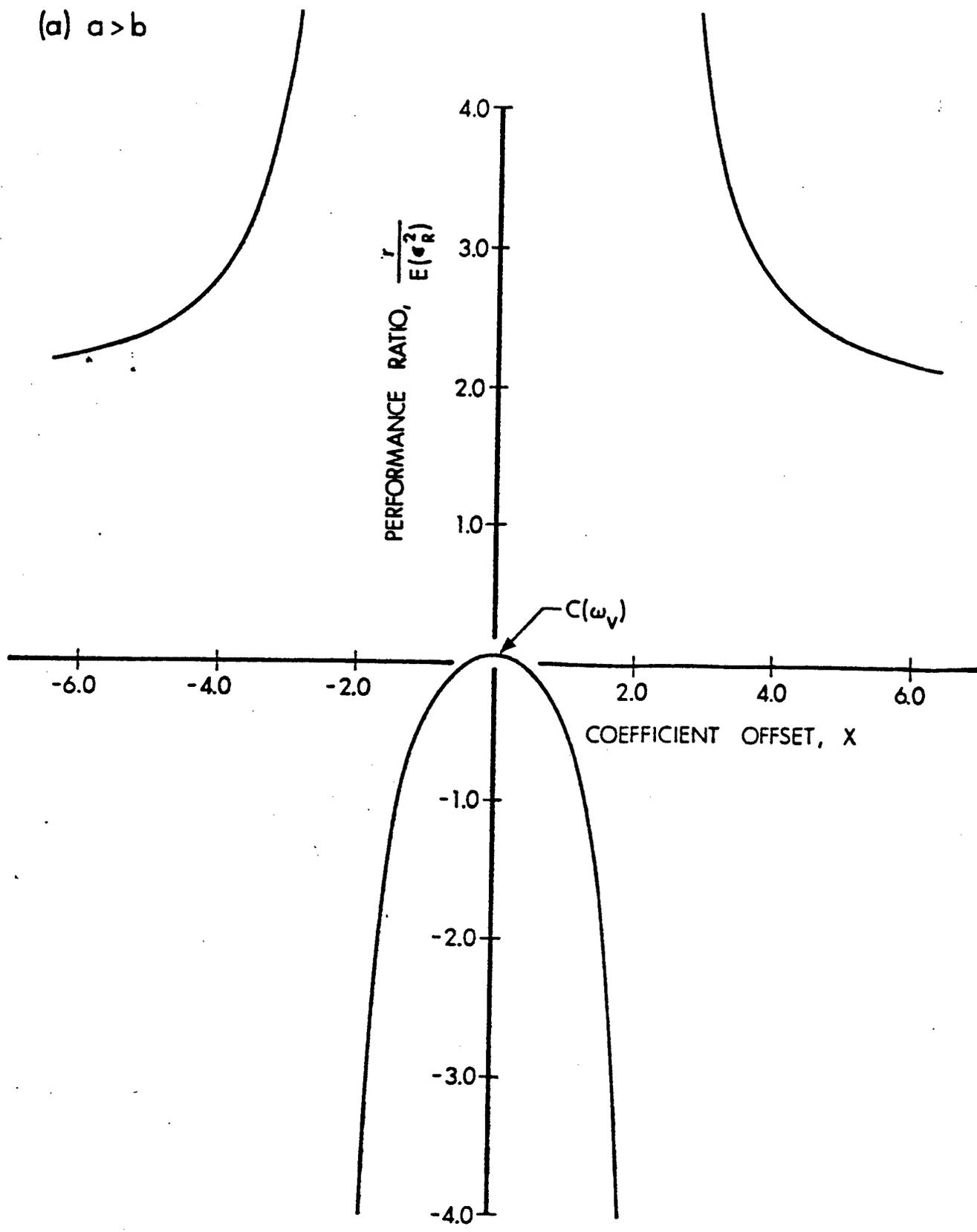
(a) a > b

PERFORMANCE RATIO, $\frac{r}{E(\varepsilon_R^2)}$

COEFFICIENT OFFSET, X

$C(\omega_V)$

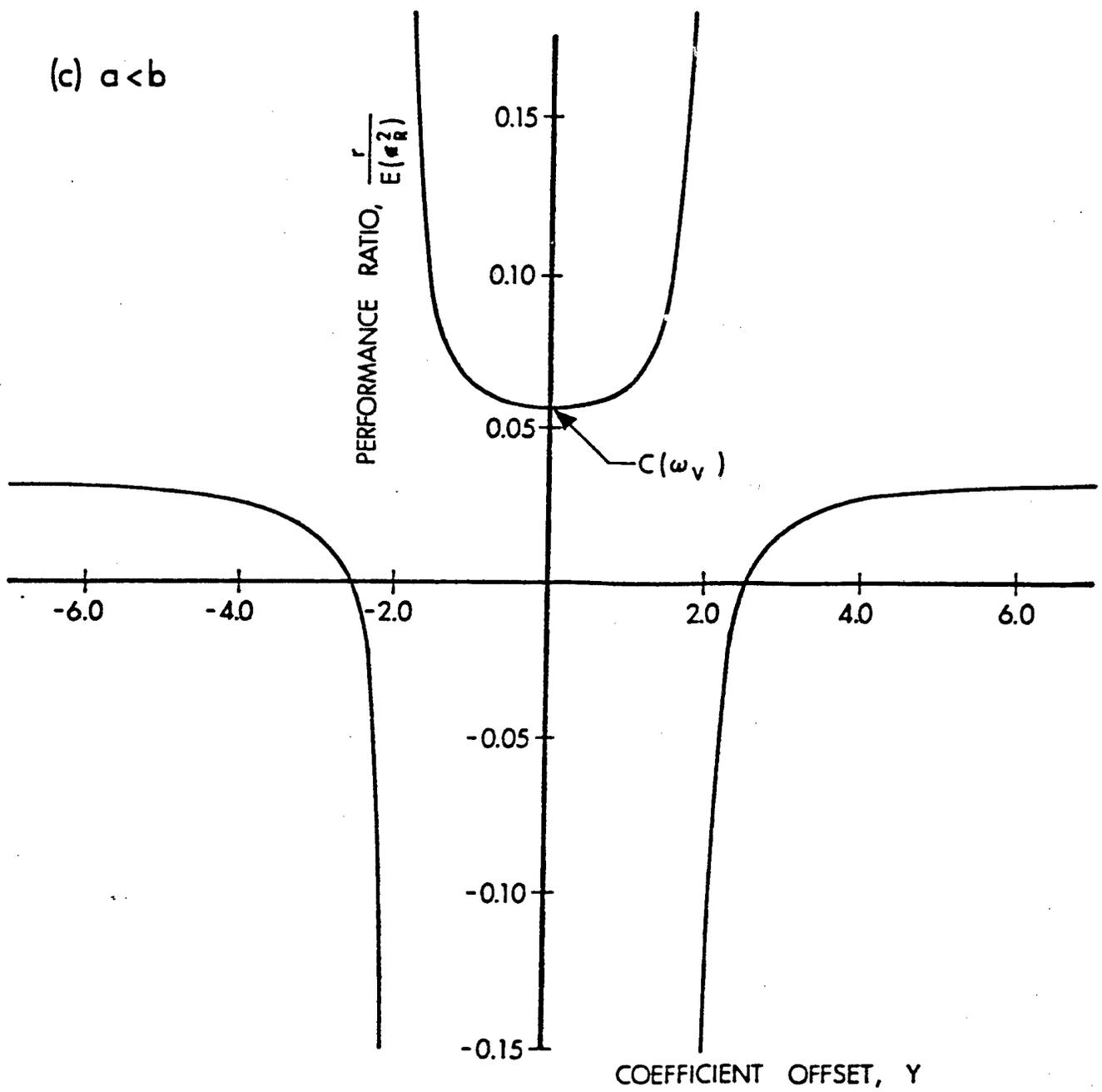Figure 1 (a) Contours of Predictor, Performance Functions.
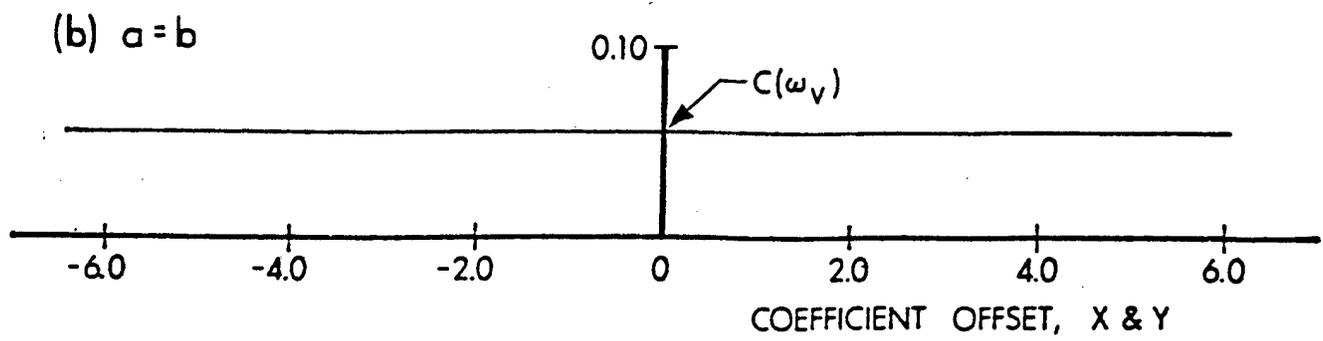
Figure 1(b) & (c) Contours of Predictor, Performance Functions.

MICROPROCESSOR IMPLEMENTATION OF AN ADAPTIVE SECOND ORDER TRACKING/PREDICTION ALGORITHM FOR TANK FIRE CONTROL

P. T. Yip
US ARMY ARMAMENTS RESEARCH & DEVELOPMENT COMMAND
FIRE CONTROL & SMALL CALIBER WEAPONS SYSTEMS LABORATORY
Dover, NJ 07801

ABSTRACT

This study is to investigate the feasibility and performance of an adaptive fire control filter-predictor system in the micro-processor environment. The filter model used is our previous design which includes a Kalman estimator for tank target state estimation and an UD-factorization scheme to propagate the state error covariance matrix. This method provides excellent computation stability and accuracy. In addition, the parallel structure of filters in this model is particularly suitable for microprocessor implementation. Three Intel 86/12A single board computers are used to process the parallel filters simultaneously. The computation accuracy of the target state estimates and the processing time are examined.

INTRODUCTION

This study is to investigate the feasibility of implementing and the performance of an advanced adaptive fire control filter-predictor system in real time and in the microprocessor environment. The filter model used is our previous design, which includes a Kalman estimator for tank target state estimation and an UD-factorization scheme, to propagate the state error covariance matrix. This method provides excellent computation stability and accuracy. In addition, the parallel structure of filters in this model is inherently suitable for microprocessor implementation.

We start our exercise with the UD-factorization of the state error covariance matrix. The system configuration is considered next. Then the interface of microprocessors is described. The requirements of implementation are stated. Lastly, the results and conclusions are addressed.

UD-FACTORIZATION OF THE STATE ERROR COVARIANCE MATRIX

In the conventional Kalman filter algorithm, the error information propagates through updating the state error covariance matrix. They are

$$\overline{P}_{k/k-1} = \Phi_{k,k-1}\,\widehat{P}_{k-1}\,\Phi_{k,k-1}^T + GQ_{k-1}G^T \qquad (1)$$

$$K_k = \overline{P}_{k/k-1}\,H_k(H_k^T\overline{P}_{k/k-1}\,H_k + r)^{-1} \qquad (2)$$

$$\widehat{P}_k = \overline{P}_{k/k-1} - K_k H_k^T\,\overline{P}_{k/k-1} \qquad (3)$$

where $\widehat{P}$ is the a posteriori state error covariance matrix, $\overline{P}$, the a priori state error covariance matrix, Φ, the state transition matrix, H, the measurement matrix, G, the distribution matrix, K, the Kalman gain matrix, Q, the plant noise covariance matrix, and r, the measurement noise variance.

The P matrix is required to be positive semi-definite in order that the system is stable. As we may see in Equation (3) that the difference of two semi-definite matrices can produce a negative definite P especially when the accumulated round-off error becomes significant. Hence, the UD-factorization method is adopted for its inherent stability and enhanced accuracy.

The recursive formula of the UD-algorithm for updating the state error covariance matrix in each measurement cycle are

$$\widetilde{W}\widetilde{D}\widetilde{W}^T = \Phi\widehat{U}\widehat{D}\widehat{U}^T\Phi^T + GQG^T \qquad (4)$$

$$\overline{U}\overline{D}\overline{U}^T = \widetilde{W}\widetilde{D}\widetilde{W}^T \qquad (5)$$

$$\alpha = H^T\overline{U}\overline{D}\overline{U}^TH + r \qquad (6)$$

$$K = \overline{U}\overline{D}\overline{U}^TH/\alpha \qquad (7)$$

$$\widehat{U}\widehat{D}\widehat{U}^T = \overline{U}\left[\overline{D} - \frac{1}{\alpha}(\overline{D}\,\overline{U}^TH)(\overline{D}\,\overline{U}^TH)^T\right]\overline{U}^T \qquad (8)$$

where $\quad \widetilde{D} = \begin{bmatrix} \widehat{D} & \vline & \emptyset \\ \hline \emptyset & \vline & Q \end{bmatrix}$ is N by N and

$N = n + N_w$, $W = [\Phi U \vdots G]$ n by N,

$$G = \begin{bmatrix} \emptyset \\ 1 \cdot \emptyset \\ \emptyset \cdot 1 \end{bmatrix} \text{ n by N } ,$$

$$U = \begin{bmatrix} 1 & U_{1,2} & \text{-------} & U_{1,n} \\ & & & \text{-} \\ & & & U_{n-1,n} \\ \emptyset & & & 1 \end{bmatrix} \quad n \text{ by } n,$$

$H^T = (h_1 \text{---} h_n)$

D, n by n diagonal matrix and

$\emptyset$, zero elements.

with $\underset{\sim}{b} = \bar{U}^T H$, $\underset{\sim}{v} = \bar{D} \bar{U}^T H$ and initial conditions

$\hat{d}_1 = \bar{d}_1 \, r/\alpha_1$, $\alpha_1 = r + v_1 b_1$, and

$k_2^T = (v_1 0 \text{---} 0)$

where U_{ij} and K_{ij} are the ith element of the column vector U_j and K_j respectively.

Then, the elements of d, U, and K are computed recursively as the following:

For j=2, ---,n (Equations 9 through 13)

$$\alpha_j = \alpha_{j-1} + v_j b_j \tag{9}$$

$$\hat{d}_j = \bar{d}_j \, \alpha_{j-1}/\alpha_j \tag{10}$$

$$\lambda_j = -b_j/\alpha_{j-1} \tag{11}$$

For i=1, ---,n (Equations 12 through 13)

$$\hat{U}_{ij} = \bar{U}_{ij} + \lambda_j K_{ij} \tag{12}$$

$$K_{i,j+1} = K_{ij} + v_j \, \bar{U}_{ij} \tag{13}$$

The Kalman gain K of this measurement cycle is given by

$$K = K_{n+1}/\alpha_n$$

Since r is always positive, the positive definite condition of D is assured by Equation (10). As cancellation type errors that may happen in Equation (3) are avoided in Equation (10), the accuracy of computation is enhanced.

SYSTEM CONFIGURATION

In our previous estimator-predictor design, three types of target
models have been incorporated. Type 1 is a constant velocity model.
Type 2 is a first order Markov acceleration model and type 3 is
a second order acceleration model with one zero and two poles.
The parameters of these models have been identified with real
test data to account for various target maneuvering levels. Noised
corrupted data of range and azimuth angle of target are measurement
inputs to the three parallel extended Kalman filters modified with
the UD-factorization scheme. The adaptive prediction comes in
when one of the filters with the largest likelihood function is
selected to provide estimates for gun lead prediction.

Three microprocessors are used and each processes one filter. The
one with the constant velocity model is the master board which also
processes the filter selection and gun lead predictions by virtue
of its smaller load of computational burden. The communication
control and data transfer between the master board and the other
two microprocessor boards will be described in the next section.

MICROPROCESSORS AND THEIR INTERFACE

Three Intel 86/12A single board computers (SBC) are used to process
the parallel filters simultaneously. Each has 32K bytes of random
access memory (RAM) and 8K bytes of electronic programmable read
only memory (EPROM) which can be extended to 32K bytes. If more
memory is needed, extra RAM and EPROM boards can be attached. The
memory in own board is accessed by the central processing unit
(CPU) of the board through the local bus. Additional memory up
to one megabyte can be planned and accessed through the system bus.

The communication between the keyboard or the microprocessor develop-
ment system and the master board is established through a serial
interface cable. Two out of the three programmable peripheral
interface input/output ports are used to take care of the communi-
cation traffic control between the master board and the other two
boards.

The data transfer uses the multibus interface which requires only
one bus clock of 9.22 MHz for synchronized communication among the
SBC. The local CPU must reside in that part of its own memory which
has not been assigned as dual port RAM inside the megabyte addres-
sing plan when another CPU actually accesses the dual port RAM
area.

The 86/12A single board computer which has twelve 16-bit registers
performs floating point computations with the help of a floating
point mathematics library simulating 32-bit operation. The test
chip of 8087 coprocessor was made available for development on
August 1981. This coprocessor which can be attached to the 86/12A
computer board easily has eight 80-bit registers capable of per-

forming 32- and 64-bit floating point multiplication with very
high speed such as tens of microseconds.

IMPLEMENTATION

After the proper interfacing of the microprocessors, some real
target paths of various noise statistics are selected. The function
of the entire set-up, the prediction estimates and the processing
time of the second order algorithm in this system are investigated.

a. A rather linear portion of a target path is used to verify the
proper functioning of the entire microprocessor set-up. A similar
program is run on an IBM 360 computer to obtain results for com-
parison.

b. A segment of real target path data with an average maneuvering
noise level 1.176 meters per second and an average speed 13 miles
per hour is corrupted with random Gaussian noise of 3 meters in
range measurement and 0.3 milliradians in angle measurement. These
corrupted data is sampled at 10 s/s as input to the system and the
prediction estimates are compared with the results from previous
study using a conventional extended Kalman filter without modifi-
cation.

c. With the same data the system performance is evaluated for pro-
cessing the data at 5 s/s instead of 10 s/s.

d. The processing times for the floating point multiplication,
division and square root operation with the 86/12A CPU are compared
to that with the 8087 numerical coprocessor.

e. The actual processing time of the second order algorithm with
a 8087 coprocessor test unit is examined. The number of measure-
ments processed in 10 seconds is noted.

RESULTS AND CONCLUSIONS

Under the implementation conditions in the previous section, results
are summarized as follows:

a. Results from IBM 360 and Intel 86/12A SBC show a 1.2 percent
or less difference in lead angle estimates and much less in impact
range estimates. The proper functioning of the multi-microprocessor
set-up is verified.

b. From previous study for the given target path in implementation
b and averaging over seventeen points, the estimated prediction
errors in milliradians are 1.29, 1.72 and 0.91 for constant velocity,
first order acceleration and second order acceleration filter types
respectively. From the multi-microprocessors under the same con-
ditions, the estimated prediction errors in milliradians are 1.2,
1.49 and 0.88 for constant velocity, first order acceleration and

second order acceleration filter types respectively.

The accuracy of the estimates from this algorithm are highly competitive or better than that from the conventional extended Kalman filter algorithm.

c. With a sampling rate of 5 s/s the estimated prediction errors in milliradians are 1.16, 1.54 and 0.9 for constant velocity, first order acceleration and second order acceleration filter types, respectively. The change in performance is about 3 percent.

d. Averaging over ten thousand iterations, the floating point operation of the command group LOAD, MUL, STORE and WAIT takes 4 milliseconds with the 86/12A CPU while the same takes 63.6 microseconds with the 8087 coprocessor. It is a 63 times faster in multiplication with the latter.

For the command group LOAD, DIV, STORE and WAIT, the floating point operation takes 5.5 milliseconds with the 86/12A CPU and 85.6 microseconds with the 8087 coprocessor. It is 64 times faster in division with the latter.

For the command group LOAD, SQRT, STORE and WAIT, the 86/12A CPU takes 40 milliseconds to process a square root procedure while the 8087 coprocessor with its micro program for SQRT takes 77.6 microseconds. It is 515 times faster with the latter.

e. With a test unit of 8087 coprocessor planted in the 86/12A board, the second order algorithm is processed for 10 seconds. Only 88 sets of measurements are processed. This indicates that a 12 percent improvement in speed is needed to do 10 samples per second real time processing. Fine tuning the program code or changing the programming language to assembler type may help eliminate this time lag.

In all, the impressive numerical characteristics of the UD-factorization deserves our attention. It has been encouraging to know that microprocessor technology has caught up in speed and flexibility to process advanced parallel algorithms with heavy load of computation. We see that great many applications of microprocessor to multiple input, multiple output and parallel processing are forthcoming.

REFERENCES

1. P. T. Yip, N. P. Coleman, "An Adaptive Lead Prediction
    Algorithm for Maneuvering Target Engagement", ARO Report
    81-1, Trans. of the 26th Conference of Army Mathematicians,
    pp 141-152, Jan 81.

2. G. J. Bierman, "Factorization Methods for Discrete Sequential
    Estimation", Academic Press, New York, 1977.

ON THE CREDIBILITY OF MODELS

Naim A. Kheir
School of Science and Engineering
The University of Alabama in Huntsville, Huntsville, AL 35899

Model Credibility is becoming increasingly important in today's world of complex systems. One reason is due to the awareness and discretion being exercised on spending on simulations; a second reason might be the fact that more and more models and simulation results are being used in decision-making. Models, whether representing the broad spectrum of engineering applications (energy, power, aerospace, military systems, etc.) or, say, biological systems such as that of blood circulation would require the same attention in terms of model credibility. More recently, reliance on valid models has become a necessity in areas such as energy forecasting,[7] (energy models and their integrity have been the subject of many congressional hearings since 1975). Thus, the ultimate use of a model is for decision-making and its final evaluation is in terms of the decisions being made.

Three major areas appear to be the focus of progress, or lack of it, in arriving at a higher level of agreement among simulationists on model credibility and what it is all about. These areas are related to:

(i)   Terminology
(ii)   Issues
(iii)   Qualifying Measures

The question of _Terminology_ has been the subject of many previous efforts by the Technical Committee on Model Credibility (TCMC) of the Society of Computer Simulation. Ref. (1) summarizes a complete set of definitions beginning with the understanding and distinction between Reality, Conceptual Model, and Computerized Model, and proceeding to introduce the important concepts of Model Verification and Model Validation. The document also introduced statements on model qualification, domain of applicability, certification and documentation. The definitions adopted by the TCMC on verification and validation are; "Model Verification: The substantiation that a Computerized Model represents a Conceptual Model within specified limits of accuracy. Model Validation: The substantiation that a Computerized Model within its domain of applicability possesses a satisfactory range of accuracy consistent with the intended application of the model." However, all too frequently in process modeling the concepts of verification and validation are reduced, respectively, to simply the tasks of debugging and input-output comparison of model and system data. One should note that this terminology was arrived at with the intent that it could be employed in all types of simulation applications. Thus, adherence to the terminology is highly recommended to facilitate communication between simulation developers, users and decision-makers.

For example, it is simple to recognize the difficulty in communication between a mathematically-oriented modeler and a linguistically-oriented public policy-maker.

A work of caution is in order, even if one adheres to the above terminology and arrives at a validated model, one may be tempted to make an obvious and simple change in the model. Since it is easy to err, revalidation of the model, for the same reasons that validation was required in the first place, is necessary whenever any modification, even an apparently minor one, is made. Thus, once having demonstrated the model validity, it should be considered INVIOLABLE.**

In order to be able to judge the adequacy of a model for its intended purposes, the TCMC is engaged in a discussion of an understanding of important Issues including these:

(a) The real purpose of a credibility measure – is it to make a decision to use a "more-credible model" at perhaps greater cost versus a "less-credible model" at a lower cost? Is it to establish a confidence or reliability factor for the model, i.e., X% reliable for Y% confidence?

(b) In modeling reality in terms of ultimate simplicity (a more detailed model is not necessarily a better model), an issue is that of "simple" versus "complex" models and cost considerations. Simple models have the added merit of closing communication gaps between "non-technical" decision-makers and modelers.

(c) Should a credibility measure be "absolute" defining the agreement of dynamic computer simulation model (Computerized Model) with actual system (Reality), or "relative" (model versus model)?

(d) How to keep simulations under configuration control so that credible ones remain credible.

(e) The absence of an effective grasp of how to achieve parsimony in modeling makes it virtually impossible to develop an efficient, understandable, credible model of a large-scale system.

Next we focus on the real question of which Qualifying Measure(s) one may adapt to express the credibility of a model. Basically, the objective from using a measure is to quantify how well a model matches the performance of reality being modeled. Comparison of time trajectories from the model and the instrumented system is often used (data collected from an actual system may be rare and/ or expensive to get while simulation results may be abundant). A summary of measures used in previous studies follows:

(a) Theil Inequality Coefficient (TIC) was recommended in regards with missile systems validation [2],

** Personal discussion with Dr. Lester H. Fink, of Systems Engineering for Power, Oakton, Virginia.

(b) A modified TIC was applied to validation study with sparse random data [6],

(c) In addition to TIC, correlation coefficient and a similarity coefficient were recommended in Ref. (3),

(d) In a recent study[5], cross-correlation coefficient and Bayesian updating were suggested in a credibility investigation of an RF environmental model,

(e) Use of FFT (Fast Fourrier Transform) to obtain frequency domain error measure of a trajectory was introduced in a boiler-turbine-generator system study[4],

(f) Also in Ref. (4), digital filtering technique was employed to extract frequency bands of an error signal; the band-limited measures of signals could be further analyzed.

(g) Error trajectory could be qualified in terms of measures such as the integral of its square and/or the largest absolute value.

REFERENCES

(1) The Technical Committee on Model Crediblity, "Terminology for Model Credibility", _Simulation_, pp. 103-104, March, 1979.

(2) Naim A. Kheir and Willard M. Holmes, "On Validating Simulation Models of Missile Systems", _Simulation_, pp. 117-128, April, 1978.

(3) Gary M. Griner, John M. Mango, and Harold L. Pastrich, "Validation of Simulation Models, Using Statistical Techniques", Proceedings 1978 Summer Computer Simulation Conference pp. 54-59.

(4) M. J. Damborg and L.F. Fuller, "Model Validation Using Time and Frequency Domain Error Measures", September 1976, Energy Research and Development Administration, (publication ERDA 76-152).

(5) A. M. Baird, R. B. Goldman and N. C. Randall, "Verification and Validation of RF Environmental Models-Methodology Overview", Technical Report #RFSS 106-005, Analytics, Willow Grove, Pennsylvania, July, 1980.

(6) J. R. Rowland and W. M. Holmes, "Simulation Validation with Sparse Random Data", _Computers and Electrical Engineering_, Vol. 5, No. 1, pp. 37-49, March 1978.

SESSION II: CONTROL THEORY & APPLICATIONS II/SIMULATION

20 OCT 1981

(AFTERNOON)

THIRD MEETING OF THE COORDINATING

GROUP ON MODERN CONTROL THEORY

HOSTED BY: US ARMY MISSILE COMMAND

Next page is blank.

A LINEAR NONLINEAR CONTROL PROBLEM

Leon Kotin

Center for Tactical Computer Systems

US Army Communications-Electronics Command, Fort Monmouth, NJ 07703

INTRODUCTION

Many, perhaps most, of the ordinary differential equations of applied mathematics are second-order linear equations $d^2x/dt^2 + a(t)dx/dt + b(t)x = 0$ or their nonhomogeneous variants. Their importance is indicated by the famous names given to such equations: Bessel, Legendre, Hill, Hermite, Airy and Laguerre, to name just a few. By an elementary transformation, such equations can be put into the form of the following system

$$x' \equiv dx/dt = p(t)y, \quad y' \equiv dy/dt = q(t)x. \tag{1}$$

We shall consider this system where the control vector (p,q) belongs to the class of piecewise continuous vector functions of t with bounded norm, say

$$p^2 + q^2 \leq 1. \tag{2}$$

We shall determine that control for which a nontrivial integral curve or trajectory initially on the x-axis reaches the y-axis in least possible time. We shall also determine this shortest time and the corresponding geodesic $(x(t), y(t))$.

We remark that by changing the time scale, we can see that no generality was lost by setting the bound of the norm of (p,q) equal to unity.

This paper is a detailed exposition of results which were obtained in collaboration with G. Birkhoff in the broader context of elliptic autonomous families of differential systems; these appear in concise form in [2].

The title of this paper derives from the fact that although (1) is
a system of linear differential equations in x and y and is linear
in the control variables p and q, it is not linear jointly in
(x,y) and (p,q).

THE MINIMUM TIME

From (1) and (2), we see that for any trajectory,

$$p^2 + q^2 = x'^2/y^2 + y'^2/x^2 \leqq 1 \qquad (3)$$

or

$$1/y^2 + (dy/dx)^2/x^2 \leqq (dt/dx)^2. \qquad (4)$$

Consequently, the time t required for a trajectory initially at the
point (x_0, y_0) to go to (x,y) satisfies

$$t \geqq \int_{x_0}^{x} (1/y^2 + (dy/dx)^2/x^2)^{\frac{1}{2}} dx. \qquad (5)$$

To evaluate this integral, we introduce the modified polar
coordinates ϕ and λ defined by

$$e^{2\phi} = x^2 + y^2, \quad \lambda = y/x \qquad (6)$$

whence

$$x = e^{\phi}/(1+\lambda^2)^{\frac{1}{2}}, \quad y = \lambda e^{\phi}/(1+\lambda^2)^{\frac{1}{2}}. \qquad (7)$$

We note that ϕ and λ are related to the standard polar coodinates
r and θ by the equations $\phi = \log r$ and $\lambda = \arctan \theta$.

In order to compute the integral in (5) we first obtain, by the
chain rule,

$$dx = e^{\phi}(1+\lambda^2)^{-3/2} [(1+\lambda^2)d\phi - \lambda d\lambda],$$

$$dy = e^{\phi}(1+\lambda^2)^{-3/2}[\lambda(1+\lambda^2)d\phi + d\lambda]. \qquad (8)$$

Then

$$dy/dx = \frac{\lambda(1+\lambda^2)\phi' + 1}{(1+\lambda^2)\phi' - \lambda}, \qquad \phi' \equiv d\phi/d\lambda. \tag{9}$$

Furthermore, from (6) and (7)

$$d\lambda = (x\ dy - y\ dx)/x^2$$
$$= e^{-\phi}(1+\lambda^2)^{3/2}[(1+\lambda^2)\phi' - \lambda]^{-2}\ dx. \tag{10}$$

After replacing these in (5), the integral in terms of ϕ and λ becomes $\int F(\lambda,\phi')d\lambda$, where

$$F(\lambda,\phi') = \frac{1}{\lambda(\lambda^2+1)}[(\lambda^2+1)^2(\lambda^4+1)\phi'^2 + 2\lambda(\lambda^4-1)\phi' + 2\lambda^2]^{\frac{1}{2}}. \tag{11}$$

The bracketed quadratic expression in ϕ' is a minimum when

$$\phi' = -\lambda(\lambda^2-1)/(\lambda^2+1)(\lambda^4+1). \tag{12}$$

Substituting this into the integrand $F(\lambda,\phi')$ and integrating from $\lambda = 0$ to ∞, we obtain the minimum time T in going from the x-axis to the y-axis. This is found to be, through the use of the beta function,

$$T = \int_0^\infty d\lambda/(\lambda^4 + 1)^{\frac{1}{2}} = \Gamma^2(\tfrac{1}{4})/4\pi^{\frac{1}{2}} = 1.85407\ldots \tag{13}$$

([1], p. 258; [4], pp. 254,524). We shall show later that this value is actually attained. We state this as Theorem 1:

The smallest t-interval between a zero of y and zero of x for a nontrivial solution (x,y) of (1) - (2) is given by T in (13).

THE GEODESICS AND CONTROLS

By definition, the geodesics are the solution of (1) - (2) which yield the minimum time T in (13). This time T is realized by the trajectories of (1)-(2) which satisfy the differential equation (12). Although this equation is separable, solving it in its present form involves some complicated computation. It is easier

to rewrite (12) in terms of x and y alone. Using (6), (9) and (12), after some simple algebra we obtain $dy/dx = -x^3/y^3$ from (12); this integrates to the implicit form of the solution

$$x^4 + y^4 = \text{const.} \tag{14}$$

By linearity, we may take const. = 1, getting

$$x^4 + y^4 = 1. \tag{15}$$

To obtain the explicit form of the solution (15), we first invoke the bang-bang property; i.e., the minimizing solution will correspond to a control (p,q) which is on the boundary of the control region in the (p,q)-plane. Then the inequality (2) becomes the equation

$$p^2 + q^2 = 1. \tag{16}$$

Differentiating (14) with respect to t, we get $x^3x' + y^3y' = 0$ or, using (1), $px^2 + qy^2 = 0$. But from (14) and (16), this yields

$$p^2 = y^4 \tag{17}$$

whence $x' = py = \pm(1-x^4)^{3/4}$.

We shall consider the trajectory (15) which is moving clockwise and which is initially on the line $y = x$ and, with no loss in generality, in the first quadrant, so that $x_o \equiv x(0) = 2^{-\frac{1}{4}}$. Then

$$x' = -(1-x^4)^{3/4} \tag{18}$$

whence

$$-t = \int_{x_0}^{x} (1-x^4)^{-3/4}dx. \tag{19}$$

To evaluate this integral in closed form, we introduce a series of substitutions which telescope to

$$x^4 = \tfrac{1}{2}(1 - (1-w^2)^{\frac{1}{2}}). \tag{20}$$

76

Then (19) becomes

$$-2^{-3/2}t = \int_1^w (w(1-w^2))^{-\frac{1}{2}}dw. \tag{21}$$

In terms of Legendre's canonical form [3, p. 59]

$$F(\phi) \equiv F(\phi, 2^{-\frac{1}{2}}) = \int_0^\phi (1 - \tfrac{1}{2}\sin^2 v)^{-\frac{1}{2}}dv, \tag{22}$$

by [3, pp. 78, 163] (20) becomes

$$-2^{-3/2}t = 2^{\frac{1}{2}}(F(\phi) - F(\pi/2)) = 2^{\frac{1}{2}} \int_{\pi/2}^\phi (1 - \tfrac{1}{2}\sin^2 v)^{-\frac{1}{2}}dv \tag{23}$$

where

$$w = (1 - \cos^2 \phi)/(1 + \cos^2 \phi)$$

$$= (1 - cn^2 F(\phi))/(1 + cn^2 F(\phi)) \tag{24}$$

[3, pp. 59, 163] in terms of the Jacobian elliptic function $cn\ F \equiv cn\ (F, 2^{-\frac{1}{2}})$. From (23), $F(\phi) = -2t + F(\pi/2)$. Letting $K \equiv F(\pi/2)$, by the addition formula [4, p. 497] for $cn(u-v)$ in terms of the other Jacobian elliptic functions sn and dn, and by the values $sn\ K = 1$, $cn\ K = 0$ and $dn\ K = 2^{-\frac{1}{2}}$ [4, p. 499], we can show from (24) that

$$w = cn^2(2t). \tag{25}$$

Applying this to (20) gives us

$$x^4 = \tfrac{1}{2}[1 - (1 - cn^4(2t))^{\frac{1}{2}}]. \tag{26}$$

Then y^4 by (14) becomes

$$y^4 = \tfrac{1}{2}[1 + (1 - cn^4(2t))^{\frac{1}{2}}]. \tag{27}$$

The trajectory given by these two equations is initially on the line $y = x$ in the positive quadrant and reaches the y-axis when t

is the smallest positive zero of $cn(2t, 2^{-\frac{1}{2}})$; this is $\frac{1}{2}T = \Gamma^2(\frac{1}{4})/8\pi^{\frac{1}{2}}$ [4, p. 524] (cf. eq. (13) above). To determine the entire trajectory in the first quadrant, we simply reflect this trajectory through the line $y = x$. Therefore, because $cn(2t)$ is an even function, for $-T \leq t \leq 0$, x^4 and y^4 are given by the right-hand side in (27) and (26) respectively.

The corresponding control variables p and q can now be obtained immediately. From (17), $p = \pm y^{\frac{1}{2}}$, but the negative sign is chosen by (18); similarly, $q = x^{\frac{1}{2}}$ when $y \geq x \geq 0$.

This is all summarized in the following result, which incorporates Theorem 1.

Theorem 2. The smallest t-interval between a zero of x and a zero of y for a nontrivial solution of (1)-(2) is $\Gamma^2(\frac{1}{4})/4\pi^{\frac{1}{2}} = 1.85407 \ldots$. The corresponding geodesic, normalized by (15), and control functions are given by

$$x^2 = q = [\tfrac{1}{2}(1 - [1-cn^4(2t)]^{\frac{1}{2}})]^{\frac{1}{2}}$$

$$y^2 = -p = [\tfrac{1}{2}(1 + [1-cn^4(2t)]^{\frac{1}{2}})]^{\frac{1}{2}}$$

when $y \geq x \geq 0$.

REFERENCES

1. M. Abramowitz and I. Stegun, "Handbook of Mathematical Functions," Dover Publications, Inc., New York, 1965.
2. G. Birkhoff and L. Kotin, Autonomous families of differential systems, J. Math. Anal. Appl. 55 (1976), 466-475.
3. W. Gröbner and N. Hofreiter, "Integraltafel," part I, Third edition, Springer-Verlag, Vienna, 1961.
4. E. T. Whittaker and G. N. Watson, "A Course of Modern Analysis," Macmillan, New York, 1948.

APPLICATION OF MODERN ESTIMATION AND CONTROL TECHNIQUES TO THE GLAADS TEST VEHICLE

D.P. Glasson
The Analytic Sciences Corporation
Reading, Massachusetts 01867

B.L. Shulman
U.S. Army ARRADCOM
Dover, New Jersey 07801

ABSTRACT

Application of modern estimation and control techniques to the tracking, stabilization, and pointing functions of a mobile air defense system is addressed in this paper. A multiple-model estimator structure is applied to tracking tactical missile targets. Modeling, design, and performance evaluation of an instrument platform stabilization system to reject terrain-induced errors are outlined. An optimal predictor for ballistic lead angle compensation is formulated; its prediction error characteristics and propagation of these errors through the gun pointing controller are derived. Future areas of development and field test validation for the concepts investigated are described.

INTRODUCTION

BACKGROUND

Performance requirements of modern mobile air defense systems have placed stringent specifications on the tracking, stabilization and pointing performance of these systems. The tracking subsystem must accurately estimate the position and velocity of a highly-maneuvering target without explicit knowledge of the target's maneuvering capabilities or intended trajectory. The stabilization system must reject vibration disturbances to the tracking sensor assembly and gun pointing system due to gun recoil and vehicle travel over a wide range of terrain. The gun pointing system is limited by the extrapolation accuracy of a target trajectory predictor and by the dynamic capabilities of the gun gimbal actuation system. These demanding system requirements call for correspondingly powerful design and analysis tools.

Modern control methodologies offer a systematic framework of synthesis and analysis techniques for air defense fire-control system design. Modern estimation/control techniques were developed specifically for multiple input-output systems which potentially are stochastic, nonlinear, and uncertain (i.e.,

the dynamics of the system and disturbances are not known precisely); all of these considerations are present in an air defense fire-control system.

The goal of the study described here was to assess the potential benefit of using modern control techniques in designing a fire-control system for a representative air defense system. Using mathematical models of the Gun Low Altitude Air Defense System (GLAADS), a number of modern estimation and control concepts were developed and analyzed. The concepts investigated and a summary of results are described in the following section.

SYSTEM OVERVIEW

Figure 1 is a block diagram of the air defense fire-control system concept developed in the present study. For purposes of demonstrating new estimation and control concepts the system is restricted to planar engagements, i.e., only range and elevation pointing and tracking are considered.

The integrated system is comprised of tracking, pointing, and stabilization subsystems. The tracking subsystem generates estimates of the target range ($\hat{R}$), elevation ($\hat{\theta}_t$) and elevation
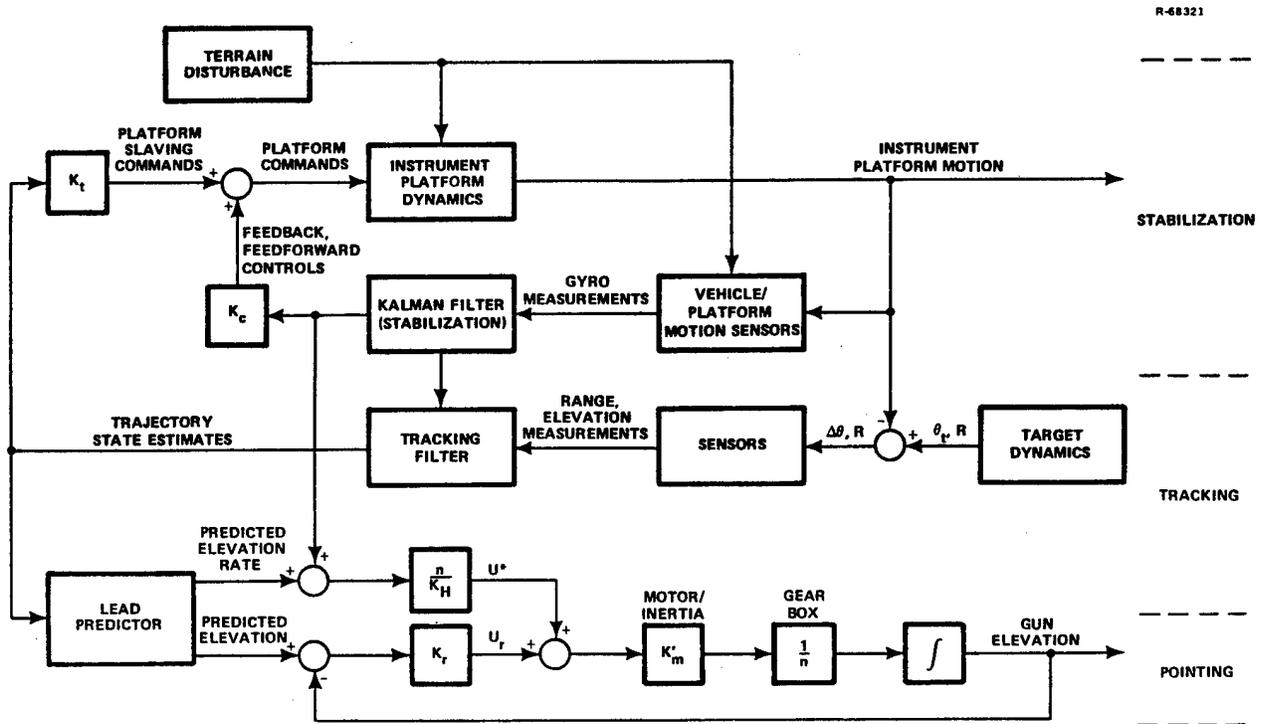

Figure 1   Integrated Fire-Control System

80

rate ($\hat{\dot{\theta}}_t$) from noisy range and elevation measurements. The estimates generated by the tracking subsystem are routed to the pointing system where these quantities are extrapolated through the estimated projectile time-of-flight (T_f) by a prediction algorithm (i.e., the ballistic lead angle is computed). The extrapolated elevation and elevation rate are then used by a feedforward controller to command the gun pointing angle and slew rate; the dynamic response of the gun itself is regulated by a feedback controller. The instrument platform stabilization system serves the dual function of slaving the instrument platform attitude to the current target elevation (via feedforward control) and rejecting terrain induced disturbances (via a feedforward-feedback controller).

Modern control concepts applied to the three subsystems and evaluated in the present study include:

- A tracking filter based on multiple model estimator structure

- Statistical linearization of the nonlinear target tracking dynamics

- An optimal one-step prediction algorithm for extrapolating target motion estimates over the projectile time-of-flight

- Command-generator-tracker (CGT)/optimal regulator control of the gun pointing dynamics

- A robust (i.e., insensitive to variations of terrain type) instrument platform stabilization system designed by optimal estimation/control techniques.

Applications of these concepts to the GLAADS vehicle and performance benefits derived from them are discussed in the following sections.

TRACKING FILTER SUBSYSTEM

Through application of multiple-model structuring and statistical linearization, an accurate and robust tracking filter is designed. This filter produces unbiased estimates of the target motion with range and elevation errors substantially lower than the noise levels of the range and elevation sensors. It is shown that the multiple model filter obviates the need for precise knowledge of the target maneuver model; i.e., the filter performs well given only knowledge of the expected range of target maneuver dynamics. The formulation and performance of the tracking filter is described in the following subsections.

81

TRAJECTORY AND SENSOR MODELS

The variables used to describe the target trajectory and measurements are shown in Fig. 2. The target position is defined by the target altitude (y) and horizontal distance from the gun (x). The instantaneous target velocity vector ($\underline{v}$) is characterized by the target airspeed (V) and flight path angle (γ). The maneuver characteristics of the target are described by the flight path angle rate ($\dot{\delta} = \omega$). Measurements of two polar components of target position, range (r) and elevation (θ), are available to the fire control system.
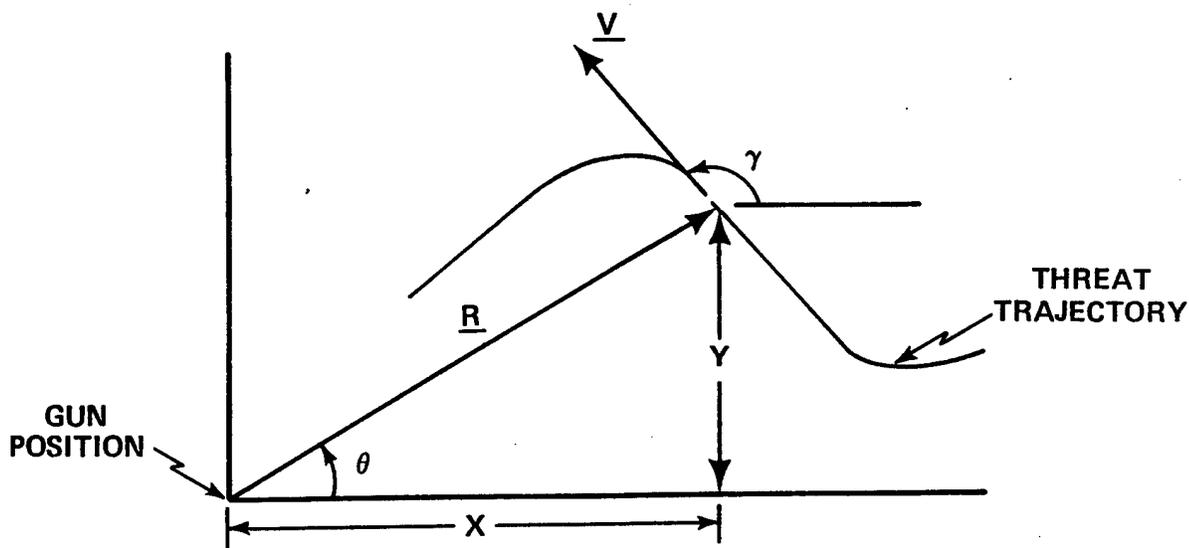
R-64315

Figure 2   Engagement Geometry

The dynamic equations of the target trajectory and the equations relating the target state to the tracking instrument measurements are listed in Table 1. The notation, N(m,v), denotes white noise of mean, m, and variance, v.

The maneuver characteristics of the target vehicle are embodied in the flight-path-angle-rate (ω) equation; as discussed in Ref. 1, the flight path angle rate is directly related to the normal acceleration of the vehicle which is the usual command variable for maneuvering manned aircraft and tactical missiles. The parameters that govern the dynamics of flight path angle rate, τ and q, are never precisely known in any real engagement; hence, the dynamics shown in Table 1 are both stochastic and uncertain.

82

SUMMARY OF TRAJECTORY AND MEASUREMENT EQUATIONS

TRAJECTORY DYNAMICS

$$\dot{x} = V \cos \gamma \qquad = \dot{x}_1$$

$$\dot{y} = V \sin \gamma \qquad = \dot{x}_2$$

$$\dot{V} = -g \sin \gamma - f_D V^2 = \dot{x}_3$$

$$\dot{\gamma} = \omega \qquad = \dot{x}_4$$

$$\dot{\omega} = -\frac{1}{\tau} \omega + w \qquad = \dot{x}_5$$

$$w \sim N(0,q)$$

RANGE MEASUREMENT

$$r_m = x^2 + y^2 + v_r \; ; \; v_r \sim N(0,4 \text{ m}^2)$$

ELEVATION MEASUREMENT

$$\theta_m = \tan^{-1} (y/x) + v_\theta \; ; \; v_\theta \sim N(0,0.25 \text{ mrad}^2)$$

The thrust/drag balance of the vehicle is quantified by the parameter f_D; for example, in an unpowered segment of a tactical missile trajectory f_D relates the drag of the vehicle to the vehicle airspeed. The drag parameter, f_D, is usually unknown in a real engagement, but its <u>range</u> of values can be estimated; hence f_D is an uncertain but bounded parameter.

The range and elevation measurements are related to the trajectory states by nonlinear equations. The rms levels of sensor noise listed were taken from Ref. 2 and represent the performance of state-of-the-art instrumentation.

FILTER FORMULATION

The target trajectory dynamics and measurement models listed in Table 1 are stochastic, nonlinear, and uncertain (i.e., the model parameters are not precisely known). Due to the nonlinear and uncertain properties of the trajectory and measurement models the standard linear optimal estimator (Kalman filter) cannot be directly applied; in the present study, two modifications of the standard Kalman filter structure were employed to accommodate nonlinearity and uncertainty:

- A statistically-linearized formulation of the Kalman filter to accommodate nonlinearities

•   A multiple model estimator structure
to accommodate the uncertainty of the
model parameters.

The structure of a statistically-linearized filter is shown in
Fig. 3. The structure is substantially similar to the linear
Kalman filter; it consists of a state estimator that generates
estimates of the trajectory state, $\hat{\underline{x}}_k$, using a model of the
dynamics ($\dot{\underline{x}}=\underline{f}(\underline{x})$), the measurement model ($\underline{z}=h(\underline{x})$) and the
tracker measurements, $\underline{z}_k$, and a error covariance (P) propagator.

The major differences between the statistically-linearized
filter and an extended Kalman filter are that expected values
of the state derivative ($\hat{\underline{f}}(\underline{x})$) and measurement ($\hat{\underline{h}}(\underline{x})$) are used
rather than direct functions of the estimates (i.e., $\underline{f}(\hat{\underline{x}})$ and
$h(\hat{\underline{x}})$) and statistical describing functions (Ref. 3) for the
linearized dynamics (N) and measurements (M) are used rather
than Taylor series approximations (the mathematical derivations
of the expected values and describing functions are detailed
in Ref. 1). At the expense of some additional calculations,
the statistically-linearized filter will yield unbiased esti-
mates of the nonlinear dynamics and avoid filter divergence
problems typically encountered in applications of extended
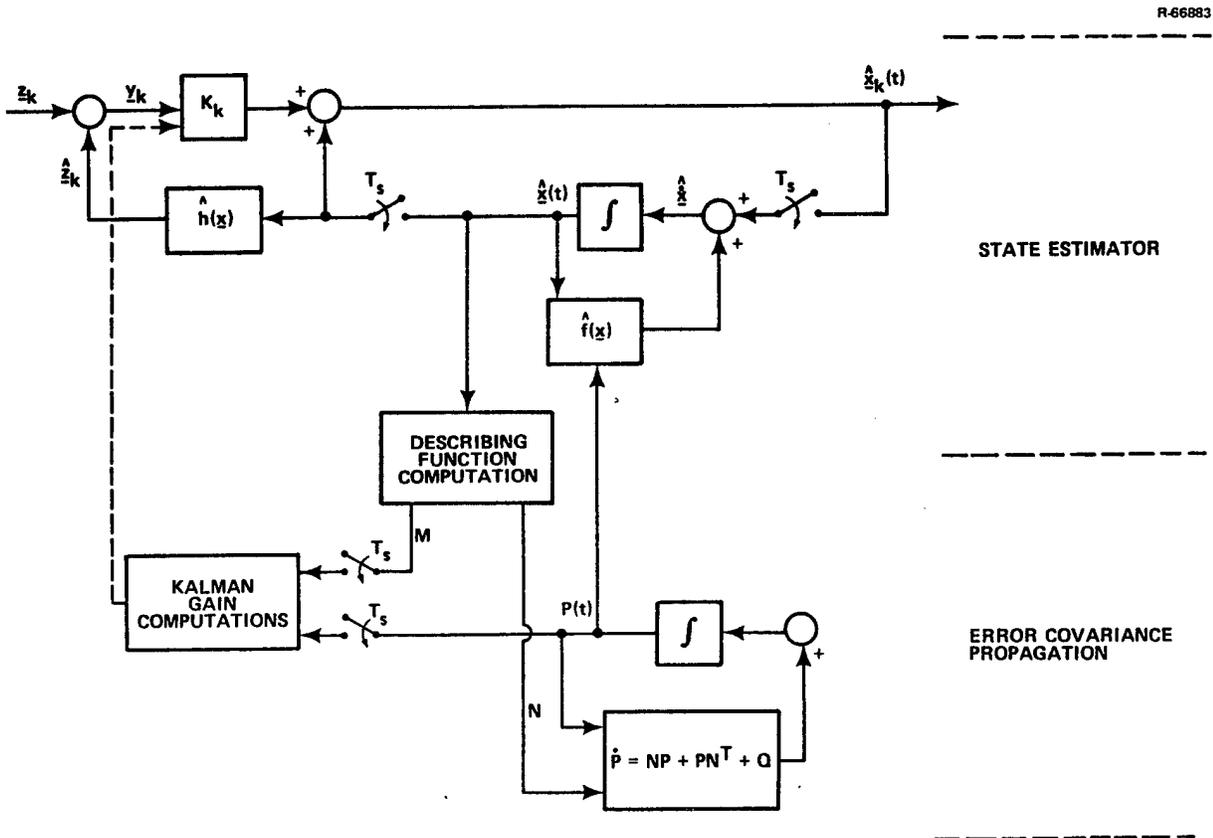Kalman filters.

Figure 3   Statistically-Linearized Kalman Filter

84

Uncertainty of the dynamic model parameters is accommodated
through a multiple-model estimator structure. Figure 4 is a
functional diagram of a two-model estimator structure, as it
would be applied to an air defense tracking system. Here the
range and elevation measurements (z) are processed by two fil-
ters. The choice of the parameters τ_i and Q_i (correlation
time and process noise level of the flight path angle rate
dynamics) are chosen to represent likely target maneuver char-
acteristics in the individual filters. For example, a choice
of large τ_1 and small Q_1 (long correlation time, low normal
acceleration rms) would represent a level-flight trajectory in
filter 1; small τ_2 and moderate Q_2 in filter 2 would represent
a vertical plane "jinking" maneuver. The dynamic models used
in the two filters would "bracket" the expected range of target
maneuvers while the averaging algorithm would combine the esti-
mates of the two filters to tune the estimator structure to
the current target maneuver level. An alternative application
to the dual filter structure for tracking an anti-radar missile
having uncertain but bounded drag is described in the following
section. Mathematical details of the dual-filter structure in
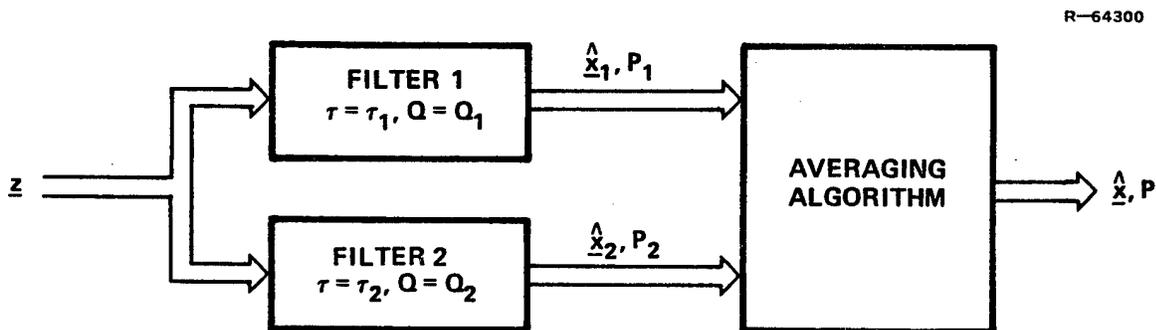air defense system applications are covered in Ref. 1.

Figure 4   Multiple Model Estimator Structure

FILTER PERFORMANCE

The performance of the dual statistically-linearized filter in
tracking the unpowered midcourse trajectory of anti-radar mis-
sile is described here. A segment of the example trajectory
is shown in Fig. 5; the segment shows a planar, unpowered,
non-maneuvering gravity-turn through the atmosphere.

The parameters used in the dual filter structure were chosen
to provide an adaptation of the estimator to the unknown drag
characteristics of the target vehicle. The maneuver parameters,
τ and σ_w, are identical for the two filters with values appro-
priate to a low maneuver level gravity turn. The drag param-
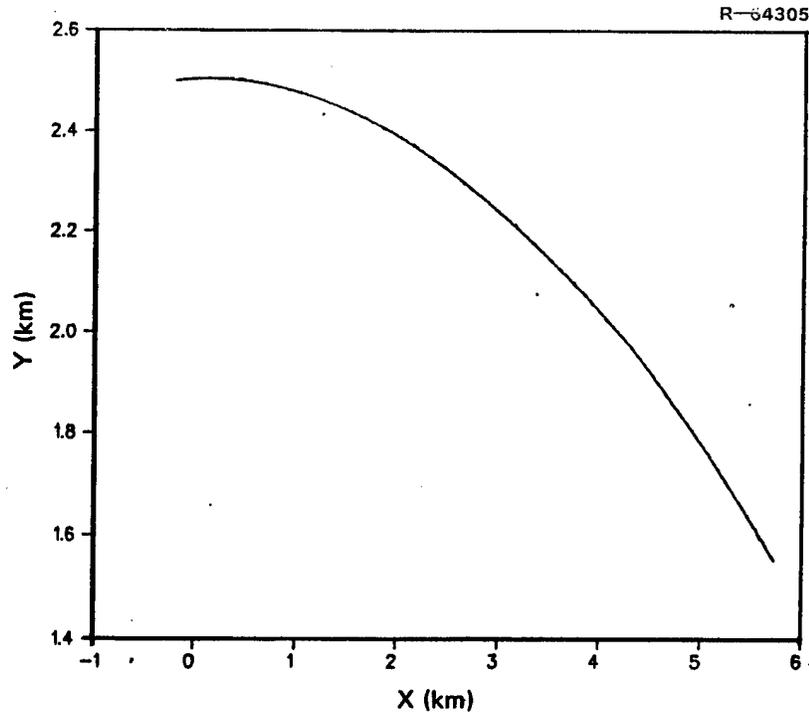eter, f_D, is set to zero in one filter and to a value $2\bar{f}_D$ in
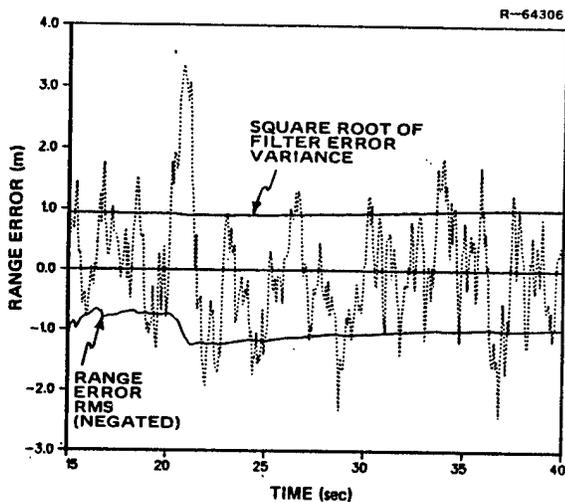
Figure 5   Anti-Radar Missile Midcourse Segment

the other filter, where $\bar{f}_D$ is an estimate of the vehicle drag parameter derived from intelligence data (Ref. 4). The two values of f_D "bracket" the range of variation of f_D; the dual-filter averaging algorithm then combines the estimates of the two filters to "tune" to the current value of f_D.

The performance of the dual-filter in tracking the example trajectory is shown in Fig. 6. Unbiased errors in range and elevation estimates are obtained. Substantial improvement of rms range and elevation error over the measurement accuracies is achieved; range error is reduced to 1 meter rms as opposed to 2 meters rms measurement error and elevation is reduced to 0.25 mrad rms as opposed to 0.5 mrad rms measurement error. There is good agreement between the true estimation error variance and the error variance computed by the dual filter, thereby validating the use of statistical linearization, the choice of parameters in the present application, and the viability of a dual filter structure in adapting to unknown drag characteristics of the target.

STABILIZATION SYSTEM

An instrument platform stabilization system design based on a Kalman filter/optimal feedforward-feedback control structure is described in this section. Using this optimal structure,

86

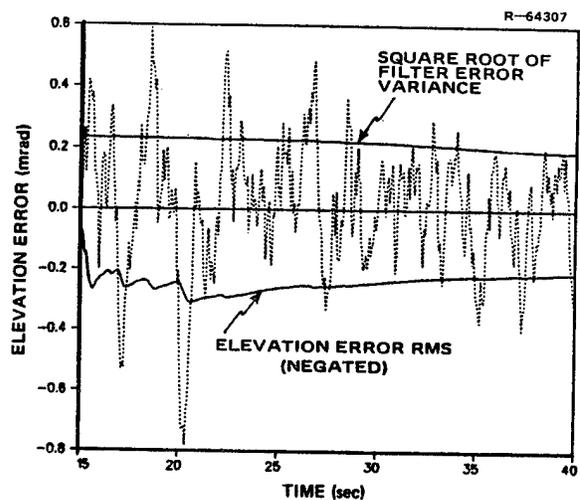RANGE ERROR HISTORY   ELEVATION ERROR HISTORY

Figure 6 . Anti-Radar Missile Tracking Performance

point designs for various levels of terrain-induced vibration
were performed and analyzed. Suboptimal systems were then
designed and their performance compared with that of the opti-
mal designs; by this means, major simplifications of the system
structure were shown to be possible with little degradation of
stabilization performance. The most significant of these sim-
plifications is that the stabilization system can be decentral-
ized from the tracking system.

SYSTEM DESIGN

The structure of the stabilization system is shown in Fig. 7.
Using the platform rate integrating gyro and hull mounted rate
gyro measurements, a full-order Kalman filter (i.e., a filter
designed using the coupled dynamics of the platform, rate in-
tegrating gyro, and terrain-induced disturbance) generates
estimates of the gyro output angle ($\hat{\theta}_g$), the platform eleva-
tion angle and elevation rate ($\hat{\theta}_e$ and $\hat{\dot{\theta}}_e$), and the disturbance
state ($\hat{q}_h$). The estimates are then multiplied by a control
gain matrix, K_c, to compute the platform torquer and gyro com-
mands (u_e and u_g).

The optimal control gain matrix, K_c, is partitioned into gains
that multiply the gyro and platform states and gains that mul-
tiply the disturbance states, i.e.,:

$$K_c = [K_p \vdots K_d]$$

87

Figure 7   Structure of Instrument Platform
            Stabilization System

With this partitioning, the control system can be described in
terms of feedback and feedforward control functions. Desirable
platform dynamic response is achieved by proper values of the K_p
gains; optimum disturbance rejection is accomplished by the K_d
gains.

The terrain disturbance model used in the present study was
derived from data presented in Ref. 5 and is described in
Ref. 1. This model represents travel over road and country
terrain at speeds from 5 to 25 km/hr.

Th noise characteristics of the rate integrating gyro and the
hull rate gyro are given in Table 2. These noise characteris-
tics are typical of tactical aircraft quality instruments.

PERFORMANCE AND SENSITIVITY ANALYSIS

The method used to analyze the stabilization system performance
was steady-state covariance analysis. The covariance matrix
of the stabilization system is derived from the steady-state
covariance equation:

TABLE 2
MEASUREMENT NOISE LEVELS

INSTRUMENT	RMS NOISE	BANDWIDTH
RIG	0.31 μrad	600 Hz
Hull Rate Gyro	2.9 mrad/sec	600 Hz

$$\tilde{F}\tilde{X} + \tilde{X}\tilde{F}^T + Q = 0 \qquad (1)$$

Here $\tilde{X}$ is the covariance matrix of the system which consists of subsets related to the covariances of the platform states, the disturbance states and the state estimator errors. The matrices $\tilde{F}$ and $\tilde{Q}$ are the dynamics and process noise matrices, respectively, for the coupled platform, disturbance, controller and state estimator error dynamics.

The performance metric chosen in the present case is the steady-state variance of the platform elevation angle; performance sensitivity analyses yielded the following significant results:

- Stabilization of the instrument platform to 3.3 μrad rms over the entire range of terrain and vehicle speed using fixed gains (computed for worst case design point)

- Elimination of the feedforward branch of the controller providing a major simplification of control structure with negligible degradation of performance

- Stabilization error rms increases by a factor of 4 with hull rate gyro removed

- Platform residual stabilization error is sufficiently low (i.e., two orders of magnitude lower than the tracking elevation sensor) that the stabilization and tracking functions can be decentralized.

GUN POINTING

The pointing system design is based on a recently-developed type of feedforward controller, the command generator tracker

89

(CGT). This controller causes the plant output (gun pointing angle) to track exactly the output of a specified deterministic linear system; in tracking stochastic processes (such as a maneuvering target) the CGT has shown performance superior to that of optimal feedforward controllers.

SYSTEM DESIGN

The structure of the predictor/gun pointing system developed in this chapter is shown in Fig. 8. The model of the gun elevation dynamics is comprised of a gain, K_m' to represent the hydraulic motor command response and inertia; the dynamics of the hydraulic motor valve are very high frequency and were therefore neglected in the present design. The rotation rate of the hydraulic motor is geared-down by a factor of $1/n$ in the gear box; the gun elevation, θ_{GUN}, is the integral of the gun rotation rate.
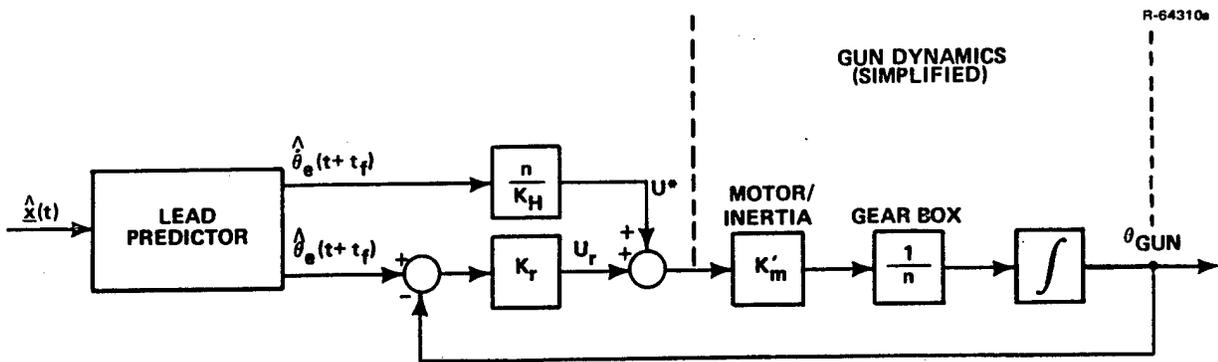

Figure 8   Predictor/Gun Pointing System Structure

Elevation and elevation-rate estimates from the tracking filter are extrapolated forward in time through a computed projectile time-of-flight. The extrapolated elevation rate ($\hat{\dot{\theta}}_e(t+t_f)$) is multiplied by a feedforward control gain (n/K_H) to drive the gun elevation rate to match the target elevation rate. The error between the extrapolated target elevation ($\hat{\theta}_e(t+t_f)$) and the gun elevation is driven to zero by a regulator gain, K_r; the magnitude of this gain determines the control bandwidth of the closed-loop gun dynamics.

PREDICTOR/POINTING SYSTEM ERROR ANALYSIS

The mathematical relationship between gun pointing error and the trajectory state prediction errors is summarized in this section. First, the predictor elevation and elevation rate errors are derived in terms of the errors in the extrapolated

trajectory state. The gun pointing error is then derived from the predictor errors and the dynamics of the gun/controller system. Figure 9 shows the geometrical relationships used to derive the elevation and elevation rate errors.
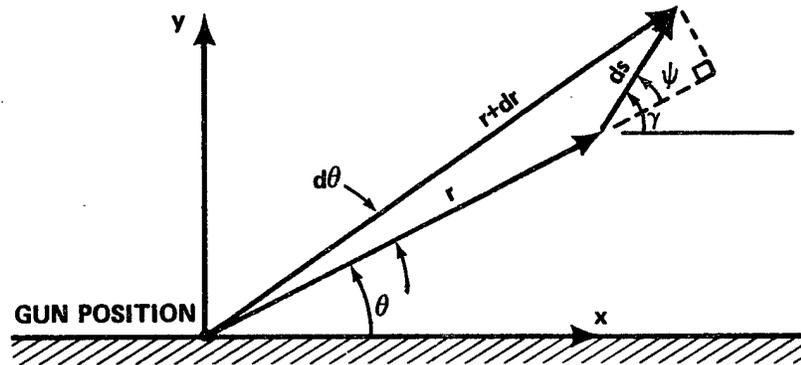

Figure 9   Geometrical Relationships for Prediction
              Error Analysis

After analyzing the differential geometry of Fig. 9 (Ref. 1) one obtains the following expressions for the predictor errors:

$$e_\theta = \frac{1}{\hat{R}^2} \; (-\hat{y} \; e_x + \hat{x} \; e_y) \tag{2}$$

$$e_{\dot{\theta}} = \hat{\dot{\theta}} \; [e_V/\hat{V} - e_R/\hat{R} + \cot(\hat{\theta}-\hat{y})(e_y-e_\theta)] \tag{3}$$

where the notation e_a denotes the prediction error for variable a, and $\hat{B}$ denotes the predicted value of variable B. Equations 2 and 3 relate the elevation and elevation rate errors (e_θ and $e_{\dot{\theta}}$), which corrupt the control commands to the gun, to the predicted trajectory states ($\hat{x}$, $\hat{y}$, $\hat{V}$, $\hat{y}$) and predictor errors (e_x, e_y, e_V, e_y, e_θ, and e_R).

By expressing the true target elevation and elevation rate (which, if commanded to the gun pointing system would yield exact target tracking) in terms of their predicted values and prediction errors; i.e.,

$$\hat{\theta}_T = \theta_T + e_\theta \tag{4}$$

91

$$\dot{\hat{\theta}}_T = \dot{\theta}_T + e_{\dot{\theta}} \qquad (5)$$

the following equation is derived (Ref. 1) for the gun pointing errors:

$$\dot{e}_{gun} = -\frac{1}{\tau} e_{gun} + \frac{1}{\tau} e_\theta + e_{\dot{\theta}} \qquad (6)$$

where e_{gun} is the gun pointing error and $\tau(=n/(K_m K_r))$ is the time-constant of the closed-loop gun regulator dynamics. Equation 6 defines the dynamics of the gun pointing error in response to errors of the extrapolated elevation and elevation rate. As indicated by Eq. 6, the gun pointing errors are frequency limited by the bandwidth $(1/\tau)$ of the gun regulator. The static gain of elevation error to gun error is unity; the static gain of elevation rate error to gun error is τ.

Equations 2, 3 and 6 could be used in a Monte-Carlo simulation to determine the time-history and statistics of the gun pointing error in a particular air-defense scenario. The predictor errors would be computed as the difference between the predicted elevation and elevation rate and the elevation and elevation rate of the truth model trajectory. A linear combination of the computed predictor errors (i.e., $(1/\tau) e_\theta + e_{\dot{\theta}}$) would be the input to a first-order linear filter with time constant, τ; the output of the filter would be the gun pointing error.

CONCLUSIONS

In this paper, modern estimation and control design techniques were applied to the GLAADS air defense system. Specific concepts considered in this study include: application of statistical linearization to the nonlinear trajectory dynamics and tracking sensor measurements, multiple-model estimator structuring of the tracking filter to accommodate modeling uncertainty, stabilization system design by optimal estimation and control techniques, optimal prediction algorithm design, and command-generator-tracker/optimal regulator control of gun pointing. The performance benefits obtained through applications of these concepts were demonstrated through subsystem examples.

Further developments of these concepts should include:

- Extension and evaluation of the design formulations for non-planar engagement scenarios

- Development of practical implementation structures for eventual field testing

- Global performance evaluation of a mobile air defense system (i.e., error budget structure) to identify high-payoff areas for subsystem improvement and development.

REFERENCES

1. Glasson, D.P., and Acharya, N.A., "Gun/Sensor Stabilization and Control Technology," Report No. ARSCD-CR-81028, Fire Control and Small Caliber Weapon Systems Laboratory, U.S. Army ARRADCOM, Dover, New Jersey, July 1981.

2. Huling, S., Mintz, M., Goodman, S., and Dziwak, W., "Robust Autoregressive Models for Predicting Aircraft Motion from Noisy Data," Proceedings of IEEE Conference on Decision and Control, Ft. Lauderdale, FL, 1979.

3. Gelb, A., (Ed.), Applied Optimal Estimation, M.I.T. Press, Cambridge, 1974.

4. Information provided by Foreign Intelligence Office, U.S. Army ARRADCOM, Dover, New Jersey (SECRET).

5. Goldgraben, J.R., and Buchanan, B., "Hull Motion Studies," Vol. 1 and 2, Report No. DAAA25-76-A-0441/0001, Decilog, Inc., Melville, NY, January 1979.

6. Thodos, et. al., "Gun Low Altitude Air Defense System," Technical and Management Summary, Report No. RIA-R-TR-76-006, Aircraft and Air Defense Weapon Systems Directorate, Gen. Thomas J. Rodman Laboratory, Rock Island, IL, June 1976.

ON DESIGNING ROBUST PREDICTORS USING FINITE STATE MARKOV CHAINS

E. B. Pate & M. Mintz
Dept. of Systems Eng.
Univ. of Pennsylvania
Phila., PA   19104

W. Dziwak & S. A. Goodman
US Army Armament Research
    and Development Command
Dover, NJ   07801

ABSTRACT

Traditionally, control systems oriented studies of uncertain dynamic processes with continuous state descriptions have relied primarily on the identification and estimation of models based on ordinary differential equations, partial differential equations, or related difference equations. Recently, the authors have explored the use of finite markov chains to approximate processes with continuous state descriptions. Our applications of these techniques have focused on the determination of robust models of evasive targets in the context of AAA fire control.

We have developed a practical technique for estimating robust finite state markov chain models. This technique is based on game theory and provides a minimax method for determining robust approximations of markov chain state transition matrices, which are used to construct target motion predictors. The importance of this new approach lies in its ability to provide easily implemented predictors which can outperform traditional autoregressive models in a noisy environment.

This paper outlines this new methodology and provides examples of fire control applications based on flight test data.

INTRODUCTION

The present study is an outgrowth of an earlier study (1) which characterized, identified, and validated robust mathematical models for the motion of an attack aircraft during its weapon delivery pass against a defended target.

These new maneuver models provided the basis for enhanced filtering and prediction algorithms for AAA fire control systems. The development of these models and algorithms was based on a synthesis of univariate time series methods and game theoretic analysis. This synthesis lead to (i) the development and validation of a practical design procedure for high performance target state estimators in the presence of moderate to large parameter uncertainty, and (ii) a technique for designing a class of "worst case" maneuver processes to blunt the effectiveness of AAA systems.

A central aspect of the research reported in (1) was the use of authentic flight test data, which consisted of eleven sample flight profiles an aircraft might perform while attacking a defended ground target. The actual data was gathered during flight tests with an A7-E aircraft at the NWTC, China Lake, California. These attack profiles, which also constitute the flight test data base for this present study, are described in detail in Chapter II of reference (1). This kinematic data base describes the aircraft motion in a cartesian coordinate system, where the origin of this coordinate system is the aircraft's intended target, as well as the assumed location of the AAA weapon system. The kinematic data describing the eleven flight profiles in the XYZ coordinate system includes consistent position, velocity, acceleration, and acceleration-dot data in each coordinate with a time increment of 0.1 sec. The primary models developed in (1) characterize the aircraft motion in terms of "decoupled" autoregressive (AR) models for the individual acceleration-dot time series in X, Y, and Z. We summarize the salient results of this earlier study with the following remarks:

(i) Although the eleven flight paths appear significantly different to the "naked eye," the thirty-three acceleration-dot time series in the data base -- eleven flight paths times three directions -- are shown to be accurately modeled by a single robust fifth-order autoregressive model. The eleven flight paths in this data base include three dive toss maneuvers, five dive maneuvers, and three pop-up maneuvers. The acceleration-dot processes were incorporated in the model development since the acceleration, velocity, and position time series are all significantly nonstationary.

(ii) Substantial improvements in overall prediction capability are achievable by using robust, high-order filter-predictor algorithms based on a fifth-order AR model of acceleration-dot instead of the "usual" (benchmark) third-order algorithms based on a first-order AR model of acceleration.

(iii) Typical improvements in average hit probability achieved by the new models developed in (1) versus the

standard benchmark model based on a first-order AR model of acceleration, ranged from 25 to 35 per cent. The specific enhancement in average hit probability associated with these new filter-predictor algorithms depended on the specific flight path, and the noise levels in the unfiltered observations. The unfiltered observations were modeled by target range, azimuth, elevation, and the respective rates.

ALTERNATIVE MODELS

Motivation

The consideration of dynamic stochastic models for target motion based on alternatives to the AR models described in this Introduction and detailed in (1) is motivated by the observation that predictors, designed on the basis of nominal fifth-order AR models for acceleration-dot, showed extreme sensitivity to observation noise. Here, a nominal AR model refers to a model obtained by a standard least squares identification procedure in conjunction with the usual goodness of fit tests. This extreme sensitivity to observation noise was eliminated in (1) by the following ad hoc approach: the nominal fifth-order AR model used in the predictor was replaced by a modified fifth-order model with greater damping and reduced bandwidth. The overall filter/predictor system was characterized by three decoupled channels for the X, Y, and Z coordinates. The individual Kalman filters were implemented based on the nominal values of the X triple-dot AR coefficients for Pass 10. The performance of this simplified filter structure with these specific coefficients was studied extensively through simulation experiments. The results of this study indicated that this simplifed filter provided good performance against all of the observed flight profiles. A worst case analysis based on game theoretic techniques revealed that this simplified nominal filter should be replaced by a structurally identical filter with different AR parameter values to counter plausable worst case maneuver processes which were not part of the flight test data base. We refer the reader to (1) for a complete description of this worst case analysis and filter design technique. The coefficients for the individual X, Y, and Z coordinate predictors were obtained by adjusting the overall bandwidth and damping to achieve good prediction performance based on the filtered observations. A common choice of modified AR coefficients was implemented for each of the three predictors. This adjustment of predictor bandwidth and damping necessitated some empirical analysis via simulation studies. It is worth emphasizing that these "decoupled" eighth-order nominal filter/modified predictors provided 25 - 35 per cent improvement in average hit probability compared with the usual "decoupled" third-order benchmark algorithm. We note that although the nominal predictors based on fifth-order AR

models of acceleration-dot showed extreme sensitivity to observation noise, which necessitated modifying the predictor's frequency response, a nominal predictor based on the Pass 10 X triple-dot AR coefficients provided excellent prediction capability against each of the eleven flight paths in a noiseless environment. This substantial sensitivity to observation noise is of more than academic interest. It suggests that the underlying process (truth model) which actually characterizes the aircraft motion may exhibit structural details which are not embraced by AR or more generally by autoregressive integrated moving average (ARIMA) approximations. This last statement is <u>not</u> intended to imply that ARIMA models are unsuited for maneuver process modeling, but rather that, in the set of all possible maneuver process models, there may be alternative classes of models which provide better explainations of the underlying process. One recognizes, in applications oriented model building, that there is a delicate balance which must be sought between process explaination (complexity) and implementation approximations (simplicity). The choice of pivot point for this balance is strongly influenced by the model's intended application.

Models Based on Aerodynamic Variables and Aircraft Aspect

We began our consideration of alternative models for evasive attack aircraft motion by examining an overall model structure which was delineated in terms of aerodynamic variables and aircraft aspect. This new model was based on an integration of finite markov chain models for aircraft normal acceleration with ARIMA models for aircraft tangential acceleration and bank angle. The consideration of dynamic stochastic models for target motion based on target aspect (bank angle) as well as aerodynamic variables (normal and tangential acceleration) was motivated by an earlier investigation reported in (2). These earlier results indicated that enhanced prediction capability might be achievable based on prediction algorithms defined in terms of target aspect, airspeed, and normal acceleration, particularly over extended prediction intervals (e.g. 3 - 5 sec.). We remark that other investigators working in the air-to-air fire control environment have recently considered state estimation algorithms based on target aspect and normal acceleration. However, these collateral works, which are reported in (3 - 5), do not make use of any flight test data.

The factors which suggest modeling target motion in terms of bank angle, normal acceleration, and tangential acceleration are:

(i) A desire to describe target motion in terms of decision variables under the control of the pilot.

(ii) The recognition, based on theoretical considerations as well as empirical studies, that the stochastic dynamic behavior of the individual X, Y, & Z acceleration-dot time series for a given flight profile are strongly coupled in a noncausal fashion.

(iii) The recognition that alternative models for target motion based on aspect and aerodynamic variables could allow the exploitation of partially redundant dynamic data in the context of seeking enhanced prediction capability through multisensor integration.

Preliminary Results

(i) The first phase of the present study focused on the identification and estimation of univariate time series models for target bank angle (BA), normal acceleration (NA), and tangential acceleration (TA). These results indicate that the eleven BA, NA, & TA time series can be adequately modeled by three separate ARIMA models. By the phrase "adequately modeled," we mean that based on noiseless data there is inadequate evidence to support the rejection of the null hypothesis. The phrase "adequately modeled" is not intended to imply that these models necessarily have good sensitivity properties. The prediction capabilities of these models in a noisy environment will be described subsequently.

(ii) A single input single output (SISO) transfer function analysis indicates that while there are weak causal relations between BA and NA, and between NA and TA, it is adequate to treat the individual BA, NA, & TA time series for a given flight path as independent series.

(iii) The NA time series for each flight path exhibits significant piecewise linear behavior. This suggests that the rate of change of normal acceleration can be modeled approximately as a finite state markov chain. Detailed analysis indicates that this finite state markov chain model is quite competitive with the previously described ARIMA model for NA as judged by the relative prediction capability of each model in a noiseless environment.

(iv) A comparative analysis of predictor performance for the case of noiseless data indicates that:
    (a) The hybrid predictor (based on a nominal markov chain model for NA-dot, and nominal ARIMA models for TA & BA) performs comparably to the predictor comprised of nominal ARIMA models for NA, TA, & BA.
    (b) The performance of both of these new predictors is comparable to that of the robust predictor based on acceleration-dot obtained in (1).
    (c) The nominal fifth-order AR models based on acceleration-dot obtained in (1) performs noticeably better

than each of the other predictors cited in (iv-a) and (iv-b). The high performance capability of these nominal fifth-order AR models in a noiseless environment is not practically useful because of the severe noise sensitivity of these models as noted previously.

(v) A comparative analysis of predictor performance for the case of noisy data indicates that:
    (a) The nominal ARIMA models of NA, TA, & BA exhibit the same extreme sensitivity to observation noise as was found for the nominal fifth-order AR models of acceleration-dot obtained in (1).
    (b) The nominal finite state markov chain model for NA-dot showed substantial noise immunity.

Preliminary Conclusions

We draw the following conclusions from these preliminary results:

(i) The nominal finite state markov chain model has substantially better noise immunity than its nominal ARIMA counterpart.

(ii) Logical directions for further research include:
    (a) A study of the behavior of finite state markov chain approximations to the TA & BA processes.
    (b) A study of the behavior of finite state markov chain approximations to the X, Y, & Z acceleration-dot processes resolved in a cartesian coordinate system.

We decided to direct our phase-two efforts towards a detailed study of finite state markov chain approximations of the acceleration-dot processes resolved in a cartesian coordinate system. We chose this direction over the finite state markov chain study of NA, TA, & BA, since current sensor capabilities do not suggest the immediate availability of direct or indirect aircraft bank angle data with a suitable S/N ratio.

MARKOV CHAIN MODELS of A-DOT

In this section we describe the determination and validation of nominal finite state markov chain approximations to the individual X, Y, & Z acceleration-dot processes for the flight paths in our data base. The following approach is justified if we assume that the underlying A-dot data is generated by a (possibly) infinite state wide-sense stationary markov process with sample paths that exhibit piecewise constant behavior over intervals of random duration. We refer the reader to reference (6) for a more

rigorous probabilistic description of the class of underlying processes for which our approximation algorithm is theoretically valid. In the following discussion we focus our attention on a generic sample path, for example, the X triple-dot realization for Pass 1.

An Approximation Algorithm

Our approximation algorithm has the following steps:

Step 1 - Dynamic Range: Determine the dynamic range (maximum & minimum values) of the time series data.

Step 2 - State Assignment: Determine a finite set of "states" for the time series data.

Step 3 - Transition Matrix Estimation: Estimate the probabilities in the one-step state transition matrix -- based on the state assignments made in Step 2.

Step 4 - Repeat Steps 1 - 3 for the remaining time series data sets.

Step 5 - Hypothesis Testing: Perform the appropriate statistical tests to evaluate the validity of the hypothesis that the derived finite state markov chains have a common underlying distribution. (We refer the reader to reference (7) for an excellent treatment of hypothesis tests for finite state markov chains.)

Some Comments on the Algorithm

Step 2: There is no canonical method to resolve the state assignment question. We have explored two methods in this preliminary analysis. These methods are: (a) the method of uniform dynamic range, and (b) the method of uniform duration. The method of uniform dynamic range breaks the dynamic range of the time series into M equal intervals. (In this analysis we chose M = 5.) The center point of each interval was defined to be the value of the associated state. The method of uniform duration selects the M "state intervals" such that the number of "occupancies" in each interval are identical (or approximately identical). Here again, the value of M was chosen to equal 5, and the center point of each interval was used to designate the state value. The selection of M = 5, as well as the state assignment procedure represents judgmental calls on the part of the investigators. Further research on these issues is currently being pursued.

Step 3: The underlying one-step state transition matrices were estimated using the method of maximum likelihood (7).

Structural and Statistical Results

Although the flight paths all look very different to the "naked eye," the estimated one-step state transition matrices showed remarkable similarity between the X, Y, & Z directions for a given flight path, and between all of the flight paths. This result corresponds to the related behavior of the acceleration-dot spectra reported in (1). Use of the uniform dynamic range rule for state assignment led to one-step transition matrices which exhibit a pronounced birth-death behavior.

Prediction Using Markov Chains

Prediction based on a MMSE criterion is easily carried out for a finite state markov chain model. The propagation of the conditional expectation of the state n steps into the future is obtained by raising the one-step state transition matrix to the nth power and then multiplying the resulting matrix by a column vector of state values. The desired value of the conditional expectation is merely a weighted sum of n-step state transition matrix entries.

Numerical Results

In this section we present the results of a series of simulation experiments which were carried out to test the validity of this finite state markov chain approximation concept. These results represent two separate classes of finite state markov chain approximations. The first model denotes a finite state markov chain approximation to X, Y, & Z triple-dot. The predictions are based on a "multiple integration" of the predicted values of acceleration-dot, acceleration, and velocity in each coordinate. A standard Taylor series model defines the overall predictor structure. The second model, which we introduce very briefly, denotes a finite state markov chain approximation to the individual components of the derivative of the aircraft's angular velocity vector (Omega-dot). Detailed motivation for this choice of state variable description of the aircraft motion appears in (6). Our purpose in presenting these additional results here is to illustrate that the choice of state variable description or model coordinatization is not uniquely or canonically determined. Both classes of models have been exercised against the benchmark predictor. Since sensitivity to observation noise is a critical issue, predictor performance with and without noise has been investigated. The signal to noise ratios used in these experiments correspond roughly to the low level noise figure experiments performed in (1). In the current experiments, uncorrelated observation noise was added to the data prior to the prediction calculations. No filtering was carried out on these data prior to the prediction calculations. Since Kalman filters were employed in the experiments

102

PASS NO.	XYZ TRIPLE-DOT				OMEGA-DOT				BENCHMARK			
	AVG HIT PROB	SEC TOF	Miss Distance Histogram 0-5	5-10 Meters # of Rounds	AVG HIT PROB	SEC TOF	Miss Distance Histogram 0-5	5-10 Meters # of Rounds	AVG HIT PROB	SEC TOF	Miss Distance Histogram 0-5	5-10 Meters # of Rounds
1 No Noise	.397192	0 - 1	46	0	.376014	0 - 1	46	0	.322085	0 - 1	46	0
		1 - 2	28	13		1 - 2	23	11		1 - 2	15	11
		2 - 3	0	7		2 - 3	2	3		2 - 3	0	5
		3 - 4	0	0		3 - 4	0	0		3 - 4	0	0
		4 - 5	0	0		4 - 5	1	2		4 - 5	0	0
1 Noise	.348228	0 - 1	46	0	.353139	0 - 1	45	1	.317263	0 - 1	45	1
		1 - 2	19	14		1 - 2	22	14		1 - 2	12	13
		2 - 3	0	3		2 - 3	1	3		2 - 3	3	3
		3 - 4	0	2		3 - 4	0	0		3 - 4	0	0
		4 - 5	0	1		4 - 5	0	1		4 - 5	1	0
2 No Noise	.331401	0 - 1	27	0	.321864	0 - 1	27	0	.225967	0 - 1	26	1
		1 - 2	23	4		1 - 2	22	5		1 - 2	15	9
		2 - 3	2	8		2 - 3	6	4		2 - 3	0	1
		3 - 4	0	1		3 - 4	0	0		3 - 4	0	0
		4 - 5	0	1		4 - 5	0	0		4 - 5	0	0
2 Noise	.287723	0 - 1	27	0	.305919	0 - 1	27	0	.213553	0 - 1	24	3
		1 - 2	15	11		1 - 2	18	9		1 - 2	14	9
		2 - 3	2	5		2 - 3	6	2		2 - 3	0	0
		3 - 4	0	2		3 - 4	0	0		3 - 4	0	0
		4 - 5	0	0		4 - 5	0	1		4 - 5	0	0
3 No Noise	.411553	0 - 1	29	0	.353486	0 - 1	29	0	.309004	0 - 1	26	3
		1 - 2	44	7		1 - 2	33	12		1 - 2	28	14
		2 - 3	1	1		2 - 3	0	4		2 - 3	0	0
		3 - 4	0	2		3 - 4	0	0		3 - 4	0	0
		4 - 5	0	0		4 - 5	0	4		4 - 5	0	0
3 Noise	.344399	0 - 1	28	0	.329188	0 - 1	28	0	.282348	0 - 1	26	2
		1 - 2	34	16		1 - 2	28	18		1 - 2	26	15
		2 - 3	0	2		2 - 3	0	4		2 - 3	0	1
		3 - 4	0	0		3 - 4	0	0		3 - 4	0	0
		4 - 5	0	0		4 - 5	0	0		4 - 5	0	1
7 No Noise	.402733	0 - 1	47	0	.362481	0 - 1	47	0	.352018	0 - 1	43	4
		1 - 2	21	2		1 - 2	15	7		1 - 2	15	5
		2 - 3	0	7		2 - 3	0	5		2 - 3	3	2
		3 - 4	0	0		3 - 4	0	0		3 - 4	0	1
		4 - 5	1	0		4 - 5	0	0		4 - 5	0	0
7 Noise	.351804	0 - 1	47	0	.319388	0 - 1	47	0	.323917	0 - 1	42	5
		1 - 2	17	8		1 - 2	6	17		1 - 2	13	7
		2 - 3	0	2		2 - 3	0	0		2 - 3	1	3
		3 - 4	0	0		3 - 4	0	0		3 - 4	0	0
		4 - 5	0	0		4 - 5	0	0		4 - 5	0	0
10 No Noise	.408987	0 - 1	49	0	.348071	0 - 1	49	0	.344829	0 - 1	49	0
		1 - 2	27	11		1 - 2	18	13		1 - 2	16	17
		2 - 3	2	4		2 - 3	1	2		2 - 3	0	4
		3 - 4	0	0		3 - 4	0	0		3 - 4	0	0
		4 - 5	0	0		4 - 5	0	0		4 - 5	0	0
10 Noise	.362005	0 - 1	49	0	.324366	0 - 1	49	0	.327280	0 - 1	45	4
		1 - 2	16	16		1 - 2	13	15		1 - 2	16	15
		2 - 3	3	3		2 - 3	0	2		2 - 3	0	5
		3 - 4	0	0		3 - 4	0	0		3 - 4	0	0
		4 - 5	0	0		4 - 5	0	0		4 - 5	0	0
14 No Noise	.395702	0 - 1	44	0	.345427	0 - 1	44	0	.298755	0 - 1	44	0
		1 - 2	30	15		1 - 2	22	15		1 - 2	9	29
		2 - 3	0	2		2 - 3	0	0		2 - 3	1	1
		3 - 4	0	0		3 - 4	0	0		3 - 4	0	0
		4 - 5	0	0		4 - 5	0	0		4 - 5	0	0
14 Noise	.351072	0 - 1	44	0	.287483	0 - 1	44	0	.288187	0 - 1	44	0
		1 - 2	22	15		1 - 2	13	14		1 - 2	9	22
		2 - 3	2	2		2 - 3	0	0		2 - 3	0	2
		3 - 4	0	0		3 - 4	0	0		3 - 4	0	0
		4 - 5	0	0		4 - 5	0	0		4 - 5	0	0

TABLE 1.

reported in (1), a complete correspondence between these preliminary experiments and the results reported in (1), cannot be made. The results of the present experiments should be viewed as preliminary, since the markov chain predictors which were implemented in each case were based solely on the Pass 1 time series data. This choice represents a first cut, and illustrates the excellent performance of the markov chain approximations, which did not require any tuning. The results of the prediction experiments are contained in Table 1. We remark that both classes of markov chain models performed well against the benchmark model, and both exhibited significant noise immunity. The performance of the nominal (non robust) fifth-order AR models for acceleration-dot yield corresponding average hit probabilities significantly less than 0.1 at this noise figure. Further results relating to the robustization of these preliminary markov chain approximations are reported in (6, & 8). Reference (6) includes a worst case analysis of the markov chain approximation process, as well as the saddle-point theory which justifies the worst case analysis.

CONCLUSIONS

This study has presented substantial evidence to support the assertion that finite state markov chain approximations can be used in place of AR (and ARIMA) models as the basis for predictors in a realistic AAA fire control application. The value of the markov chain approximations lie in their substantial immunity to observation noise. It has been shown previously in (1) that high order AR models can provide a substantial enhancement in prediction performance in comparison with the usual decoupled third-order benchmark model. However, the application of these high order AR models requires that the nominal parameter values be adjusted to reduce the bandwidth and increase the damping of the given predictor. This adjustment procedure requires a degree of numerical experimentation to obtain a suitable design. Whereas, the markov chain approximations need essentially no tuning to obtain a design with excellent observation noise immunity, and therefore these models can be used "directly off the shelf".

REFERENCES

(1) S. F. Huling, and M. Mintz, "ENHANCED FILTERING & PREDICTION FOR AAA FIRE CONTROL: An Application of Game Theory and Time Series Analysis," Final Report on Contract No. DAAK10-78-C-0186, Submitted to US Army ARRADCOM, May 1980. Published as Contractor Report ARSCD-CR-80015.

(2) S. F. Huling, and M. Mintz, "ROBUST AUTOREGRESSIVE PREDICTORS FOR AIRCRAFT MANEUVERS: A Comparative Study," Final Report on Contract No. DAAA25-76-C-0435, Submitted to US Army Frankford Arsenal, October 1978.

(3) J. D. Kendrick, "Estimation of Aircraft Target Motion Using Pattern Recognition," Ph. D. Dissertation, Air Force Institute Of Technology, 1978.

(4) J. D. Kendrick, P. S. Maybeck, and J. G. Reid, "Estimation of Aircraft Target Motion Using Orientation Measurments," IEEE Transactions On Aerospace And Electronic Systems, Vol. AES-17, No. 2, March 1981, pp. 254-259.

(5) C. A. McNary, et. al., "Motion Estimation Using Target Aspect (META) Feasibility Study," Interim Report on Contract No. F33615-77-C-1227, Submitted to US Air Force Avionics Laboratory, October 1979, AFAL-TR-79-1077.

(6) E. B. Pate, and M. Mintz, "NEW TECHNIQUES FOR DESIGNING ROBUST PREDICTORS FOR AAA FIRE CONTROL SYSTEMS: An Application of Markov Chain Models and Game Theory," Final Report on Contract No. DAAK10-79-C-0232.

(7) T. W. Anderson, and L. A. Goodman, "Statistical Inference About Markov Chains," Annals Of Mathematical Statistics, Vol. 28, 1957, pp. 89-110.

(8) E. B. Pate, M. Mintz, W. Dziwak, and S. A. Goodman, "On Designing Robust Predictors Based On Finite State Markov Chains: A Game Theoretic Approach," Proceedings of the Nineteenth Annual Allerton Conference, October 1981.

Next page is blank.

ROBUST KALMAN FILTERING

Dr. G. A. Hewer
RF Anti-Air Branch
Weapons Synthesis Division
Naval Weapons Center
China Lake, California 93555

ABSTRACT

This is a preliminary report on the current research on the applicability of robust Kalman filtering in monopulse radar tracking systems. (An estimation procedure is robust if small perturbations in the noise model from the assumed (Gaussian) noise model result in only small changes in the mean-squared-error of estimate.)

INTRODUCTION

Optimal guidance laws for accelerating targets depend on adequate estimates of key states such as line-of-sight rate and target normal accelerations. When optimum state estimates of these parameters are available, superior missile performance can be demonstrated. These estimates are usually provided by some Kalman filter algorithm. In the classical Kalman filter, noise sources are characterized by uncorrelated Gaussian statistics. Unfortunately, as the research of Masreliez and Martin [1] demonstrates, the behavior of Kalman filter algorithms can be severely degraded when the actual noise disturbances are non-Gaussian, particularly when the non-Gaussian behavior is heavy tailed. The latter behavior is characterized by outliers. In monopulse radars this heavy tailed non-Gaussian behavior is present in the angle tracking signals because of target glint. A monopulse tracker will turn until the central axis of the receiver antenna is aligned with the normal of the incoming (scattered) wavefront. For a point target the scattered wavefront is spherical, and thus the gradient is always along a radial vector directed from the receiver aerial to the target. A complex target is composed of a number of spatially separated scatterers and thus the spherical wavelets from the individual "point" scatterers will interfere. As a result of this interference the phase of the received signal will not, in general, be independent of the target aspect. The component of the phase gradient vector orthogonal to the radial direction is directly related to tracking error. It is this type of error that constitutes glint. Since the phase of a complex target varies as a function of target aspect and motion, the statistics for the Kalman filter are non-stationary. Thus the Kalman filter must adapt to the non-stationary glint statistics. Moreover, the pulse repetition rate of the radar is generally much higher than the requisite tracking rate. For this reason the Kalman filter generally processes a set of statistics based on a fixed number of sampled radar measurements. If these statistics are the mean and variance of the

angular glint based on a sequence of radar pulses, then they will be sensitive to intrinsic signal outliers (i.e., large glint spikes). For this reason robust statistical alternatives to the mean and variance are considered. Informally, a robust estimate is one whose performance remains quite good when the true distribution of the data deviates from the assumed distribution. The mean and variance are sensitive to large changes in a small fraction of data points. Robust estimates are more resistant to outliers. The purpose of this research is to clarify the role of robust estimates in angle tracking.

In this paper the basic angle tracking loop simulation is outlined and some preliminary results are presented. In addition, the role of robust estimates in the tracking loop are identified and some comparisons of the mean and variance with robust estimates are presented using some simulated glint data.

TRACKING LOOP MODEL

The basic angle tracking loop is defined in Figure 1. The tracking loop and Kalman filter equations are derived and discussed in the paper by Pearson and Stear [2]. In this section the Kalman filter equations, the controller and the antenna stabilization loop denoted by G(S) are defined.
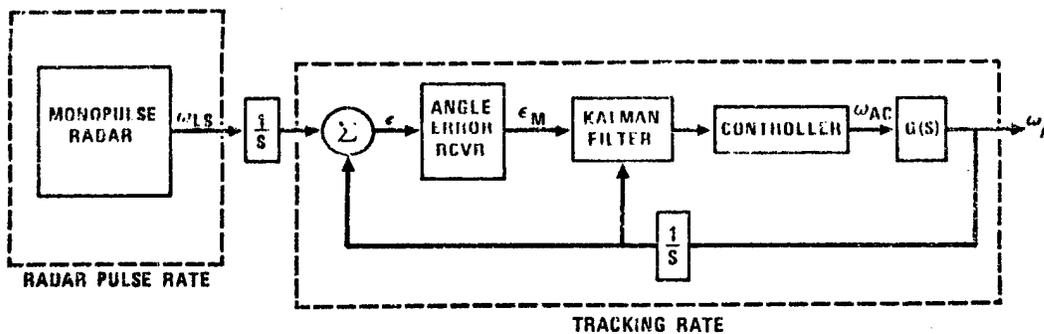
ω_{LS} – LOS RATE $\qquad$ ϵ – ANGLE POINTING ERROR

ω_A – ANTENNA RATE $\qquad$ ϵ_M – MEASURED POINTING ERROR

ω_{AC} – COMMANDED
$\qquad$ ANTENNA RATE

FIGURE 1. Pointing Error Control System.

For this simulation a planar engagement is assumed and for the initial studies the radar is fixed and the target is executing a constant g turn. Also, it is assumed that line of sight and antenna gimbal coordinate frames are almost coincident. Let ϵ denote pointing error, which is the integrated difference between the line-of-sight rate ω_{LS} and antenna rate ω_A. Let a_T and a_I denote the

target and interceptor accelerations. The Kalman filter state equations are

$$\dot{\varepsilon} = \omega_{LS} - \omega_A$$

$$\dot{\omega}_{LS} = -\frac{2\dot{R}}{R}\omega_{LS} + \frac{1}{R}(a_T - a_I)$$

$$\dot{a}_T = -\frac{1}{\tau}a_T + q$$

with observation equation

$$y = k\varepsilon + r,$$

where k is the angle error receiver slope and r and q denote additive noises. This formulation of the Kalman filter in line-of-sight coordinates is appealing because the filter is linear and the second state equation reduces to the formula for the transverse . acceleration of a particle moving in a plane. The constants R, $\dot{R}$ and τ are respectively range, range rate and target acceleration time constant. The estimates of R and $\dot{R}$ are provided by the radar.

The estimates $\hat{\varepsilon}$ and $\hat{\omega}_{LS}$ produced by the Kalman filter are combined linearly to produce an antenna rate command of the form

$$\omega_{AC} = G_1\hat{\omega}_{LS} + G_2\hat{\varepsilon}$$

where G_1 is usually unity and G_2 is proportional to the tracking loop rate.

The antenna stabilization loop is modeled as a third order system whose states are antenna postion, rate and acceleration, which are denoted by x_1, x_2 and x_3. Let ζ denote the damping ratio and ω the undamped natural frequency. Finally, let $u(t)$ denote a continuous real valued input function. The state equations can be written as

$$\dot{x}_2 = x_3$$

$$\dot{x}_3 = -2\zeta\omega x_3 - \omega^2 x_2 + \omega^2 u(t)$$

$$\dot{x}_1 = x_2.$$

EXACT SOLUTIONS OF THE STATE TRANSITION MATRICES

In this section the state transition matrices for the Kalman filter and the antenna stabilization loop are derived. First, the transition matrix for the Kalman filter is derived. Next, the transition matrix that is used to represent the antenna stabilization loop and integrator in the pointing error control system using Kalman estimates is derived. Finally, the transition matrix is used to obtain the sampled-data time domain representation of the stabilization loop integrator with a hold circuit. Both of these transition matrices are derived using spectral operator theory. These techniques for finite dimensional operators are discussed in Lancaster [3] and Zadeh and Desoer [4].

Before deriving the exact solutions of these systems, the concepts and formulas that are essential in the development of spectral operator theory for functions of matrices are presented. Assume the following state variable formulation

$$\dot{x} = Ax + Bu \tag{1}$$

$$y = Cx \tag{2}$$

where A, B anc C are respectively n x n, n x 1 and 1 x n constant matrices and x, y and u are real valued state vectors of compatible dimensions. To simplify the discussion it is assumed throughout this section that the eigenvalues of A are distinct. Let $\lambda_1 \ldots , \lambda_n$ denote the eigenvalues of A. The basic strategy of this section is to solve the linear system (1) by first deriving an exact expression for exp(At) and then solving the forced system by integrating the general solution. The spectral operator theory develops an exact expression for elementary functions with matrix arguments. For example, the theory justifies the substitution of a matrix A for the real variable ℓ in the power series expansion of the elementary functions such as $\exp(\ell)$ and $\sin(\ell)$. However, computing the matrix exp ($A\ell$) by the infinite power series can be difficult except in very special cases or for small values of t. A finite power series expansion can be obtained by using the following fundamental formula for the function of a matrix. Given any real valued function f, which is analytic at the eigenvalues of A

$$f(A) = \sum_{k=1}^{n} f(\lambda_k) Z_k \tag{3}$$

where $\lambda_1 \ldots , \lambda_n$ are the distinct eigenvalues of the n x n matrix A and the matrices Z_k have constant elements and depend exclusively on A. The n x n matrices Z_k are called the <u>components</u> of A. The component matrices are linearly independent nonzero matrices that commute with A and satisfy the following identities

110

(a) $\sum\limits_{k=1}^{n} Z_k = I,$

(b) $Z_k Z_k = Z_k$ for each k

(c) $Z_k Z_j = 0$ for $k \neq j$

Where I and 0 are respectively the n x n identity and null matrix. Property (a) follows from the fundamental formula (3) by letting $f(\lambda) = 1$. Matrices that satisfy properties (b) and (c) are called respectively idempotent and orthogonal. Since the eigenvalues of A are assumed to be distinct, the Z_k can be computed by the formula

$$Z_k = \prod_{\substack{j=1 \\ j \neq k}}^{n} (A - \lambda_j I) / \prod_{\substack{j=1 \\ j \neq k}}^{n} (\lambda_k - \lambda_j)$$

where $\prod$ is the product symbol. An alternative method for computing the component matrices is given in Lancaster and Zadeh. When $f(\lambda) = e^\lambda$ or $f(\lambda) = \lambda$ there results

$$\exp(At) = \sum_{k=1}^{n} \exp(\lambda_k t) Z_k$$

$$A = \sum_{k=1}^{n} \lambda_k Z_k.$$

The spectral theory of an operator can be very useful in computing some fundamental properties of exp(At). By property (a) for t = 0

$$\exp(At) = \sum_{k=1}^{n} Z_k = I,$$

which is one of the basic properties of the state transition matrix. To show that exp(At) when computed by the fundamental formula (3) is a solution of (1) with zero-input (i.e., the input vector u is zero for all time) first form the product

$$A \exp(At) = \left(\sum_{k=1}^{n} \lambda_k Z_k \right) \left(\sum_{k=1}^{n} \exp(\lambda_k t) Z_k \right)$$

and then apply the idempotent and orthogonality properties of the component matrices to the product to obtain

$$\sum_{k=1}^{n} \lambda_k \exp(\lambda_k t) Z_k = \frac{d}{dt} \left(\sum_{k=1}^{n} \exp(\lambda_k t) Z_k \right)$$

111

which proves that exp(At) is a solution of (1) with zero-input response.

These techniques are now used to solve for the state transition matrix in the Kalman filter. The 3 x 3 A matrix is

$$\begin{pmatrix} 0, & 1, & 0 \\ 0, & -\dfrac{2\dot{R}}{R}, & -\dfrac{1}{R} \\ 0, & 0, & -\dfrac{1}{\tau} \end{pmatrix},$$

where R, $\dot{R}$ and τ are respectively range, range rate and the target acceleration time constant. Since A is an upper triangular matrix the eigenvalues of A are the diagonal entries. These are

denoted by $\lambda_1 = 0$, $\lambda_2 = -\dfrac{2\dot{R}}{R}$ and $\lambda_3 = -\dfrac{1}{\tau}$. Using the product formula, the formal expressions for the correstponding component matrices become

$$Z_1 = \left(A^2 - (\lambda_2 + \lambda_3)A + \lambda_2\lambda_3 I \right) / \lambda_2\lambda_3$$

$$Z_2 = \left(A^2 - \lambda_3 A \right) / \lambda_2(\lambda_2 - \lambda_3)$$

$$Z_3 = \left(\lambda_2 A - A^2 \right) / \lambda_3(\lambda_2 - \lambda_3),$$

where A^2 denotes the product of a matrix. After some tedious computations these expressions become

$$Z_1 = \begin{pmatrix} 1, & \dfrac{R}{2\dot{R}}, & -\dfrac{\tau}{2\dot{R}} \\ 0, & 0, & 0 \\ 0, & 0, & 0 \end{pmatrix}$$

$$Z_2 = \begin{pmatrix} 0, & -\dfrac{R}{2\dot{R}}, & \dfrac{R\tau}{2\dot{R}(R - 2\dot{R}\tau)} \\ 0, & 1, & \dfrac{\tau}{2\dot{R}\tau - R} \\ 0, & 0, & 0 \end{pmatrix}$$

112

$$Z_3 = \begin{pmatrix} 0, & 0, & \dfrac{\tau^2}{2R\dot{\tau}-R} \\[2em] 0, & 0, & \dfrac{\tau}{R-2R\dot{\tau}} \\[2em] 0, & 0, & 1 \end{pmatrix}$$

Using the fundamental formula the exact finite series expansion for exp(At) can be written as

$$\exp(At) = \exp(0)Z_1 + \exp\left(\dfrac{-2\dot{R}}{R}\,t\right)Z_2 + \exp\left(\dfrac{-t}{\tau}\right)Z_3.$$

This solution clearly exhibits the dependence of exp(At) on the eigenvalues of A; thus, the transient response of the zero-input response system can be readily analyzed.

If t<<1 so that $\exp(\lambda t)$ can be approximated by the first two terms in its series expansion, then the transition matrix becomes the sum of two matrices, which are

$$\begin{pmatrix} 1, & 0, & 0 \\[1em] 0, & 1, & 0 \\[1em] 0, & 0, & 1 \end{pmatrix} + \begin{pmatrix} 0, & 1, & 0 \\[1em] 0, & \dfrac{-2\dot{R}}{R}, & -\dfrac{1}{R} \\[1em] 0, & 0, & -\dfrac{1}{\tau} \end{pmatrix} t.$$

This expression is equivalent to integrating the linear system with zero-input response by Euler's method.

Consider the 3 x 3 A matrix

$$\begin{pmatrix} 0, & 1, & 0 \\[1em] -\omega^2, & -2\zeta\omega, & 0 \\[1em] 1, & 0, & 0 \end{pmatrix},$$

which is the A matrix in the state space representation of the antenna stabilization loop and of the integrator in the pointing error block diagram. In this matrix ω is the undamped natural frequency and ζ is the damping ratio. The eigenvalues of A are

$\lambda_1 = 0$, $\lambda_2 = -\zeta\omega \pm j\omega\sqrt{1 - \zeta^2}$ and $\lambda_3 = \bar{\lambda}_2$, where lambda bar denotes complex conjugate and $j = \sqrt{-1}$. Let $\omega_d = \omega\sqrt{1 - \zeta^2}$ denote the damped frequency and $\sigma = \zeta\omega$ denote the reciprocal of the time constant of the antenna stabilization loop. For a matrix with one real eigenvalue and two complex conjugate eigenvalues the transition matrix exp(At) can be decomposed into the following useful expression that is given in Zadeh and Desoer (page 611).

$$\exp(At) = \exp(\lambda t)Z_1 + \exp(-\sigma t)\left(R\cos(\omega_d t) + X\sin(\omega_d t)\right)$$

where $2Z = R - jX$.

Again the spectral decomposition of the matrix A clearly exhibits the dependency of the transition matrix on σ and the damping frequency ω_d. By utilizing the product formula for the component matrices and some tedious algebra the following expressions for the component matrices can be obtained

$$Z_1 = \begin{pmatrix} 0, & 0, & 0 \\ 0, & 0, & 0 \\ \dfrac{2\zeta}{\omega}, & \dfrac{1}{\omega^2}, & 1 \end{pmatrix}$$

$$R = \begin{pmatrix} 1, & 0, & 0 \\ 0, & 1, & 0 \\ \dfrac{-2\zeta}{\omega}, & \dfrac{-1}{\omega^2}, & 0 \end{pmatrix}$$

$$X = \dfrac{1}{\omega_d} \begin{pmatrix} \zeta\omega, & 1, & 0 \\ -\omega^2, & -\zeta\omega, & 0 \\ 1-2\zeta^2, & -\dfrac{\zeta}{\omega}, & 0 \end{pmatrix}$$

In the digital simulation of the error tracking loop the antenna response and the integrator are computed as a state variable sampled data system. The general solution of the linear system (1) with initial conditions given at t = 0 and x(0) is

$$x(t) = \exp(At)x(0) + \int_o^t \exp\Big(A(t-\tau)\Big)Bu(\tau)d \ .$$

Suppose the input is sampled with period T and between sampling times the input is a hold circuit

$$Bu(t) = Bu(NT) \quad \text{for} \quad NT \leq t < (N+1)T.$$

Therefore at sample time $t = NT$

$$x\Big((N+1)T\Big) = \exp(AT)x(NT) + h(T)u(NT)$$

where

$$h(T) = \int_o^T \exp(A\ell)Bd\ell.$$

The only task left in computing this expression is the evaluation of h(T), since for our applications exp(AT) is solved exactly. If A is nonsingular, then formally

$$\int_o^T \exp(A\ell)Bd\ell = \int_o^T (A^{-1})A \exp(A\ell)Bd\ell = A^{-1}\Big(e^{AT} - I\Big)B.$$

This expression for h(T) is a direct generalization of the calculus for one dimensional real variables.

In our application one of the eigenvalues of A is zero and so the integral must be evaluated directly. Since the constant matrices commute with the real valued exponential and trigonometric functions in the expansion of exp(AT), the integral h(T) is evaluated' by integrating the following real valued functions

$$\int_o^T \exp(-\sigma\ell) \cos (\omega_d\ell)d\ell \text{ and}$$

$$\int_o^T \exp(-\sigma\ell) \sin (\omega_d\ell)d\ell.$$

Now the solution of the first integral is

$$f_1(\sigma,\omega_d) = \frac{e^{-\sigma T}}{\sigma^2+\omega_d^2} \left[\Big(\omega_d \sin (\omega_d T) - \sigma \cos (\omega_d T)\Big) + \sigma\right]$$

and the solution of the second integral is

$$f_2(\sigma,\omega_d) = \frac{e^{-\sigma T}}{\sigma^2+\omega_d^2} \left[\Big(-\sigma \sin (\omega_d T) - \omega_d \cos (\omega_d T)\Big) + \omega_d\right]$$

Thus, the exact solution of $h(T)$ is

$$h(T) = Z_1 T + f_1(\sigma, \omega_c) R + f_2(\sigma, \omega_d) X.$$

For our application the 3 x 1 input matrix is

$$B = \begin{pmatrix} 0 \\ K \\ 0 \end{pmatrix}$$

where K is a constant gain matrix. The exact value of K depends on the requirements of the sampled data system in the error tracking loop.

EXPONENTIALLY CORRELATED TARGET NOISE

In this section a brief discussion of first order exponentially correlated noise or colored noise is presented. A more complete discussion is found in Jazwinski [5]. A formal mathematical description of such a process is

$$\frac{da}{dt} = -\sigma a + \sigma \alpha \omega \qquad 0 \leq t \tag{4}$$

where α and $\sigma > 0$ are fixed constants and ω is zero mean, white Gaussian noise with correlation function

$$E\left[\omega(t)\omega(\tau)\right] = \delta (t - \tau).$$

As usual $\delta(t)$ is the Dirac delta function and E is the expectation operator. Formally, the solution of this equation is

$$a(t) = e^{-\alpha t} a(0) + \alpha \sigma \int_0^t e^{-\alpha(t-S)} \omega(S) dS.$$

The constant σ is the variance of the target acceleration and α is the reciprocal of the maneuver (acceleration) time constant. Singer [6] proposed the exponentially correlated noise process as a model for maneuvering targets. By using this process with the appropriate Kalman filter, he proposed a tracking algorithm for piloted threats. In his paper, Singer proposes the following density model for the target acceleration variance. For completeness, a derivation of his model is included.

Let A_{max} denote the maximum target acceleration rate. Let X be the random variable that denotes the target acceleration state. According to Singer, X is a random variable with the following assigned probabilities

$$P(X = \pm A_{max}) = P_{max}$$

$$P(X = 0) = P_0$$

and otherwise the target accelerates between the limits $-A_{max}$ and A_{max} according to the appropriate uniform distribution. In order to insure that X is a bona fide random variable (i.e., $P(-\infty < X < \infty) = 1$), the probability of the mutually exclusive events $(-A_{max} < X < 0)$, $(0 < X < A_{max})$ must be $1 - (2P_{max} + P_0)$. This implies that the uniform density function for these events is

$$f(X) = \frac{1 - \dfrac{(2P_{max} + P_0)}{2A_{max}}}{} \quad .$$ The variance σ of target acceleration

is calculated by finding the variance of the random variable X. The expectation of X is zero and so the variance of X is given by

$$\sigma^2 = E(X^2) = \left(\frac{1 - \dfrac{(2P_{max} + P_0)}{2A_{max}}}{} \right) \frac{2A_{max}^3}{3} + 2A_{max}^2 P_{max}$$

$$= \frac{A_{max}^2}{3} (1 + 4P_{max} - P_0).$$

This completes the derivation of the Singer target acceleration model.

When the exponentially correlated noise model is used with a sensor having a constant data rate with sampling period T, then (4) can be converted to discrete form. By sampling the solution of (4), starting with t = 0, the recursive form becomes at the sampling instances jT

$$a_{j+1} = Ma_j + \omega_j$$

where

$$a_j = a(jT)$$

$$M = \exp(-\alpha T)$$

$$\omega_j = \sigma\alpha \int_{jT}^{(j+1)T} \exp\left(-\alpha(j+1)T - \lambda\right) \omega(\lambda) d\lambda.$$

The statistics of ω_j are formally

$$E(\omega_j) = 0$$

$$E(\omega_j \omega_i) = 0 \qquad j \neq i$$

$$E(\omega_j^2) = .5\alpha(1 - M^2)\sigma^2.$$

The latter equation shows how the sampled noise variance is related to its continuous time noise variance. Since ω_j is a Gaussian process, these statistics specify its density.

POINTING ERROR CONTROL SYSTEM SIMULATION EXAMPLE

In this section the pointing error control system simulation is briefly discussed. After listing the initial conditions and parameter values, some preliminary plots of the simulation output are presented. The primary purpose of these plots is to verify the simulation and to illustrate the effect of outliers. The requisite initial conditions and parameters to implement the sampled data Kalman filter algorithm, sampled data antenna stabilization loop and controller gains are now defined.

Tracking Period	$\Delta t = .03$ sec
Observation Variance	$R = .0001$ (rad^2)
Target Acceleration Variance	$Q = 1.$ (meters^2/sec^4)
Antenna Damping Factor	$\zeta = .4$
Antenna Undamped Natural Frequency	$\omega = 100$ (rad/sec)
Controller Gains	$G_1 = 1$, $G_2 = 1./\Delta t$
Target Acceleration Time Constant	$\tau = 2.$

The Kalman filter 3 x 3 initial covariance matrix was initialized by setting all diagonal elements equal to unity and the off diagonal elements equal to zero. For this example, the point target executed a full 360 degree constant 6 g turn with target velocity of 250 meters/sec. The outlier noise was added to angular position of the target with respect to the radar antenna. The outlier noise model was generated as contaminated distribution as discussed in Tukey [7]. The contaminated model was generated as the mixture of two normal distributions, each with zero mean and one with variance equal to observation variance and one with ten times the first variance. Let us denote these distributions as N(0,R) and N(0, 10R), respectively. The mixture of the two distributions defined as

$$F(x) = pN(0,R) + (1 - p)N(0, 10R) \qquad 0 < p < 1$$

generates the contaminated normal distribution. The random variable X with this distribution can be generated by first taking a uniform deviate U; if U < p, X is generated by independent samples from N(0, R) and otherwise choose N(0, 10R).

As noted by Maybeck [8] and Bierman [9], the usual Kalman filter algorithm is subject to numerical difficulties. To overcome these difficulties the UDU^T estimate-covariance updating algorithm and the modified Gram-Schmidt algorithm for the time update algorithm of Bierman were employed in this simulation. These algorithms solve the Kalman gain

$$K = \hat{P}H^T\left[H\hat{P}H^T + R\right]^{-1}$$

the error covariance matrix

$$\hat{p} = \hat{p} - KH^T\hat{p}$$

and the covariance time update

$$\tilde{P} = \Phi\hat{P}\Phi^T + GQG^T$$

where the subscripts have been omitted for notational simplicity. In these equations Φ is the Kalman filter state transition matrix, which is derived in the previous section, H is the observation row matrix (H = (1,0,0)) and Q is the process noise column matrix (G = $(0,0,1)^T$), P is the covariance matrix, K is Kalman gain matrix and Q and R are defined in the parameter list.

A few selected plots from the simulation are illustrated in Figures 2, 3, 4 and 5. Figure 2 is a comparison of the estimated target position with actual position. Figure 3 is a comparison of the estimated line of sight rate with the actual line of sight rate. Figure 4 is a plot of the contaminated normal noise added to the target position. The outliers are clearly evident in the plot. Figure 5 is a plot of the tracking loop innovations, which is the difference between the true measurement and the best prediction of it before sampling. Note that even with the nonoptimum initial estimates and sampling period, the loop maintains track.
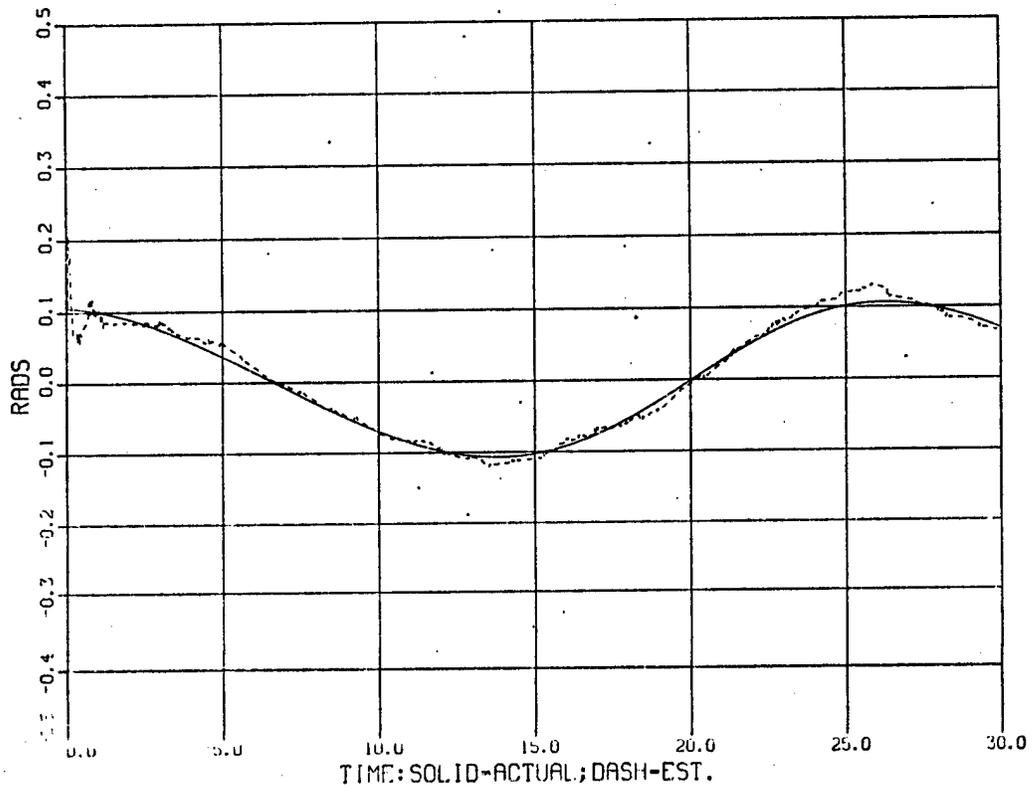
FIGURE 2.   Estimated Target Position vs Actual.
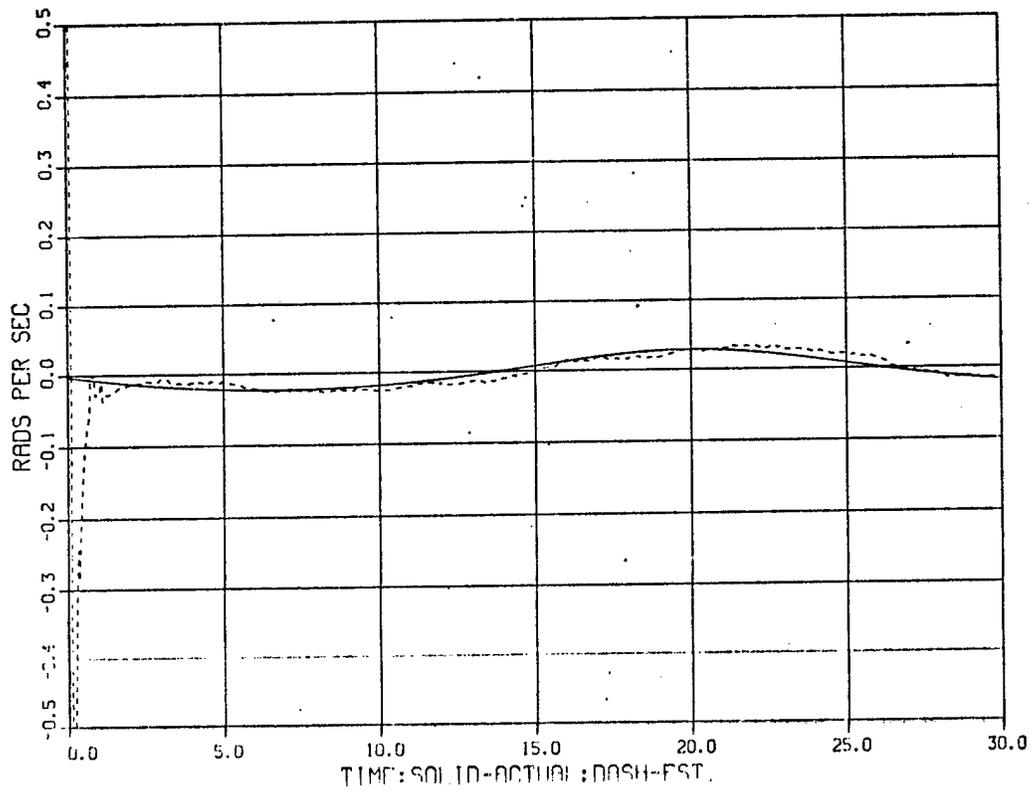
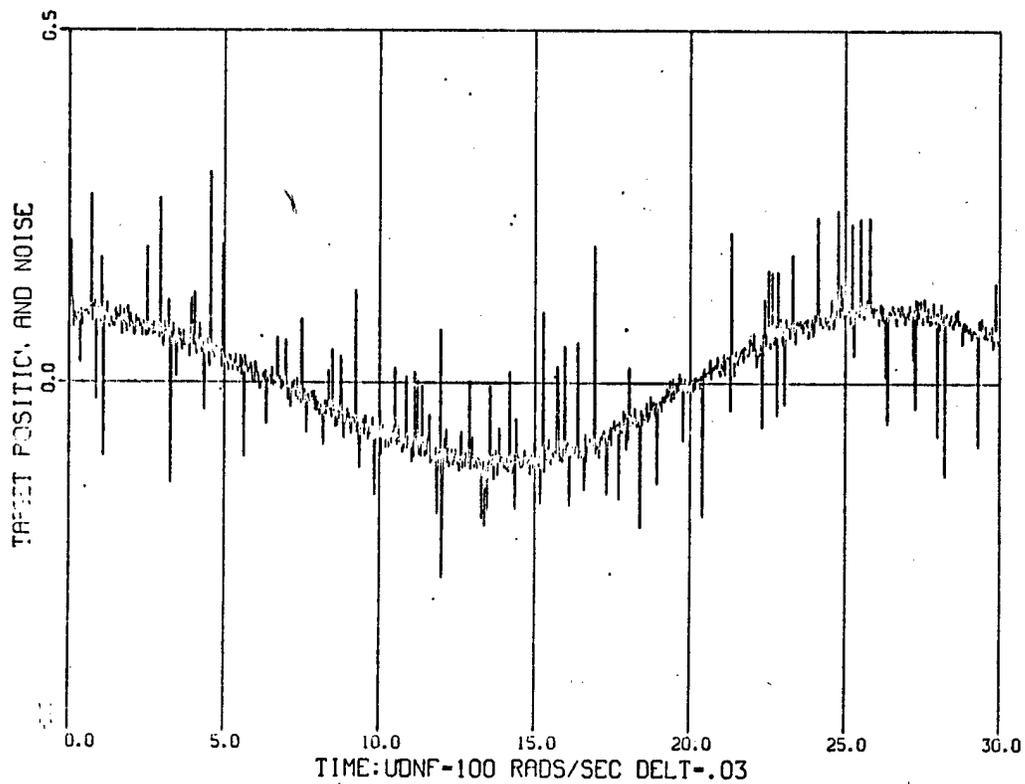FIGURE 3.   Estimated Target L.O.S. Rate vs Actual.
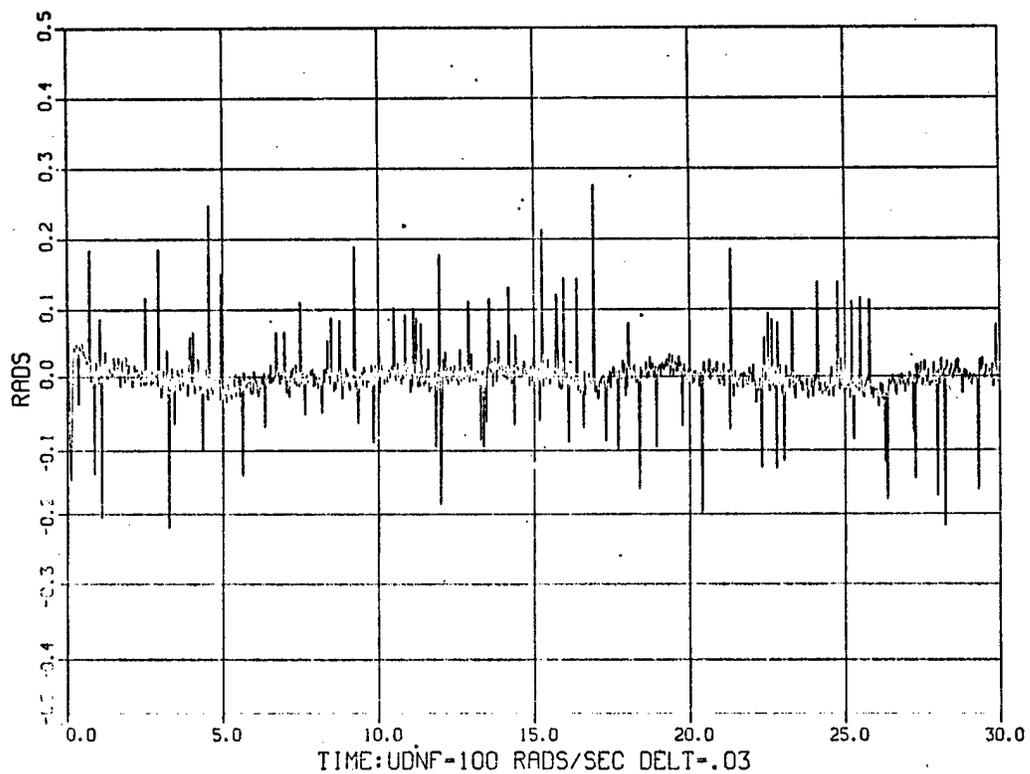
FIGURE 4.   10% Contaminated Normal Noise.

FIGURE 5.   Innovations.

121

A statistical procedure is <u>resistant</u> [10] if the value of esti-
mate is insensitive to a small change in all of the data values
or to large changes in a few of the data values. According to
Huber [11] this is a working definition that can be used to define
robustness. Figure 6 is a plot of linear glint, which clearly
exhibits the presence of outliers (glint spikes) that are intrin-
sic in the glint signature. Figure 6 is a sample of glint gener-
ated for a complex target using a radar target model developed by
Mumford [12]. Mumford's model computes the backscatter from a
complex target by decomposing the complex target into simple
component shapes for which scattering solutions have been derived.
This modeling technique is known informally as "N-shape" modeling.
Angular glint is defined as the linear displacement of the center
of radar reflection from the defined physical center of the target
measured along a line in the plane passing through the target
center, at right angles to the sightline, to the physical center.
Its magnitude is equal to the tangent of the angle between the
true and apparent directions of the target times the range.
Linear glint is simple range independent angular glint. Thus,
the strategy of robustifying the Kalman filter is based on making
it resistant to glint spikes. There are at least two ways to im-
plement this strategy. The first way is to preprocess the mono-
pulse radar pulses in a robust manner using summary statistics as
inputs to the pointing error control system flowcharted in Figure
1. This is a natural approach in tracking radars, since the radar
pulse rate is much higher than the requisite tracking rate. The
second way is based on the robustified Kalman filter developed by
Martin [13]. Both of these techniques are outlined in this
section.

Generally, for a complex target, the resulting glint signature
is non-stationary time series. Thus, both robust techniques
rely on adaptive noise estimates of the input noise statistics.
For the moment we ignore the interaction of target maneuver and
the glint signature. The two summary statistics of the input
noise that are required are an estimate of location and scale.
For a symmetric distribution estimate of location is the center
of the distribution, while an estimate of scale is the spread of
the distribution. For a Gaussian distribution the optimum esti-
mate of location is the mean and optimum estimate of scale is the
variance (standard deviation). For the moment in this discussion,
the correlation structure in the glint signature is also ignored.
As amply demonstrated by Tukey [7] for non-Gaussian heavy tailed
symmetric distributions these classical estimates are unsafe.

Following Martin [14] the following definitions are introduced
for completeness. Let $Y_1, \ldots, Y_n$ denote a univariate data
sample. A <u>statistic</u> is simple a function of the data
$T(Y) = T(Y_1, \ldots, Y_n)$. An <u>estimator</u> is a statistic whose value
is supposed to provide an indication of a parameter in a para-
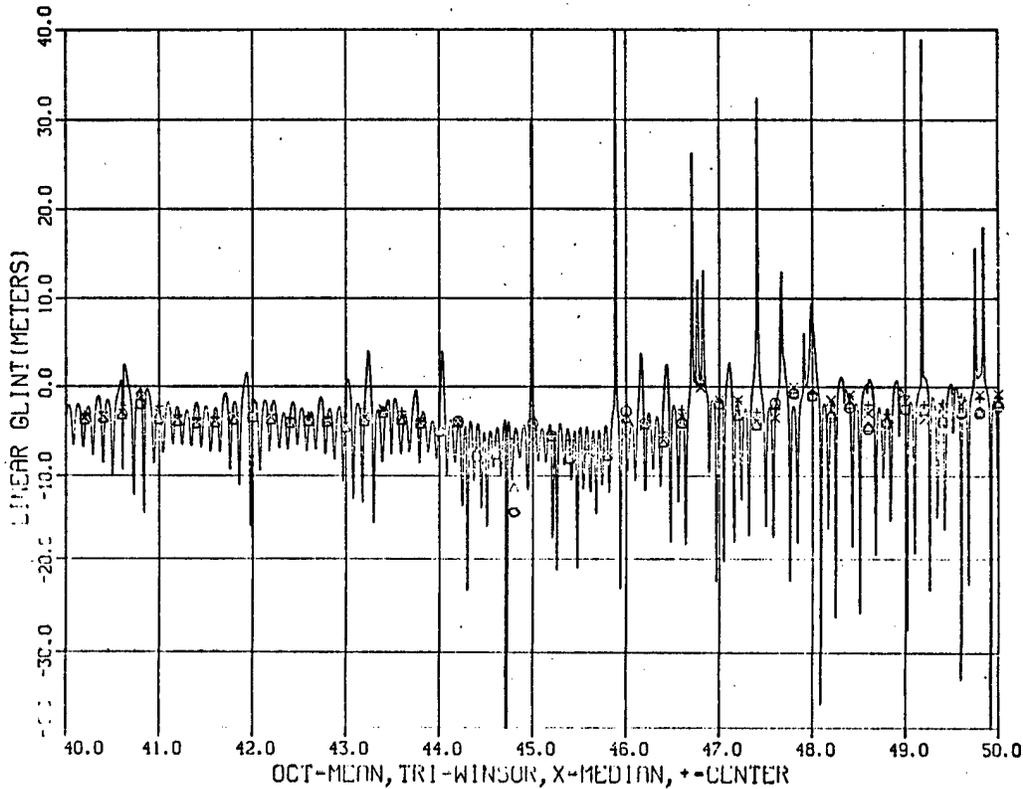metric statistical model for the data. A real scalar-valued esti-

FIGURE 6. Location Comparison (N-Shape Glint).

mate is <u>translation</u> invariant if for any real number C and the constant n-dimensional unit vector 1

$$T(Y + C\vec{1}) = T(Y);$$

<u>translation equivariant</u> if

$$T(Y + C\vec{1}) = T(Y) + C;$$

<u>scale invariant</u> if for any real constant C > 0

$$T(CY) = T(Y);$$

and <u>scale equivariant</u> if

$$T(CY) = CT(Y).$$

The <u>sample mean</u>

$$T(Y) = \frac{1}{N} \sum_{L=1}^{N} Y_i$$

is translation and scale equivariant. The sample <u>standard deviation</u>

123

$$S(Y) = \sqrt{\frac{1}{N-1} \sum_{L=1}^{N} (Y_i - T(Y))^2}$$

is translation invariant and scale equivariant. The robust estimate of scale CMADM = Median Absolute Deviation from the Median = median $|Y_i - $ median $(Y)|/.6745$ is translation invariant and scale equivariant. The divisor .6745 makes CMADM a consistent estimate of the standard deviation if the sample is drawn from a normal population. A robust estimate of location can be achieved by Winsorizing (see Huber, p. 18) the data. To metrically Winsorize the data, the observations $Y_1, \ldots, Y_n$ are replaced by pseudo-observations. In this study the pseudo-observations were obtained by setting all observations beyond 3S(Y) equal to S(Y) and then recomputing the sample mean. This procedure is translation invariant and scale equivariant. Another robust-estimate is Tukey's biweight [7, p. 353], which is defined as

$$T(Y) = \frac{\sum W_i Y_i}{\sum W_i}$$

where

$$W_i = \begin{cases} \left(1 - \left(\dfrac{Y_i - Y^*}{CS}\right)^2\right)^2 & \text{when } \left(\dfrac{Y_i - Y^*}{CS}\right) < 1 \\ 0 & \text{otherwise} \end{cases}$$

and S = CMADM. The constant C is callled the cutoff parameter, in this study C = 6. Biweight is translation and scale equivariant. Associated with each of these estimates is an influence function, which in exploratory data analysis governs the effect of the value of one data point on the estimate. Some influence functions are graphed in Figure 7. The linear influence curve in Figure 7(i) is the influence curve for the sample mean and shows that the sample mean is directly affected by a change in one data point. The influence curve labeled (ii) is Huber's monotone function and the influence curve (iii) is Hampel's two-part redescending function. The role of these influence functions in robust statistics is discussed in Huber [11]. Both of the latter influence functions ignore changes in measurement outside of a band and respond within the band; thus, outliers outside the acceptance band are rejected.

Martin's robustified Kalman filter modifies the state correction equation and the conditional error covariance matrix equation with a suitable scaled influence function. Two excellent candidates for an influence function in the Martin filter are the Huber and Hampel functions in Figure 7. The details of his filter are beyond the scope of this paper and the interested reader should consult Martin [13].

Figures 6 and 8 illustrate the different estimates of location and scale as provided by the different statistics. The data in Figure 6 represents the glint signature of a complex target sampled every .001 degree of target aspect in a 10 degree sector. Each of the statistics in Figures 6 and 8 are derived from successive non-overlapping .02 degree intervals containing 20 samples. In Figure 6 the points labeled by octagons are sample means, the triangular labels are the Winsorized estimates, the X labels are sample medians and the pluses are center or Tukey's biweight.

The resistence of median and biweight are clearly indicated in the 44 to 45 degree interval. In Figure 8, square labels represent standard deviation, the octagons represent the Winsorized estimates, and the triangles represent CMADM. Again, the resistance of CMADM versus the standard deviation is clearly illustrated.

CONCLUSION

Preliminary results indicate that the classical Kalman filter will be a suboptimal design in the presence of heavy tailed non-Gaussian distributions. The theory of robust statistics and robust Kalman filters offers an important set of tools that can be used to optimize the design. Future research will be directed towards this goal.
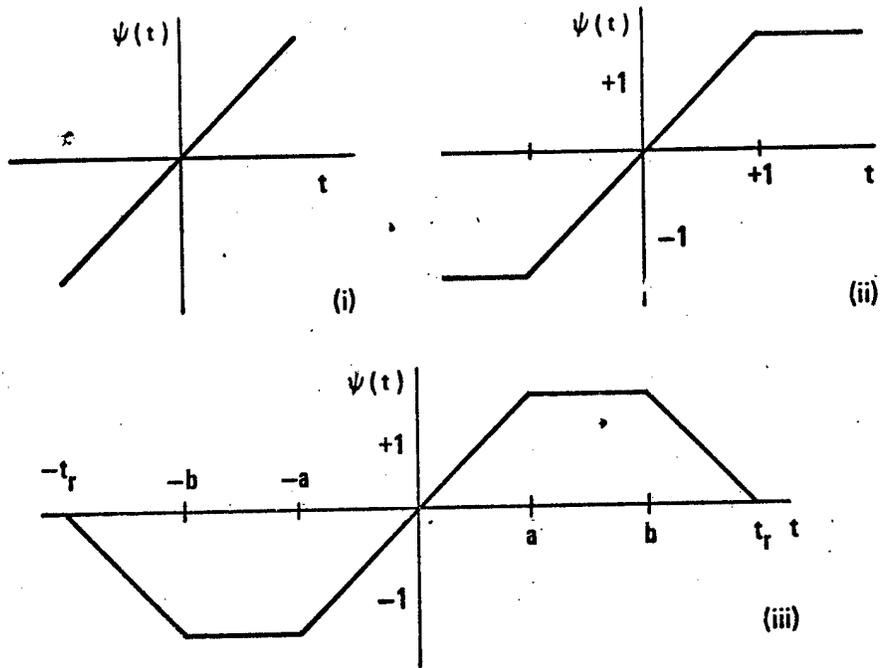
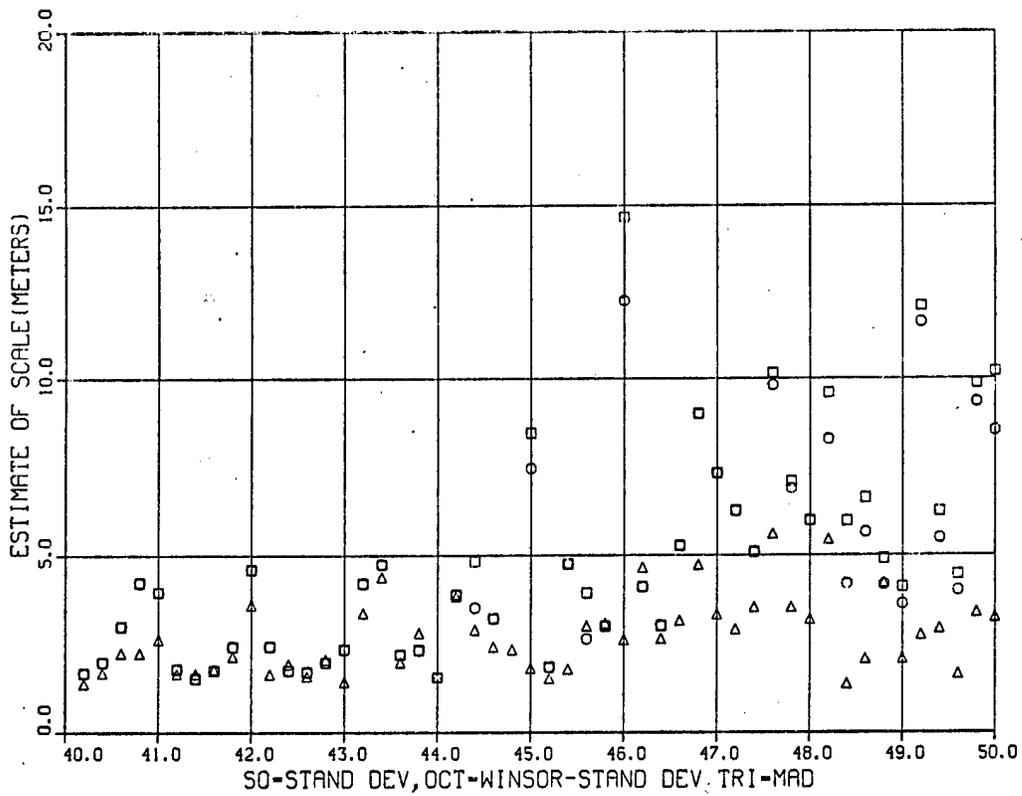## ACKNOWLEDGMENT

FIGURE 7.   Influence Functions

FIGURE 8.   Scale Comparison (N-Shape Glint).

REFERENCES

1. Masreliez, C. J. and Martin, R. D. "Robust Bayesian Estimation for the Linear Model and Robustifying the Kalman Filter," *IEEE Trans. on Auto. Control*, AC-22, pp. 361-371.

2. Pearson, J. B. and Stear, E. B. "Kalman Filter Applications in Airborne Radar Tracking," *IEEE Trans. on Aero and Elec. Systems*, AES-10, 1972, pp. 319-329.

3. Lancaster, P. *Theory of Matrices*, Academic Press, New York, 1969.

4. Zadeh, L. A. and Desoer, C. A. *Linear System Theory*, McGraw-Hill, New York, 1963.

5. Jazwinski, A. H. *Stochastic Processes and Filtering Theory*, Academic Press, New York, 1970.

6. Singer, R. A. "Estimating Optimal Tracking Filter Performance for Manned Maneuvering Targets," *IEEE Trans. on Aero. and Elec. Systems*, AES-6, 1970, pp 473-482.

7. Tukey, J. W. "A Survey of Sampling from Contaminated Distributions," *Contributions to Probability and Statistics*, Ed. Olkin, Ingram and others, Standford University Press, Standford, Calif., 1960.

8. Maybeck, P. S. *Stochastic Models, Estimation and Control*, Vol. 1, Academic Press, New York, 1979.

9. Bierman, G. J. *Factorization Methods for Discrete Sequential Estimation*, Academic Press, New York, 1977.

10. Mosteller, F. and Tukey, J. W. *Data Analysis and Regression*, Addison-Wesley, London, 1977, p. 203.

11. Huber, P. J. *Robust Statistics*, John Wiley, New York, 1981, p. 7.

12. Mumford, M. L. *Reflections Upon Target Modeling*, Naval Weapons Center Technical Memorandum 4124, Naval Weapons Center, China Lake, Calif., 1980.

13. Martin, R. D. "Approximate Conditional Mean Type Smoothers and Interpolators," Heidelberg Workshop on Smoothing Techniques for Curve Estimation, Heidelberg, Germany, 1979.

14. Martin, R. D. Unpublished Lecture Notes, Dept. of Statistics, University of Washington, Seattle, Washington, 1980.

Next page is blank.

A CASE STUDY OF MODERN DIRECT DIGITAL AUTOPILOT DESIGN

George B. Doane III, Sherman M. Seltzer, and H. Eugene Worley
Control Dynamics Company, Huntsville, Alabama 35801

ABSTRACT

This paper describes, by means of a missile autopilot design case study, a technique currently in use for determining the stability and dynamic characteristics of a digital control system in terms of several selected system parameters. The method requires that the system characteristic equation be available in the complex z-domain. It is the ability to handle more than one free system parameter, which need not be (but often is) a controller gain which makes this method more powerful than most design techniques. The paper also demonstrates the generation of the system equations by the Systematic Analysis Method. This method, an alternative to, for instance signal graph methods, is applicable to both simple and complex systems. The final design was evaluated by the method of Digital Control System Response by Cross-Multiplication.

INTRODUCTION

This paper is expository in nature concerning the design of digital control systems. The case study presented in this paper is that of the design of a missile digital autopilot. The methods used in the design are those currently in use to produce such designs which are coming about with ever greater frequency since the advent of the ubiquitous microprocessor. The paper traces through the formulation of the equations of motion, the rationale for autopilot transfer function selection, the application of the Parameter Plane Method of autopilot parameter selection and ends with a simulation to evaluate the missile response, at the sampling instants, to a test input. References are included so that readers may pursue in greater depth if they desire the details of the various procedures used.

PROBLEM FORMULATION AND AUTOPILOT DESIGN

The case study selected for this paper is that of an autopilot design of a tactical US Army missile. To formulate the study mathematically, the equations of motion of a missile were derived assuming planar motion. Thus two differential equations are required, one describing translation of the missile's center of mass in the plane, the other describing rotation of the missile airframe about the center of mass. With reference to Figure 1 the following quantities are defined:

$$F \triangleq \text{engine thrust force}$$
$$A \triangleq \text{aerodynamic axial force}$$
$$N \triangleq \text{aerodynamic normal force (note: N defined a positive quantity in the \underline{negative} 3b direction)}$$

M $\triangleq$ aerodynamic pitching moment about the center of mass

ℓo $\triangleq$ distance from vehicle center of mass to moment reference point

I $\triangleq$ polar moment of inertia of missile about an axis normal to the plane and directed through the center of mass

m $\triangleq$ the mass of the missile

g $\triangleq$ the acceleration due to gravity

1n, 2n, 3n $\triangleq$ designate unit vectors in the n-coordinate frame according to the usual right hand rule i.e., $1\hat{n}$ x $2\hat{n}$ = $3\hat{n}$

Rm $\triangleq$ the vector relating the origin of the r-coordinate system to the origin of the b-coordinate system (thus relating the missile's center of mass in the b-coordinates to the assumed inertial space coordinates i.e. the r-coordinate system)

θ $\triangleq$ the angle between the missile's longitudinal (roll) axis and the local horizontal (thus an inertial coordinate under the non-rotating earth assumption)

V $\triangleq$ the missile's velocity vector

α $\triangleq$ the angle between V and the missiles longitudinal axis
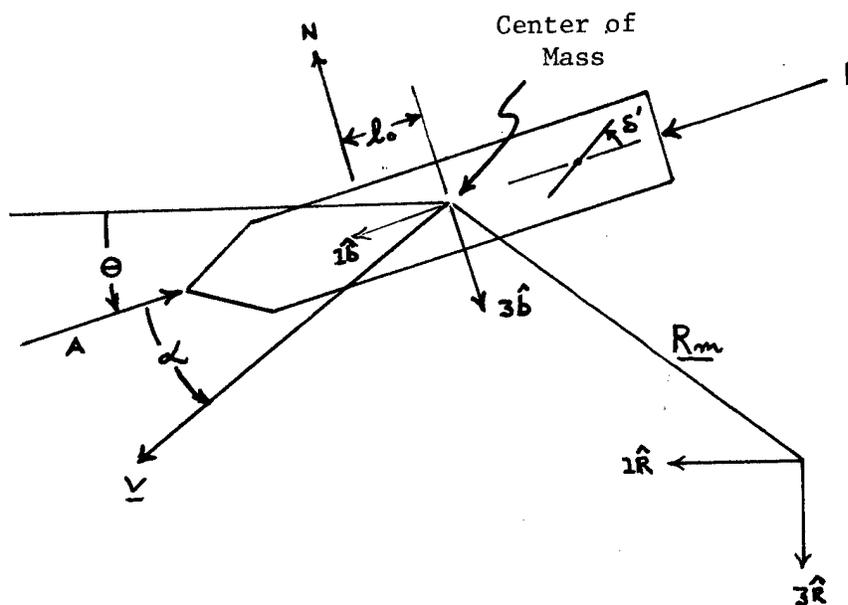
δ' $\triangleq$ aerodynamic fin deflection

Figure 1

The equations of motion are found by applying D'Alembert's Principle to obtain the translational and rotational differential equations

$$m \ \underline{\ddot{R}}m = (F-A) \ \hat{1b} - N \ \hat{3b} + mg \ \hat{3r} \tag{1}$$

$$I \ \ddot{\theta} = M - \ell oN \tag{2}$$

The vector notation has been omitted from equation (2) because of the assumed one degree of rotational freedom.

Typically there is only weak interaction or coupling between the translational equation (1) and the rotational equation (2). Thus this interaction will be, for the purposes of this paper, ignored. It is further assumed that the missile is in nominally level flight. Therefore the variable θ, usually denoted by

$$\theta = \theta o + \theta(t) \tag{3}$$

becomes merely $\theta(t)$. Linearizing the aerodynamics leads then to a transfer function between vehicle pitch rate and fin deflection of the form [1]

$$\frac{\dot{\theta}(s)}{\delta'(s)} = \frac{b \ (s + d)}{s^2 + 2\zeta\omega_n s + \omega_n^2} \tag{4}$$

For a particular missile in level flight this transfer function becomes

$$\frac{\dot{\theta}(s)}{\delta'} = \frac{(-216.6) \ (s + 0.693)}{(s^2 + 1.963 + 60.196)} \tag{5}$$

With negligible loss in modeling fidelity this may be approximated to

$$\frac{\dot{\theta}(s)}{\delta'} = \frac{(-216.6)(s)}{(s^2 + 60.196)} \tag{6}$$

This then is the pitch plane rotational transfer function with which the autopilot is to work such that the actual missile angular rate, $\dot{\theta}$, controlled by δ' (the fin angle) corresponds to a commanded angular rate $\dot{\theta}c$, furnished by the missile guidance system. For the sake of simplicity in early analyses it is assumed that the vehicle's angular rate, $\dot{\theta}$, is sensed perfectly and that the fin deflection, δ', follows perfectly its input command. If it is postulated that the missile rate, $\dot{\theta}$, should follow a step command of rate, $\dot{\theta}c$, with negligible error then the use of some form of integration process between the system error, $\dot{\theta}c-\dot{\theta}$, and the fin deflection, δ', is suggested. Recognizing that the damping of rotational motion of the missile is virtually non-existent and, indeed, is modeled as zero, suggests the use of some form of missile airframe rate feedback to fin deflection, δ', to stabilize the airframe rotation. The most efficacious autopilot algorithms

131

for final, eventual flight use are the subject of further study. However, the methodology expostulated above allows one to arrive quickly at workable first designs which could be evaluated in three or six degree of freedom simulations and "tuned up" as the results of such simulations, as well as more information, v.g. rate sensor and actuator models, becomes available. Based on these considerations one possible block diagram for the autopilot loop is given in Figure 2.
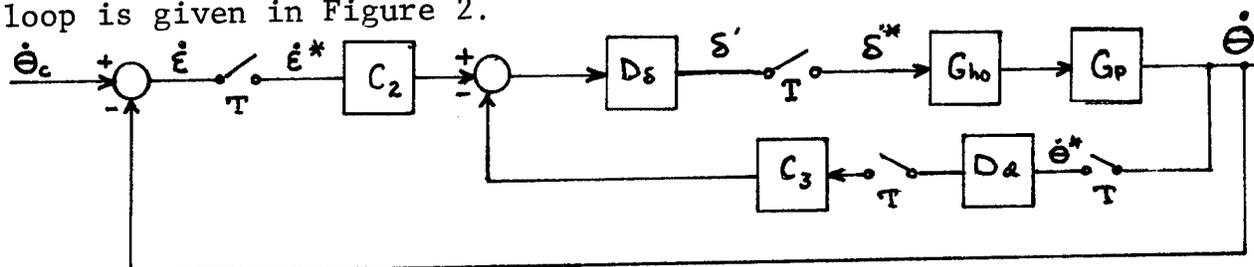

Figure 2

Starring denotes a sampled quantity and

D_i denotes a digital compensator transfer function

G_{ho} denotes the transfer function of a zero order or "box car" hold

G_p denotes the transfer function between missile angular rate, $\dot\theta(s)$, and the fin deflection, $\delta'(s)$.

T denotes sampling period of the synchronous samplers

A number of methods[2] are available with which to develop the transfer function between $\dot\theta$ and $\dot\theta c$, which is necessary to study stability and performance. The method used here, called the Systematic Analysis Method or SAM, is a general, easily applied technique applicable to both simple and complex systems. First one selects the variables at the inputs to the samplers as the unknowns. Then the original equations are written and tabulated in Table 1. If any of these equations contain the product of an unsampled system variable and an unsampled transfer function they are modified by substitution to eliminate unstarred (or unsampled) variables and tabulated in Table 1. Finally, a column in the table is constructed in which the equations from the first or second steps, as appropriate, are transformed into the sampled domain according to the relationships

$$(RG)^* = \overline{RG}^*$$
$$(RG^*) = R^*G^*$$
$$(R\ )^* = R^*$$

Application to the problem at hand yields for the first column

Original Equations

$$\dot\varepsilon(s) = \dot\theta_c(s) - \dot\theta(s)$$

$$\delta'(s) = D\delta(s)C_2\ \dot\varepsilon(s) - D\delta(s)C_3\ \{Dd(s)\dot\theta^*(s)\}^*$$

$$\dot\theta(s) = G_p(s)G_{ho}(s)\delta'^*(s)$$

132

and for the second column

$$\dot{\epsilon}*(s) = \dot{\theta}_c^*(s) - \dot{\theta}*(s)$$

$$\delta'*(s) = D_\delta^*(s)C_2\dot{\epsilon}*(s) - D_\delta^*(s)C_3D_d^*(s)\dot{\theta}*(s)$$

$$\dot{\theta}*(s) = \overline{G_p(s)G_{ho}(s)}* \ \delta'*(s)$$

Table 1

Lastly the desired input output relationship is found by substitution to be

$$(7)$$

$$\frac{\dot{\theta}*(s)}{\dot{\theta}_c^*(s)} = \frac{C_2\overline{G_pG_{ho}}*(s)D_\delta^*(s)}{(1+C_2D_\delta^*(s)\ \overline{G_{ho}G_p}*(s) + C_3\ D_\delta^*(s)D_d^*(s)\overline{G_{ho}G_p}*(s))}$$

or, expressed in the z-domain,

$$(8)$$

$$\frac{\dot{\theta}(z)}{\dot{\theta}_c(z)} = \frac{C_2\ \overline{G_pG_{ho}}(z)\ D_\delta(z)}{(1+C_2D_\delta(z)\ \overline{G_{ho}G_p}(z) + C_3D_\delta(z)\ D_d(z)\overline{G_{ho}G_p}*(z))}$$

Based upon the design goals and approaches expressed above D_δ should perform an integration operation whereas D_d should be selected such that missile rate propagates to fin deflection. These considerations suggest letting

$$D_\delta(z)D_d(z) = 1 \qquad\qquad\qquad (9)$$

and
$$D_\delta(z) = \frac{Tz}{(z-1)} \qquad\qquad\qquad (10)$$

where it is recognized that equation ten corresponds to the integration operation by means of a rectangular rule. The plant transfer function, $G_p(s)$, has already been tabulated as equation (6). The first order hold transfer function, $G_{ho}(s)$, is known to be

$$G_{ho}(s) = \frac{1-e^{-Ts}}{s} \qquad\qquad\qquad (11)$$

Thus

$$G_p(s)G_{ho}(s) = \frac{b\ s}{(s^2+\omega n^2)}\ \frac{(1-\epsilon^{-Ts})}{s} = \frac{b(1-\epsilon^{-Ts})}{(s^2+\omega n^2)} \qquad . \quad (12)$$

This becomes, in the z-domain,

$$\overline{G_{ho}G_p}(z) = \frac{b(sim\ \omega n^T)(z-1)}{\omega n(z^2-2(\cos\ \omega n^T)z+1)} \qquad . \qquad (13)$$

Substituting equations (9),(10), and (13) into (8) yields the desired overall transfer function

133

$$\frac{\dot{\theta}(z)}{\dot{\theta}_c(z)} = \frac{(^T C_2 b \, \sin \, \omega n^T) z}{L(z)} \qquad (14)$$

where $L(z)$ is the polynominal $\omega n \, z^2 + (^T b C_2 \sin \, \omega n^T - 2\omega n \cos \omega n^T + C_3 b \sin \omega n^T) z + (\omega n - b C_3 \sin \omega n^T)$ and where C_2 and C_3 are constants yet to be selected. The equation will be examined first to see how the missile responds to a unit step input. Applying a unit step of command and using the final value theorem (assuming a final value exists) produces

$$\lim_{nT \to \infty} \dot{\theta}(nT) = \lim_{z \to 1} \frac{z}{(z-1)} \frac{(z-1)}{z} \frac{\dot{\theta}(z)}{\dot{\theta}_c(z)} \qquad (15)$$

which when evaluated yields

$$\dot{\theta}(\infty) = \frac{T \, C_2 b \, \sin \, \omega n \, T}{T \, C_2 b \, \sin \, \omega n T + 2 \, \omega n (1 - \cos \, \omega n T)} \, . \qquad (16)$$

To continue, T was selected to be 0.10 second on reasonableness grounds, and b and ωn are missile parameter previously stated viz. -216.6 and 7.76 sec^{-1}. Substituting yields an expression for the limit in terms of the free parameter C_2 as follows

$$\dot{\theta}(\infty) = \frac{C_2}{C_2 - 0.276} \qquad (17)$$

Defining the error as the amount by which the output fails to attain a value of unity allows the construction of Table 2

% error	C_2
21.7	-1
5.24	-5
2.7	-10
0.5	-50

Table 2

Thus to keep the error indicated by this particular measure of performance below a few percent a value of C_2 less than -10 is indicated (note that, as will be shown below, C_2 must be negative to insure a stable system).

What remains to be done in this quick look design procedure is to select the free parameters, C_2 and C_3. This is done in such a way as to bound the static error as indicated in Table 2 and to meet stability requirements. Noting that there are two free parameters to select it is necessary to decide upon a particular technique. By freezing C_3, one might, for example, apply root locus or frequency response techniques in the z and w domains respectively. However, there is no need to specify either parameter independently of the other if one utilizes the Parameter Space Method[3] of design.

The method is based upon analysis and synthesis methods described in Siljak's monograph [4] as extended. Briefly put, the method allows one to map the location of the roots of the system's characteristic equation into a plane whose coordinates are the system's free parameters and which is readily divided into regions identified with system stability and instability. It is noted that the free parameters need not be gains but could just as well be some other system parameter. In addition to the characteristic root locations, such things as contours of constant relative damping factors and specified exponential time constants may be transformed as contours into the parameter plane. Thus in a manner somewhat reminiscent of the classical root locus a portrait may be presented of all pertinant aspects of the system's transient response with, however, the cogent difference that they may be presented as functions of several parameters rather than the simple parameter open loop gain. The method will be exemplified by application to the problem at hand viz. that described by equation (14).

As detailed in reference three, this design technique deals directly with the system's characteristic equation. As shown in the reference, the coefficients of the characteristic equation are cast if possible into the linear form

$$\sum_{j=0}^{2} (d_j K_0 + f_j K_1 + g_j) z^j \qquad (18)$$

for systematic generation of the computer program input data. If this linear combination is not possible, the method can still be used but becomes more tedious. In this form the K_0, K_1 variables are the parameters to be selected i.e. they are the coordinates of the parameter plane. It is convenient to fill out a table where columns are d_j, f_j, g_j. The transpose of these columns provide the input to the computer program used. Noting that the denominator of (14) corresponds to this problem's characteristic equation, allows the construction of Table 3 below.

j	d_j	f_j	g_j
0	$-b \sin \omega nT = +2.1632$	0	1.0
1	$b \sin \omega nT = -2.1632$	$Tb \sin \omega nT = -2.1632 \times 10^{-2}$	$-2 \cos \omega nT = -1.994$
2	0	ω_n 0	1.0

Table 3

In the particular computer program used the transpose of the d_j column becomes the A matrix, the transpose of the f_j column the B matrix and the transpose of the g_j column the F matrix. The program was run with the result exhibited as Figure 3.

By applying the appropriate "shading rules" (or factoring the CE for a number of test points) it can be established that the interior of the triangle in the C_2, C_3 plane corresponds to system stability i.e. a condition wherein all roots of the CE lie within the unit circle in the z-plane. Also plotted are contours of constant

135

relative damping factor, zeta, for two values i.e. 0.5 and 0.707.
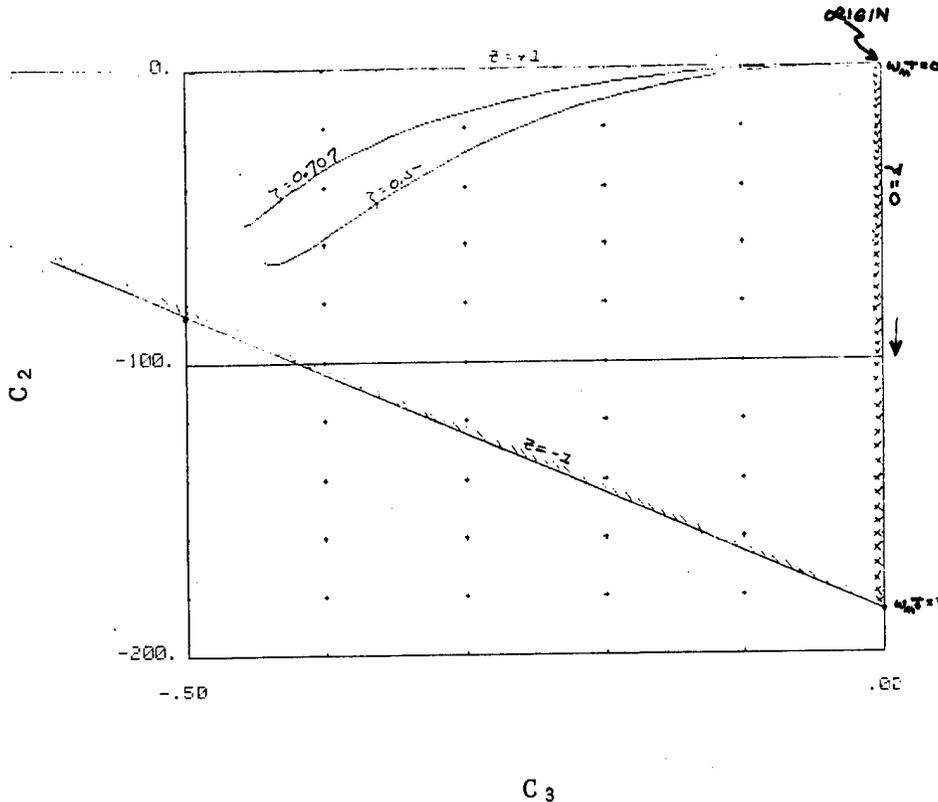

C_3

Figure 3

Although no system parameter sensitivity studies were performed on this example it seems prudent to stay some distance from the stability boundaries at this point in the design. Thus a set of values for C_2 and C_3 of C_2= -50 and C_3= -0.4 was chosen. One notes this point lies between the 0.5 and 0.707 zeta contours in the C_2-C_3 plane and at some distance from the various stability boundaries. In addition, the choice of C_2= 50 will insure a small error in response to a unit step, as previously discussed.

SIMULATION RESULTS

An evaluation of the response of the system at the sampling instants is presented as Figure 4. It was evaluated by means of a computer program implementing the "Determination of Digital Control System Response by Cross-Multiplication" as presented by Seltzer in reference five. The input to this program consists merely of the coefficients of the numerator and denominator polynomials of the overall transfer function (equation 14) and for plotting purposes
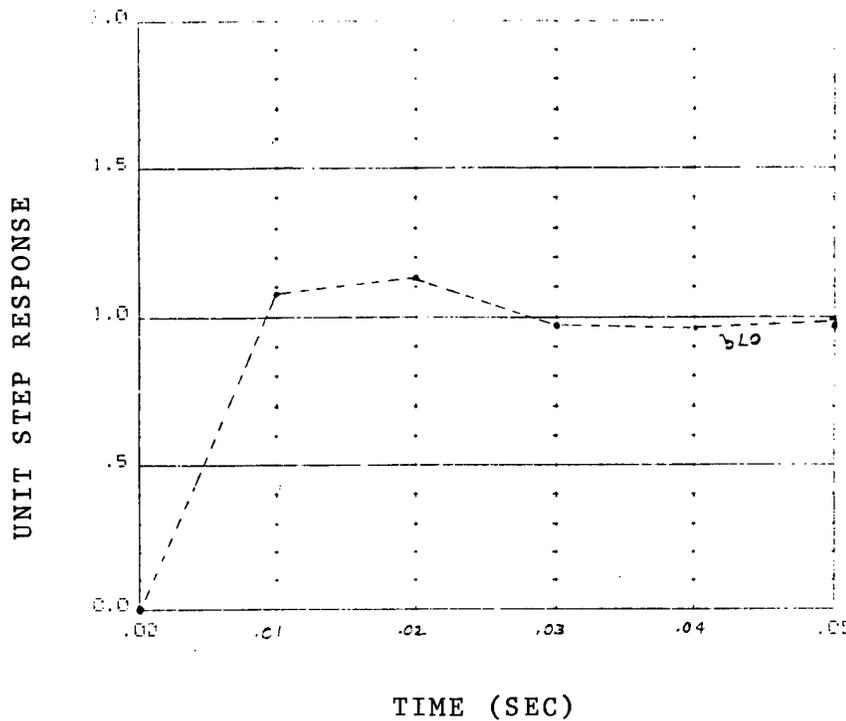
the sampling interval, T.

TIME (SEC)

Figure 4

From the Figure and the associated printout it is seen that the maximum percent overshoot occuring at the sampling instants is

$$\% \text{ o.s.} = \frac{1.126 - 1.000}{1.00} \times 100 = 12.6\%$$

which occurs at the third (nT = 0.02 sec) sampling instant. This compares favorably with Franklin and Powell's [6] approximation relating percent overshoot to relative damping factor for a second order system with no finite zeros

which is

$$\zeta \leq (0.6)(1 - \frac{\% \text{ o.s.}}{100})$$

here then

$$\zeta \leq (0.6)(1 - \frac{12.6}{100}) = 0.52$$

The degree of correlation can be judged when it is recalled that the C_2, C_3 values were chosen such that their set of values lay between the $\zeta = 0.5$ and $\zeta = 0.707$ loci.

137

CONCLUSION

Presented in this paper, by means of the case study of a digital autopilot design, is a modern method of designing digital control systems without regard to continuous system considerations. The Parameter Space Method of generating free system parameter values is employed to ensure stability in both the absolute and relative sense. Sufficient detail has been included such that, given the availability of Parameter Space and Response Cross-Multiplication computer programs, one may rapidly and methodically design digital control systems and keep them updated as plant characteristics change. This capability is especially useful during the initial design phases of a system. The methods presented are currently being used in the design of US Army missile autopilots, space vehicles control systems and have been used to design aircraft control systems. It is of course understood that when final configurations become available the total system design would be validated by appropriate simulation. Such simulation would include time varying, non-linear and certainly more detailed descriptions of the system and its components v.g. the missile fin actuation subsystem. In fact such additional simulations have been performed in various instances and confirmed the efficacy of the design method. Additional work needs to be done in such areas as mapping points on the real axis of the z-plane into the parameter plane in order to control further the system response time.

REFERENCES

1. S. M. Seltzer and H. E. Worley, "Analysis of Sampling Rate On SAM Accuracy", US Army Missile Command, Final Report on Contract DAAH01-81-M-A118.
2. S. M. Seltzer, "SAM: An Alternative to Sampled-Data Signal Flow Graphs", Technical Report T-79-49 US Army Missile Research and Development Command.
3. S. M. Seltzer, "Application of the Parameter Space Method to Aerospace Vehicle Digital Control System Design", IEEE Transaction on Automatic Control, Vol. AC-26, No. 2, April 1981.
4. D. D. Siljak, "Nonlinear Systems", New York, Wiley, 1969.
5. S. M. Seltzer, "Determination of Digital Control System Response by Cross-Multiplication", Conference Proceedings IEEE Southeastcon '81, Huntsville, Alabama, April 5-8, 1981.
6. G. F. Franklin and J. D. Powell, "Digital Control of Dynamic Systems", Addison-Wesley Publishing Company, 1980.

ROBUST MISSILE GUIDANCE
D. O. Molnar
The Boeing Aerospace Company,
Guidance and Navigation Technology Group,
P. O. Box 3999,
Seattle, Washington 98124

GENERAL INTRODUCTION

INTRODUCTION

A new guidance law is derived for tactical missiles that undergo significant acceleration and drag. Past guidance laws based on constant velocity missile dynamic engagement models result in sub-optimal trajectories when applied to missiles used most often in tactical engagements. Recall that in most tactical engagements the missile accelerates (booster burn, or "boost to mach") and coasts to intercept. The new guidance law is based on a more complete dynamic engagement model that contains the missile expected axial accelerations and the control direction constraint normal to the missile velocity vector. The non-linear two point boundary value problem [1] is solved by separating the missile axial velocity dynamics from the control dynamics to obtain a time varying linear dynamic constraint model. The results are verified by simulation, and indicated significant performance improvement in a crossing target surface to air engagement.

The history of short range missile guidance is very rich, for an excellent summary the reader is referred to an article by Pastrick et. al. [2]. We assume, as before, that a well designed missile autopilot is implemented; so that for guidance law derivation we can assume a simple relationship between commanded accelerations and missile response [1-6,8,9]. We also assume that the intercept time is know or approximately known by estimation, [2,3,9]. Under benign conditions any monotonic function of predicted miss can serve as the guidance law. However the more optimal use of hardware resources is made possible by implementation of more nearly optimal guidance laws which will translate into more robust guidance, or wider engagement envelope. The optimal guidance law derived here can be reformulated as a biased PNG guidance law. Hence the bias values can be computed at a reduced rate for computer implementation economy. The traditional approximations are: Two-dimensional motion, Point-mass, Instantaneous Control response, linear dynamic model, and constant speed [9]. Non linearities are traditionally ignored to facilitate the use of linear optimization methods to obtain the desired feedback control law. In this note we retain the Point-mass approximation, and use a slightly more accurate dynamic model, and incidentally provide a new explanation of three dimensional PNG.

PAST RESULTS

The Proportional Navigation Guidance (PNG) was shown to be optimal by Bryson [1] if neither missile or target are accelerating. Three dimensional guidance including the effects of accelerating target and new methods of estimating the time of intercept have been presented [4,3]. Recall that 'optimal' has only meaning relative to the cost function minimized and the dynamic constraint model used. The relative completeness of the dynamic constraint model is the issue of this note. Expected missile acceleration have in the past been included in the time-to-go to intercept calculation, but not included in the dynamic constraint model used in the optimal guidance law calculation. Because of past use of inconsistent dynamic constraint models [1,3-5], the resulting guidance laws generated unusable control commands along the missile velocity axis.
In this paper we also show that the same constant missile and target dynamic models are used in

deriving both PNG [1] and the 'optimal' three dimensional control law of Riggs [3]. And hence the improved guidance performance reported in [3] is the result of using better time-to-intercept calculations than is implicit in PNG.

The problem of target tracking in the presence of noise is not considered here. However the improved guidance law presented here leaves more control authority for countering unexpected target maneuvers. Also the target is assumed to be non accelerating, control modifications to account for random target accelerations might be included as in [4]. We next summarize the result of Reference [3], for use as the starting point for the developments of this note.

A LINEAR OPTIMAL GUIDANCE PROBLEM SOLUTION

Consider the dynamic model, Equation (1), of the missile engagement relative to the target, with no target acceleration, as used in References [3-5]. The optimal guidance problem (or the two point boundary value problem) is to minimize the cost function (2) subject to dynamic constraints (1), with time of intercept given.

$$
\left.
\begin{array}{l}
dR/dt = V \\
dV/dt = -u
\end{array}
\right\}
\tag{1}
$$

where :

R = relative position vector of missile from target in inertial coordinates

V = $V_t - V_m$ = relative velocity vector of missile from target

u = missile control acceleration vector (not constrained in direction or magnitude)

The cost function 'J' is given by (2):

$$
J = R(t_f) \cdot R(t_f)/2 + \int_t^{t_f} B \ u(t) \cdot u(t)/2 \ dt
\tag{2}
$$

(i.e. terminal miss plus integrated cost of control weighted by B).

Recall from references [1 & 3] that the solution to the optimal guidance problem is:

$$
u = -\Lambda \ t_g [R + V \ t_g] \ /(3 B + t_g^3)
\tag{3} *
$$

where: $t_g = (t_f - t)$ = estimated time-to-go to intercept is given

140

It is well to note that the <u>dynamic model</u> Equation (1) contains no provision for the expected missile boost acceleration and drag. Also note that the acceleration control vector 'u' is in the plane spanned by (R,V) vectors. Since the missile velocity vector 'V_m' is not necessarily in the (R,V)-plane, the control vector 'u' may have a component along 'V_m'. In other words axial acceleration is commanded which is typically not usable.

In appendix A it is show that Equation (3) reduces to the familiar Proportional Navigation Guidance (PNG) law Eq. (4), if (a) 't_g' is estimated by range/range rate, and (b) use of control effort is not penalized, (B = 0).

$$\mathbf{u} = - \Lambda \, \dot{\sigma} \, \dot{R} \mathbf{p} \tag{4}$$

where

$\dot{\sigma}$ = angular rotation rate of the line-of-sight
vector in inertial space (**)

$\dot{R}$ = missile closing rate on target

Λ = guidance gain factor equal to 3;
used as a design parameter with value 3 to 6

$\mathbf{p}$ = unit normal to line of sight vector in the (R,V) plane

---

*   See Bryson [1, pp287; Eq. 9.4.27] The equivalence is apparent if the energy coefficients are equated as follows: $C_p = 1$, and $C_e = 0$, with $\Lambda = 3$.

(**)   This concept of coordinate free vector rotation in three-space is the key to generalized Proportional Navigation concept. To appreciate the simplification achieved by this concept compare the results developed here with [7].

In other words, the improved guidance performance of Eq. (3) is the result of including the effect of expected missile axial acceleration in the time-to-go estimation; since both guidance laws (3) and (4) are based on dynamic constraint models that do not include anticipated missile accelerations. Next we develop the more accurate dynamic constraint model that includes the expected missile acceleration, which together with the cost function results in the improved guidance law, ~~introduced above~~.

NEW OPTIMAL CONTROL LAW FOR ACCELERATING MISSILES

The new optimal control law is based on the two point boundary value mathematics [1] as above, but using a more complete dynamic constraint model as derived next. Consider the inertial acceleration equation (1), with the missile inertial acceleration expressed as orthogonal components relative to the missile velocity vector as follows:

$$dV_m/dt = \dot{\theta} \times V_m + \dot{V}_m \tag{5}$$
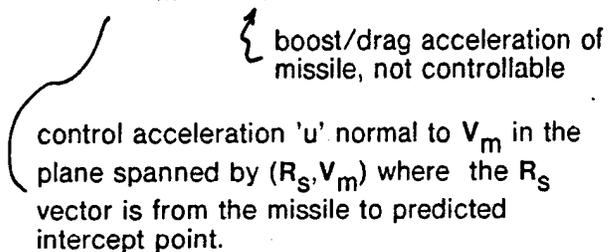
{ boost/drag acceleration of missile, not controllable

(control acceleration 'u' normal to V_m in the plane spanned by (R_s, V_m) where the R_s vector is from the missile to predicted intercept point.

Equation (5) constitutes the modifications to (1) which results in the new more accurate dynamic constraint model (6) summarized below.

MISSILE TARGET DYNAMIC MODEL THAT INCLUDES EXPECTED MISSILE ACCELERATIONS

The new dynamic missile-target engagement model is given by Eq.(6).

$$dR/dt = V$$

$$dV/dt = -a_m - u$$

$$a_m = \begin{cases} a & \text{for } t < t_b \\ -a_D & \text{for } t > t_b \end{cases}$$

missile axial acceleration boost and drag

$$\dot{\theta} = u/V_m = \text{inertial turning rate of missile velocity vector}$$

(6)

142

where:

a , a_D = missile expected boost & drag acceleration along V_m

V_m = missile velocity vector in inertial coordinates

u = control acceleration applied in the plane normal to the missile velocity axis. (the direction is defined later by the control law)

t_b = missile boost burn out time

As noted above, this model is more complete than past dynamic constraint models used for guidance law derivation. Selected variables are illustrated in Figure 1. below.
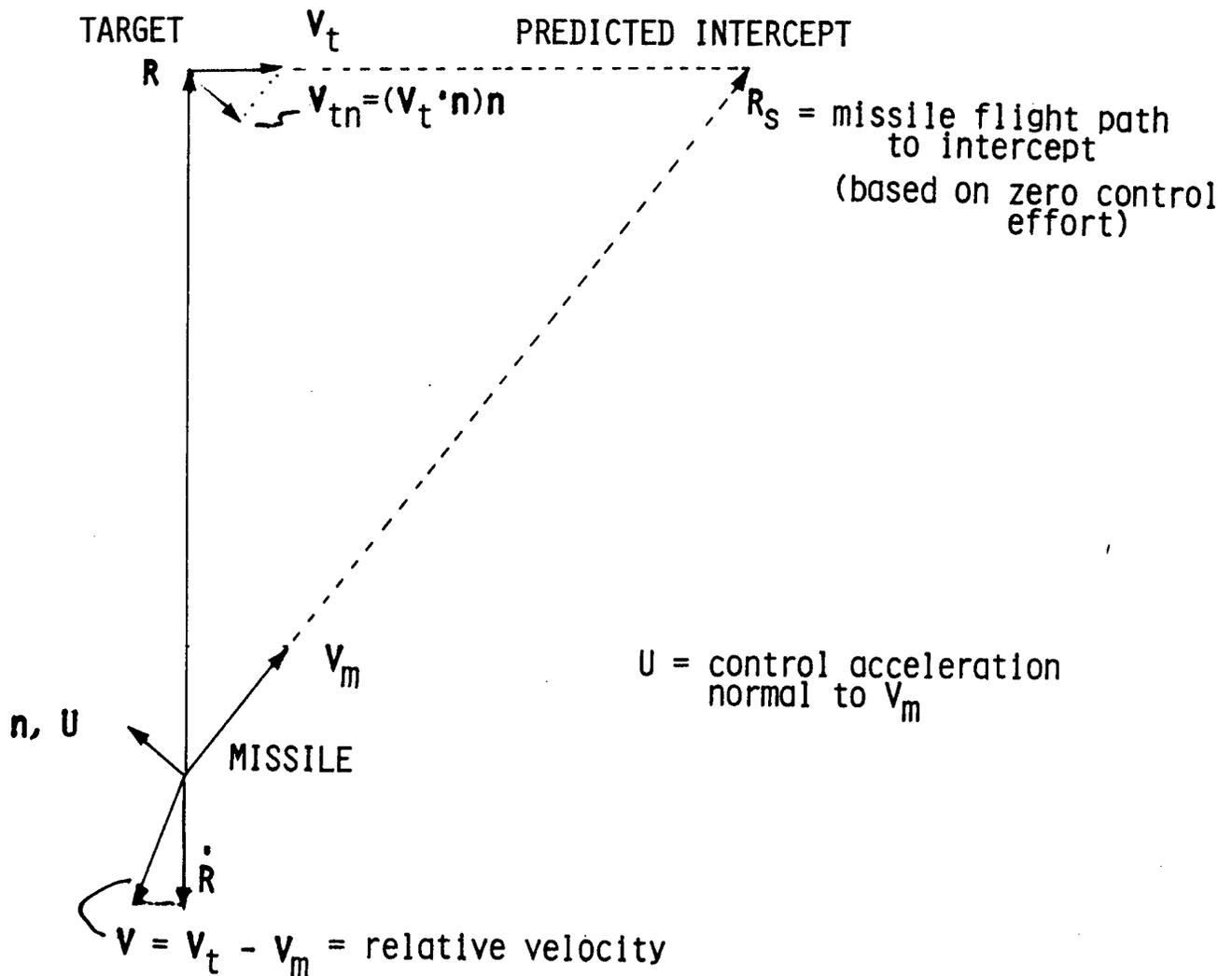
TARGET V_t PREDICTED INTERCEPT

$V_{tn} = (V_t \cdot n)n$

R_s = missile flight path to intercept (based on zero control effort)

U = control acceleration normal to V_m

V_m

MISSILE

n, U

$\dot{R}$

$V = V_t - V_m$ = relative velocity

Figure 1. Illustration of missile-target parameter; where R_s= missile estimated path length to intercept.

NEW OPTIMAL CONTROL LAW SOLUTION

The non linear dynamic constraints are changed to a linear time varying constraint by use of the assumed separability of the missile axial dynamics from the control dynamics, see Eq. (6). It is convenient to formulate the 'zero effort predicted miss function' normal to the missile velocity vector (*). The other inertial coordinate system axis is <u>along</u> the missile velocity vector; for which the time history of the missile is specified by the expected accelerations, (see time-to-go calculation in Appendix B). In actual implementation of the guidance law the missile target data may be available in arbitrary coordinate system which we anticipate by our use of coordinate free vector notation.

Consider Eq. (6) with the inertial axis oriented along the missile velocity axis so that Θ is small. In this case the component of predicted zero effort final miss orthogonal to the missile velocity axis is:

$$z = \int_{t}^{t_f} V_{tn} \, d_t + z_0 + \Theta R_s n \tag{7}$$

where:

$$V_{tn} = (V_t \cdot n) \, n = \text{component of target velocity}$$
$$\text{normal to missile velocity axis}$$

$$n = \text{unit normal to } V_m \text{ in the } (R_s, V_m) \text{ plane}$$

$$z_0 = (R \cdot n)n$$
$$= \text{component of range vector } (\cdot R)$$
$$\text{normal to missile velocity axis}$$
$$\Theta = 0 = \text{current attitude of } V_m \text{ in the inertial reference frame}$$

Figure 1 is a summary of the above illustrating the variables of interest for this guidance law derivation.

Differentiating Eq. (7) and substituting from Eq. (6) yields the terminal miss dynamic equation (8) in terms of the control vector:

---

* Past guidance law predicted miss formulations are normal to the line of sight vector, [1,2,4,5]; which is also implicit in [3] because of the equivalence to PNG presented above.

144

$$\dot{z} \quad = \quad \text{-u } R_s/V_m \tag{8}$$

where

$$R_S \quad = \quad V_m(\xi)\xi \cdot \xi^2 a/2 + (a + a_D)(\xi \cdot T_x)U_s(\xi \cdot T_x)/2 \tag{9}$$
$$= \quad \text{the predicted path length traveled by the missile to intercept in terms of time-to-go}$$

$$T_x \quad = \quad \text{the time between target intercept}$$
$$\text{and missile boost burn out time } (= t_f \cdot t_b)$$

$$U_s \quad = \quad \text{the unit step function}$$

$$\xi \quad = \quad \text{variable of integration equal to 't}_g\text{'}$$

Using the familiar methods of optimal control [1]; we obtain the control in terms of __final__ predicted miss (z_f) :

$$u \quad = \quad -(z_f/B)(R_s/V_m) \tag{10}$$

Equation (10) is substituted into (8) to obtain the terminal miss differential Equation:

$$\dot{z} \quad = \quad -(z_f/B)(R_s/V_m)^2 \tag{11}$$

With some effort Equation (11) is solved and is substituted into Eq. (10) to give the desired optimal guidance law Eq. (12):

$$\boxed{u \quad = \quad R_s \, z \, /[V_m \{ B + t_g^3/3 + D \}]} \tag{12}$$

Where :

$$D = \{ F(a_m, V_c, B_v, V_b) - F(a_m, V_c, B_v, V_m)$$

$$+ F(a_D, V_f, V_f, V_b) - F(a_D, V_f, V_f, V_f) \} U_s(t_b \cdot t)$$

$$+ \{ F(a_m, V_f, V_f, V_m) - F(a_m, V_f, V_f, V_f) \} U_s(t \cdot t_b)$$

The function 'D' is expressed in terms of the unit step function '$U_s(.)$' and function 'F' which is defined as follows:

$$F(a, V_c, B_v, V) =$$

$$\{ -V^3/4 + V_c V^2 - (V_c^2 + B_v/2)V - (B_v/2)^2 /V \}/a^3$$

where:

$$B_v = V_c - (a + a_D)a \, T_x$$

V_f = estimated final velocity of the missile

V_b = estimated missile velocity at burn out

$$V_c = V_f + (a + a_D)T_x$$

It is well to note that the above guidance law reduces to the familiar Proportional Navigation Guidance law if the missile axial velocity remains constant and if the missile axis is aligned with the line-of-sight to the target. The scalar function 'D' becomes zero for constant missile velocity. The factor (R_s/V_m) denotes expected missile path length to target divided by missile velocity becomes 't_g', the time-to-go. And the remaining zero effort miss distance 'z' becomes equal to the product of Range, angular line of sight rate, and 't_g', $z = (\dot{\sigma} R \, t_g)$.

146

SIMULATION RESULTS

To illustrate the guidance laws, we simulate a Surface-to-Air (SAM) engagement scenario. For this guidance law performance evaluation, we represent the "real world" missile by Eq. (1) together with a first order lag imposed on the control acceleration of 0.3 sec; and a maximum limit on control of 3g.

THE ENGAGEMENT GEOMETRY AND RESULTS

The target travels at a constant velocity of 500 ft/sec, and is crossing initially, at which time the missile velocity is 50 ft/sec; see Figure 1. The missile accelerates for 2 sec at 20g . Figure 2 indicates the benefit of the more complete guidance law, Eq. (12), note the reduced miss distance. Figure 3 indicates the control accelerations associated with the trajectories indicated in Figure (2); note that the new guidance law uses less control effort to intercept the target than the other guidance laws (3) and (4), leaving more control authority to counter unexpected target maneuvers. Recall that the missile axial velocity is assumed not controllable, hence a component of the commanded acceleration due to Eq. (4) or (5) along the missile velocity vector is not used.

Recall that the true time of intercept (t_f) is unknown, hence various algorithms have been proposed to estimate $t_g = (t_f\text{-}t)$, the remaining time to intercept [2,3,6].

Further guidance law refinement are possible if we include the effect of missile auto pilot dynamic delay into Eq. (6). Another improvement is the inclusion of control normal to the body axis rather than normal to the velocity vector as assumed above.

Of potentially greater performance benefit would be the combining of the target tracking and missile guidance problems.

CONCLUSION

We have derived a new guidance law for missiles experiencing significant axial acceleration. This guidance law is demonstrated to give superior intercept performance compared to PNG and another "optimal" guidance law in a surface-to-air intercept scenario. This guidance law is obtained through the use of modern control methodology applied to a more complete kinematic missile target engagement model. The kinematic constraint model used includes the missile axial accelerations and the constraint on the direction of the missile control effort normal to the velocity vector. The resultant non-linear dynamic model is solved by first solving the axial dynamic equation, which results in a time varying linear dynamic constraint model. Recent "optimal" guidance laws have used missile acceleration estimates in the estimation of the "time-to-go" to intercept, however have not included acceleration in the missile-target dynamics as in this note.

147

BSTHM   1221DXXS   PNG, *SAM* SCENARIO
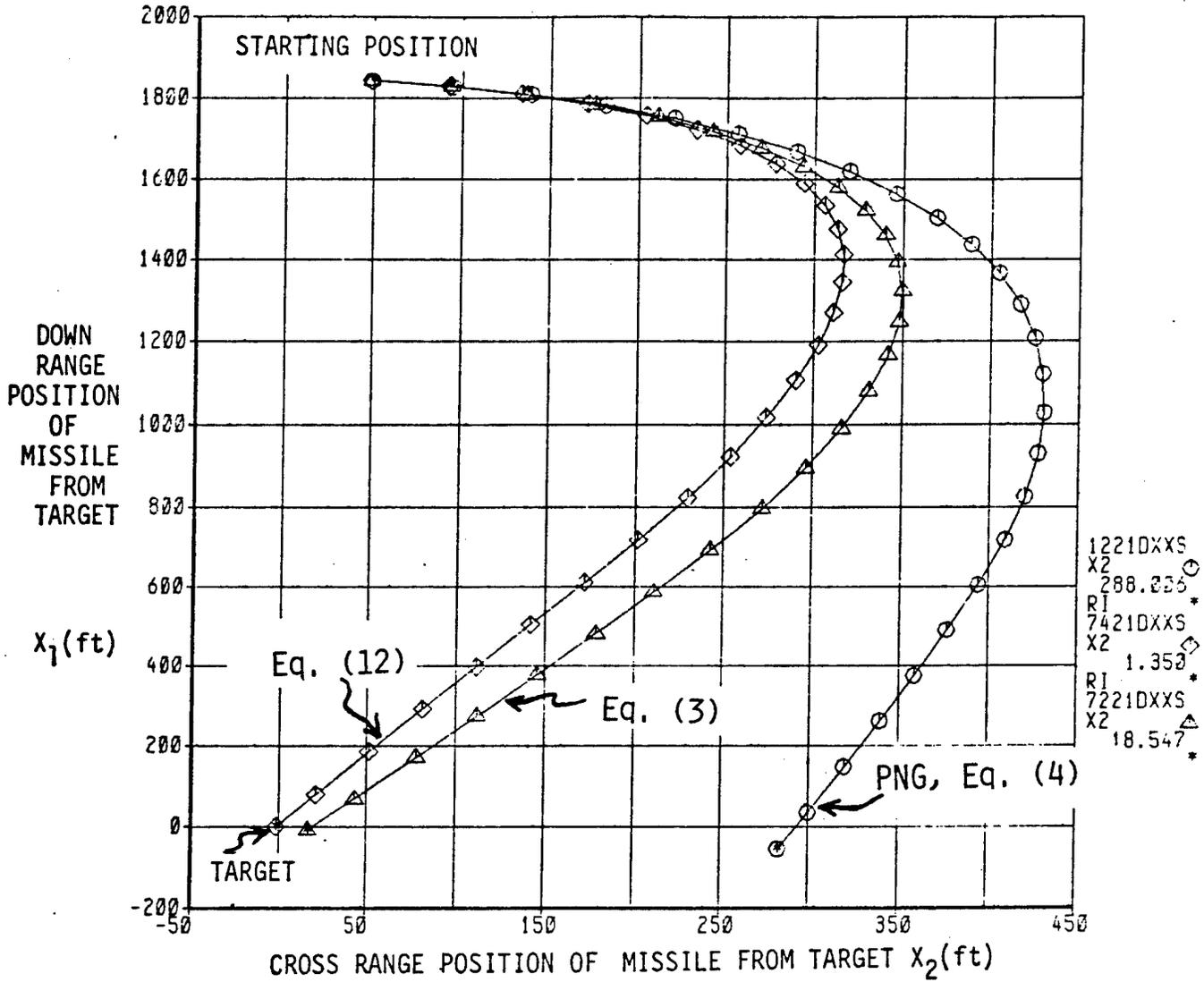GN = 3.0; B = 0.000; RI = 288.006 AT TI = 2.580

Figure 2.

Relative Trajectory of Missile to Target Illustrating Sensitivity to control laws; Equations (3), (4) and (12), resulting in terminal miss distances of 18.5 ft, 288 ft, and 1.4 ft respectively. With time-to-go estimated by Eq. (13).
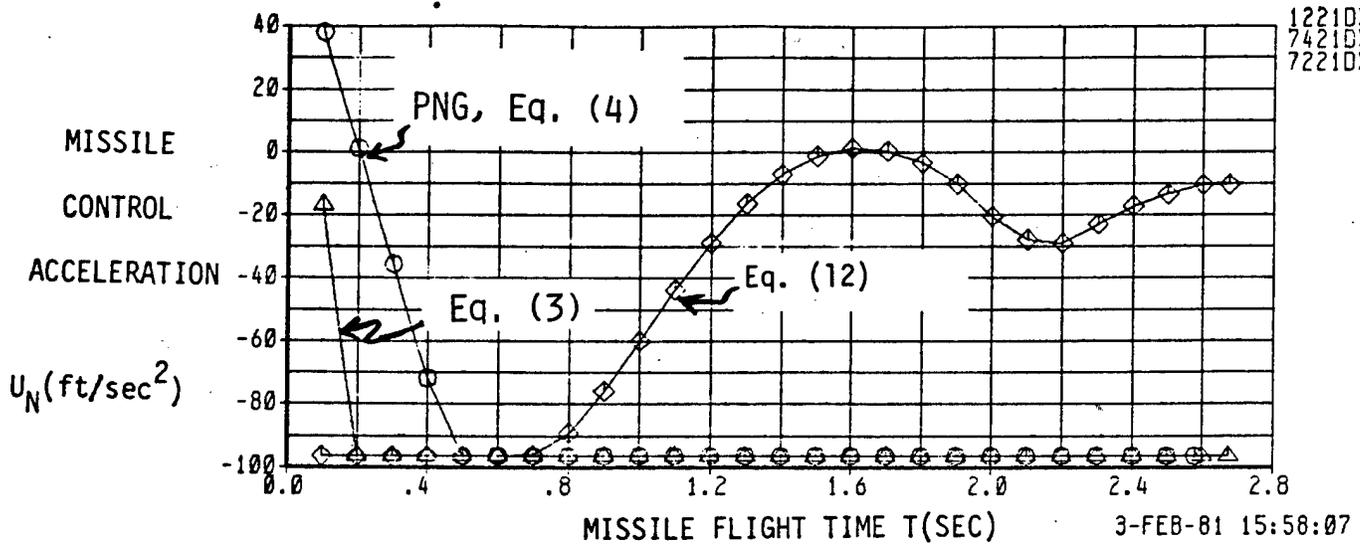
Figure 3.

Control acceleration normal to missile velocity axis; note that less control authority is used with new guidance law, leaving more for countering target maneuvers. Maximum control effort is limited to 3 g's.

The optimal guidance law of Riggs et. al. [3] is shown to be equivalent to PNG under less restrictive conditions. The conditions for the equivalence of equations (3) to equation (4) are: (a) the time to go 'tg' intercept is range divided by range rate, and (b) the optimal guidance cost function assign zero penalty to control effort; see the cost function Equation (2).

Consider figure A1, where we indicate the orthogonal coordinate system with one axis along the line of sight vector 'R', and the normal 'p' to 'R' in the (R,V)-plane.

$$\dot{\sigma} = \cdot V_p / R$$

$$V = V_t \cdot V_m$$

$$V_m$$

$$\dot{R} = (V \cdot R) R / R^2 = \dot{R} r$$
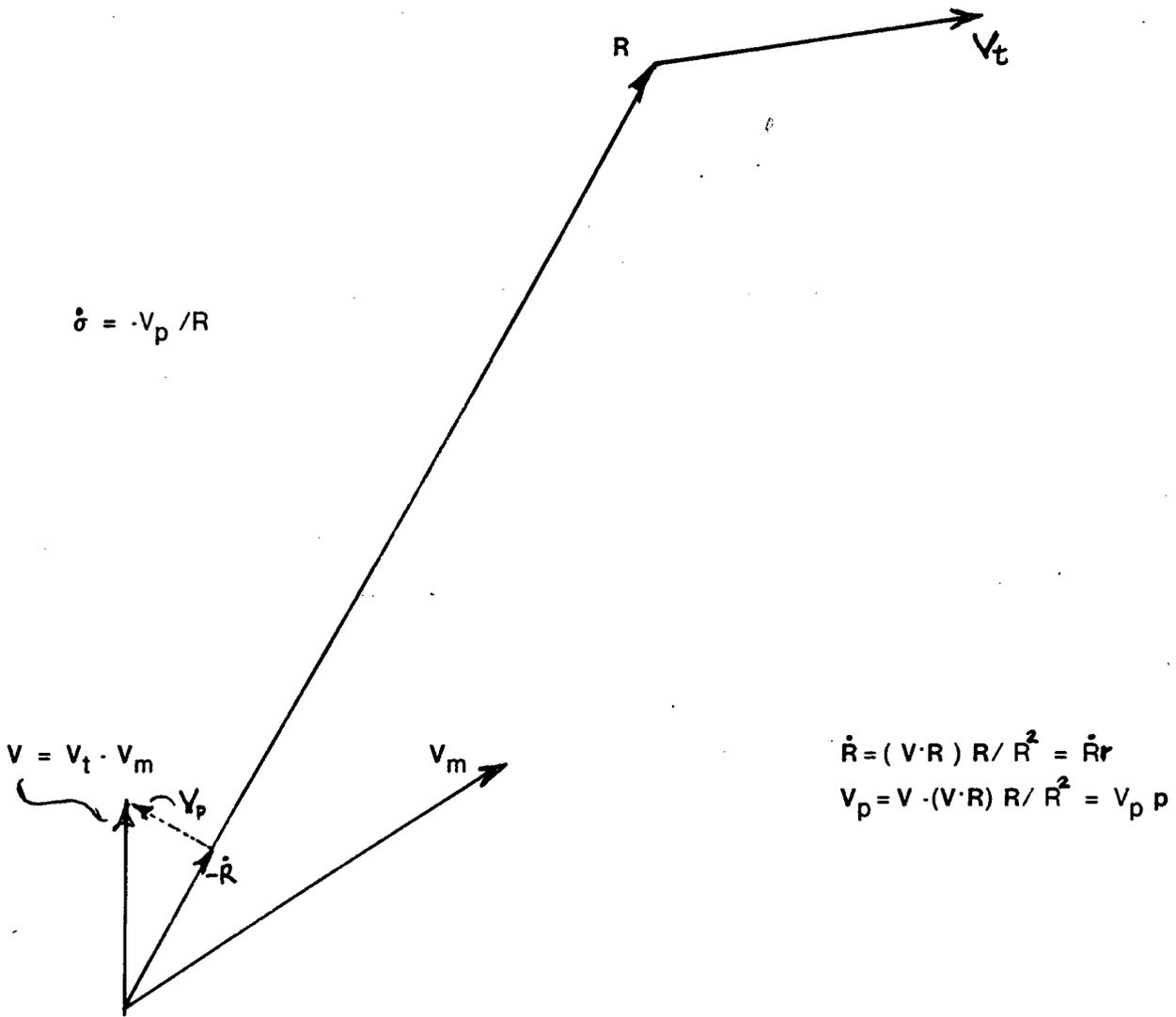
$$V_p = V \cdot (V \cdot R) R / R^2 = V_p \, p$$

Figure A1 Vector and Scalar quantities for three dimensional PNG

Consider the orthogonal unit basis vectors (r,p) along the line of sight vector and normal in the (R,V)-plane as indicated in Figure A1.

It is convenient to define the following :

$$\mathbf{R} = R\,\mathbf{r} = \text{the line of sight vector}$$

$$\mathbf{V} = \dot{R}\,\mathbf{r} + V_p\,\mathbf{p} = \text{relative velocity} \;(\,V_t - V_m)$$

$$t_g = -R/\dot{R} \qquad \text{time-to-go to intercept}$$

(A1)

Substituting definitions A1 into Eq. (3) with B = 0, gives:

$$u = -\Lambda\,t_g\,[\,\mathbf{R} + (\dot{R}\,\mathbf{r} + V_p\,\mathbf{p})\,t_g\,]\,/\,tg^3 \tag{A2}$$

$$u = -\Lambda\,\dot{R}^2\,[\,R\,\mathbf{r} + \dot{R}\,(-R/\dot{R})\,\mathbf{r} + V_p\,(-R/\dot{R})\,\mathbf{p}\,]/\,R^2 \tag{A3}$$

$$u = -\Lambda\,V_p\,(\dot{R}\,/R\,)\,\mathbf{p} = -\Lambda\,\dot{R}\,\dot{\sigma}\,\mathbf{p} \tag{A4}$$

Where the concept line of sight vector rotation rate in inertial space is represented by $\dot{\sigma}$. Note that Equation A4 is the familiar PNG guidance law with the gain factor Λ = 3; typically Λ is made to take on values between 3 and 6, in order to more quickly head the missile to the predicted intercept point. Various time-to-go 't_g' algorithms have been developed [2,3], it is noted that the use of smaller than true 't_g' improves performance, and is equivalent to varying Λ. This observation is indicative of the inconsistency of using the above control laws (3,4) in a situation where the actual missile dynamics does not have axial velocity control, and moreover experiences uncontrolled boost acceleration to 'mach' and drag.

151

APPENDIX B TIME-TO-GO TO INTERCEPT ESTIMATION

The estimation of the time of target intercept is motivated by the subsequent great simplification of the general (free final time) two point boundary value problem [1].

Consider Equation (6), and note that for zero control effort, the missile velocity and path length is uniquely specified by (a) the initial velocity, (b) the expected axial acceleration, and (c) the time-to-go to intercept. Both the missile velocity and the remaining path length are expressed in terms of 't_g', hence the indicated solution (B1) is obtained.

$$t_g = [\cdot C_1 \cdot Sqrt(C_1{}^2 \cdot 2 \, a_D \, C_0)]/ \, a_D \tag{B1}$$

where during missile boost; or $t < t_b$ and $t_f > t_b$

$$C_0 = R \cdot (a \cdot a_D)(t_b \cdot t)^2/2$$

$$C_1 = dR/dt + (a \cdot a_D)(t_b \cdot t)$$

and for after burn out we use; ($t > t_b$, $t_f > t_b$)

$$C_0 = R \; ; \; and \; C_1 = dR/dt$$

where:

t_b = missile boost burn out time.

For convenience we repeat a time-to-go estimation algorithm used in Reference [3]; and provide a comparitive illustration in Figure B1.

```
DATA R,U,A,DT,TB,TF/3500.0,-1000.0,-600.0,0.04,1.6,2.175/
C
88     CONTINUE
          TT = TF-T
C
C                                    TT = TRUE TIME-TO-GO
C
       TG1 = -R/U
                                 TG1 = RANGE/(CLOSING VELOCITY)
                                       IMPLICIT IN PNG; SEE APPENDIX B
C
C
       TG3 = 2.0*R/(-U + SQRT(U*U - R*A/0.75))
C
                                    TG3 = TIME TO GO; RIGGS, AGARD
C
C
       TG6 = (R - A*(TB - T)**2/2.0)/(-U - A*(TB - T))
C
                                       TG6 = NEW ACCURATE TIME TO GO ESTIMATE
C
C
C
C
       T = T + DT
                                  T = TIME
       IF (T.GT.TB) A = 1.0E-5*U*U
                                  A = ACCELERATION ALONG
                                      LINE OF SIGHT
       U = U + A*DT
                                  U = CLOSING VELOCITY
       R = R + U*DT
                                  R = RANGE TO TARGET
       IF (R.GT.-500.0) GOTO 88
```
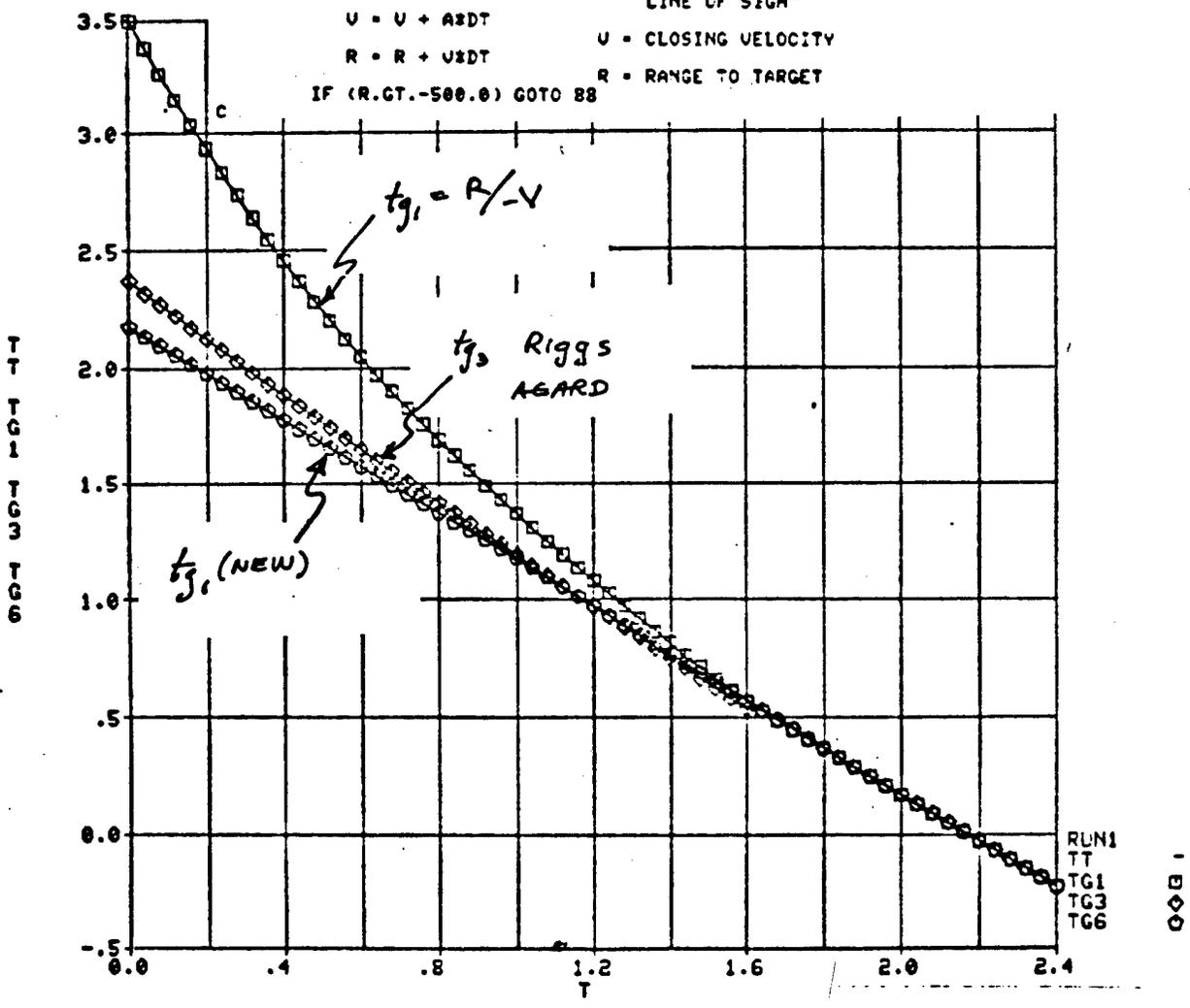

Figure B1

Comparison of time-to-go to intercept algorithms in a tail chase scenario; tg_1 is implicit in PNG, tg_3 is from Reference [3], and tg_6 is a simplified form of Equation (B1) for the case where drag acceleration is much smaller than the boost acceleration. 153

REFERENCES

[1] Bryson, A.E. and Ho, Y.C.
     "Applied Optimal Control", Blaisdell, Waltham, Mass 1968, Chapter 5.

[2] Pastrick, H. L.; S. M. Seltzer; and M. E. Warren "Guidance Laws for
     Short Range Tactical Missiles"
     J. Guidance and Control Vol. 4, No. 2 March -April 1981.

[3] Riggs, T.L. "Optimal Control and Estimation for Terminal Guidance of Tactical Missiles"
     May 1980 NATO AGARD Guidance Conference at Eglin AFB
     (also see NAECON 1979 proceedings)

[4] Asher, R.B. and J.P. Matuszewski, "Optimal Guidance with Maneuvering Targets
     J. Spacecraft Vol II, No. 3, March 74; pp204-206.

[5] Stockum, L.A. and F.C. Weimer,
     "Optimal and Suboptimal Guidance for a Short-range Homing Missile", IEEE
     Transaction on Aerospace Electronics Vol. AES-12, No. 3, May 1976; pp355-360.

[6] York, R.J. and H.L. Pastrick, "Optimal Terminal Guidance with Constraints at Final Time";
     Journal of Spacecraft and Rockets, Vol 14, No. 6, June 77, pp 381-383

[7] Adler, F. P. "Missile Guidance by three Dimensional Proportional Navigation" Journal of
     Applied Physics, Vol. 27, No. 5 May 1956; pp 500- 507,

[8] Anderson, G. M.; "Comparison of Optimal Control and Differential Game
     Intercept Missile Guidance Laws" AIAA Journal of Guidance and Control; Vol. 4, No. 2,
     March-April 1981; pp 109-115.

[9] Shinar, Josef, "Solution Techniques for Realistic Pursuit-Evasion Games" in CONTROL
     AND DYNAMIC SYSTEMS, Advances in Theory and Application Vol 17,
     Edited by C. T. Leondes, Academic Press 1981.

SESSION III: CONTROL THEORY & APPLICATIONS III/SIMULATION

21 OCT 1981
(MORNING)

THIRD MEETING OF THE COORDINATING

GROUP ON MODERN CONTROL THEORY

HOSTED BY: US ARMY MISSILE COMMAND

Next page is blank.

A NEW CLASS OF GUIDANCE LAWS FOR AIR-TO-AIR MISSILES*

Joseph N. Craig, Roger L. Barron, and Francis J. Cook
Adaptronics, Inc.
McLean, Virginia 22102

ABSTRACT

Adaptive Learning Network synthesis has been used to develop a new class of guidance laws for short-range air-to-air missiles. ALN guidance laws are trained to estimate target range, range rate, time-to-go, and other trajectory parameters not explicitly observable by passive sensors but required to implement advanced guidance laws. This development permits economical implementation of modern optimal guidance laws in passive systems, yielding considerable performance improvements over other passively realizable guidance laws.

INTRODUCTION

Research and development activities directed toward improved guidance laws for tactical air-to-air missiles have been vigorously pursued over the last thirty or more years [1]. The most impressive improvements have come from guidance laws developed using optimal control theory [2,3,5]. Unfortunately, the best performing of the modern guidance laws require knowledge of the relative missile-target position, velocity, and acceleration. Typically, air-to-air missiles are equipped only with passive sensor systems (infrared seekers) so straightforward implementation of modern guidance laws is not possible. Additionally, most optimal guidance laws also require an estimate of time-to-go.

The traditional solution to the problem of implementing modern guidance laws when faced with limited information has made use of Kalman filters to estimate the unknown states [4]. This approach requires that the missile be equipped with fairly sophisticated data processors, and does not solve the problem of estimating time-to-go.

Recently, a new approach to implementing modern guidance laws in passive systems has been developed using Adaptive Learning Networks (ALNs) to estimate the unknown combinations of data [6]. In this approach, ALNs are "trained" to mimic the modern guidance

---

law, using only passively available information. Because the ALNs are trained from a library of simulated engagements, it is now possible to implement a wide variety of guidance laws that are not amenable to Kalman filter approaches. For instance, non-deterministic or iterative solutions can be implemented once the appropriate training data base is obtained.

The use of trainable ALN guidance laws also has a considerable impact on hardware implementation requirements. The trained ALN algorithms are a computationally simple set of algebraic expressions. They can be realized using simple microprocessor circuitry.

ADAPTIVE LEARNING NETWORK SYNTHESIS METHODOLOGY

The classical approach in the design of signal processing functions has been to determine explicitly all of the relevant characteristics, deterministic and/or statistical, of the process being observed and to use these measurements with simplifying assumptions in the design synthesis. Often the mathematical structure of the processor is assumed and its design consists of calculating the values of the coefficients in this structure. In many applications, however, little is known about the characteristics of the structure and the best or even an acceptable structure for the process cannot be determined a priori. In these cases, it is desirable to determine the model structure as well as the model coefficients from a representative data base. The Adaptive Learning Network (ALN) methodology [7,8,9] provides a realization of this goal. Many useful references are found in Reference 10.

To explain the ALN approach, let us assume that we observe a scalar variable y, called the output, and N other variables, x_1, x_2, ..., x_N which are called inputs (in the present case, the desired output is a command to a missile control system; the independent variables are data available from the sensor system). The inputs are also referred to as the observables or independent variables and the output as the dependent variable. Here, "independent" means independently observed; the input variables need not be statistically independent. We seek a relationship between the independent and dependent variables that, in general, is a nonlinear function:

$$\hat{y} = f(x_1, x_2, ..., x_N; c_1, c_2, ..., c_L) \qquad (1)$$

Here and elsewhere, the caret is used to denote the calculated value of the indicated variable. If f is known, then estimates of the L coefficients (c_1, c_2, ..., c_L), may be obtained by minimizing M differences between the calculated and observed dependent variables in the least-squares sense,

158

$$\sum_{i=1}^{M} [y_i - \hat{y}_i]^2 = \sum_{i=1}^{M} [y_i - f(x_{i1}, x_{i2}, \ldots, x_{iN};$$

$$c_1, c_2, \ldots, c_L]^2 = \text{minimum} \qquad (2)$$

In many applications, however, the function f is not known and simplified analytical models fail to reflect the complexity of the observed data. In these cases, the ALN methodology provides an empirical solution to the structure of f based on a network interconnection of basic elements whose individual structures, as well as the interconnections, are learned from a representative data base.

Under fairly general conditions, a function of N variables (x_1, x_2, ..., x_N) may be expressed as a power series,

$$\hat{y} = a_o + \sum_{i=1}^{N} a_i x_i + \sum_{i=1}^{N} \sum_{j=1}^{N} a_{ij} x_i x_j +$$

$$\sum_{i=j}^{N} \sum_{j=1}^{N} \sum_{k=1}^{N} a_{ijk} x_i x_j x_k + \ldots \qquad (3)$$

This polynomial expression in many variables is referred to as a multinomial expression or a Kolmogorov-Gabor polynomial [11]. It is extremely difficult to evaluate the coefficients of Kolmogorov-Gabor polynomials when there are more than several variables. The evaluation is considerably easier when the variables are introduced successively, which can be done in pairs using second-order partial polynomials, also called basic elements:

$$\hat{y}_{jk} = w_0 + w_1 x_j + w_2 x_k + w_3 x_j x_k + w_4 x_j^2 + w_5 x_k^2 \qquad (4)$$

Here $\hat{y}_{jk}$ is used to denote the output of the basic element to inputs x_j and x_k, and the w_i's (i=0,1, ..., 5) are the coefficients of the basic element whose values are determined by the least-squares error criterion.

Training of the ALN (ALN synthesis) consists of building up, layer by layer, a structure that synthesizes the Kolmogorov-Gabor polynomial by using basic elements $\hat{y}_{jk}$. In the first layer of the network, $N(N-1)/2$ basic elements are constructed from the N inputs. Some of the best performing input variables are also used to form triplets and third-order partial polynomials. Only basic elements producing acceptable model errors are allowed to pass their outputs to the second layer. The outputs of each surviving basic element as well as the original features are used as inputs to the second layer of basic elements. This process can be repeated with succeeding layers until overfitting is detected.

physical, and engineering processes [10]. Application of the ALN methodology has been successful where conventional and/or theoretical modeling techniques have produced poor results.

APPLICATION TO GUIDANCE LAW SYNTHESIS

To synthesize an ALN guidance law, the ALN is trained on example guidance commands for a variety of typical engagements. This is accomplished by building a training data base: an advanced guidance law (usually a law requiring complete, explicit observability of the target's trajectory) is used in conjunction with a computer program that simulates air-to-air engagements, and the analyst compiles a library of typical simulated engagements. The library ideally encompasses the range of launch conditions over which the resulting guidance law is expected to perform. For example, launch range, initial aiming error (off-boresight angle), and the target aspect angle are important launch parameters. At each time step of each simulated engagement, outputs available from the target seeker and other sensors in the missile are tabulated along with the actual acceleration commands generated by the advanced guidance law. The target seeker and other sensors in the missile will, in general, deny explicit observability of some quantities used in computing the advanced guidance law commands, but the latter is computed using all denied information when generating the training data base. The time histories of the available sensor observables are used as input variables in the ALN synthesis process, while the commands are the dependent variables. In this way, the sensor data are used to estimate the information not explicitly observed and to generate the appropriate guidance commands as if that information were available. The resulting ALNs embody an economical realization of the advanced guidance law.

ILLUSTRATIVE EXAMPLE

As an example of ALN implementation of a guidance law, let us consider implementation of proportional navigation (PNG). In this example, as in many tactical missile applications, the primary (and perhaps only) explicitly observable external quantity is the line-of-sight angle (λ) or its rate of change ($\dot{\lambda}$). (Note that although we are limiting this illustrative example to a two-dimensional engagement for which there is only one line-of-sight angle, the extension to three dimensions is straightforward.) Other variables and/or constants of the engagement kinematics are usually unknown, although explicit identification of some of them is sometimes possible through the application of techniques of modern control theory.

The limited information in this situation largely accounts for the popularity of PNG, wherein the rate of change of λ is measured and the commanded missile normal acceleration (a_{mn}) is set proportional to this rate:

Avoidance of overfitting is a key aspect in the training of ALNs [12,9]. The network must be taught to generalize properly on its experience in fitting the training observations so that error rates for new, but statistically similar data, will also be low. Overfitting is detected by cross-validation and by employing an information theoretical criterion [13]. When cross-validation is used to detect overfitting, the known data base is divided into two independent but statistically similar subsets called training and selection subsets. The training subset is used to determine the coefficients of the elements. The selection subset is used to reject the poorly performing basic elements and to detect overfitting. While the error rate on the training subset is continuously decreased by incorporating additional layers, the error rate on the selection subset increases when overfitting occurs.

When the number of observations in the data base is too small to form the two independent subsets, the growth of the model, i.e., the increase in the number of coefficients, is controlled by the use of Akaike's information criterion (AIC) [14]. The AIC measures the poorness of the model and consequently needs to be minimized:

$$AIC = -2\ell n(\text{maximum likelihood}) \quad (5)$$
$$+2(\text{number of coefficients}) = \text{minimum}$$

The AIC can be considered as an adaptive F test where the risk level changes with the number of observations and the number of model coefficients in the two models to be compared [15]. Also, the AIC is asymptotically equivalent to the maximum likelihood model [13]; i.e., the model selected by the independent selection subset based on the least-squares error criterion approaches the model selected by the AIC as the number of observations approaches infinity.

If the size of the data base permits, an independent evaluation subset is used to estimate the overall performance. Since the evaluation subset is not used for network synthesis, the performance of this subset is an accurate estimate of the ability of the network to generalize to new, previously unseen data.

In summary, the ALN method is an empirical technique to obtain the structure of a process and requires no a priori knowledge and/or assumptions about the process itself. The relevant features are selected by the learning algorithm from the candidate feature list and are introduced into the learning network in the optimum order. Features discovered by the learning algorithm to be of little or no use are discarded automatically. The learning algorithm permits the structure of the network to grow, i.e., to approximate the general Kolmogorov-Gabor polynomial, but only to the extent required by the data base. As a general modeling tool, the ALN methodology is applicable to detection, classification, prediction, and control of a wide range of complex biological,

physical, and engineering processes [10]. Application of the ALN methodology has been successful where conventional and/or theoretical modeling techniques have produced poor results.

APPLICATION TO GUIDANCE LAW SYNTHESIS

To synthesize an ALN guidance law, the ALN is trained on example guidance commands for a variety of typical engagements. This is accomplished by building a training data base: an advanced guidance law (usually a law requiring complete, explicit observability of the target's trajectory) is used in conjunction with a computer program that simulates air-to-air engagements, and the analyst compiles a library of typical simulated engagements. The library ideally encompasses the range of launch conditions over which the resulting guidance law is expected to perform. For example, launch range, initial aiming error (off-boresight angle), and the target aspect angle are important launch parameters. At each time step of each simulated engagement, outputs available from the target seeker and other sensors in the missile are tabulated along with the actual acceleration commands generated by the advanced guidance law. The target seeker and other sensors in the missile will, in general, deny explicit observability of some quantities used in computing the advanced guidance law commands, but the latter is computed using all denied information when generating the training data base. The time histories of the available sensor observables are used as input variables in the ALN synthesis process, while the commands are the dependent variables. In this way, the sensor data are used to estimate the information not explicitly observed and to generate the appropriate guidance commands as if that information were available. The resulting ALNs embody an economical realization of the advanced guidance law.

ILLUSTRATIVE EXAMPLE

As an example of ALN implementation of a guidance law, let us consider implementation of proportional navigation (PNG). In this example, as in many tactical missile applications, the primary (and perhaps only) explicitly observable external quantity is the line-of-sight angle (λ) or its rate of change ($\dot{\lambda}$). (Note that although we are limiting this illustrative example to a two-dimensional engagement for which there is only one line-of-sight angle, the extension to three dimensions is straightforward.) Other variables and/or constants of the engagement kinematics are usually unknown, although explicit identification of some of them is sometimes possible through the application of techniques of modern control theory.

The limited information in this situation largely accounts for the popularity of PNG, wherein the rate of change of λ is measured and the commanded missile normal acceleration (a_{mn}) is set proportional to this rate:

$$a_{mn} = V_m N \dot{\lambda} \qquad\qquad (6)$$

where V_m is missile velocity and N is the so-called navigation constant.

In the simplified example at hand, the analyst could postulate a family of intercept engagements, the family being characterized by a given value of the navigation constant, N = N´. Each member of this family would have its unique combination of values for the initial conditions and constants. Literally, thousands of engagements could be "run off" on the computer, and the results could be put into a data base, shown schematically in Figure 1.

$Y = a_{mn}$	$X_1 = t$	$X_2 = \dot{\lambda}$
y_1	x_{11}	x_{21}
y_2	x_{12}	x_{22}
$\vdots$		
y_M	x_{M1}	x_{M2}

M = number of observed points in data base.

FIGURE 1: EXAMPLE DATA BASE

The ALN training procedure could be used to synthesize a small network in which the output (Y) would be a_{mn} and the inputs (X_1 and X_2) would be t and λ. At the conclusion of this training, one would undoubtedly find that the ALN is one which generates a close approximation to the original guidance law, Equation (6). Examination would show that the output of the ALN and a_{mn} from Equation (6) agree fairly closely for all values of t and $\dot{\lambda}$ in the data base. In this case, the ALN methodology has "discovered" the value of N´ used to generate the family of solutions. More importantly, the methodology has "discovered" a way to infer the unknown V_m (unknown because it was assumed to be explicitly unobservable within the missile system). Even though V_m varied with time and was different -- in general -- for each solution in the data base, and not an explicit input to the ALN, the procedure for ALN synthesis created an approximate relationship for its identification.

163

Perhaps, after creating the above ALN function, it would be found that the ALN solution is not a sufficiently close approximation to Equation (6). In this case, a more complete record of the histories of λ and a_{mn} might be used to provide addditional input information during ALN training. The results of the engagement simulations could be put into data base records, each record being of the form:

$$y_i(t), \; y_i(t-\Delta t), \; \ldots, \; y_i(0),$$

$$x_{2i}(t), \; x_{2i}(t-\Delta t), \; \ldots, \; x_{2i}(0), \; t$$

where Δt is a constant sampling interval. In other words, samples of a_{mn} and λ would be kept from the time of missile launch until the time of "present" calculation, t.

We do not know, a priori, how far back in time the guidance law might best go in fetching inputs from such data files as have just been described. But, no matter. The ALN methodology will find this for us, using only the most relevant samples in generating the desired approximation. From a practical standpoint, we may wish to enforce a limit on the amount of memory available for the guidance system, in which case, the data records could be constructed in the form:

$$y_i(t), \; y_i(t-\Delta t), \; \ldots, \; y_i(t-k\Delta t),$$

$$x_{2i}(t), \; x_{2i}(t-\Delta t), \; \ldots, \; x_{2i}(t-k\Delta t); \; t$$

where k is an integer (say 5 or 10). At the beginning of the intercept mission, the observed values of $y_i(0)$ and $x_{2i}(0)$ could be loaded into appropriate memory locations within the missile guidance unit, and after collecting k consecutive samples, the ALN solution would be fully "initialized."

ALN SYNTHESIS FOR AN OPTIMAL GUIDANCE LAW

The basic principles of guidance law synthesis using ALN training outlined for the illustrative example have been applied to a guidance law (MG) derived using known optimal control theory [2]. The optimal guidance command is:

$$\vec{a} = \frac{3}{t_{go}^2} (\vec{R} + t_{go} \dot{\vec{R}}) \tag{7}$$

where $\vec{a}$ is the optimal missile acceleration measured in an inertial reference frame, $\vec{R}$ is the missile-target line-of-sight (LOS) vector, $\dot{\vec{R}}$ is the time rate of change of the LOS vector, and t_{go} is the remaining time to go until intercept. In terms of the relative range, R, range rate, $\dot{R}$ and the line-of-sight angles λ_E and λ_A depicted in Figure 2, the vectors are:

164

$$R_x = R \cos \lambda_E \cos \lambda_A \tag{8a}$$

$$R_y = R \cos \lambda_E \sin \lambda_A \tag{8b}$$

$$R_z = R \sin \lambda_E \tag{8c}$$

$$R_x = \dot{R} \cos \lambda_E \cos \lambda_A - R \dot{\lambda}_E \sin \lambda_E \cos \lambda_A \tag{8d}$$
$$- R \dot{\lambda}_A \cos \lambda_E \sin \lambda_A$$

$$R_y = \dot{R} \cos \lambda_E \sin \lambda_A - R \dot{\lambda}_E \sin \lambda_E \sin \lambda_A \tag{8e}$$
$$+ R \dot{\lambda}_A \cos \lambda_E \cos \lambda_A$$

$$R_z = \dot{R} \sin \lambda_E \qquad + R \dot{\lambda}_E \cos \lambda_E \tag{8f}$$

If the subject missile is equipped with a gimballed, inertially stabilized IR seeker, the inertial LOS angles and LOS rates are readily available. Then acceleration commands given by Equation (7) and (8a-f) can be calculated in the (inertial) seeker reference frame. Control of the missile requires that acceleration commands be specified relative to a coordinate system fixed to the missile body axes. This is easily accomplished if the orientation of the seeker is known. In practice, the longitudinal acceleration of the missile is often uncontrollable due to the type of propulsion system that is used. In these instances, a_{Mx} is unrealized and a_{My} and a_{Mz} are calculated using Equations (7) and (8a-f). These equations express the acceleration in terms of the LOS angles and LOS rates typically encountered in PNG applications.
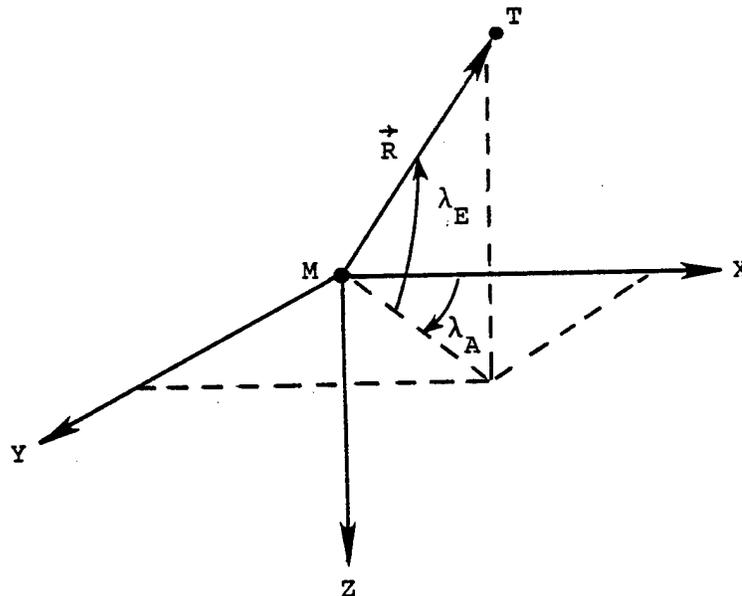

FIGURE 2: MISSILE-TARGET LINE-OF-SIGHT GEOMETRY IN INERTIAL COORDINATES

The missile acceleration commands in the seeker inertial reference frame can be written [6]:

$$A_{sx} = \kappa_1 \cos\sigma_q \cos\sigma_r - \kappa_2(\dot{\sigma}_r \cos\sigma_q \sin\sigma_r + \dot{\sigma}_q \sin\sigma_q \cos\sigma_r) \quad (9a)$$

$$A_{sy} = \kappa_1 \cos\sigma_q \sin\sigma_r + \kappa_2(\dot{\sigma}_r \cos\sigma_q \sin\sigma_r - \dot{\sigma}_q \sin\sigma_q \cos\sigma_r) \quad (9b)$$

$$A_{sz} = \kappa_1 \sin\sigma_q - K_2 \dot{\sigma}_q \cos\sigma_q \quad (9c)$$

where:

$$\kappa_1 = \frac{3R}{g t_{go}} \left(\frac{1}{t_{go}} + \frac{\dot{R}}{R} \right) \quad (10a)$$

$$\kappa_2 = 3R/g t_{go} \quad (10b)$$

and σ_r and σ_q are the pitch and yaw LOS angles in the seeker reference frame.

The orientation of the seeker, relative to the missile body axes, is specified by two angles, ψ_g and θ_g. The transformation between the missile body coordinates and seeker coordinates may be written as:

$$\vec{A}_M = \begin{pmatrix} a_{Mx} \\ a_{My} \\ -a_{Mz} \end{pmatrix} = \begin{pmatrix} \cos\psi_g \cos\theta_g & -\sin\psi_g \cos\theta_g & \sin\theta_g \\ \sin\psi_g & \cos\psi_g & 0 \\ -\cos\psi_g \sin\theta_g & \sin\psi_g \sin\theta_g & \cos\theta_g \end{pmatrix} \vec{A}_S \quad (11)$$

where $\vec{A}_M$ and $\vec{A}_S$ are measured in the body and seeker frames, respectively.

For the gimballed, initially stabilized, IR seeker, the passively unknown data are completely contained in the optimum gain terms, κ_1 and κ_2. Thus, if estimates of these values can be obtained from the passively observable data, a passive implementation of the modern guidance law can be obtained.

Several approaches to estimating t_{go} exist. An iterative, non-deterministic approach to the estimation of t_{go} is particularly suited to generating training acceleration commands in an off-line mode. The procedure is:

(a) Simulate the engagement using the complete MG equations with a typical calculation of t_{go} [2].

(b) Save the duration of the engagement, t_f.

(c) Simulate the engagement again as in (a), except use t_{go} = t_f-t, where t is the elapsed time past launch.

(d) Save the corrected duration of the engagement, t_f.

166

(e) Repeat (c) and (d) until t_f converges, whence t_{go} is known exactly throughout the engagement.

Engagements produced by this procedure are more nearly optimal than those that make use of estimates of t_{go}.

The ALN training approach to synthesizing the modern guidance law for the inertially stabilized gimballed IR seeker consists of the following:

(a) Acquire time histories of the passive observables.

(b) Use the data from (a) to estimate the optimum gains, κ_1 and κ_2.

(c) Use the estimates of κ_1 and κ_2 together with Equations (9) and (11) to calculate the required accelerations relative to the missile body coordinate system.

Note that, although R, $\dot{R}$, and t_{go} are required to implement MG, only two combinations of these quantities in the form of the optimal gains, κ_1 and κ_2 are required. Thus, the ALNs can be trained to estimate the required optimal gain rather than to estimate the three separate values.

Training Data Base

To demonstrate the application of this method, a training data base for the modern guidance law was obtained by simulating air-to-air engagements using a six-degree-of-freedom (6DOF) simulation program provided by the Air Force Armament Laboratory. The 6DOF program implemented MG for a realistic model of a highly measurable, short-range, bank-to-turn missile. An evasive target maneuver is also included in the simulation program.

Simulated engagements were run for a variety of initial engagement conditions. For each set of launch conditions, the simulation was iterated to achieve the best estimate of t_{go}. For the final iteration, values for each of the passive observables, together with the optimal guidance commands and κ_1 and κ_2, were saved in a training data file. The training data base was limited in this example to the following launch conditions:

- Missile and target were co-speed, flying straight and level at missile launch (0.9 mach).

- Missile and target were co-altitude at launch (10,000 feet).

- Initial aspect angle (angle between target velocity vector and LOS vector) varied from 0 to 180 in 45 increments. (Zero-degree aspect angle is tail-on.)

167

- Initial off-boresight angle (angle between missile velocity vector and LOS vector) was either $25°$ leading or lagging or $0°$.

- The target flew straight and level until missile range was less than 6000 feet, at which time the target performed a 9-g, dual-plane maneuver into the attack.

ALN Training

Approximately 1500 time points from a total of 200 training engagements were used to train ALNs to estimate the optimal values of κ_1 and κ_2 from the passively available data. Candidate ALN inputs included:

o Missile-Target LOS angles in Missile Body Coordinates: ET,AT

o Seeker Gimbal Orientation angles: ψ_g, θ_g

o Missile Target LOS rates determined by the Seeker: $\dot{\sigma}_q, \dot{\sigma}_r$

o Time since launch: t, $1/t$ ($t > 0$)

For each of the angle variables, the current and four previous samples of each variable were saved for training ($\Delta t = 0.05$ sec).

The structure of the trained ALN that estimates the optimal gains, κ_1 and κ_2, is shown in Figure 3. Each element of the ALN calculates up to a cubic polynomial of its inputs. The ALN estimator is a complicated function of the candidate input variables, but not all of the candidate inputs are used. Those inputs that provided redundant or unnecessary data were discarded by the ALN training routine.

ALN Guidance Performance

The performance of the ALN guidance law was determined by using it to guide the hypothetical missile in simulated engagements. The engagement launch conditions were generally different from those used in training the ALN. Two comparisons of the ALN guidance law have been carried out:

o comparison of passive ALN guidance with the full modern guidance law (assuming observability of all states), and

o comparison of ALN guidance with PNG. This comparison shows the level of performance improvement that can be obtained over current systems.

Initial evaluation of the passive ALN guidance laws was carried out by comparing ALN guidance with the active modern guidance law
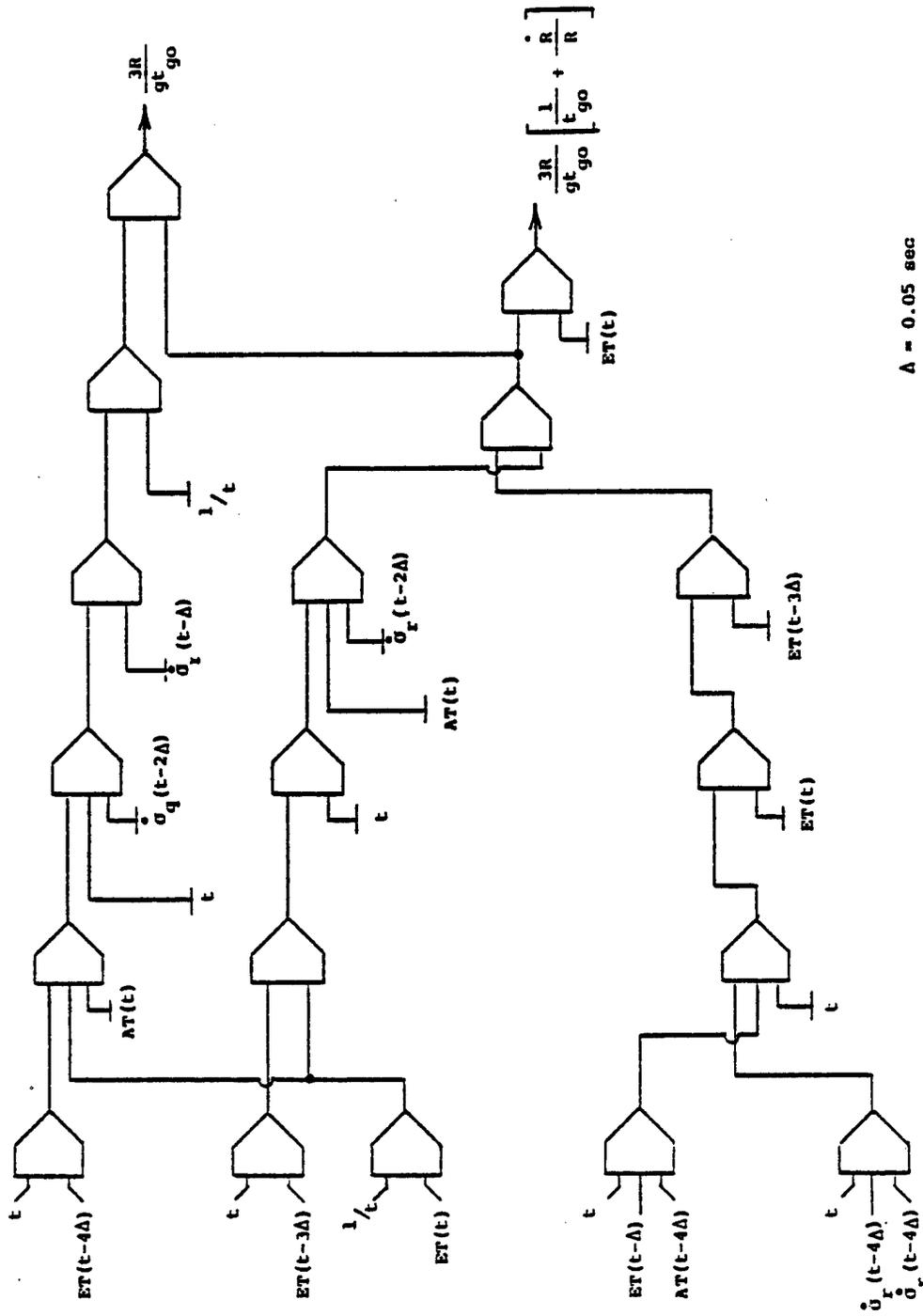
FIGURE 3: ALN STRUCTURE FOR MODIFIED PROPORTIONAL NAVIGATION FOR A GIMBALLED SEEKER SYSTEM: ALNG1

$\Delta = 0.05$ sec

169

for the same launch conditions included in the training data base. Defining a hit as an engagement for which the terminal miss distance was less than 10 feet, the ALN guidance law scored hits for 82% of the engagements hit by active modern guidance. ALN guidance was generally inferior to MG for longer-range launches that generally terminate in a tail chase. A linear combination of PNG with ALN guidance diagrammed in Figure 4, was therefore used to slowly turn off ALN guidance. ALN-PNG guidance was successful for 91% of the engagements hit using MG . Additionally, 20% of the engagements not hit using MG were hit by the combined ALN-PNG guidance law.

A complete comparison of the ALN-PNG guidance law with MG and with PNG was obtained for 266 engagement conditions, including off-boresight angles up to ±45 . Note that the training data included only off-boresight angles to ±25 . The detailed comparison is presented in Reference 6; the important trends noted are summarized here.

First, the ALN-PNG guidance law generally achieved intercept with smaller terminal-miss distances, slightly shorter flight times, and less total guidance impulse than did PNG. Most importantly, the ALN-PNG guidance law produced successful intercepts more often than PNG. This was especially true for launches with larger aspect angles (> 90°) and larger off-boresight angles (>20 , especially noticeable for OBA = ± 45). While providing a realizable implementation of modern guidance, the ALN-PNG guidance laws also produced successful intercepts over a considerably wider range of launch parameters than PNG.

Summary performance matrices are presented in Figures 5 and 6. The performance evaluation was carried out for the ALN-PNG guidance law. It can be readily ascertained that the passive combined ALN-PNG guidance law was greatly superior to PNG. It had 19% more hits when the initial OBA was 0 and ±15 , 35% more hits when the initial OBA was ±25 , and 61% more hits when the initial OBA was ±45 .

On comparing the passive (ALN-PNG) guidance law with the active modern guidance law, Figure 6, there were a number of engagements (13) hit by the ALN-PNG law that were missed by MG, while only one engagement missed by the ALN-PNG law was hit by the MG. This shows again that the ALN-PNG guidance law was an excellent representation of MPN over the envelope of tested launch conditions. Further, the engagements in which the ALN guidance hit and the MPN missed were engagements near the outer-launch body of the missile. This indicated that the phasing in of PNG in the ALN provided a guidance law that was, in some respects, better than MG. Additional independent testing of the ALN-PNG guidance law showed that dramatic increases are obtained in the outer launch boundaries over those available using either PNG or MG.

Additional testing has compared the ALN-PNG guidance law with an extended Kalman filter implementation of MG[16]. In both cases,
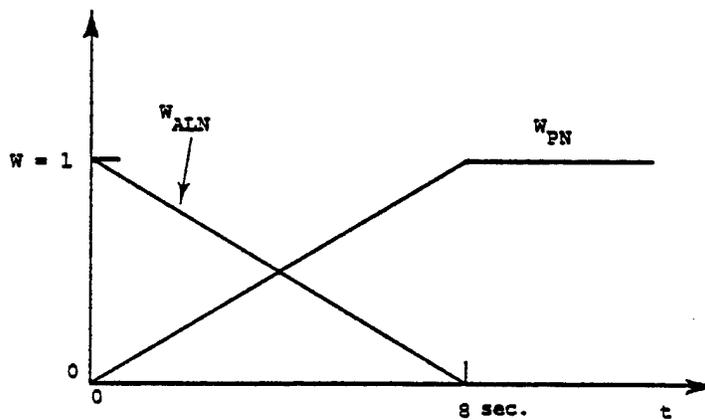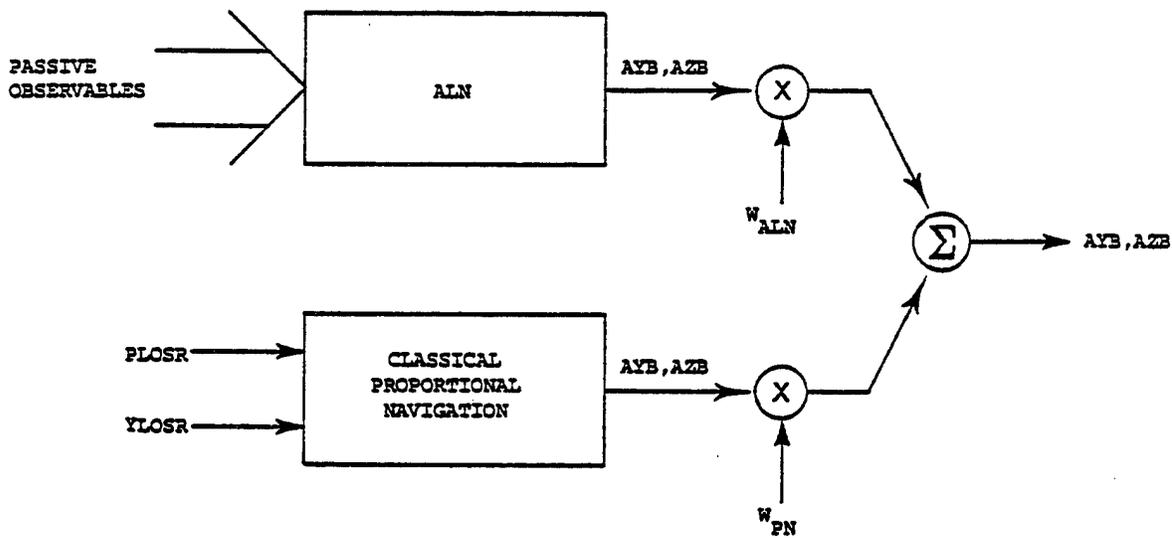
170

FIGURE 4: COMBINATION OF ALN GUIDANCE LAW WITH CLASSICAL
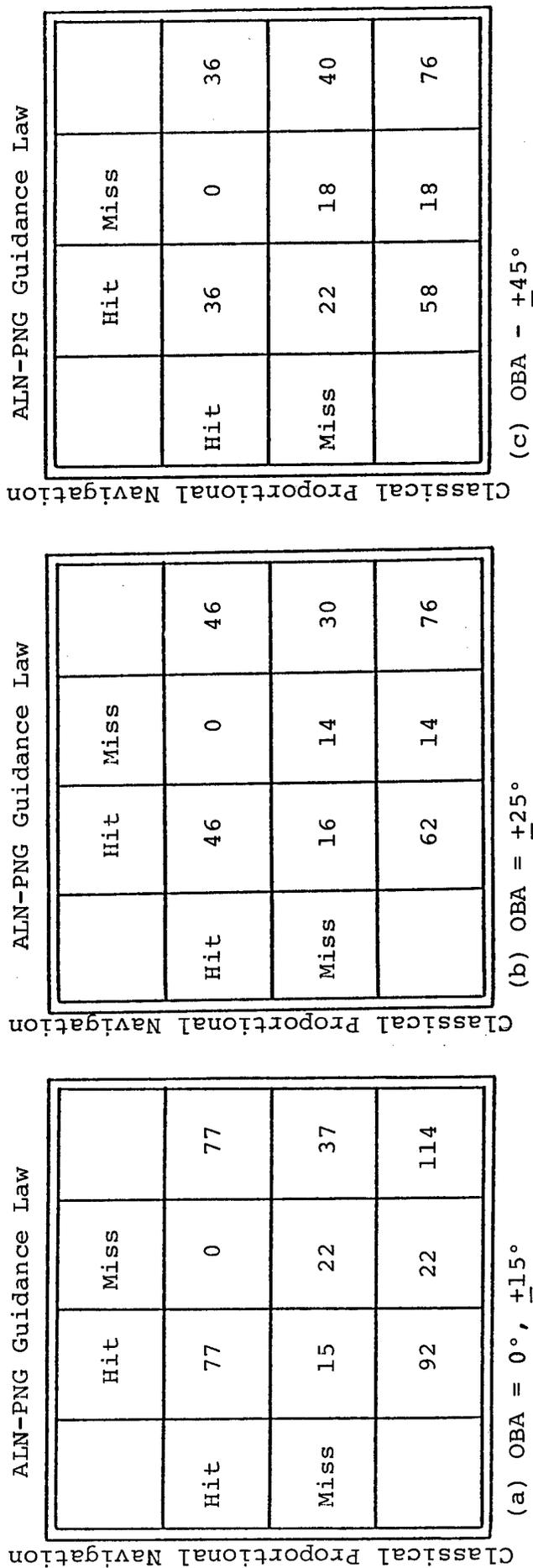PROPORTIONAL NAVIGATION

171

FIGURE 5: COMPARISON OF THE COMBINED ALN-PNG GUIDANCE LAW WITH CLASSICAL, PASSIVE PNG FOR TEST PLAN ENGAGEMENTS

(a) OBA = 0°, ±15°

(b) OBA = ±25°

(c) OBA = ±45°

172

ALN-PNG Guidance Law

(a) OBA = 0°, ±15°

Active Modern Guidance Law	Hit	Miss	
Hit	87	0	87
Miss	5	22	27
	92	22	114

(b) OBA = +25°

Active Modern Guidance Law	Hit	Miss	
Hit	58	0	58
Miss	3	15	18
	61	15	76

(c) OBA = ± 45°

Active Modern Guidance Law	Hit	Miss	
Hit	53	1	54
Miss	5	17	22
	58	18	76

FIGURE 6: COMPARISON OF THE COMBINED ALN-PNG GUIDANCE LAW WITH ACTIVE MODERN GUIDANCE LAW FOR TEST PLAN ENGAGEMENTS

realistic noise models were used to degrade the sensor noise. These tests showed that ALN-PNG produced better inner-launch boundaries than PNG. MG produced better inner-launch boundaries than either ALN-PNG or PNG, but ALN-PNG produces the best outer-launch boundaries. In the presence of noisy sensor data, the performance of ALN-PNG was not greatly degraded.

CONCLUDING REMARKS

The ALN guidance law synthesis approach permits the use of advanced, "active" guidance laws with seeker hardware of the type normally used to implement classical, passive proportional navigation. In their explicit deterministic forms, the advanced guidance laws require knowledge of range, range rate, and time-to-go, in addition to the usual LOS angular rates. By estimating gain factors involving range, range rate, and time-to-to, the ALNs permit implementation of the advanced laws using only passive observables.

The computations required by ALN guidance laws could be implemented by adding a small microprocessor-based subsystem to the passively-guided missile. The microprocessor would be supplied the time histories of the passively-observable data and calculates the ALN outputs. The capabilities required by the ALN are well within the capabilities of current microprocessors using ROM-based software and a small amount of RAM for temporary storage.

Previously, advanced guidance laws have not been generally utilized in air-to-air missiles because much of the data necessary for their implementation has been denied by operational missile sensor systems. Now, through the use of ALN techniques, this missing information can be largely recovered in an efficient and noise-insensitive manner from the time histories of the data available from the sensors. This opens up a new world of possibilities for missile guidance applications.

REFERENCES

1. Pastrick, H.L., S.M. Seltzer, and M.E. Warren, "Guidance Laws for Short-Range Tactical Missiles," J. Guidance and Control, Vol. 4, No. 2, p. 98, 1981.

2. Riggs, T.L., "Linear Optimal Guidance for Short-Range Air-to-Air Missiles," Proc. of NAECON 1979, Vol. II, pp. 757-764, May 1979.

3. Fuller, J.W., et al.,"Tactical Missile Guidance and Control Methodology," Report No. AFATL-TR-80-20, January 1980.

4. Sammons, J.M., et al., "Development and Comparison of Optimal Filters," Report No. AFATL-TR-79-87, October 1979.

5. Andersen, G.M., "Guidance and Control Methodology," Report No. AFATL-TR-79-86, October 1979.

6. Craig, J.N., R.L. Barron, and F.J. Cook, "A Priori Training of Guidance and Control Algorithms for Tactical Missiles, Task I: Air-to-Air Guidance Law Implementation," Report No. AFATL-TR-80-102, August 1980.

7. Barron, R.L., "Adaptive Transformation Networks for Modeling, Prediction, and Control," Proc. IEEE/ORSA Joint Nat. Conf. on Major Systems, Anaheim, CA, 1971.

8. Gilstrap, L.O., Jr., "Keys to Developing Machines with High-level Artificial Intelligence," Proc. ASME Des. Eng. Conf., pp. 1-16, 1971.

9. Mucciardi, A.N., "Neuromine Nets as the Basis for the Predictive Component of Robot Brains," Cybernetics, Artificial Intelligence, and Ecology, Robinson and Knight (eds.), Spartan Books, pp. 159-193, 1972.

10. Cook, F.J., and J.N. Craig, "Adaptive Learning Networks and Image Processing for Missile Guidance," Proc. Soc. Photo-Opt. Instr. Eng. 238, pp. 293-302, 1980.

11. Gabor, D., W. Wildes, and R. Woodcock, "Universal Nonlinear Filter Prediction Which Optimizes Itself by Learning," IEEE Proc. 108, Part B, 1961.

12. Ivakhnenko, A.G., "Polynomial Theory of Complex Systems, IEEE Trans. Syst., Man, Cybern, SMC-1, pp. 364-378, 1971.

13. Stone, M., "An Asymptotic Equivalence of Choice of Model by Cross-validation and Akaike's Criterion," J. R. Statist. Soc., B., 39, pp. 44-47, 1977.

14. Akaike, H., "Information Theory and an Extension of the Maximum Likelihood principle," 2nd International Symposium on Information Theory, B.N. Petrov and F. Csaki (eds.), Akademia, Budapest, Hungary, pp. 267-281, 1973.

15. Maklad, M.S., and S.T. Nichols, "A New Approach to Model Structure Discrimination," IEEE Syst., Man, Cybern. SMC-10, pp. 78-84, 1980.

16. Vergez, P.L., private communication.

Next page is blank.

ESTIMATING TIME-TO-GO FOR USE IN ADVANCED GUIDANCE LAWS

Tom L. Riggs, Jr., Capt, USAF
Department of Astronautics and Computer Science
United States Air Force Academy, Colorado 80840

INTRODUCTION

The modern air-to-air missile engagement scenario dictates the need for high performance terminal guidance laws that are capable of steering missiles towards successful intercepts against highly maneuverable and intelligent targets. Numerous studies [1,2,3] over the past few years have shown that linear optimal control theory can yield extremely effective guidance algorithms that are capable of meeting and exceeding this demanding mission objective. However, these guidance laws require more information than is directly available from existing hardware, such as relative range, relative velocity, possibly target acceleration, and time-to-go. To meet the information needs of these advanced guidance laws research into developing estimation algorithms has been pursued nearly as enthusiastically as in the guidance area. Most notably is the work in estimation performed for the U.S. Air Force Armament Laboratory by the University of Texas.[4] In this effort, it was shown that by using optimal estimation techniques important state information including the relative range vector, relative velocity vector and target acceleration vector can be accurately estimated from very restricted and noisy passive (infrared) seeker measurements and on-board body-fixed missile acceleration and angular-rate measurements. Vergez and Riggs [5] showed that by combining those state estimation techniques with even the most simple linear feedback guidance law, drastic missile performance improvements could be realized over conventional guidance methods (proportional navigation) if and only if those laws were mechanized with an accurate estimate of time-to-go. As in any practical problem, the desire for high performance is weighted and often limited by the issue of complexity. This is the basis of the research on time-to-go estimation. That is, what is the most accurate method for estimating time-to-go given the restriction that it must be implementable in a microprocessor based missile guidance computer?

THEORETICAL DEVELOPMENT

Background

The need for an accurate measure of time-to-go (the amount of time remaining to intercept) arises from the theory that is used in deriving the guidance laws. The parameter time-to-go appears naturally in the solution of optimal control problems where time

is the independent variable and final time is assumed to be fixed. Of all the optimal control formulations that have been developed over the last twenty years, the one that most often yields practical solutions is the linear regulator formulation. The missile intercept problem can be, and has been, mathematically described such that it lends itself to a special case of the linear regulator formulation. The advantage of this approach is that the resulting solution is a set of algebraic equations in feedback form. Thus the solution is concise, relatively simple, and to some degree self-correcting. The drawback to this approach is the need for complete state information and knowledge of final time. As noted earlier, the state information problem has been addressed with successful results. Because of this, for this effort it will be assumed that complete state information is available. The final time issue is the subject of this research.

The missile intercept problem is in reality a free final time problem within certain physical constraints. To wit, there is a set of final times at which the missile can intercept the target within the lethal range of the warhead. This set is bounded and determined by the degree of controllability of the missile and the chosen trajectory of the target. Obviously if the missile has complete control of its acceleration vector both in magnitude and direction, the set of final times becomes the positive real number set. However, the missile only has partial and finite control of its acceleration vector through the use of lateral aerodynamic control. This controllability restriction greatly limits the size of the final set. Further, this set shrinks as the engagement proceeds, ultimately resulting in one possible time, the time at which the point of closest approach is reached. Realizing these physical constraints, one might ask why not derive the guidance law assuming partial acceleration control and allowing final time to be free. The answer is simple. If the problem is formulated in that manner then the solution is not in closed form nor can it be easily implemented on-board the missile.

These practical constraints along with the desire to obtain a practical good performing but not necessarily optimal guidance algorithm makes it attractive to solve the problem using the optimal linear regulator formulation. Given this approach the mechanization of the resultant guidance law requires the estimation of final time (and subsequently time-to-go) in order to satisfy the original fixed final time assumption.

Guidance Law

The guidance law that was used for this study is given by equation (1).

$$\bar{A}_M = \left[\frac{3}{tgo^2}I \; \vdots \; \frac{3}{tgo}I \; \vdots \; 3K_TI \right] \begin{bmatrix} \bar{S}_R \\ \overline{} \\ \bar{V}_R \\ \overline{} \\ \bar{A}_T \end{bmatrix} \tag{1}$$

where

$$K_T = (e^{t\,tgo} + t\,tgo - 1)/(t\,tgo)^2$$

I = 3 x 3 Identity Matrix

$\bar{A}_M$ = Commanded Missile Acceleration Vector

$\bar{S}_R$ = Relative (Target/Missile) Range Vector

$\bar{V}_R$ = Relative (Target/Missile) Velocity Vector

$\bar{A}_T$ = Target Acceleration Vector

The complete derivation of the guidance law is given in Section II of Reference [5]. This law is based on a linear kinematic engagement model and a linear first-order target dynamic model and is designed to minimize final range. The term t in the gain K_T is a constant and is a function of the time constant of the target model. All of the vectors are made up of three orthogonal components with respect to some arbitrary cartesian coordinate system. The predominance of time-to-go, denoted by tgo is clear in the equations.

Time-to-go Assuming Constant Closing Velocity

The most commonly used method for estimating time-to-go is given by equation (2). This method is based on the assumption that the

acceleration along the line-of-sight is zero for all time.

$$tgo = -R/\dot{R} \tag{2}$$

Estimating Time-to-go Numerically

The problem of estimating time-to-go involves the prediction of the line-of-sight acceleration for all future time. This is indeed a formidable task since this acceleration is the dot product of the target/missile relative acceleration vector (a function of time) with a unit vector that lies along the line-of-sight (also a function of time). Obviously this cannot be determined in general because of the uncertainty of future target maneuvers. However, the acceleration along the line-of-sight can be approximated by assuming that the target acceleration is zero and the missile's axial acceleration is the dominant contributor to the line-of-sight acceleration. Once this assumption is made the problem reduces to the construction of a time dependent function that represents the missile's axial acceleration. This was done with a very simple function (given by·equation 3) in [6] resulting in a time-to-go algorithm that not only was accurate under many launch conditions but greatly increased the missile's performance over conventional time-to-go mechanizations. Unfortunately those results did have limitations, especially on the long range launches. This was due to the function used to model the missile's axial acceleration.

$$A_{MX} = \begin{cases} A_{max}, \text{time} < \text{time of engine burnout} \\ \\ A_{min}, \text{time} > \text{time of engine burnout} \end{cases} \tag{3}$$

where A_{max} and A_{min} are constants determined from missile thrust/drag characteristics.

An improved approach was suggested by York [7] in that actual missile axial acceleration data is used to curve-fit an approximate function of exponential form during thrust off and of linear form during thrusting. This is the basis of the following numerical.algorithm.

Algorithm Development

Based on an assumed model of the line of sight acceleration, the algorithm is constructed to determine the time at which the range will be minimized given the present range and range rate. To do this, the following assumptions will be made.

1. Assume non-maneuvering target

2. Assume acceleration along line-of-sight can be modeled as

$$A_{los} = \ddot{R}(t) = \begin{cases} k \,, & 0 < t < t_{bo} \\ \\ ae^{bt}, & t > t_{bo} \end{cases}$$

note – t_{bo} is time of burnout

$$\dot{R}(t) = \int \ddot{R}\, dt$$

$$R(t) = \int \dot{R}\, dt = \iint \ddot{R}\, dt$$

Since $\ddot{R}(t)$ is a piecewise continuous function with one discontinuity there will be three possible solutions for $\dot{R}(t)$ and $R(t)$. Those solutions are

Definitions

t_o – present time

t_f – final time

R_o – present range

$\dot{R}_o$ – present range rate

<u>Case</u> <u>1</u> – $t_o < t_{bo}$, $t_f < t_{bo}$

$$\dot{R}(t) = k(t-t_o) + \dot{R}_o$$

$$R(t) = \frac{k}{2}(t-t_o)^2 + \dot{R}_o(t-t_o) + R_o$$

<u>Case</u> <u>2</u> – $t_o > t_{bo}$, $t_f > t_{bo}$

$$\dot{R}(t) = \frac{a}{b}e^{bt} - \frac{a}{b}e^{bto} + \dot{R}_o \qquad (4)$$

$$R(t) = \frac{a}{b^2}e^{bto}e^{b(t-to)} + (\dot{R}_o - \frac{a}{b}e^{bto})(t-t_o) + R_o - \frac{a}{b^2}e^{bt}o \qquad (5)$$

181

<u>Case 3</u> - $t_o < t_{bo}, t_f > t_{bo}$

This case is a combination of Case 1 and 2.

Use eqns for Case 1 and solve for $\dot{R}(t_{bo})$ and $R(t_{bo})$ and substitute those quantities into the equations for Case 2.

Therefore

$$\dot{R}(t) = \frac{a}{b} e^{bt} - \frac{a}{b} e^{bt_{bo}} + \dot{R}(t_{bo}) \tag{6}$$

$$R(t) = \frac{a}{b^2} e^{bto} e^{b(t-t_{bo})} + (\dot{R}(t_{bo}) - \frac{a}{b} e^{bt_{bo}})(t-t_{bo})$$

$$+ R(t_{bo}) - \frac{a}{b^2} e^{bt_{bo}} \tag{7}$$

where

$$\dot{R}(t_{bo}) = k(t_{bo} - t_o) + \dot{R}_o \tag{8}$$

$$R(t_{bo}) = \frac{k}{2}(t_{bo} - t_o)^2 + \dot{R}_o(t_{bo} - t_o) + R_o \tag{9}$$

Mechanization of the Algorithm

The mechanization of the algorithm requires logic to first determine in which case (1, 2, or 3) the missile is operating. This will be a function of present time, range, range-rate, and the near future acceleration profile. Once the case is determined, the appropriate equations are solved by the following methods:

    1. For Case 1 time-to-go can be calculated in closed form by

$$tgo = \frac{2R_o}{-\dot{R}_o + \sqrt{(\dot{R}_o)^2 + 2kR_o}} \tag{10}$$

182

2. For Case 2. A Newton iteration technique is used to determine the time at which R(t) = 0 in equation (5).*

3. For Case 3. A Newton iteration technique is used to determine the time at which R(t) = 0 in equation (7)* using the values of $\dot{R}(t_{bo})$ and $R(t_{bo})$ determined by equations (8) and (9).

*NOTE: Prior to solving equation (5) or (7), a check must be made to determine if R(t) = 0 is a valid solution. This is done by determining the time at which the range rate will go to zero. To do this equation (4) or (6), as appropriate, is set to zero and solved for t. That t is then substituted into equation (5) or (7), appropriately, and R(t) is calculated. If R(t) is negative the algorithm proceeds. If not, then the time at which $\dot{R}(t)$ = 0 is used as the final time.

This process, although involved, is solvable with a digital computer. The algorithm is intended to be solved every Δt as the missile flys toward the target. If sample time causes throughput bottlenecks the appropriate modifications could be made, such as solving for new t_f's, every two or three guidance computations, as required.

Closed-Form Method

Recall that the reason for needing time-to-go in the guidance law stems from the original assumptions made in deriving the law; that is, that final time is fixed and the missile has complete control of its acceleration vector. The following time-to-go algorithm attempts to rectify these deviate assumptions.

Consider a rewritten form of the guidance law given in equation (1), and referenced to the missile body coordinate frame.

$$A_{MX} = 3\ (S_{RX}/tgo^2 + V_{RX}/tgo + K_T A_{TX}) \tag{11a}$$

$$A_{MY} = 3\ (S_{RY}/tgo^2 + V_{RY}/tgo + K_T A_{TY}) \tag{11b}$$

$$A_{MZ} = 3\ (S_{RZ}/tgo^2 + V_{RZ}/tgo + K_T A_{TZ}) \tag{11c}$$

Given knowledge of the vector quantities $\bar{S}_R$, $\bar{V}_R$, and $\bar{A}_T$ (recall this information will be supplied by the state estimator) then the unknowns in equation (11) are A_{MX}, A_{MY}, A_{MZ} and tgo. The

183

quantity A_{MX} is the missile's axial acceleration command. This quantity is not controllable and would normally not be of interest. However, if the commanded axial acceleration were forced to be the actual measured axial acceleration then there would be only one unknown in equation 11a, tgo. This is the basis for this time-to-go algorithm. That is, pick a tgo that forces the commanded axial acceleration to equal the present missile axial acceleration measurement. The value of tgo is then used to solve equations 11b and 11c for A_{MY} and A_{MZ}. With this logic and the use of the Quadratic Formula the following closed form solution for time-to-go results.

$$ tgo = \frac{2S_{RX}}{-V_{RX} + \sqrt{(V_{RX})^2 + 4S_{RX}A_{RX}/3}} \tag{12} $$

where

$$ A_{RX} = A_{MX} - 3K_T^- A_{TX} $$

$$ K_T^- = K_T \Big|_{t_o - \Delta t} $$

Mechanization of the Algorithm

To mechanize the algorithm all the vector components must be known with respect to the missile body coordinate system. The terms S_{RX}, S_{RY}, and A_{TX} are obtained from the state estimator and A_{MX} is the measured axial acceleration from an onboard accelerometer. The term K_T^- is an approximation of the proper value of K_T. Recall that K_T is a function of time-to-go. This creates a problem in mechanizing equation (12) directly since we are solving for time-to-go. Fortunately, K_T varies slowly as a function of time-to-go. Using this fact, equation (12) can be solved using a value of K_T calculated from the most recent past estimate of time-to-go, hence the notation K_T^-.

Exact Non-realizable Method

In order to evaluate any method for estimating time-to-go an exact truth model must be established. This is more complicated than flying the missile and post priori determining final time. The reason for this is simple. The time-to-go estimate used at

184

each guidance command interval will cause a different accelera-
tion command, hence a different trajectory and hence a different
final time. To determine the exact trajectory the missile will
fly with the exact knowledge of time-to-go requires an impracti-
cal iterative method comprised of multiple flyouts. Although
such a method is non-realizable for real world applications, it
is useful as an evaluation tool. Such a method was developed to
determine the missile's performance using exact knowledge of
time-to-go. The results are surprising as will be seen later.

The algorithm is a straight forward recursive iteration scheme
often used to solve transcendental equations and is depicted in
Figure 1. It has one check in it to insure stability and is
exited when the change in two subsequent flight times is less
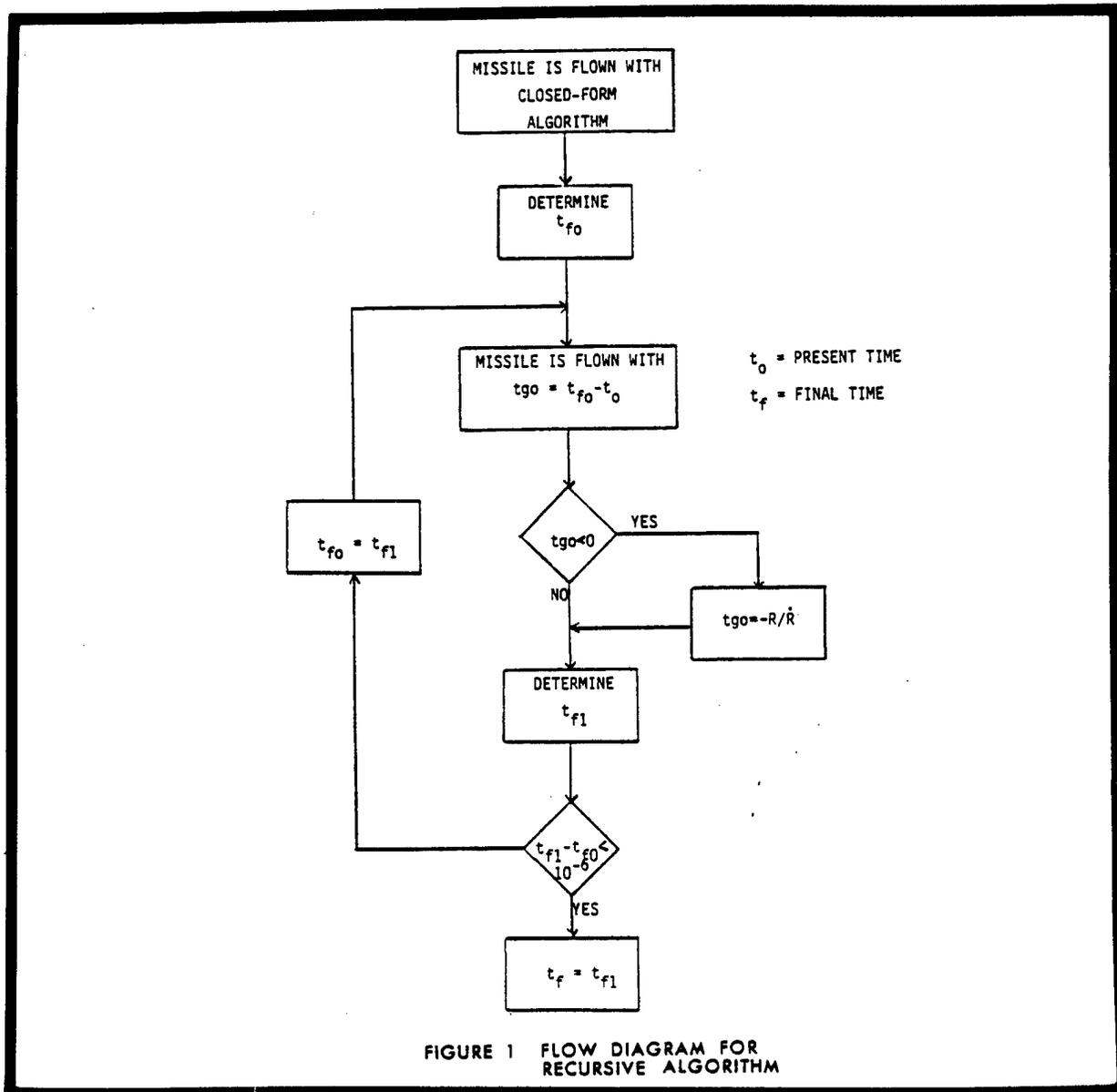than 10^{-6} seconds.

FIGURE 1   FLOW DIAGRAM FOR
RECURSIVE ALGORITHM

ANALYSIS

Approach

The most economical and effective method to evaluate any time-to-go algorithm is to implement it in a detailed simulation of a missile system and perform simulated missile fly-outs against realistic target maneuvers. This was accomplished in the analyses of the techniques presented in this paper.

The simulation consists of a six-degree-of-freedom (6-DOF) missile model of a conceptual high performance bank-to-turn short range air-to-air missile. The simulation contains detailed non-linear math models of the major missile subsystems including the seeker, autopilot, and propulsion; detailed aerodynamic models of the missile airframe characteristics supported by wind tunnel generated aero data; and the models that describe the missile's equations of motion. Additionally, the simulation contains a three-degree-of-freedom target model which incorporates a nine "g" out-of-plane evasive maneuver algorithm.

To perform the analysis the guidance law given by equation (1) was implemented with each time-to-go algorithm into the simulation and provided all required information assuming zero errors. Although this method of evaluation deviates from the "real" world, it does provide a common method for at least comparing one time-to-go technique to another. To be sure, if a particular technique does not perform well under these ideal conditions, it certainly won't perform well under more realistic and restrictive conditions. Therefore, this analysis provides an intermediate step in determining the comparative performance of the candidate algorithms.

Comparison of Algorithm's Accuracy

For reference purposes the four algorithms presented in this paper will be indexed by the following shorthand names:

TG01 — $-R/\dot{R}$ (Equation 2)

TG02 — Numerical Method (Equations 4-10)

TG03 — Closed-form Method (Equation 12)

TG04 — Recursive Method (Figure 1)

Figure 2 is a plot of the time-to-go estimates versus time for the four algorithms. As can be seen, TG02 and TG03 and of course TG04 (recall it is forced to be accurate) accurately estimate

186

time-to-go whereas TG01 has considerable error. However, all techniques resulted in a small final miss distance (less than 2 ft) in this rather mundane engagement.

Figure 3 shows the time-to-go estimate versus time from TG01 during a difficult forward hemisphere off-boresight shot. Note that the algorithm over estimates time-to-go early in the flight during thrusting and then underestimates time-to-go for the remaining flight (coasting phase begins at 2.6 seconds). This happens in all cases for TG01 due to the fact that the algorithm assumes constant closing velocity although the missile sustains high acceleration levels due to thrust and drag. For this case, the missile attained a final miss distance of 15.6 feet.

Figure 4 plots the time-to-go estimates for TG02, TG03, and TG04 made during the same initial engagement as in Figure 3. Each time-to-go algorithm caused a different final time, hence the three different asymtotes. In this case, TG03 performs the worst in terms of estimation accuracy, however; unexpectedly, the most accurate time-to-go method, TG04, results in an extremely poor miss distance. Other similar shots were tried to determine if this was an isolated case or a general problem. It was found that the same problem occurs in many other large off-boresight forward hemisphere launches. To help determine the reason for this deviation from expected performance consider the differences in TG03 and TG04. TG03 underestimated time-to-go during the thrusting phase and then tracked true time-to-go nearly exactly from burnout to intercept. The only significant difference in TG03´s accuracy as compared to TG04 was during the thrusting phase. Now consider how this affected the missile´s acceleration commands over the subsequent flights. Figure 5 plots the commanded normal acceleration profiles associated with TG03 and TG04. First consider the profile due to TG03. It is clear that the missile commanded an extremely hard initial turn and then from about two to five seconds it commanded a low g level turn. The peak that occurs at 5.1 seconds is in reaction to a last ditch target maneuver which is activated at approximately 1 second before intercept. Intercept occurs at 6.1 seconds. Now consider the profile associated with TG04. For the first five seconds it is nearly a constant 26 g turn. At 5.7 seconds the missile reacts to the target maneuver. During the last half second the steering errors are large and the missile is commanding large acceleration. Unfortunately the missile dynamics can´t process these commands instantaneously resulting in a large miss. It appears that the major difference in the commanded acceleration profiles is the hard initial turn. This turn occurs during the same time frame that TG03 is underestimating time-to-go. Since this occurs early in the launch, the geometry of the engagement is virtually the same indicating that the different ac-
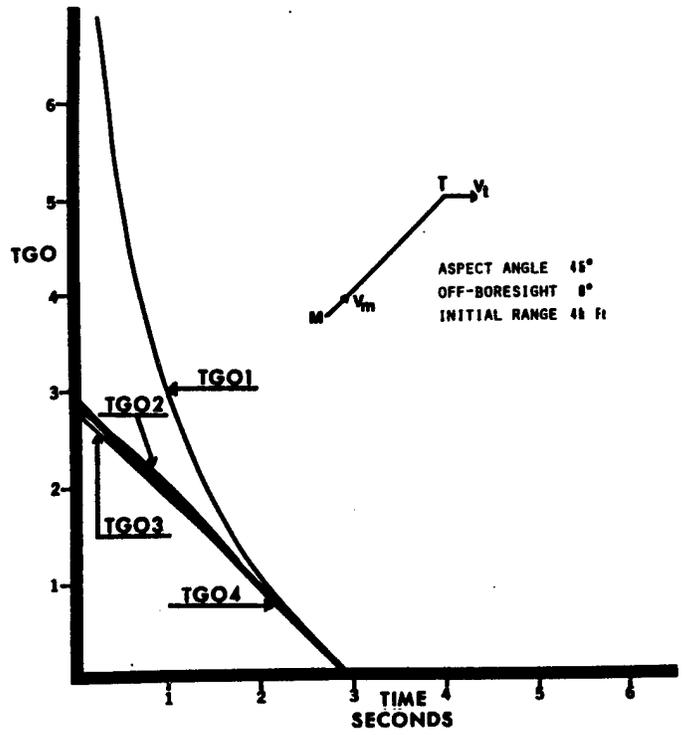
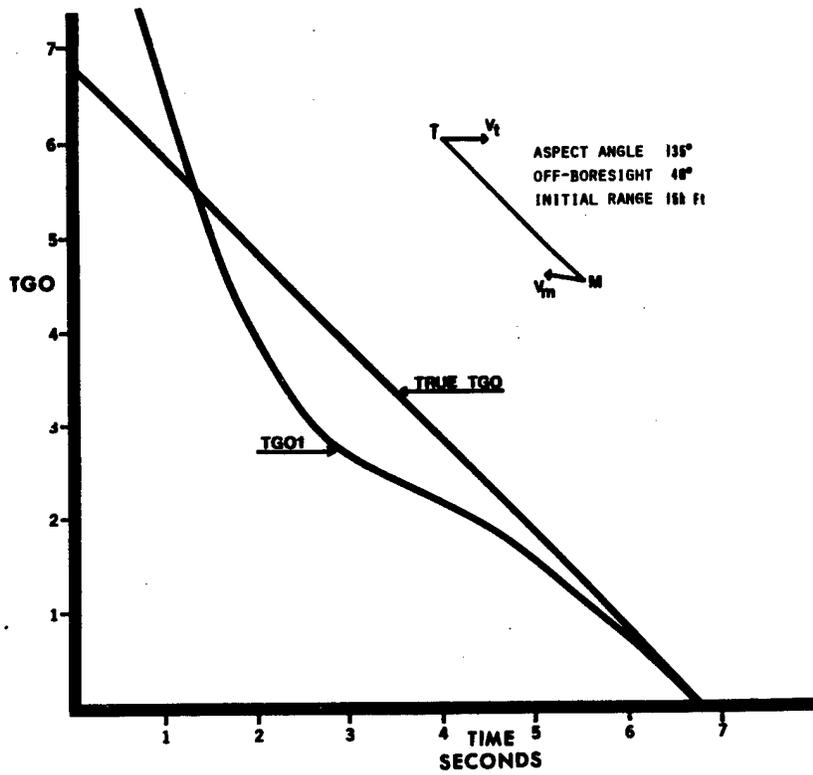**FIGURE 2 COMPARISON OF TIME—TO—GO ALGORITHMS**
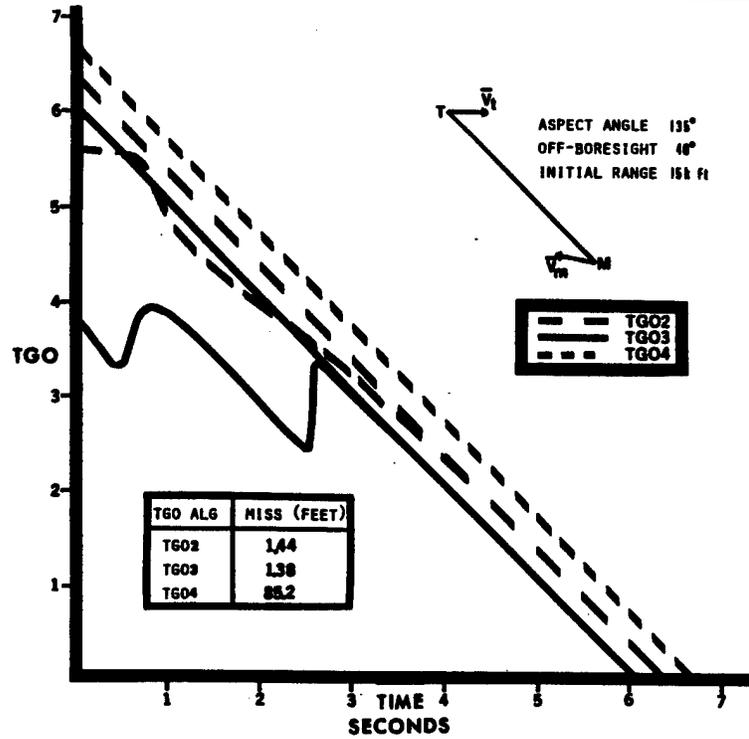

FIGURE 3 TGO1 VERSUS TRUE TIME—TO—GO

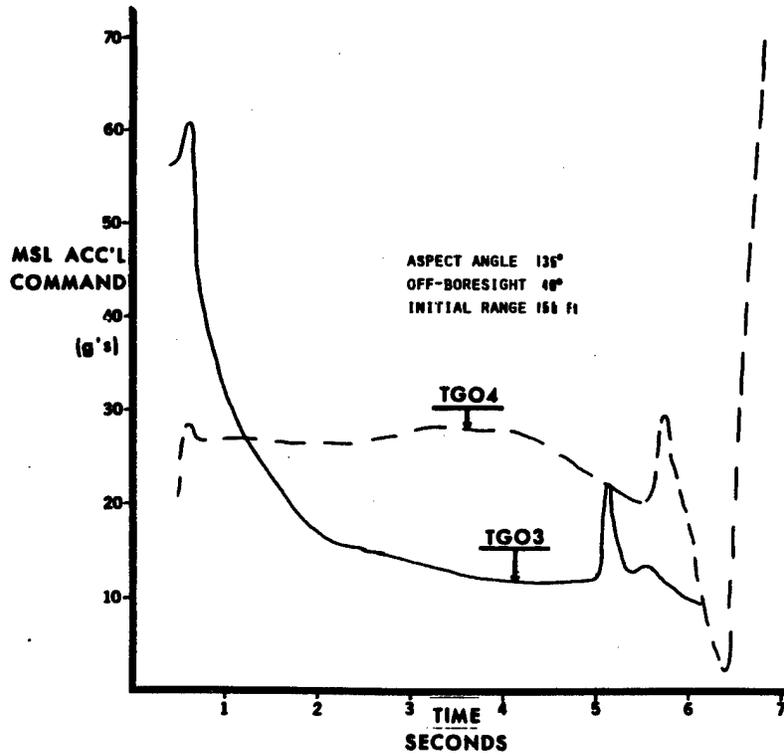FIGURE 4 TGO2, TGO3, TGO4 VERSUS TRUE TIME—TO—GO

FIGURE 5 MSL ACC'L COMMANDS VERSUS TIME FOR TGO3 AND TGO4

celeration profiles are directly attributable to the time-to-go algorithm.

To help verify this claim the mechanization of TG04 was modified such that a value of .75 of the true time-to-go was used for guidance during the thrusting phase. After burnout, the true time-to-go was used as in the original TG04. The missile was then reflown with the modified TG04 resulting in a miss distance of .49 feet. More importantly the acceleration profile for the modified algorithm was examined to see if it exhibited the same characteristics as TG03. Not surprisingly it did. In fact, the profiles were nearly the same. Figure 6 shows the commanded acceleration profile due to the modified TG04. This is a very significant result. It suggests that in terms of missile performance one does not always want to predict time-to-go accurately for mechanizing linear feedback laws. However, this raises the question how and when should the time-to-go estimate be inaccurate? To help answer this question further analyses were performed.

Aspect Angle	O-B Angle	Range (FT)	TGO3	TGO4	MOD TGO4	
					*.75	*.50
45	0	4000	1.85	.61	.81	30.8
45	40	4000	.35	.31	.52	.55
90	0	6000	2.37	.69	.87	75.1
90	40	6000	.51	.51	.63	.63
90	0	10000	.48	.32	.45	.41
90	40	10000	.58	333.	.73	.47
135	0	15000	.83	.59	.51	.78
135	40	15000	1.38	85.2	.49	.17

TABLE 1.   Comparison of Miss Distances
for TG03, TG04, & Modified TG04

Experience with TG01 clearly establishes that time-to-go should not be overestimated. Doing so makes the missile wait until the steering errors become excessively large, forcing drastic end-game maneuver requirements, possibly exceeding the missiles capability. This means that if there is to be error in the time-to-go parameter then it should be such that the estimate is less than the true value. To help determine when and by how much time-to-go should be underestimated, the modified TG04 was used with values of .75 and .5 true time-to-go during thrusting to evaluate the missile's performance in various engagements. The results of this study are given in Table 1. The results show that knowledge of true time-to-go can result in large miss distances. However, this only happens in initial large off-boresight launches and not when the missile is launched on a near intercept trajectory. Further, the results show that underestimating time-to-go by a factor of .5 during thrusting can cause the missile's performance for on-boresight launches to significantly decrease. The combination of these results indicates that time-to-go should only be underestimated in large off-boresight launches in order to null out the large steering errors as soon as possible. Doing this forces the missile to attain a collision course early in flight minimizing the chances of late evasion due to drastic target maneuvers. A further benefit of the resulting trajectory is that the missile performs its hard turning at lower velocities prior to realizing the total effects of thrusting, thus minimizing induced drag effects and increasing the missile's energy. This will naturally result in extended range capabilities.

Compensating For Large Off-Boresight Errors

To be sure, there are a number of ad hoc approaches to compensating for large off-boresight errors. For instance, a direct approach could be to add a bias term to the guidance law that would be directly proportional to off-boresight angle. This is certainly a feasible but possibly very involved approach. A more subtle method involves mechanizing the time-to-go algorithm in missile body coordinates. Recall that TG03 does this. To understand the rationale behind this approach consider Figure 7. Figure 7 depicts the relative position geometry for a planar engagement. The line-of-sight vector has a magnitude equal to the relative range and lies along the target/missile sight line. The vectors $\bar{R}_x$ and $\bar{R}_y$ are orthogonal vectors aligned in the missile's axial and normal directions respectively. The missile guidance problem is simply to drive and maintain the magnitude of the vector $\bar{R}_y$ to zero prior to the time that the magnitude of the vector $\bar{R}_x$ goes to zero. Ideally, at final time $\bar{R}_x$ and $\bar{R}_y$ will both go to zero simultaneously. The optimal guidance law attempts to do this. Most approaches to estimating time-to-go are concerned with determining the time at which the magnitude of the line-of-sight

vector will be minimized but not necessarily zero. This is an important yet subtle point. The only scenario in which the line-of-sight vector goes to zero is in the special case of a direct hit. However, for any given control logic there will be a time at which the line-of-sight is minimized hence a valid final time for use in calculating time-to-go. Now consider the scenarios in which the vector $\bar{R}_x$ goes to zero. To wit, the vector $\bar{R}_x$ goes to zero in every case that the missile can overtake the target. In other words, if the missile has a velocity advantage over the target, the magnitude of $\bar{R}_x$ will go to zero. This includes all cases in which an intercept can occur. By calculating the time at which this vector goes to zero, that time can naturally be used by the guidance to command normal accelerations such that the magnitude of $\bar{R}_y$ will go to zero before or at that final time.

The way in which the use of the body referenced range vectors for time-to-go calculations relates to off-boresight angle is simple. The ratio of $\bar{R}_y$ and $\bar{R}_x$ is a direct function of the off-boresight angle. The larger the angle, the smaller the magnitude of $\bar{R}_x$ and hence for a given thrust profile the smaller the value for time-to-go. Since the guidance gains are inversely proportional to the value of time-to-go, larger normal accelerations will be commanded to drive the magnitude of $\bar{R}_y$ to zero.

A further benefit of calculating time-to-go using missile body referenced information is that the acceleration in the missile axial direction is well defined reducing to sources of error to essentially the uncertainty in target acceleration. This is in contrast to the uncertainty in line-of-sight acceleration which is a function of the missile's axial acceleration, normal acceleration and target acceleration.

Missile Performance

The ultimate performance criteria for any guidance technique is its ability to hit the target under all possible initial engagement conditions. One commonly used method for measuring how well a missile meets the performance criteria is through a determination of the missile's inner and outer launch boundaries. This was done to evaluate the time-to-go algorithms' effect on the missile's performance. Each of the three realizeable time-to-go algorithms (TG01, TG02, and TG03) was interfaced with the guidance law and mechanized in the 6-DOF simulation. Using a binary search algorithm the inner and outer launch boundaries were computed for each time-to-go/guidance configuration. (This was not accomplished for TG04 because of the extremely large number of runs that would be required).
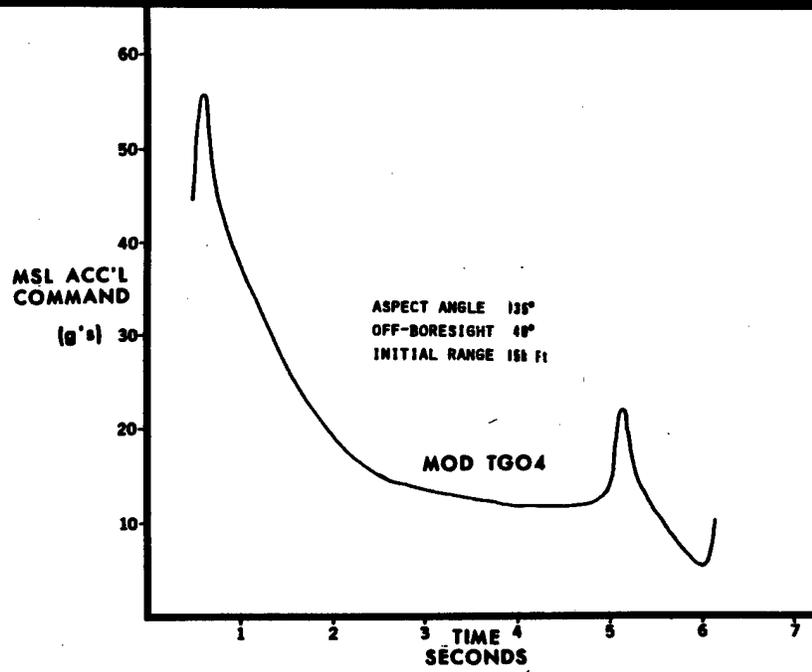
192

ASPECT ANGLE 135°
OFF-BORESIGHT 40°
INITIAL RANGE 15k Ft

MOD TGO4

**FIGURE 6 MSL ACC'L COMMAND VERSUS
TIME FOR MODIFIED TGO4**

$\overrightarrow{LOS} \triangleq$ LINE-OF-SIGHT VECTOR

FIGURE 7 PLANAR ENGAGEMENT GEOMETRY

ASPECT
ANGLE

OFF-BORESIGHT
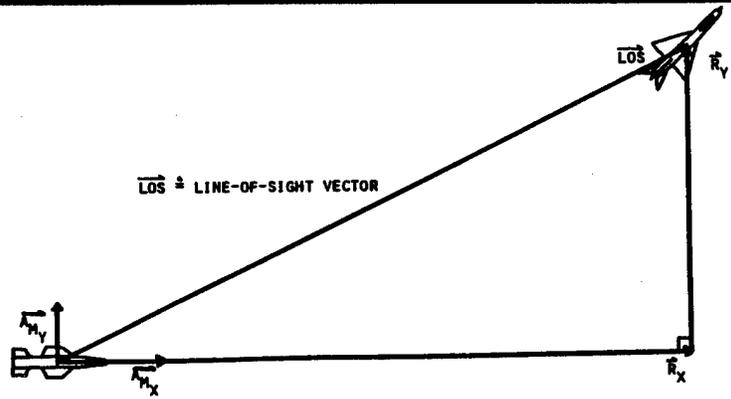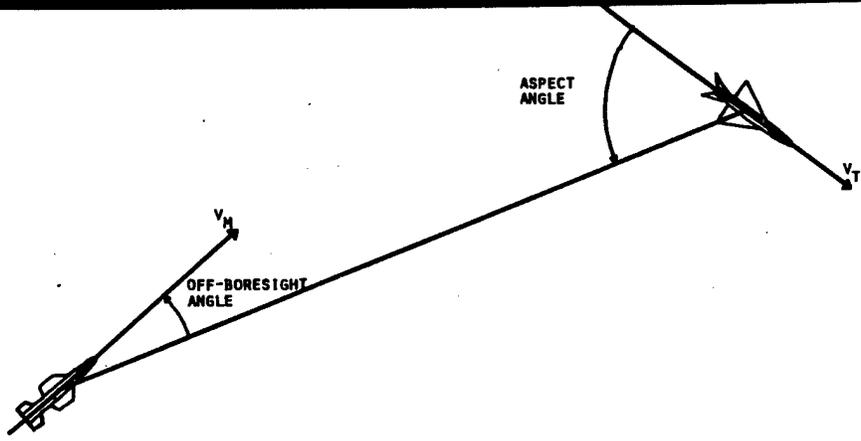ANGLE

FIGURE 8 INITIAL ENGAGEMENT GEOMETRY

193

The inner launch boundary defines the minimum range from which the missile can be launched and achieve a hit. (A hit is scored any time the point of closest approach is within ten feet of the target). The outer launch boundary defines the maximum range from which the missile can be launched and achieve a hit. Obviously, there is an infinite number of launch conditions that can be selected for evaluation. In order to limit the evaluation process a set of initial launch conditions is selected. The selection of these conditions should be done such that the evaluation will provide a good sampling of the weapon's performance over all expected initial conditions. To this end the following conditions were selected.

1. Missile and target are co-speed and flying straight and level at launch. (.9 Mach).

2. Missile and target are co-altitude at launch (10,000 ft).

3. The initial aspect angle (angle between the target's velocity vector and the line-of-sight) is varied from zero to 180 degrees in 30 degree increments. Zero degrees aspect angle is a tail-on shot whereas 180 degrees is a head-on shot.

4. The initial off-boresight angle (angle between the missile's velocity vector and the line-of-sight) is either zero degrees or 40 degrees lagging. Zero degrees off-boresight angle means the missile is launched directly at the target. Forty degrees lagging off-boresight angle means the missile is fired such that the missile's velocity vector is pointed 40 degrees behind the target.

The first two conditions (speed and altitude) were selected to be representative of dogfight conditions. The aspect angle can in reality vary from zero to 360 degrees, however, it was limited at 180 degrees because these angles represent a worst case due to the nature of the target maneuver. The two off-boresight angles were selected to evaluate the missile under a favorable off-boresight (zero degrees) and at an extremely difficult off-boresight condition (40 degrees lagging). The initial engagement geometry is depicted in Figure 8.

Table 2 gives the inner launch boundaries for the three algorithms while Table 3 gives the outer launch boundaries. The inner boundaries are accurate to within 125 feet whereas the outer boundaries have a 250 foot accuracy. Note that for the forty degree off-boresight launches the missile failed to hit the

194

		0°	30°	60°	90°	120°	150°	180°
0° O B A	TG01	1000	1000	1375	1675	3125	3125	1875
	TG02	1000	1000	1000	1125	2625	2625	1875
	TG03	1000	1000	1000	1000	2625	2875	1875
40° O B A	TG01	*	*	*	*	3625	4375	4125
	TG02	1000	1375	1875	2125	2325	3625	3875
	TG03	1000	1000	1000	1375	2125	2875	3875

*Designates a No-Hit Condition. The Missile Failed to Intercept From Any Launch Range.

TABLE 2.   INNER LAUNCH BOUNDARIES IN FEET FOR
           TG01, TG02, and TG03

		0°	30°	60°	90°	120°	150°	180°
0° O B A	TG01	8750	9250	10250	12750	16750	24750	26750
	TG02	7250	7750	9250	12250	17250	20750	23750
	TG03	9250	10250	12250	15250	20250	25250	26750
40° O B A	TG01	*	*	*	*	11250	20250	19750
	TG02	5250	5750	6750	9750	13750	19750	20250
	TG03	8250	8750	10250	13250	17250	23750	24750

*Designates a No-Hit Condition

TABLE 3.   OUTER LAUNCH BOUNDARIES IN FEET FOR
           TG01, TG02, and TG03

195

		0°	30°	60°	90°	120°	150°	180°
0°	TG02	1000	1000	1000	1125	2625	2625	1875
O B A	BODY TG02	1000	1000	1000	1000	2625	2875	1875
	TG03	1000	1000	1000	1000	2625	2875	1875
40°	TG02	1000	1375	1875	2125	2325	3625	3875
O B A	BODY TG02	1000	1000	1000	1375	2125	2875	3875
	TG03	1000	1000	1000	1375	2125	2875	3875

TABLE 4. INNER LAUNCH BOUNDARIES IN FEET FOR TG02, TG03, & TG02 COMPUTED IN BODY COORDINATES

		0°	30°	60°	90°	120°	150°	180°
0°	TG02	7250	7750	9250	12250	17250	20750	23750
O B A	BODY TG02	9750	10250	11750	15250	19750	24750	26750
	TG03	9250	10250	12250	15250	20250	25250	26750
40°	TG02	5250	5750	6750	9750	13750	19750	20250
O B A	BODY TG02	7250	7750	8750	12250	16250	22750	22750
	TG03	8250	8750	10250	13250	17250	23750	24750

TABLE 5. OUTER LAUNCH BOUNDARIES IN FEET FOR TG02, TG03, & TG02 COMPUTED IN BODY COORDINATES

target from any launch range when the guidance employed TG01. This was due to TG01's overestimation of time-to-go which caused the missile to wait too long before adequate steering, thus flying itself into a non-recoverable situation. TG02 performed much better than TG01, however, its performance fell far short of that obtained by the closed form algorithm, TG03, especially in the large off-boresight scenarios. This is due to a violation in the original assumptions used in deriving TG02, namely the assumption that the missile's axial acceleration is closely aligned to the line-of-sight vector. Based on this, it is reasonable to hypothesize that TG02's performance would increase if it was mechanized with missile body reference information as is done with TG03. To see if this was true, TG02 was remechanized using body reference information and re-evaluated. Tables 4 and 5 give the results from this study. As can be seen, the performance of the missile greatly increased. The body mechanized TG02 obtained the same inner boundaries as TG03 but the outer boundaries, although considerably better than TG02, fall short of the performance obtained by TG03. This is probably due to the fact that TG02 assumes zero target acceleration whereas TG03 does not make that assumption. Other studies have shown that target acceleration information improves outer launch boundary performance. [5]

Complexity of Solution

One of the fundamental issues involved in the selection of any time-to-go algorithm is the issue of complexity. Since the algorithm will be implemented in a small dedicated guidance computer it is mandatory that the algorithm be as simple as possible while maintaining a high level of expected missile performance.

Table 6 summarizes the complexity requirements versus the comparative performance results based on the launch boundary determinations for TG01, TG02, and TG03. The table gives the number of Fortran lines of code used to mechanize the algorithms in the simulation and the special functions needed to solve the algorithms. As can be seen TG03 performed the best and was relatively simple to mechanize.

ALG	#Lines of Code	Special Functions	Relative Performance
TG01	2	0	3
TG02	48	Square Root Exponential	2
TG03	3	Square Root Exponential	1

TABLE 6. SUMMARY OF COMPLEXITY REQUIREMENTS AND RELATIVE PERFORMANCE

SUMMARY AND CONCLUSIONS

Four time-to-go algorithms were developed and evaluated to determine both the accuracy of the algorithms and the effect of the algorithms on missile performance. The following results were found.

1. The commonly used method for estimating time-to-go, range over range-rate, severely limits the missile's performance capability.

2. If the guidance law is suboptimal as is the one used in this study, use of perfect knowledge of time-to-go can cause substandard missile performance in high dynamic engagements. In these cases, underestimation of time-to-go during the thrust phase will compensate for the suboptimality of this guidance law by nulling large initial steering errors early in the engagement.

3. Time-to-go calculations should be accomplished in missile body reference coordinates.

4. Iterative techniques for estimating time-to-go are very sensitive to modeling errors making it imperative that the algorithms contain complex equations. These methods, although solvable, tend to be very complicated.

5. The best performing yet simplistic algorithm is the closed-form algorithm that forces the commanded missile axial acceleration to be equal to the actual missile axial acceleration.

REFERENCES

1. Youngblood, J.N., "Advanced Linear Guidance Laws for Air-to-Air Missiles", AFATL-TR-80-12, January 1980.

2. Fiske, P.H., "Advanced Digital Guidance and Control Concepts for Air-to-Air Tactical Missiles," AFATL-TR-77-130, November 1977.

3. Anderson, G.M., "Guidance and Control Methodology,", AFATL-TR-79-86, October 1979.

4. Sammons, J.M., et al, "Development and Comparison of Optimal Filters," AFATL-TR-79-87, October 1979.

5. Riggs, T.L., Vergez, P.L., "Advanced Air-to-Air Missile Guidance Laws Using Optimal Control and Estimation Techniques," AFATL-TR-81-56, June 1981.

6. Riggs, T.L., "Linear Optimal Guidance for Short Range Air-to-Air Missiles," Proceedings of NAECON 1979, Volume II, pages 757-764, May 1979.

7. "Advanced Analysis For Future Missiles," MICOM Report #RG-80-8, November 1979.

MICROPROCESSOR-BASED OPTIMAL CONTROLLERS FOR A
HELICOPTER TURRET CONTROL SYSTEM

N. Coleman, E. Carroll, and R. Johnson
U.S. Army Armament Reseach and Development Command
DRDAR - SCF - CC
Dover, New Jersey 07801

N. K. Loh
Center for Robotics and Advanced Automation
School of Engineering
Oakland University
Rochester, Michigan 48063

ABSTRACT

The design and implementation of microprocessor-based discrete-time optimal controllers for the XM-97 helicopter gun-turret control system is considered. Nonfiring and firing test results are presented. Further testings and the design and implementaion of disturbance cancellating turret controllers are currently underway.

1. INTRODUCTION

The design of a high precision helicopter pointing control system using modern control and observer theory has been investigated by Coleman, Loh, et al in [1]. The pointing control system investigated was the XM-97 helicopter gun-turret control system. The continuous-time optimal controllers and observers developed in [1] were implemented by using standard analog electronic components. The resulting performance improvement of the optimal turret control system, in terms of round dispersion, turret overshoot, turret settling time, etc., ranged from a factor of 2 to 1 to a factor 10 to 1 when compared with the performance of the original system.

Recently, the continuing design efforts on helicopter turret control systems have been directed towards the development of high precision turrets employing microprocessor-based optimal controllers. Results presented in [2] demonstrated that it is indeed feasible to implement such an optimal controller in a real time environment by using state of the art microprocessors. Furthermore, numerical processor chips such as the 8087 are sufficiently fast enough to permit implementing some forms of adaptive control laws which may further enhance control system performance.

The purpose of this paper is to present some preliminary results on the performance of the XM-97 helicopter turret investigated in [1] employing microprocessor-based optimal controllers. The microprocessor sofeware was developed by using a basic Intel 220 development system expanded to 64K bytes RAM and 1.25 megabytes disc.

The organization of the paper is as follows. Section 2 gives a brief description of the existing XM-97 helicopter gun-turret control system and its step

responses. Section 3 presents a simplified mathematical model of the original system. The formulation and design of discrete-time optimal controllers for both the azimuth and elevation channels of the gun-turret based on the simplied model developed in Section 3 is presented in Section 4. The microprocessor-based implementation of discrete-time optimal turret controllers is discussed in Section 5. Section 6 presents preliminary nonfiring and firing test results. Further performance evaluations of the microprocessor-based XM-97 helicopter gun-turret control system and the design of microprocessor-based disturbance cancellating controllers are currently underway; the results will be reported elsewhere.

2. DESCRIPTION OF THE EXISTING XM-97 HELICOPTER GUN-TURRET CONTROL SYSTEM

The XM-97 helicopter gun-turret system consists of a three-barrel 20mm automatic cannon system and a turret drive system mounted under the nose section of a Cobra helicopter. For test purposes, the gun-turret and helicopter airframe are suspended from a six-degree-of-freedom simulator as shown in Fig. 1. The gun-turret control system is essentially an inertial load driven by a pulse width modulated split series DC motor through a compliant gear box. The transfer functions of the system are as shown in Fig. 2. The system consists of two controllers: one controller positions the gun turret in azimuth and the other elevates and depresses the gun cradle and the gun. The two controllers are functionally similar and independent. As shown in Fig. 2, the only difference between the two controllers is the gear ratio N which is N = 620 for the azimuth channel and N = 810 for the elevation channel.

The existing gun-turret control system essentially employs angular position feedback and angular velocity feedback. With the state variables chosen as shown in Fig. 2, the turret dynamics is described by the following 8-dimensional vector differential equation (for both azimuth and elevation channels),

$$\dot{x}(t) = Ax(t) + Bu(t), \quad x(0) = x_o, \tag{1}$$

where

$x(t) = [x'_1(t) \ x'_2(t) \ x_3(t) \ x_4(t) \ x_5(t) \ x_6(t) \ x_7(t) \ x_8(t)]^T$,

$x'_1(t)$ = gun turret angular position relative to the hull (radians),

$x_4(t)$ = gun-turret angular velocity relative to the hull (radians/second),

$x'_2(t)$ = motor angular velocity relative to the hull (radians/second),

$x_3(t)$ = motor torque (foot-pounds),

$x_5(t)$ = power amplifier output (volts),

$x_6(t)$ = low level electronics output (volts),

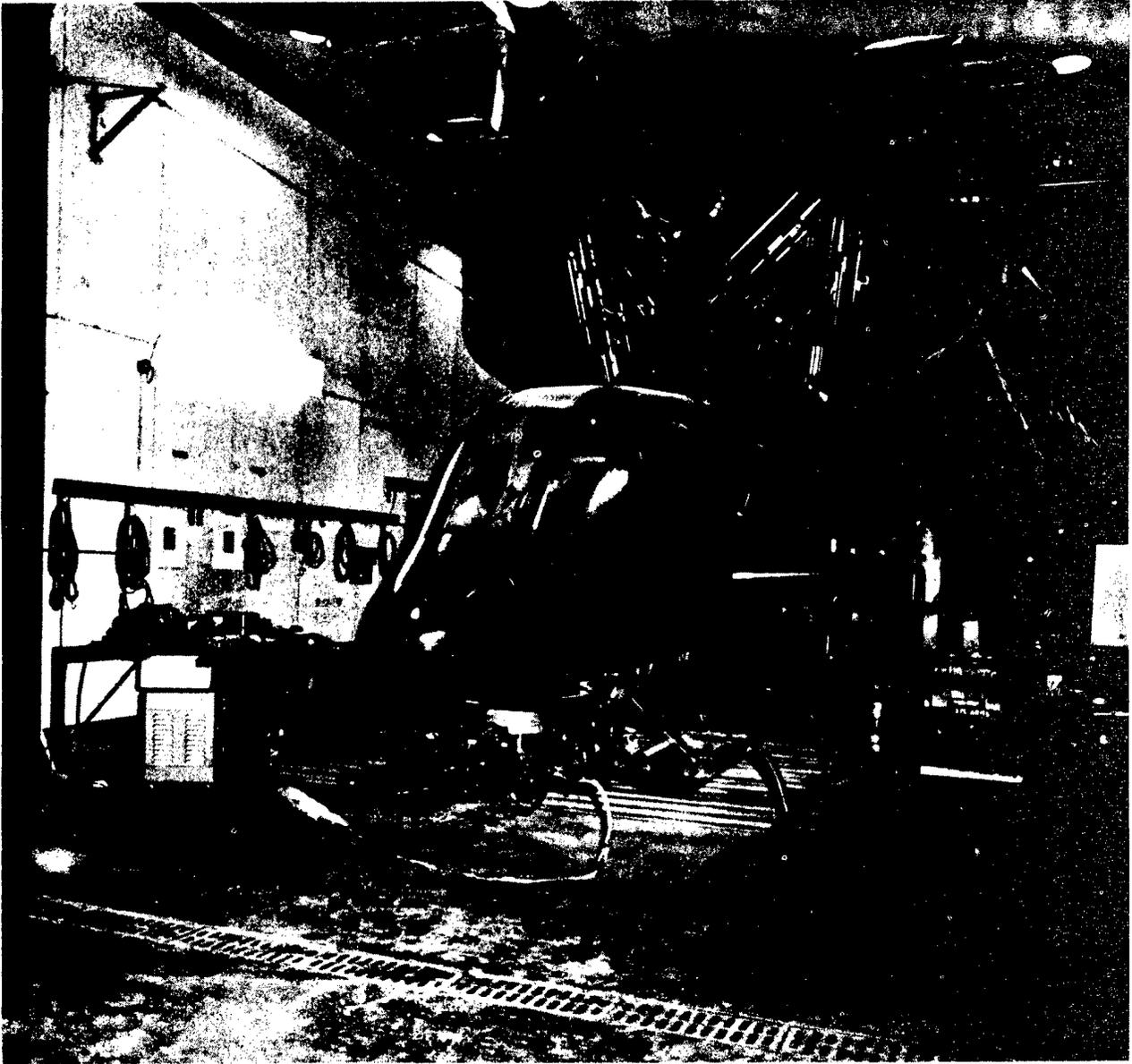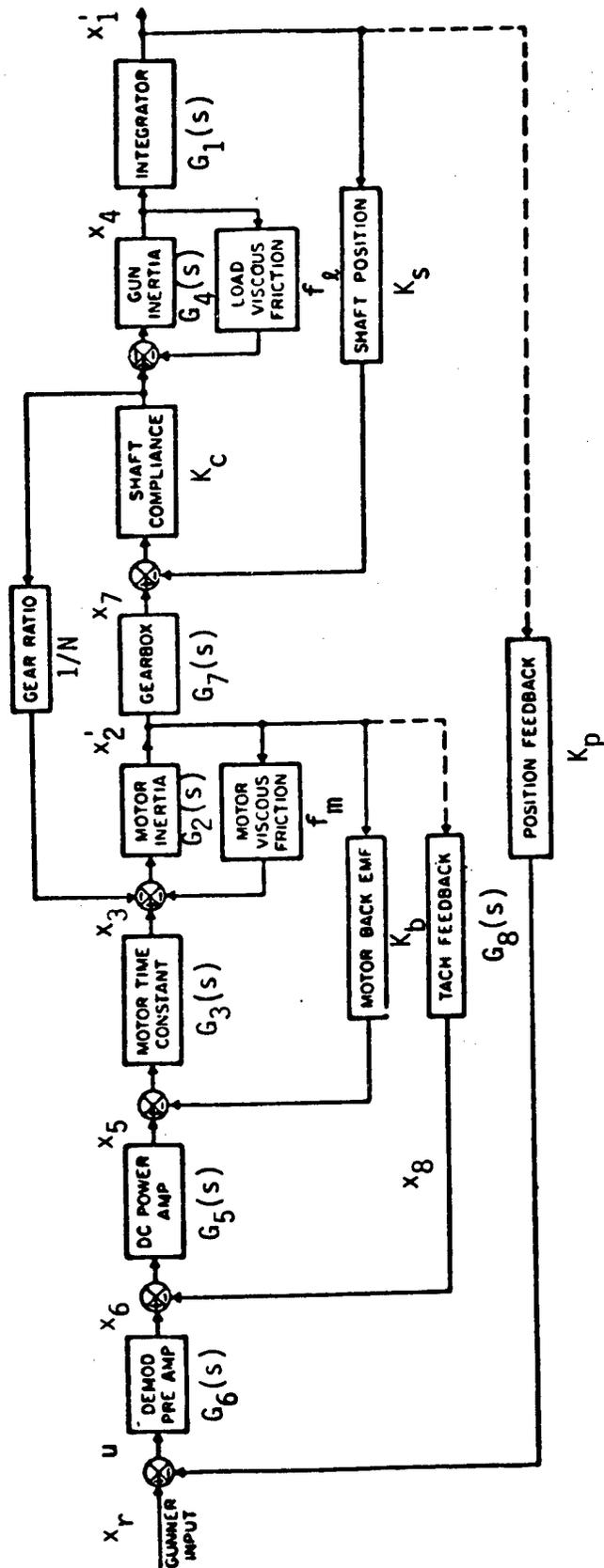$x_7(t)$ = geared-down shaft angular position relative to the hull (radians),

Fig. 1 XM-97 HELICOPTER GUN-TURRET SUSPENDED FROM SIMULATOR

Fig. 2 ORIGINAL XM-97 HELICOPTER TURRET CONTROL SYSTEMS — AZIMUTH AND ELEVATION CHANNELS

$$G_1(s) = \frac{1}{s}$$

$$G_2(s) = \frac{1}{0.00025s}$$

$$G_3(s) = \frac{p_1}{1 + 0.002s}$$

$$G_4(s) = \frac{1}{15.7s}$$

$$G_5(s) = \frac{7.5}{1 + 0.002s}$$

$$G_6(s) = \frac{535}{1 + 0.005885s}$$

$$G_7(s) = \frac{1}{Ns}$$

$$G_8(s) = \frac{p_2 s}{s + p_3}$$

$$K_p = K_s = 1.0 \qquad K_b = 0.0192 \qquad K_c = 5000000.0 \qquad f_m = 0.0 \qquad f_\ell = 50.0$$

$$N = 620 \text{ (AZIMUTH CHANNEL)} \qquad N = 810 \text{ (ELEVATION CHANNEL)} \qquad p_1 = 0.02 \qquad p_2 = .03 \text{ Az.} \qquad p_3 = 6.6 \text{ Az.}$$
$$.0375 \text{ El.} \qquad 6 \text{ El.}$$

$x_8(t)$ = output of tachometer feedback loop (volts),

$x_r(t)$ = gunner command input (radians),

$u(t)$ = control input (volts) = $x_r(t) - x'_1(t)$

and A and B are, respectively, 8x8 and 8x1 constant matrices given by

$$
A = \begin{bmatrix}
0 & 0 & 0 & 1 & 0 & 0 & 0 & 0 \\
2/Nx10^{10} & 0 & 0 & 4x10^3 & 0 & 0 & -2/Nx10^{10} & 0 \\
0 & -9.6p_1 & -5x10^2 & 0 & 5x10^2p_1 & 0 & 0 & 0 \\
-3.185x10^5 & 0 & 0 & -3.185x10^5 & 0 & 0 & 3.185x10^5 & 0 \\
0 & 0 & 0 & 0 & -5x10^2 & 3.750x10^3 & 0 & -3.750x10^3 \\
-9.095x10^4 & 0 & 0 & 0 & 0 & 0 & -1.70x10^2 & 0 \\
0 & 1/N & 0 & 0 & 0 & 0 & 0 & 0 \\
2/Nx10^{10}p_2 & 0 & 4x10^3p_2 & 0 & 0 & 0 & -2/Nx10^{10}p_2 & -p_3
\end{bmatrix},
$$

$$
B = \begin{bmatrix}
0 \\
0 \\
0 \\
0 \\
0 \\
9.095x10^4 \\
0 \\
0
\end{bmatrix}.
$$

Typical step responses of the existing turret control system described by (1) for $x_r(t)$ = 175 milliradians (10^c) are as shown in Fig. 3. The responses were oscillatory. For the azimuth channel, there was a 60% overshoot in the gun angular position $x'_1(t)$ and the settling time t_s for $x'_1(t)$ was more than t_s = 1 second.
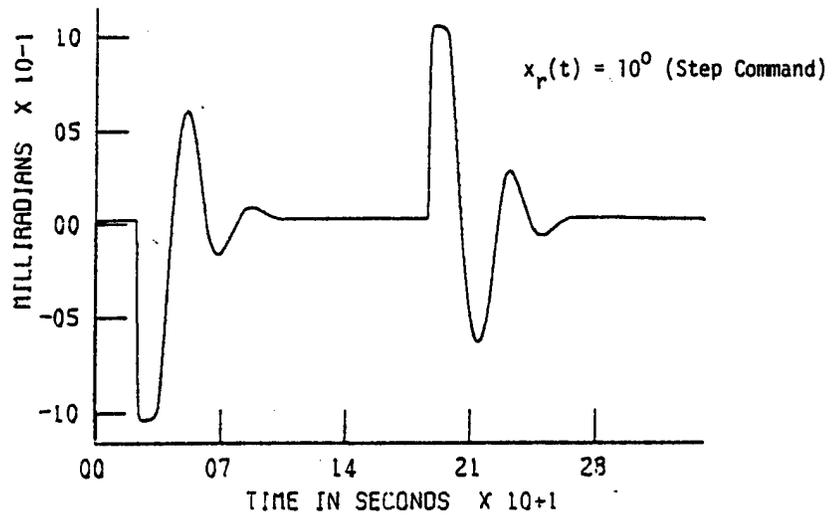
(a) Azimuth Angular Position Error
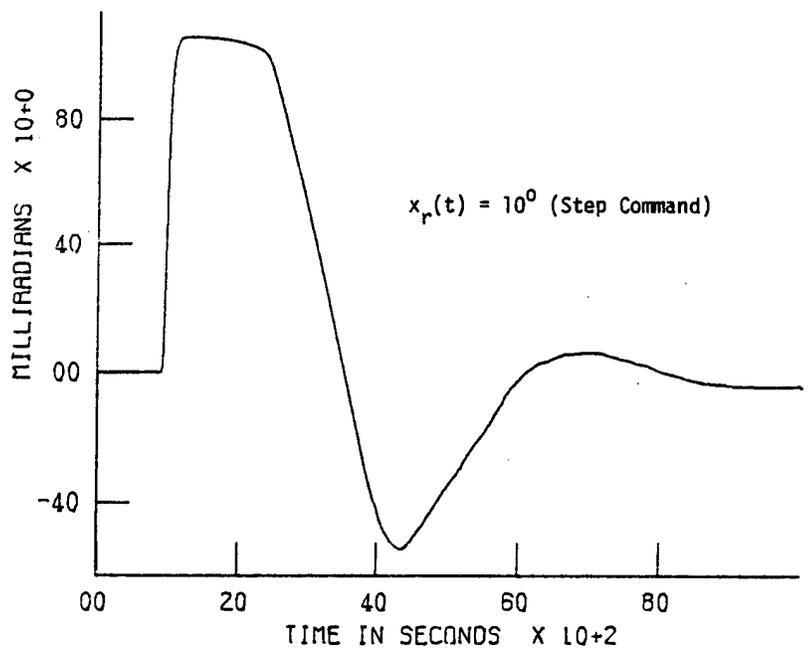
TKK 9A   DEMODULATED ELEVATION ERROR - FILTER=100HZ
TEST 132, 10MAR80, MTC / XM197

(b) Elevation Angular Position Error

Fig. 3   STEP RESPONSES OF ORIGINAL XM-97
          HELICOPTER TURRET CONTROL SYSTEM

3. GUN-TURRET MODEL SIMPLIFICATION

The first step involved in the design of suitable optimal controllers for the XM-97 helicopter turret control system was to obtain suitable open-loop models for the turret system. Hence the position and velocity feedback paths in the existing system indicated by the dotted lines in Fig. 2 were first removed; a 7th order open-loop turret control system resulted for each of the azimuth and elevation channels. The next step was to simplify the 7th order mathematical model. It was decided to ignore stable poles of magnitudes larger than 150 corresponding to a time constant of $\tau = 1/150 = 6.67$ milliseconds. Hence $G_3(s)$, $G_5(s)$ and $G_6(s)$ in Fig. 2 become, respectively,

$$G_3(s) \simeq p_1,$$

$$G_5(s) \simeq 7.5,$$

$$G_6(s) \simeq 535.$$

Furthermore, it is found that the effect of the shaft compliance K_c on the response of the helicopter gun-turret drive could be ignored. The parameter K_c was therefore eliminated by setting it to an arbitrary large value in Fig. 2. The elimination of K_c in Fig. 2 has also resulted in the elimination of the geared-down shaft angular position $x_7(t)$ which is not accessible for on-line measurement.[1] With all the simplifications as discussed above, it can be shown that the helicopter gun-turret system shown in Fig. 2 reduces to the open-loop system shown in Fig. 4 when the position and velocity feedback paths are removed.

The dynmaics of the simplified gun-turret of Fig. 4 can be shown to be described by

$$\begin{bmatrix} \dot{x}'_1(t) \\ \dot{x}'_2(t) \end{bmatrix} = \begin{bmatrix} 1 & \frac{1}{N} \\ 0 & -\frac{3.84 \times 10^3}{J} \end{bmatrix} \begin{bmatrix} x'_1(t) \\ x'_2(t) \end{bmatrix} + \begin{bmatrix} 0 \\ \frac{80.25}{J} \end{bmatrix} u(t), \qquad (2)$$

where $x'_1(t)$ and $x'_2(t)$ are the same as in (1), $J = 3 \times 10^{-4}$ for the azimuth channel and $J = 2.7 \times 10^{-4}$ for the elevation channel.

---

[1] Had $x_7(t)$ not been eliminated, a suitable filter or observer would be required to generate an estimate of $x_7(t)$ in the implementation of an optimal controller.
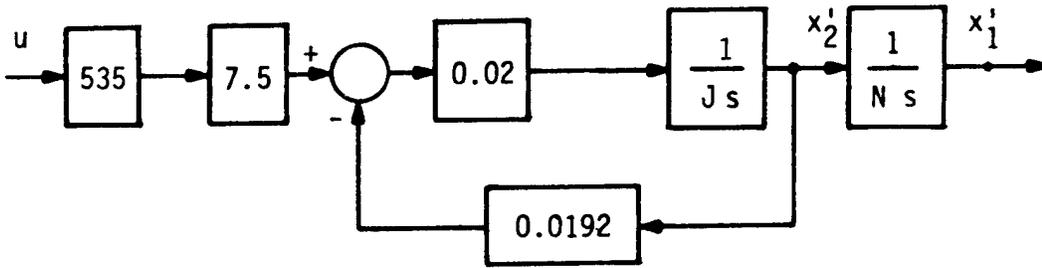
Fig. 4 SIMPLIFIED OPEN-LOOP XM-97 HELICOPTER TURRET CONTROL SYSTEMS
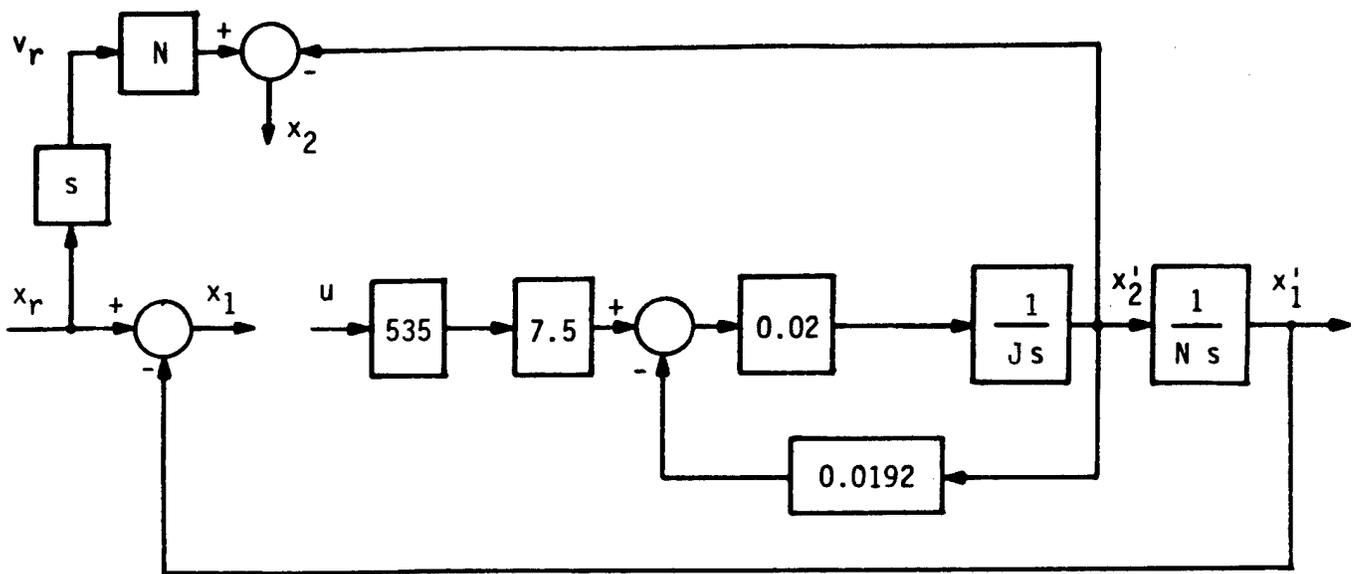WITH $J=3 \times 10^{-4}$(AZ) AND $J=2.7 \times 10^{-4}$(EL)

Fig. 5 SIMPLIFIED OPEN-LOOP XM-97 HELICOPTER TURRET CONTROL SYSTEMS
USED FOR DESIGN OF OPTIMAL TURRETS WITH $J=3 \times 10^{-4}$(AZ) AND $J=2.7 \times 10^{-4}$(EL)

4. DESIGN OF DISCRETE-TIME OPTIMAL TURRET CONTROLLER

The design of continuous-time optimal controllers for the XM-97 helicopter gun-turret control system has been investigated in [1] and [3]. In [1] and [3], the design problem was formulated as shown in Fig. 5, with the dynamics of the open-loop system described by, for both the azimuth and elevation channels,

$$\dot{\underline{x}}(t) = A\underline{x}(t) + Bu(t) + Fv_r, \quad \underline{x}(0) = \underline{x}_o, \tag{3}$$

where

$$\underline{x}^T(t) = [x_1(t) \quad x_2(t)],$$

$$x_1(t) = x_r(t) - x'_1(t)$$

  = error between the position common input x_r (radians) and the actual gun-turret angular position $x'_1(t)$ (radians),

$$x_2(t) = Nv_r - x'_2(t)$$

  = error between the velocity command v_r (radians/second) and the actual motor angular velocity $x'_2(t)$ (radians/second),

$$x_r(t) = x_r + v_r t$$

  = step-plus-ramp position command input (radians),

$u(t)$ = control input (volts),

and A, B and F are constant matrices given by

$$A = \begin{bmatrix} 0 & \dfrac{1}{N} \\ 0 & \dfrac{3.84 \times 10^3}{J} \end{bmatrix} \triangleq \begin{bmatrix} 0 & a_{12} \\ 0 & -a_{22} \end{bmatrix},$$

$$B = \begin{bmatrix} 0 \\ \dfrac{-80.25}{J} \end{bmatrix} \triangleq \begin{bmatrix} 0 \\ -b_{12} \end{bmatrix}, \quad F = \begin{bmatrix} 0 \\ \dfrac{3.84 \times 10^{-3} N}{J} \end{bmatrix} \triangleq \begin{bmatrix} 0 \\ f_{12} \end{bmatrix}.$$

To design suitable microprocessor-based optimal controllers for the helicopter gun-turret control system, equation (3) is first discretized by using a sampling interval T seconds as follows:

$$\underline{x}(k+1) = A_d\underline{x}(k) + B_d u(k) + F_d v_r, \quad \underline{x}(0) = \underline{x}_o, \tag{4a}$$

where $\underline{x}(k) \stackrel{\Delta}{=} \underline{x}(kT)$, $u(k) \stackrel{\Delta}{=} u(kT)$,

$$A_d \stackrel{\Delta}{=} e^{AT} = \begin{bmatrix} 1 & a_{d12} \\ 0 & a_{d22} \end{bmatrix},$$

$$B_d \stackrel{\Delta}{=} \int_o^T e^{At} B dt = \begin{bmatrix} b_{d11} \\ b_{d12} \end{bmatrix}, \tag{4c}$$

$$F_d \stackrel{\Delta}{=} \int_o^T e^{At} F dt = \begin{bmatrix} f_{d11} \\ f_{d12} \end{bmatrix}, \tag{4d}$$

and the components in the A_d, B_d and F_d matrices can be computed easily for each of the azimuth and elevation channels.

The design objective is to drive $\underline{x}(k)$ to the zero state and in the same time minimizing a quadratic performance measure. To achieve the objective, the control $u(k)$ is first split into two parts as

$$u(k) = u_{fb}(k) + u_{ff}(k), \tag{5}$$

where $u_{fb}(k)$ is the feedback component responsible for driving the state $\underline{x}(k)$ to the zero state, and $u_{ff}(k)$ is the feedforward component responsible for accommodating the velocity command v_r, i.e.,

$$B_d u_{ff}(k) + F_d v_r = 0. \tag{6}$$

Using (3), (4) and (6), it is not difficult to show that

$$u_{ff}(k) = \frac{f_{12}}{b_{12}} v_r = 4.785\text{N}\times10^{-5} v_r \stackrel{\Delta}{=} k_r v_r. \tag{7}$$

Substituting (5) and (7) into (4) yields

$$\underline{x}(k+1) = A_d\underline{x}(k) + B_d u_{fb}(k), \quad \underline{x}(0) = \underline{x}_o. \tag{8}$$

Equation (8) may be written as, by adding and substracting the same term $-B_d R_d^{-1} S_d^T \underline{x}(k)$ on the right-hand side of the equation[2] [4],

---

[2]The reason for using (9) is to provide an alternate method for solving the optimal control problem. See (12)-(13) and (23)-(26).

$$\underline{x}(k+1) = (A - B_d R_d^{-1} S_d^T)\underline{x}(k) + B_d[u_{fb}(k) + R_d^{-1}S_d^T\underline{x}(k)]$$

$$\stackrel{\Delta}{=} A_{eq}\,\underline{x}(k) + B_d u_{eq}(k), \quad \underline{x}(0) = \underline{x}_o \,, \tag{9}$$

where R_d and S_d are constant matrices, and

$$A_{eq} \stackrel{\Delta}{=} A - B_d \bar{R}_d^{-1} S_d^T \,, \tag{10}$$

$$u_{eq}(k) \stackrel{\Delta}{=} u_{fb}(k) + \bar{R}_d^{-1} S_d^T \underline{x}(k). \tag{11}$$

Consider the performance measure

$$J_d = \sum_{k=0}^{\infty} [\underline{x}^T(k) Q_d \underline{x}(k) + 2\underline{x}^T(k) S_d \underline{u}_{fb}(k) + \underline{u}_{fb}^T(k) R_d \underline{u}_{fb}(k)] \tag{12}$$

which may be written as [4], by completing the square for the terms inside the brackets,

$$J_{eq} = \sum_{k=0}^{\infty} [\underline{x}^T(k) Q_{eq} \underline{x}(k) + \underline{u}_{eq}^T(k) R_d \underline{u}_{eq}(k)], \tag{13}$$

where $J_d \equiv J_{eq}$, and

$$Q_{eq} \stackrel{\Delta}{=} Q_d - S_d R_d S_d^T, \tag{14}$$

while $\underline{u}_{eq}(k)$ is as defined in (11). In (12) and (13), Q_d is an nxn (n=2 for the present problem) symmetric positive-semidefinite weighting matrix, R_d is an rxr (r=1 for the present problem) symmetric positive-definite weighting matrix, and S_d is an nxr (n=2, r=1) weighting matrix. In the design of an optimal control system, the numerical values of the elements of the weighting matrices Q_d, R_d and S_d are often chosen in a trial and error basis, guided by, perhaps, the physics of the problem and design experience. However, it is important that these weighting matrices be chosen such that [4] - [5],

(i) $[A_{eq}, D_d]$, where $D_d^T D_d = Q_d - S_d^{-1} R_d S_d^T$, is completely observable, i.e.,

$$\text{rank}[D_d^T \mid A_{eq}^T D_d^T \mid A_{eq}^{2T} D_d^T \mid \dots \mid A_{eq}^{(n-1)T} D_d^T] = n, \tag{15}$$

(ii) $[A_{eq}, B_d]$ is completely controllable, i.e.,

$$\text{rank}[B_d \mid A_{eq} B_d \mid A_{eq}^2 B_d \mid \dots \mid A_{eq}^{n-1} B_d] = n. \tag{16}$$

The resultant optimal closed-loop control system will then be asymptically stable if (condition (i)) and only if (condition (ii)) conditions (i) and (ii)

are satisfied.

Given (8) and (12), or equivalently (9) and (13), we wish to find the optimal control which minimizes the performance measure J_d, or equivalently J_{eq}. It is well known that the optimal control problem posed by (8) and (12), or equivalently (9) and (13), is a discrete-time version of the following continuous-time optimal control problem:

Given the continuous-time system,

$$\dot{\underline{x}}(t) = A\underline{x}(t) + B\underline{u}(t), \quad \underline{x}(0) = \underline{x}_o \tag{17}$$

find the optimal control which minimizes the performance measure

$$J = \int_0^\infty [\underline{x}^T(t)Q\underline{x}(t) + \underline{u}^T(t)R\underline{u}(t)]dt, \tag{18}$$

where Q and R are, respectively, symmetric positive-semidefinite and symmetric positive-definite weighting matrices. The continuous-time system described by (17) may be discretized as shown in (4). The corresponding discrete-time version of (18) is then given by (12) with the following substitutions [6]:

$$Q_d = \int_0^T e^{A^T t} Q e^{At} dt, \tag{19}$$

$$R_d = \int_0^T [R + B_d^T(t)QB_d(t)]dt, \tag{20}$$

$$S_d = \int_0^T e^{A^T t} QB(t)dt, \tag{21}$$

$$B(t) = \int_0^t e^{A\sigma} Bd\sigma \tag{22}$$

We observe that although there is no cross-product term of the form $\underline{x}^T(t)S\underline{u}(t)$ used in (18), the cross-product term due to S_d in (12) is generally non-zero, unless Q = 0 as may be seen from (21). We remark also that the cross-product term in (12) may be dropped if one is not interested in establishing the corresponding relationships between the continuous-time and the associated discrete-time optimal control problems.

Now, the optimal control which minimizes the performance measure J_d given by (12) subject to (8) is given by [5]

$$u_{fb}(k) = -(R_d + B_d^T K_d B_d)^{-1}(B_d^T K_d A_d + S_d^T)\underline{x}(k) \tag{23a}$$

$$= k_1 x_1(k) + k_2 x_2(k) \tag{23b}$$

212

$$= k_1[x_r(k) - x_1'(k)] + k_2[Nv_r - x_2'(k)], \tag{23c}$$

where k_1 and k_2 are constants, and K_d is the symmetric positive-definite solution of the algebraic matrix Riccati equation

$$K_d = A_d^T K_d A_d + Q_d$$

$$-(B_d^T K_d A_d + S_d^T)^T (R_d + B_d^T K_d B_d)^{-1} (B_d^T K_d A_d + S_d^T) \tag{24a}$$

$$= A_{eq}^T K_d A_d + Q_{eq}$$

$$-A_{eq}^T K_d B_d (R_d + B_d^T K_d B_d)^{-1} B_d^T K_d A_{eq}. \tag{24b}$$

Equation (24b) follows from (24a) by simple algebraic manipulations.

Similarly, the optimal control which minimizes J_{eq} given by (13) subject to (9) is given by

$$u_{eq}^o(k) = -(R_d + B_d^T K_d B_d)^{-1} B_d^T K_d A_{eq} \underline{x}(k), \tag{25}$$

where K_d is the symmetric positive-definite solution of (24). As expected, substitution of (25) into (11) yields (23).

Combing (7) and (23), the total control is given by

$$u(k) = -(R_d + B_d^T K_d B_d)^{-1} (B_d^T K_d A_d + S_d^T) \underline{x}(k) + k_r v_r \tag{26a}$$

$$= k_1 x_1(k) + k_2 x_2(k) + k_r v_r. \tag{26b}$$

Substituting (26) into (4a) yields the optimal helicopter gun-turret control system

$$\underline{x}(k+1) = [A_d - B_d (R_d + B_d^T K_d B_d)^{-1} (B_d^T K_d A_d + S_d^T)]\underline{x}(k), \quad \underline{x}(0) = \underline{x}_o. \tag{27}$$

A block diagram for a microprocessor-based implementation of the optimal controller given by (26) is as shown in Fig. 6.
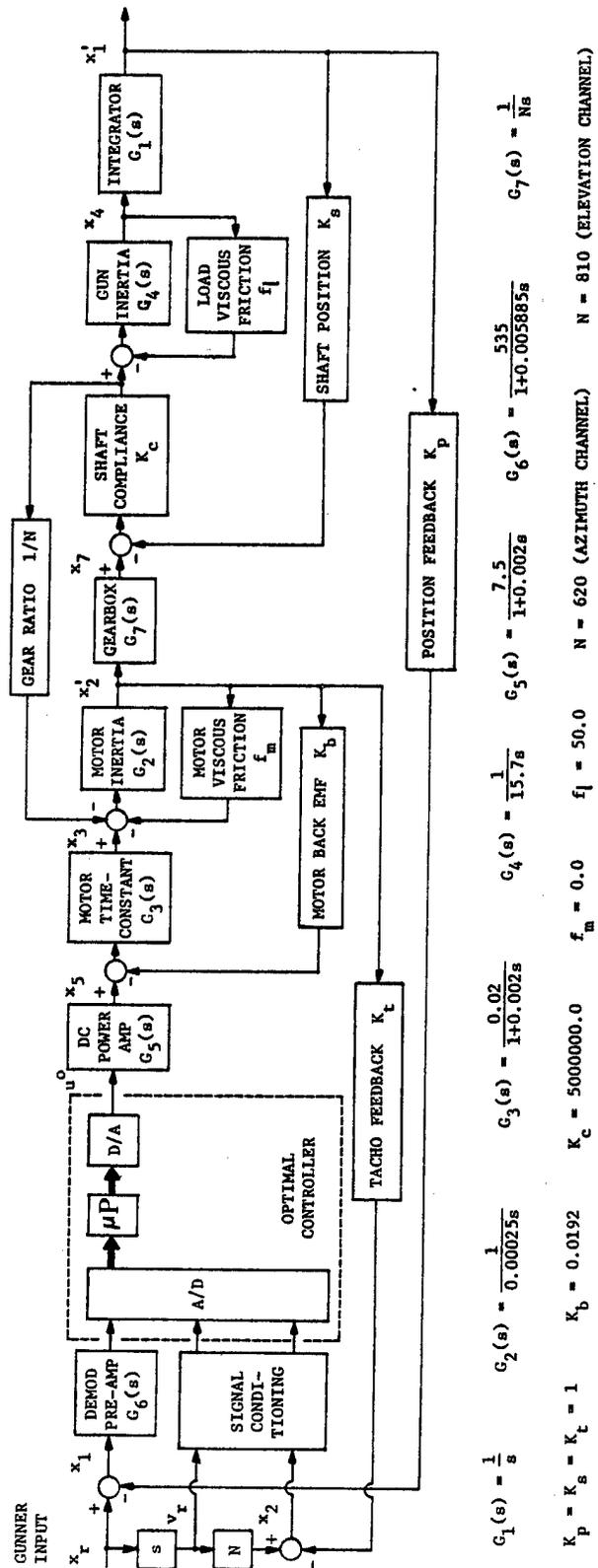
Fig. 6 OPTIMAL XM-97 HELICOPTER TURRET CONTROL SYSTEMS- AZIMUTH AND ELEVATION CHANNELS

$G_1(s) = \frac{1}{s}$ $G_2(s) = \frac{1}{0.00025s}$ $G_3(s) = \frac{0.02}{1+0.002s}$ $G_4(s) = \frac{1}{15.7s}$ $G_5(s) = \frac{7.5}{1+0.002s}$ $G_6(s) = \frac{535}{1+0.005885s}$ $G_7(s) = \frac{1}{Ns}$

$K_p = K_s = K_t = 1$ $K_b = 0.0192$ $K_c = 5000000.0$ $f_m = 0.0$ $f_l = 50.0$ $N = 620$ (AZIMUTH CHANNEL) $N = 810$ (ELEVATION CHANNEL)

214

5. IMPLEMENTATION OF DISCRETE-TIME OPTIMAL CONTROLLER

The hardware used to execute the discrete-time optimal controllers for both the azimuth and elevation channels developed for the XM-97 helicopter turret control system developed in Section 3 is as shown in Fig. 7. It consists of two SBC 310 high speed mathematics boards, an SBC 86/12 (16 bits, 8086 based) single board computer and a SBC 732 combination A/D and D/A board (12 bits). A TI Silent 700 provides the capability for quick parameter adjustment of the controller algorithms during nonfiring and firing tests. We remark that only one SBC 310 high speed mathematics board is needed to execute the control algorithms. The second SBC 310 mathematics board is used as a back-up and also to provide additional computation capability for follow-on development. To implement the controllers without disturbance cancellation, only the SBC 86/12 single board computer is needed. One complete iteration of the algorithm requires 0.8 milliseconds when implemented using fixed point assembly language code. This rapid execution time makes it possible to test and compare discrete-time optimal controllers for sample intervals of $T=1$ millisecond and $T=10$ milliseconds. The nonfiring and firing test results will be presented in the next section.

The electronic hardware is housed in a 9" x 15" x 16" aluminium case and weighs approximately 30 pounds. One of the design requirements for the system is that it be fully transportable. This has been made necessary by the fact that the software development facility is located at the Dover, New Jersey site and the nonfiring and firing testing facility is located in Rock Island, Illinois.

On power up of the XM-97 digital turret control system, an initialization routine INIT initializes all programmable devices and transfers all programs from PROM to RAM memory. The desired program is then called by executing an appropriate interrupt.

A flow diagram of the digital optimal controller software is as shown in Fig. 8. The subroutine INPAZ brings in and scales the azimuth position error, turret rate and sight rate signals and compute rate error $x_2(k)$. The subroutine INPEL performs a similar function for the elevation channel. The subroutine DAOT outputs the calculated control signals $u(k)$ for both the azimuth and elevation channels to the D/A converters. Before the signal $u(k)$ is sent to the D/A converter, however, it is converted to fixed point and clipped at 12 bits (± 10 volts) to prevent saturation of the D/A. In order to provide maximum flexibility in software development and implementation, extensive use is made of three macro routines COMP, GET and FIN. The MACRO COMP(WT, DATA1, DATA2, OPCODE, TMP) functions as follows. If WT is other than null, the program checks to determine if the high speed mathematics board has completed its computation before continuing. DATA1 and DATA2 are the address routine for the 4-byte operator and operand, respectively; if either is a null, the old values is used. OPCODE is a hexidecimal number from $\emptyset$ to F indicating the type of operation to be performed. If this value is a null, then no operation takes place. If TMP is a null, the MACRO is terminated after the high speed mathematics board is started. Otherwise the program waits until the operation is completed. The 4-byte result is then stored in the address pointed to by TMP. The MACROS GET(WT, TMP) and FIN(WT) are actually subsets of the MACRO COMP(WT, DATA1, DATA2, OPCODE, TWP). A complete
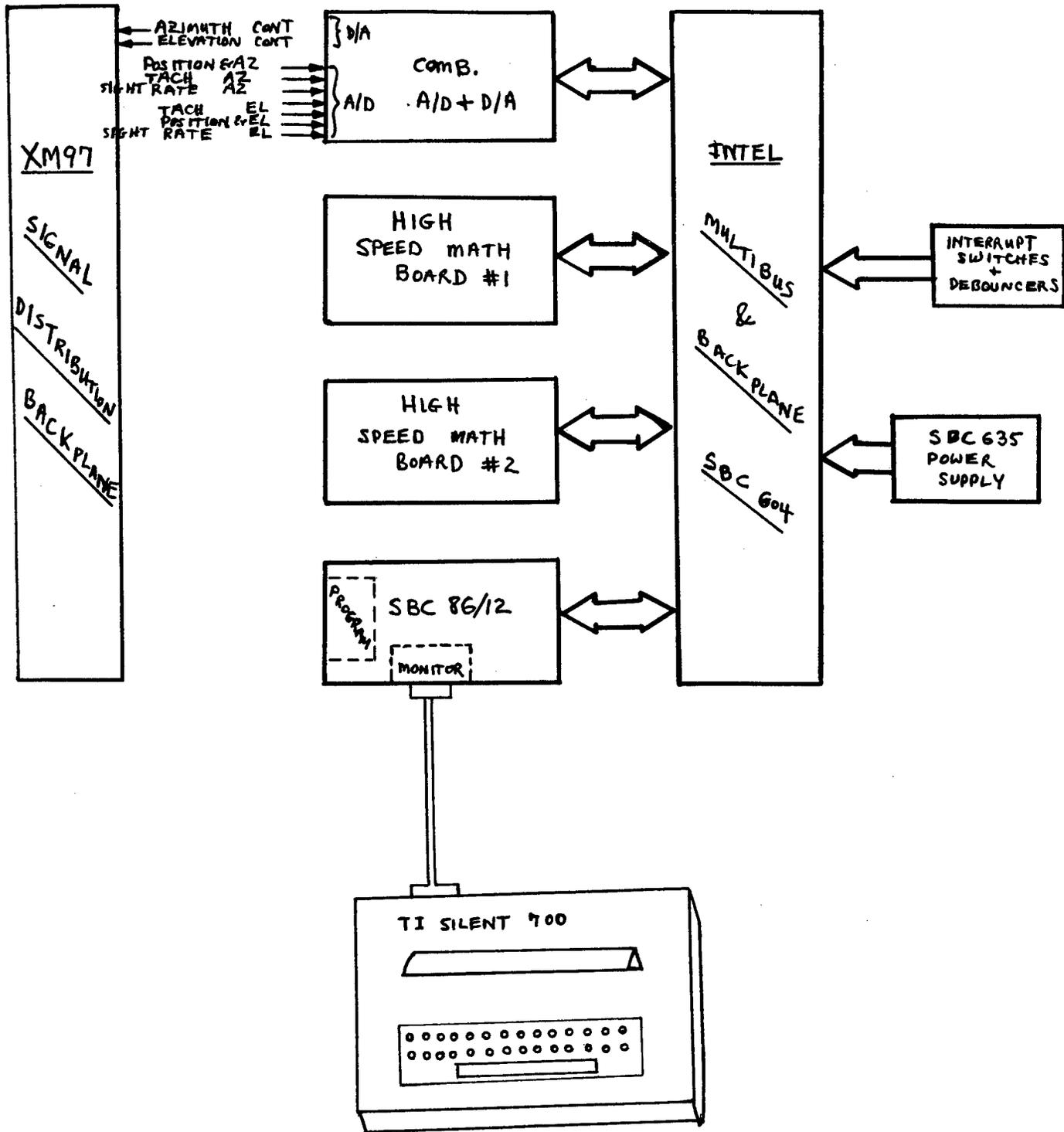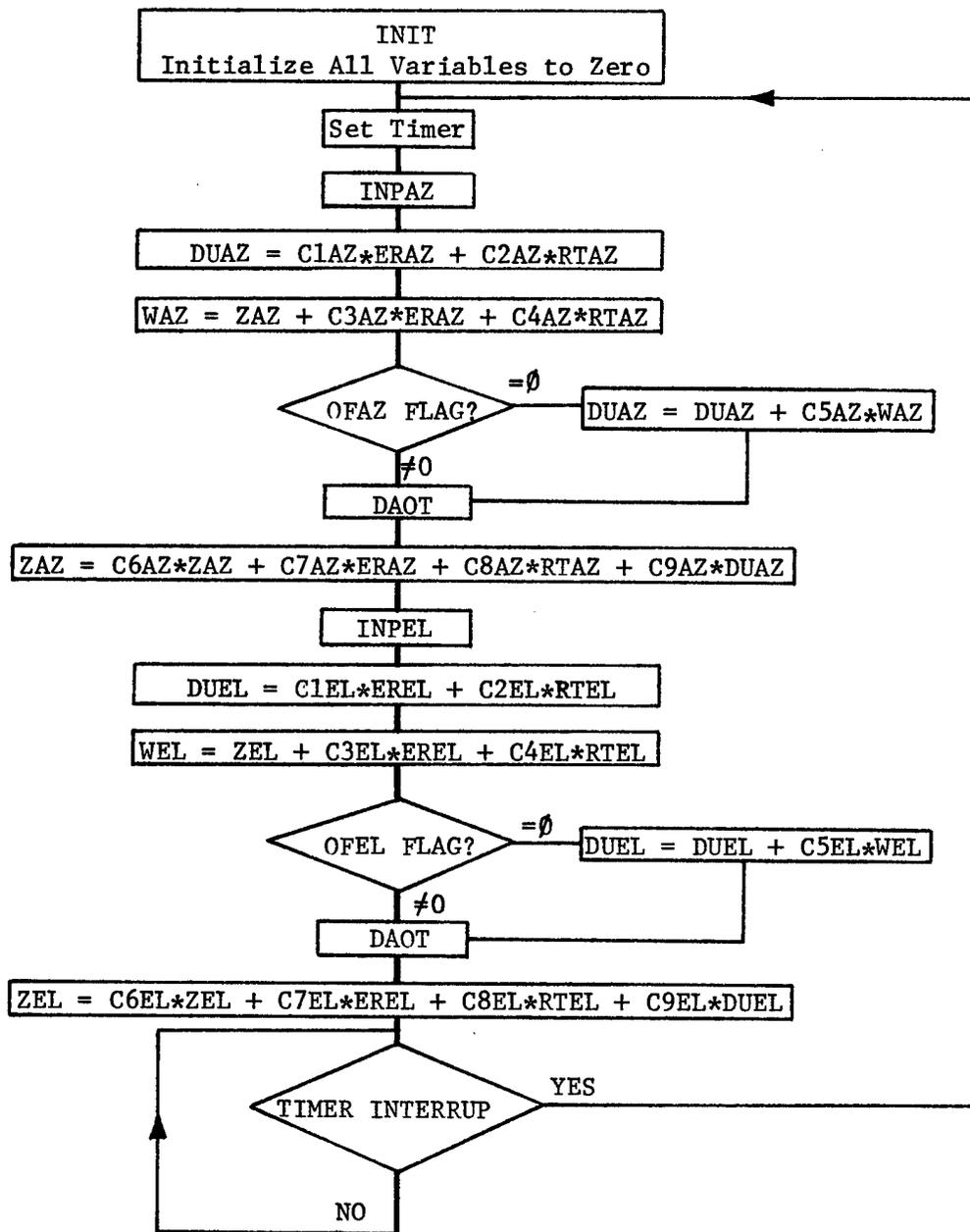
Fig. 7   XM-97 DIGITAL CONTROLLER HARDWARE

216

Fig. 8   XM-97 OPTIMAL CONTROLLER FLOW CHART
         (INCLUDING DISTURBANCE CANCELLATING CONTROL)

217

listing of the software program is available upon request.

The microprocessor development system used to debug the optimal controller algorithms is as shown in Fig. 9. The facility is located at the Army Armament Research and Development Command laboratory in Dover, New Jersey. The entire system consists of a basic INTEL 220 development system expanded to 64K bytes RAM and 1.25 megabytes disc. In addition, there is a high speed line printer, an 8-channel 12-bit A/D, a 4-channel 12-bit D/A and a PROM programmer for the 2708, 2716 and 2732 PROMS (8, 16 and 32 bits per unit, respectively). Since the 8080 requires 1.2 ms to perform a 32K bit floating point multiplication, a means of speeding up computation is required for real time execution of algorithms. Therefore, a SBC 310 high-speed mathematics board is added which does the same multiplication in 85 microseconds. However, this board must communicate with the CPU via the system bus in order to store and then load the required four byte data words. This process requires approximately 90 microseconds. To minimize this excess overhead time, another SBC 310 high-speed mathematics board was added which permits one board to compute while the other is storing data.
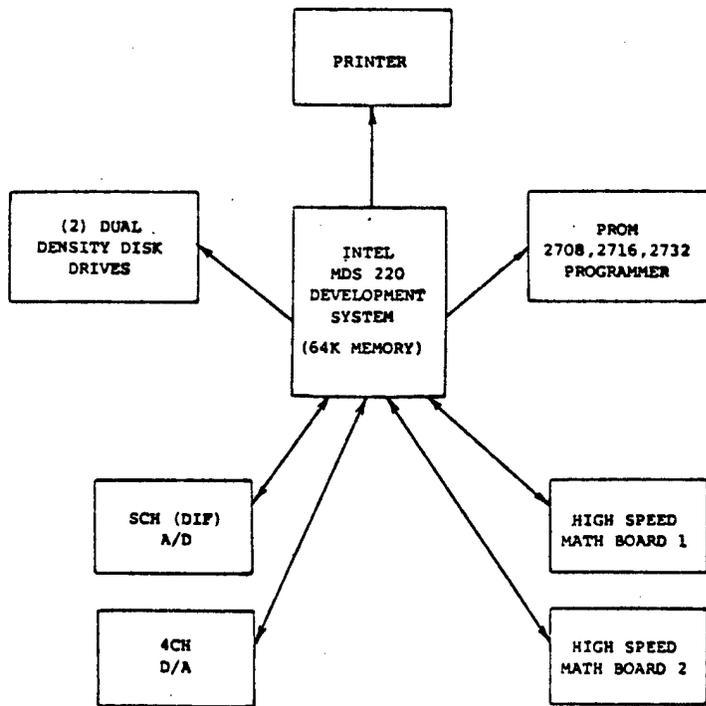

Fig. 9 MICROPROCESSOR DEVELOPMENT SYSTEM

6. TEST RESULTS

Firing and nonfiring tests of the microprocessor controlled XM-97 helicopter turret control system were conducted using the following values of Q and R in (18),

$$Q = \begin{bmatrix} q_{11} & 0 \\ 0 & 0 \end{bmatrix} \quad , \quad R = 1.$$

The corresponding Q_d, R_d and S_d were computed according to (19), (20) and (21), respectively. The above choice of Q implied that only $x_1(t) = x_r(t) - x_1'(t)$ was weighted so that large amplitudes of $x_{1d}(t)$ were discouraged.

The optimal control used was given by

$$u(k) = k_1x(k) + k_2x_2(k) + k_rv_r.$$

The following cases were investigated:

$$q_{11} = 5,$$

$$q_{11} = 10,$$

$$q_{11} = 15,$$

using a sampling intervals of T=1 millisecond and T=10 milliseconds. It was found that the case of q_{11}=5 and a sampling interval of T=1 millisecond gave the best results for both the firing and nonfiring tests.

(a) Nonfiring Tests

For nonfiring tests, the step responses of the azimuth channel of the original turret and the optimal digital turret are as shown in Fig. 10(a) - (b) and Fig. 11(a) - (b). The step inputs used were:

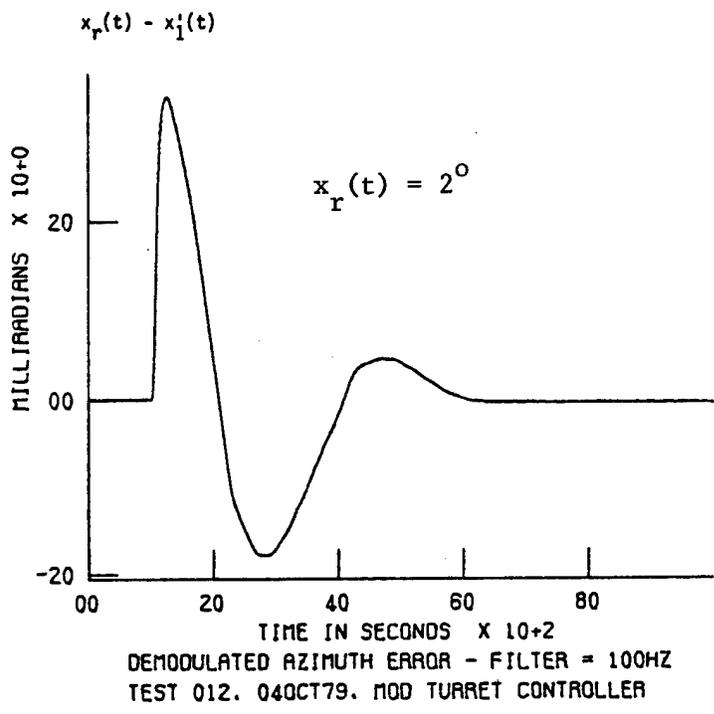### (i) Original Turret

$$x_r(t) = 2^o,$$

$$x_r(t) = 5^o.$$

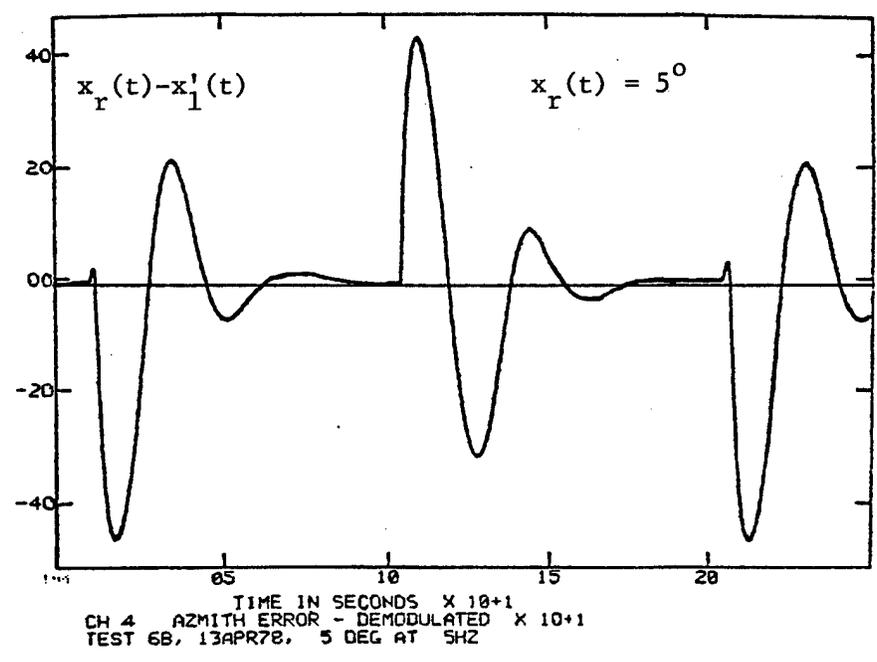### (ii) Optimal Digital Turret

$$x_r(t) = 2^o.$$

The statistics of the step responses shown in Figs. 10 - 11 are summarized in Table 1. The step responses of the original turret exhibited an average overshoot of 50% while there was no overshoot for the optimal digital turret. The settling time of the original turret was about 4.4 times longer than that of the optimal turret.

TABLE 1:   STEP RESPONSES OF ORIGINAL AND OPTIMAL
TURRETS-AZIMUTH CHANNEL

TURRET	SETTLING TIME (SEC)	% OVERSHOOT	COMMENTS
Original 2° Step 5° Step	0.50 0.74	49% 51%	Average of left & right excursions
Optimal $q_{11}=5$, T=1 ms	0.14	None	Smooth response
Optimal $q_{11}=5$, T=10 ms	0.14	None	Slight chattering response

$x_r(t) - x_1'(t)$

$x_r(t) = 2^O$

MILLIRADIANS X 10+0

20

00

-20

00   20   40   60   80

TIME IN SECONDS   X 10+2

DEMODULATED AZIMUTH ERROR - FILTER = 100HZ

TEST 012. 04OCT79. MOD TURRET CONTROLLER

(a) STEP RESPONSE - AZIMUTH CHANNEL

40

$x_r(t)-x_1'(t)$

$x_r(t) = 5^O$

20

00

-20

-40

05   10   15   20

TIME IN SECONDS   X 10+1

CH 4   AZMITH ERROR - DEMODULATED   X 10+1

TEST 6B, 13APR78,   5 DEG AT   5HZ

(b) STEP RESPONSE - AZIMUTH CHANNEL

Fig. 10   STEP RESPONSES OF ORIGINAL XM-97 GUN-TURRET

221

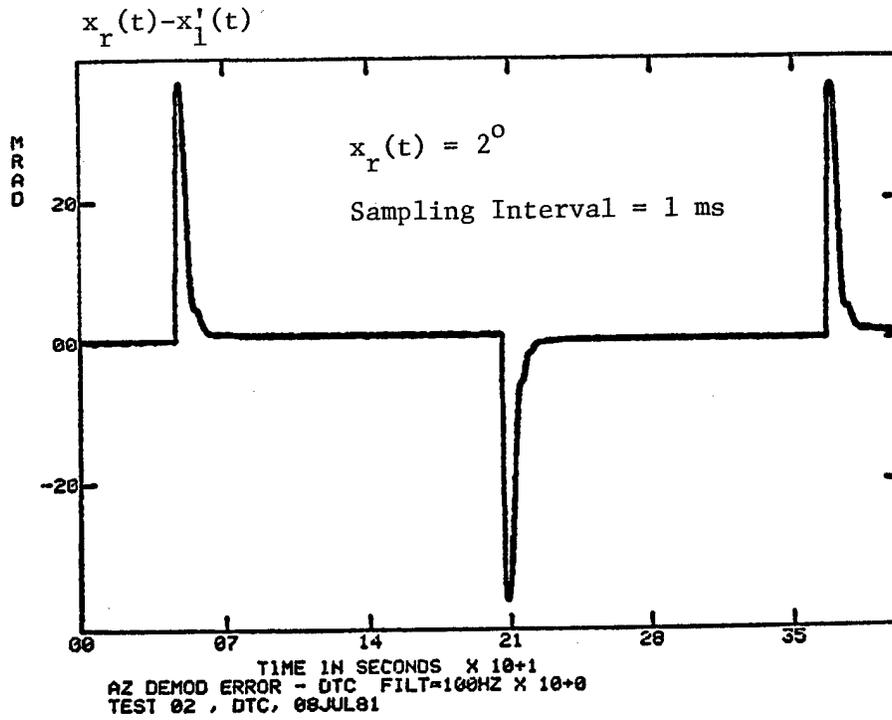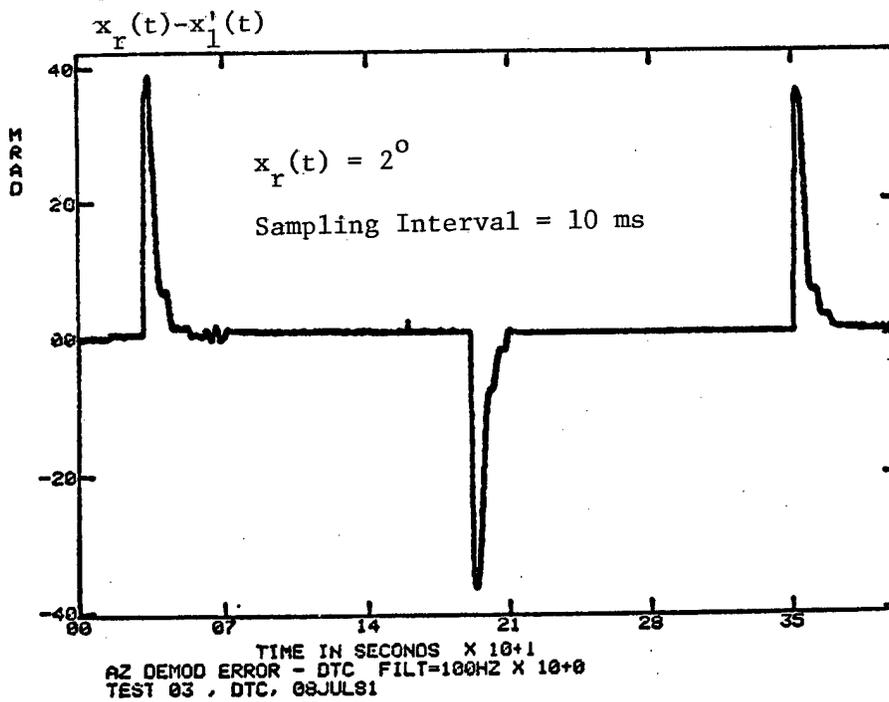(a) STEP RESPONSE - AZIMUTH CHANNEL

(b) STEP RESPONSE - AZIMUTH CHANNEL

Fig. 11 STEP RESPONSES OF OPTIMAL XM-97 GUN-TURRET

(b) Firing Tests

The firing tests were conducted using 20 rounds burst fire. The firing rate was 600 rounds per minute. In order to ignore the transient response of the turret, the statistics of the first 6 rounds, corresponding to approximately 0.6 second of firing time[3], were neglected. The performance of the original turret and the optimal digital turret in terms of the standard deviations of their rounds dispersion are summarized in Table 2. A performance improvement of approcimately 2 to 1 was obtained. Further tests using different values for q_{11} and using disturbance cancellating optimal digital controllers are currently underway. The results will be reported elsewhere.

TABLE 2: STANDARD DEVIATIONS FOR RANGE OF 85 FEET

TEST NO.	OVERALL AZIMUTH (INCH)	BARREL 1 AZIMUTH (INCH)	BARREL 2 AZIMUTH (INCH)	BARREL 3 AZIMUTH (INCH)
D 30	1.25	0.70	1.15	1.76
D 31	1.78	1.17	0.80	2.42
O 33	2.11	1.35	2.23	0.99
D 36	1.57	1.47	1.46	1.53
D 37	1.87	1.70	1.14	1.38
O 38	2.26	2.28	1.93	1.80

D = Optimal Digital Turret

O = Original Turret

---

[3]The average settling time of the original turret for nonfiring tests was about 0.62 seconds; see Table 1.

KNOWLEDGEMENT

REFERENCES

[1] N. Coleman, K. Lee, N. K. Loh and D. H. Chyung, "Application of Modern Control Theory to the Design of a Helicopter Turret Control System," Proceedings of Second Meeting of the Coordinating Group on Modern Control Theory, Army Materiel Systems Analysis Activity, Aberdeen Proving Ground, Maryland 21005, Part 1, pp. 1-20, Dec. 1980.

[2] J. Korn, E. Carroll, R. Johnson and B. Kullack, "Microcomputer Implementation of Control Algorithms for Weapon Stabilization and Control," Proceeding of Army Numerical Analysis Conference, Feb. 1981.

[3] N. K. Loh and K. C. Cheok, "Design of Optimal Controllers for XM-97 Helicopter Turret Control System," Final Report for Contract DAAA09-77-C-2040, Technical Report TR-80-11-160, School of Engineering, Oakland University, Rochester, Michigan 48063.

[4] B. D. O. Anderson and J. B. Moore, Linear Optimal Control. Englewood Cliffs, New Jersey: Prentice-Hall, 1971.

[5] B. C. Kuo, Digital Control Systems. New York: Holt, Rinehart and Winston, 1980.

[6] P. Dorato and A. H. Levis, "Optimal Linear Regulators: The Discrete-Time Case," IEEE Trans. Automat. Contr., Vol. AC-16, pp. 613-620, Dec. 1971.

DISCRETE-TIME DISTURBANCE-ACCOMMODATING CONTROL THEORY; THE DISTURBANCE-UTILIZATION MODE

C. D. Johnson
Professor of Electrical Engineering
Electrical Engineering Department
The University of Alabama in Huntsville
Huntsville, Alabama 35899

INTRODUCTION

In a recent paper [1], the theory of Disturbance-Accommodating Control (DAC) was extended to include the case of discrete-time, sampled-data control problems. The results presented in [1] covered the <u>disturbance absorption</u> (cancellation, rejection, counteraction) and <u>disturbance-minimization</u> modes of control, but did not consider the <u>disturbance-utilization</u> mode of control. In the present paper, we complete the development begun in [1] by deriving a rather general theory for the disturbance-utilization mode of digital DAC for the case of linear plants with a quadratic performance index.

The motivations for a theory of digital DAC, and the detailed derivation of the basic discrete-time models for the plant and disturbances are well-documented in [1] and therefore will not be repeated here.

SUMMARY OF DISCRETE-TIME MODELS FOR LINEAR PLANTS, DISTURBANCES AND COMMANDS

The class of plants and disturbances considered here are assumed to be such that their discrete-time response can be modeled by the following linear difference equations[*] (see [1] for the derivation of these difference equations from their continuous-time counterparts)

$$E x(nT) = \tilde{A}(nT)x(nT) + \tilde{B}(nT)u(nT) + \widetilde{FH}(nT)z(nT) + \tilde{\gamma}(nT) \tag{1a}$$

$$y(nT) = C(nT)x(nT) \tag{1b}$$

$$w(nT) = \text{external disturbance vector} = H(nT)z(nT) \tag{1c}$$

$$E\, z(nT) = \tilde{D}(nT)z(nT) + \tilde{\sigma}(nT) \tag{1d}$$

---

[*]Some possible generalizations of Eqs. (1b) and (1c,d) are described in [1].

where $E(\cdot)$ denotes the forward shift operator: $Ex(nT) = x((n+1)T)$ etc., $x = (x_1, \ldots, x_n)$ is the plant state-vector, $y = (y_1, \ldots, y_m)$ is the plant output vector, $u = (u_1, \ldots, u_r)$ is the plant control input, $w = (w_1, \ldots, w_p)$ is the plant disturbance input, and $z = (z_1, \ldots, z_\rho)$ denotes the "state-vector" for the disturbance process (1c), (1d). In the case of plants and/or disturbance processes which are governed by under-lying linear continuous-time differential equations of the form

$$\dot{x} = A(t)x + B(t)u + F(t)w(t) \tag{2a}$$

$$y = C(t)x \tag{2b}$$

$$w = H(t)z \tag{2c}$$

$$\dot{z} = D(t)z + \sigma(t) \tag{2d}$$

where $\sigma = (\sigma_1, \ldots, \sigma_\rho)$ denotes an unknown, sparse sequence of randomly arriving (once-in-a-while), random intensity impulses having a specified minimal adjacent spacing $\mu > 0$, the matrices $\tilde{A}, \tilde{B}$, etc. in Eq. (1) are related to their counterparts in Eq. (2) as follows* (see [1])

$$\tilde{A}(nT) = \Phi(t_o+(n+1)T, t_o+nT) \; ; \quad \Phi = \text{state-transition matrix for} \atop A(t) \tag{3a}$$

$$\tilde{B}(nT) = \int_{t_o+nT}^{t_o+(n+1)T} \Phi(t_o+(n+1)T,\tau)B(\tau)d\tau \tag{3b}$$

$$\widetilde{FH}(nT) = \int_{t_o+nT}^{t_o+(n+1)T} \Phi(t_o+(n+1)T,\tau)F(\tau)H(\tau)\Phi_D(\tau,t_o+nT)d\tau \tag{3c}$$

$$\tilde{\gamma}(nT) = \int_{t_o+nT}^{t_o+(n+1)T} [\Phi(t_o+(n+1)T,\tau)F(\tau)H(\tau)\int_{t_o+nT}^{\tau} \Phi_D(\tau,\xi)\sigma(\xi)d\xi]d\tau \tag{3d}$$

$$\tilde{D}(nT) = \Phi_D(t_o+(n+1)T, t_o+nT) \tag{3e}$$

$$\tilde{\sigma}(nT) = \int_{t_o+nT}^{t_o+(n+1)T} \Phi_D(t_o+(n+1)T,\xi)\sigma(\xi)d\xi \tag{3f}$$

where Φ_D denotes the state transition matrix for $D(t)$. Note that the dis-turbance-like terms $\tilde{\gamma}$, $\tilde{\sigma}$ in Eq. (1) [called "residuals" in [1]] account for the action of the $\sigma(t)$ impulses which arrive between adjacent sampling times $t_0 + nT$, $t_0 + (n+1)T$. Since the arrival times and intensities of the sparse $\sigma(t)$ impulses are completely unknown, (no probabilistic stucture) the terms $\tilde{\gamma}$, $\tilde{\sigma}$ are also completely unknown.

The primary objective of control is assumed to be expressible as the set-point regulation of, or servo-tracking by, certain specified plant variables $(\bar{y}_1, \bar{y}_2, \ldots, \bar{y}_{\bar{m}})$, where in general the $\bar{y}_i$ can be related to the plant state-variables $(x_1, \ldots, x_n)$ by the linear expression

---

*Note that the argument symbol nT appearing on the left side of Eq. (3) actually denotes the time $t = t_0 + nT$. This shorthand notation will be used consistently in this paper.

$$\bar{y} = \bar{C}(t)x \; ; \qquad \bar{y} = \left(\bar{y}_1, \cdots, \bar{y}_{\bar{m}}\right) \tag{4}$$

In many cases, the objective is to control the plant output $y(t)$ in Eq. (1b), in which case one would choose $\bar{C} = C$ in Eq. (4). On the other hand, the desire to control the entire plant state $x(t)$ would be indicated by choosing $\bar{C} = I$ in Eq. (4).

In accordance with standard procedures in DAC design [2], the <u>desired</u> (commanded) behavior of $\bar{y}(t)$ is expressed in continuous-time by the "set-point/servo-command" dynamical model

$$y(t)\Big|_{desired} = \bar{y}_c(t) = G(t)c(t) \tag{5a}$$

$$\dot{c} = \bar{E}(t)c + \mu_c(t) \tag{5b}$$

where $\{G(t), \bar{E}(t)\}$ are determined a priori by appropriate "command modeling" procedures; see [2; p. 642]; and where $c = (c_1, \ldots, c_\nu)$ represents the "state" of the command model* Eq. (5). The vector $\mu_c = (\mu_{c1}, \ldots, \mu_{c\nu})$ represents a sequence of totally unknown impulses which are sparse; similar in nature to the $\sigma(t)$ impulses in Eq. (2d). It is assumed that the set-point/servo-command vector $\bar{y}_c = (\bar{y}_{c1}, \ldots, \bar{y}_{c\bar{m}})$ might not be known a priori, but can be directly and accurately measured on-line, in real-time.

In the case of set-point regulation problems the command $\bar{y}_c(t)$ is essentially constant, or piecewise constant, in which case $\bar{E}(t) \equiv 0$ in Eq. (5b) and one can then set $G(t) \equiv I$ in Eq. (5a), assuming the $\bar{y}_i$ in Eq. (4) are independent. In the case of servo-tracking problems, the command $\bar{y}_c(t)$ is allowed to continuously vary with time and $\bar{E}(t)$ is chosen accordingly; see [2; p. 642].

For purposes of designing discrete-time controllers, it is necessary to have a discrete-time version of the set-point/servo-command model Eq. (5). Following the same procedure used for Eq. (1), the discrete-time model of Eq. (5) is obtained as

$$\bar{y}_c(nT) = G(nT)c(nT); \quad c((n+1)T) = \tilde{E}(nT)c(nT) + \tilde{\mu}_c(nT) \tag{6}$$

where

$$\tilde{E}(nT) = \Phi_{\bar{E}}\left(t_o + (n+1)T, t_o + nT\right) = \text{transition matrix for } \bar{E}(t) \tag{7a}$$

$$\tilde{\mu}_c(nT) = \int_{t_o+nT}^{t_o+(n+1)T} \Phi_{\bar{E}}\left(t_o+(n+1)T, \xi\right)\mu_c(\xi)d\xi \tag{7b}$$

The information embodied in the real-time command-state $c(nT)$ enables the DAC controller to "accommodate" uncertain servo-command behavior $\bar{y}_c(nT)$ similar to the way disturbances are accommodated.

---

*The symbols c, $\bar{E}$ in Eq. (5b) correspond to the symbols x_c, R used in [1; Eq. (43)].

DESIGN FOR THE DISTURBANCE-UTILIZATION MODE

The two modes of disturbance accommodation considered in [1] were designed to cope with disturbances by <u>counteracting</u> (absorbing) or <u>minimizing</u> their effects. This design attitude reflects the traditional view of disturbances as causing only unwanted, disruptive effects on the plant behavior. However, there are realistic situations in which disturbances are capable of producing <u>desirable</u> effects on the plant behavior. In particular, it is possible that at least some of the action of disturbances can be constructively used to assist the controller in accomplishing the primary control task. The trick, of course, is to know just how to manipulate the control $u(nT)$, in real-time, so as to harness and exploit any useful effects inherent in the (uncertain) disturbance actions.

The systemmatic design of continuous-time controllers to optimally utilize the action of uncertain disturbances was first introduced in [3], and has since been refined and applied in [2], [4], [5], [6], [7]. In this paper, we will derive discrete-time versions of "disturbance-utilizing" controller design procedures which parallel the results in [2], [4], and [6].

THE CHOICE OF A PERFORMANCE INDEX J IN DISTURBANCE-UTILIZING CONTROL PROBLEMS

The objective of disturbance-utilizing control is to make maximum (optimal) use of the disturbance $w(t)$ as an aid in accomplishing the primary control task. For instance, if the primary control task is to achieve set-point regulation or servo-tracking with minimal expediture of control resources (fuel, energy, etc.), it is conceivable that the action of disturbances $w(t)$ might be able to reduce the drain on control energy and/or achieve "better" set-point regulation or servo-tracking --- if $u(nT)$ is manipulated properly. On the other hand, if the disturbance actions are such that they are totally counter-productive to the primary control task, the use of an optimal disturbance-utilizing controller will serve to <u>minimize</u> the inevitable loss of performance contributed by the disturbance.

The optimal utilization of disturbances is achieved by application of optimal control theory, where the performance-index functional J is structured such that the minimization of J by $u(nT)$ achieves the primary control task while simultaneously making maximum "use" of $w(t)$. In the continuous-time version of disturbance-utilizing control theory [4] the most common choice of performance index J for set-point and servo-tracking problems is the classical error/control quadratic functional

$$J = \tfrac{1}{2}\epsilon^T(T_f)S\epsilon(T_f) + \tfrac{1}{2}\int_{t_o}^{T_f}\left[\epsilon^T(t)Q(t)\epsilon(t) + u^T(t)R(t)u(t)\right]dt \tag{8}$$

where $\epsilon(t)$ denotes the instantaneous "control error"; i.e. the error between desired response $\bar{y}_c$ and actual response $\bar{y}(t)$; and S, Q, R are positive definite symmetric matrices chosen by the designer. The design of $u(t)$ to minimize Eq. (8) automatically achieves the primary control task of $||\epsilon(T_f)|| = $ "small" [and $||\epsilon(t)|| = $ "small"], while simultaneously letting $w(t)$ "assist" in that task and/or in (possibly) reducing control resource consumption as measured by the time-integral of $u^T(t)R(t)u(t)$. If the disturbance $w(t)$ is such that it cannot "assist" in reducing J in Eq. (8), the

control u(t) which minimizes Eq. (8) will then automatically minimize any performance deterioration (increase in J) which w(t) contribues.

In discrete-time optimal control theory, the most common discrete-time version of Eq. (8) is expressed as

$$\tilde{J} = \frac{1}{2}\epsilon^T(NT)\tilde{S}\epsilon(NT) + \frac{1}{2}\sum_{n=0}^{n=(N-1)}\left[\epsilon^T(nT)\tilde{Q}(nT)\epsilon(nT) + u^T(nT)\tilde{R}(nT)u(nT)\right] \qquad (9)$$

where the interval of control $[t_0, T_f]$ is divided into N equal segments $t_n = t_0 + nT$; $n = 0, 1, 2, \ldots N$. Actually, if one evaluates the continuous-time performance index Eq. (8) over each segment $t_0 + nT \le t \le t_0 + (n+1)T$, using the known solution expression for Eqs. (2), (5), it can be shown [8] that Eq. (8) may finally be expressed in the form* of Eq. (9) with the exception that there is an additional term $2 u^T(nT)\tilde{M}(nT)\epsilon(nT)$ in the summation on the right side of Eq. (9). In that case, the matrices $\tilde{Q}$, $\tilde{M}$, $\tilde{R}$ are related to Q, R, B, A in Eqs. (8), (2) through some rather involved integrals. In practical applications of discrete-time optimal control it is generally preferable to adopt the format Eq. (9) as the <u>starting point</u> for structuring the performance index $\tilde{J}$ and then design the weighting matrices $\tilde{S}$, $\tilde{Q}$, $\tilde{R}$ in Eq. (9) to attach proper emphasis on the minimization of $\epsilon(nT)$, $u(nT)$; $n = 0, 1, 2, \ldots, N$. For this reason we hereafter adopt Eq. (9) as the basic performance index $\tilde{J}$ for the design of discrete-time disturbance-utilizing controllers for set-point and servo-tracking problems.

FORMULATION OF A GENERAL CLASS OF DISCRETE-TIME DISTURBANCE-UTILIZING CONTROL PROBLEMS

The systemmatic design of disturbance-utilizing controllers can be achieved by formulating the problem as a conventional (undisturbed) linear-quadratic discrete-time control problem for which solution algorithms are known. For this purpose, the discrete-time models Eqs. (1), (6), (7) are consolidated into one composite "plant" model and written as

$$\begin{pmatrix} Ex(nT) \\ Ec(nT) \\ Ez(nT) \end{pmatrix} = \begin{bmatrix} \tilde{A} & O & \tilde{FH} \\ O & \tilde{E} & O \\ O & O & \tilde{D} \end{bmatrix} \begin{pmatrix} x(nT) \\ c(nT) \\ z(nT) \end{pmatrix} + \begin{bmatrix} \tilde{B} \\ O \\ O \end{bmatrix} u(nT) + \begin{pmatrix} \tilde{\gamma} \\ \tilde{\mu}_c \\ \tilde{\sigma} \end{pmatrix} \qquad (10a)$$

$$y(nT) = \begin{bmatrix} C(nT) & O & O \end{bmatrix} \begin{pmatrix} x(nT) \\ c(nT) \\ z(nT) \end{pmatrix} \qquad (10b)$$

---

*Note that the arguments NT, nT in Eq. (9) actually represent the times $t = t_0 + NT$, $t = t_0 + nT$. This shorthand notation is consistent with that used in Eqs. (1), (6), (7) etc.; see footnote associated with Eq. (3).

For simplicity, the model Eq. (10a) is written in the more compact form

$$E\tilde{x} = \bar{A}(nT)\tilde{x}(nT) + \bar{B}(nT)u(nT) + \bar{\delta}(nT) \; ; \quad \tilde{x} = (x|c|z)^T \qquad (11)$$

where the meanings of $\bar{A}$, $\bar{B}$, $\bar{\delta}$, are clear from examination of Eq. (10a).

The instantaneous control error $\varepsilon(t)$ in Eq. (8) is the difference between the desired response and the actual response. Since $\bar{y}_c(t)$ and $\bar{y}(t)$ represent those two responses, we write $\varepsilon(t)$ as

$$\varepsilon(t) = \bar{y}_c(t) - \bar{y}(t) \qquad (12)$$

or, in terms of discrete-time $t = t_o + nT$

$$\varepsilon(nT) = \bar{y}_c(nT) - \bar{y}(nT) \qquad (13)$$

Using Eqs. (4), (6), expression (13) may be expressed in terms of $\tilde{x}$ as

$$\varepsilon = [-\bar{C}|G|O]\tilde{x} = \hat{C}\tilde{x} \; ; \qquad \hat{C} = [-\bar{C}|G|O] \qquad (14)$$

Now, the quadratic forms in the discrete-time performance-index $\tilde{J}$ in Eq. (9) may be expressed as

$$\varepsilon^T \tilde{S}\varepsilon = \tilde{x}^T \hat{C}^T \tilde{S} \hat{C}\tilde{x} = \tilde{x}^T \hat{S}\tilde{x} \; ; \qquad \hat{S} = \hat{C}^T \tilde{S} \hat{C} \qquad (15a)$$

$$\varepsilon^T \tilde{Q}\varepsilon = \tilde{x}^T \hat{C}^T \tilde{Q} \hat{C}\tilde{x} = \tilde{x}^T \hat{Q}\tilde{x} \; ; \qquad \hat{Q} = \hat{C}^T \tilde{Q} \hat{C} \qquad (15b)$$

Using Eq. (15), $\tilde{J}$ in Eq. (9) may finally be expressed in terms of the composite state $\tilde{x}$ as follows

$$\tilde{J} = \tfrac{1}{2}\tilde{x}^T(NT)\hat{S}\tilde{x}(NT) + \tfrac{1}{2}\sum_{n=0}^{n=(N-1)}\left[\tilde{x}^T(nT)\hat{Q}(nT)\tilde{x}(nT) + u^T(nT)\tilde{R}(nT)u(nT)\right] \qquad (16)$$

The optimal disturbance-utilizing control problem for discrete-time set-point regulation and servo-tracking may now be expressed precisely as follows. Find the control sequence $u(nT) = u°(nT)$, $n = 0, 1, 2, \ldots, (N-1)$, which minimizes the performance index Eq. (16) subject to the difference equation constraint Eqs. (10), (11) and for arbitrary initial conditions $\{x(0), c(0), z(0)\} = \tilde{x}(0)$. Since the $\sigma(t)$, $\mu_c(t)$ impulses which create the terms $\tilde{\gamma}$, $\tilde{\mu}_c$, $\tilde{\sigma}$ in Eq. (10a) are completely unknown and sparse, we will follow standard procedure in DAC theory and disregard the presence of those terms in Eq. (10a); see remarks in [2; p. 639].

SOLUTION OF THE DISCRETE-TIME DISTURBANCE-UTILIZING CONTROL PROBLEM

The minimization of (16) subject to Eqs. (10), (11) has the form of the conventional (undisturbed) discrete-time linear quadratic regulator problem which has already been solved; see for instance [8]. That known solution, when applied to the specific plant Eqs. (10), (11) and performance index Eq. (16) leads to the following expressions for the optimal discrete-time disturbance-utilizing control $u°(nT)$, $n = 0, 1, \ldots, (N-1)$. Assuming $\tilde{x}(nT)$ can be directly measured, the optimal control $u°(nT)$ is given by

$$u^o(nT) = -\left[\tilde{R}(nT) + \bar{B}^T(nT)\bar{P}((n+1)T)\bar{B}(nT)\right]^{-1}\left[\bar{B}^T(nT)\bar{P}((n+1)T)\bar{A}(nT)\right]\tilde{x}(nT) \qquad (17)$$

where the matrix $\bar{P}(\cdot)$ is symmetric, positive definite, and governed by the Riccati difference equation

$$\bar{P}(nT) = \left[\bar{A}^T(nT)\bar{P}((n+1)T)\bar{A}(nT) + \hat{Q}(nT)\right] - U^T\left[\tilde{R}(nT) + \bar{B}^T(nT)\bar{P}((n+1)T)\bar{B}(nT)\right]^{-1}U \; ; \qquad (18a)$$

$$U \triangleq \bar{B}^T(nT)\bar{P}((n+1)T)\bar{A}(nT)$$

with the boundary condition

$$\bar{P}(NT) = \hat{S} \qquad (18b)$$

Note that the Riccati difference equation Eq. (18) is automatically set-up for backward-time solution, "starting" at $t = T_f = t_0 + NT$ and progressing backward: $t = t_0 + (N-1)T$, $t = t_0 + (N-2)T$, ..., $t = t_0 + T$, $t = t_0$. In other words, one successively sets $n = (N-1)$, $(N-2)$, $(N-3)$..., 1, 0 in Eq. (18a). The resulting sequence of values $\bar{P}(nT)$ is then stored for future playback in the forward-time control law expression Eq. (17). In particular, at each time $t = t_0 + nT$ the "current" values of $\tilde{R}(nT)$, $\bar{B}(nT)$, $\bar{A}(nT)$ are substituted into Eq. (17), together with the "one-step-ahead" value of $\bar{P}((n+1)T)$, to compute the overall state-feedback gain matrix $\mathbb{K}(nT,(n+1)T)$ defined by

$$\mathbb{K} = -\left[\tilde{R}(nT) + \bar{B}^T(nT)\bar{P}((n+1)T)\bar{B}(nT)\right]^{-1}\left[\bar{B}^T(nT)\bar{P}((n+1)T)\bar{A}(nT)\right] \qquad (19a)$$

and $u^o(nT)$ is then computed as

$$u^o(nT) = \mathbb{K}(nT,(n+1)T)\tilde{x}(nT) \qquad (19b)$$

In practical applications, the composite state term $\tilde{x} = (x|c|z)$ in Eq. (19b) cannot be directly measured and therefore must be implemented as $\hat{\tilde{x}} = (\hat{x}|\hat{c}|\hat{z})$ where $\hat{x}$, $\hat{c}$, $\hat{z}$ are estimates of x, c, z generated on-line, in real time by a discrete-time state observer such as described in [1; Eqs. (18)-(25) and end of Section $\mathrm{V\text{-}D}$]. Note that the computation of $\mathbb{K}(nT)$ can be done off-line (it doesn't depend on knowledge of $\tilde{x}(nT)$) and therefore the time required for accurate calculation of $\mathbb{K}$ does not impact on the real-time performance of the controller.

The form of Eqs. (17), (18), (19) does not yield much insight into the fine structure of the optimal disturbance-utilizing control $u^o(nT)$. To see that fine structure, it is necessary to decompose $\bar{P}(\cdot)$ into smaller blocks corresponding to the block sturcture of $\bar{A}$ in Eqs. (10), (11). For that purpose, we set

$$\bar{P} = \left[\begin{array}{c|c|c} K_x & K_{xc} & K_{xz} \\ \hline K_{xc}^T & K_c & K_{cz} \\ \hline K_{xz}^T & K_{cz}^T & K_z \end{array}\right] \; ;$$

$$K_x = n \times n \; ; \; K_{xc} = n \times \nu \; ; \; K_{xz} = n \times \rho \qquad (20)$$

$$K_c = \nu \times \nu \; ; \; K_{cz} = \nu \times \rho \; ; \; K_z = \rho \times \rho$$

231

and substitute Eq. (20), together with the expressions for $\widetilde{R}$, $\overline{B}$, $\overline{A}$, $\hat{Q}$ and $\hat{S}$, into Eqs. (17), (18), (19) to obtain the optimal control $u^o(nT)$ expressed equivalently as

$$u^o(nT) = -\left[\widetilde{R}(nT)+\widetilde{B}^T(nT)K_x((n+1)T)\widetilde{B}(nT)\right]^{-1}\widetilde{B}^T(nT)\left[K_x((n+1)T)\widetilde{A}(nT)x(nT)+K_{xc}((n+1)T)\widetilde{E}(nT)c(nT)+\right.$$
$$\left.+\left(K_x((n+1)T)\widetilde{FH}(nT)+K_{x\widetilde{z}}((n+1)T)\widetilde{D}(nT)\right)z(nT)\right] \tag{21}$$

where the six block matrices comprising Eq. (20) obey the following set of coupled matric difference equations

$$K_x(nT)=\left[\widetilde{A}(nT)-\widetilde{B}(nT)[\widetilde{R}(nT)+\widetilde{B}^T(nT)K_x((n+1)T)\widetilde{B}(nT)]^{-1}\widetilde{B}^T(nT)K_x((n+1)T)\widetilde{A}(nT)\right]^T K_x((n+1)T)\widetilde{A}(nT)+\overline{C}^T(nT)\widetilde{Q}(nT)\overline{C}(nT);$$
$$K_x(NT)=\overline{C}^T(NT)\widetilde{S}\,\overline{C}(NT), \tag{22a}$$

$$K_{xc}(nT)=\left[\widetilde{A}(nT)-\widetilde{B}(nT)[\widetilde{R}(nT)+\widetilde{B}^T(nT)K_x((n+1)T)\widetilde{B}(nT)]^{-1}\widetilde{B}^T(nT)K_x((n+1)T)\widetilde{A}(nT)\right]^T K_{xc}((n+1)T)\widetilde{E}(nT)-\overline{C}^T(nT)\widetilde{Q}(nT)\widetilde{G}(nT);$$
$$K_{xc}(NT)=-\overline{C}^T(NT)\widetilde{S}\,G(NT), \tag{22b}$$

$$K_{x\widetilde{z}}(nT)=\left[\widetilde{A}(nT)-\widetilde{B}(nT)[\widetilde{R}(nT)+\widetilde{B}^T(nT)K_x((n+1)T)\widetilde{B}(nT)]^{-1}\widetilde{B}^T(nT)K_x((n+1)T)\widetilde{A}(nT)\right]^T\cdot\left[K_{x\widetilde{z}}((n+1)T)\widetilde{D}(nT)+K_x((n+1)T)\widetilde{FH}(nT)\right];$$
$$K_{x\widetilde{z}}(NT)=0 \tag{22c}$$

$$K_c(nT)=\widetilde{E}^T(nT)\left[K_c((n+1)T)-K_{xc}^T((n+1)T)\widetilde{B}(nT)[\widetilde{R}(nT)+\widetilde{B}^T(nT)K_x((n+1)T)\widetilde{B}(nT)]^{-1}\widetilde{B}^T(nT)K_{xc}((n+1)T)\right]\widetilde{E}(nT)+G^T(nT)\widetilde{Q}(nT)G(nT);$$
$$K_c(NT)=G^T(NT)\widetilde{S}\,G(NT), \tag{22d}$$

$$K_{c\widetilde{z}}(nT)=\widetilde{E}^T(nT)\left[K_{xc}^T((n+1)T)\widetilde{FH}(nT)+K_{c\widetilde{z}}((n+1)T)\widetilde{D}(nT)-K_{xc}^T((n+1)T)\widetilde{B}(nT)[\widetilde{R}(nT)+\widetilde{B}^T(nT)K_x((n+1)T)\widetilde{B}(nT)]^{-1}\widetilde{B}^T(nT)[K_x((n+1)T)\cdot\right.$$
$$\left.\cdot\widetilde{FH}(nT)+K_{x\widetilde{z}}((n+1)T)\widetilde{D}(nT)]\right];$$
$$K_{c\widetilde{z}}(NT)=0, \tag{22e}$$

$$\underset{z}{K}(nT) = \widetilde{FH}(nT)^T\left[\underset{xz}{K}((n+1)T)\widetilde{D}(nT) + \underset{x}{K}((n+1)T)\widetilde{FH}(nT)\right] + \widetilde{D}(nT)^T\left[\underset{xz}{K}^T((n+1)T)\widetilde{FH}(nT) + \underset{z}{K}((n+1)T)\widetilde{D}(nT)\right]$$

$$- \left[\underset{x}{K}((n+1)T)\widetilde{FH}(nT) + \underset{xz}{K}((n+1)T)\widetilde{D}(nT)\right]\widetilde{B}(nT)\left[\widetilde{R}(nT) + \widetilde{B}(nT)^T\underset{x}{K}((n+1)T)\widetilde{B}(nT)\right]^{-1}\widetilde{B}(nT)^T\left[\underset{x}{K}((n+1)T)\right.$$

$$\left.\widetilde{FH}(nT) + \underset{xz}{K}((n+1)T)\widetilde{D}(nT)\right] \quad ; \qquad\qquad \underset{z}{K}(NT) = 0 . \tag{22f}$$

Thus, to implement the disturbance-utilizing control $u°(nT)$ in Eq. (21) one must first solve for $K_x(nT)$, $K_{xc}(nT)$, $K_{xz}(nT)$ by solving Eqs. (22a,b,c) in backward time $n = (N-1)$, $(N-2)$,..., 2, 1, 0, using the indicated "initial conditions" at $t = t_0 + NT$. As already mentioned, this step can be carried-out off-line (ahead of time) and the computed values stored for future use. Note that at each time $t = t_0 + nT$, the real-time disturbance-utilizing con-trol Eq. (21) depends on the values of $\widetilde{R}$, $\widetilde{B}$, $\widetilde{A}$, $\widetilde{E}$, $\widetilde{FH}$, $\widetilde{D}$, and x, c, z evaluated at $t = t_0 + nT$ and the values of K_x, K_{xc}, K_{xz} evaluated at the "one-step-ahead" time $t = t_0 + (n+1)T$.

THE NOTIONS OF FIXED COST, ASSISTANCE, BURDEN, AND UTILITY IN DISTURBANCE-UTILIZING CONTROL PROBLEMS

The optimal disturbance-utilizing control $u°(nT)$ in Eq. (21) achieves the minimum possible value of $\widetilde{J}$ in Eq. (9). That minimum value of $\widetilde{J}$ will be de-noted by the scalar function $V = V(x(nT), c(nT), z(nT), (n+1)T)$ where $x(nT)$, $c(nT)$, $z(nT)$ denote arbitrary "initial conditions" in (x, c, z)-space.

It can be shown [8] that the function $V(x,c,z,(n+1)T)$ for the disturbance-utilization problem Eqs. (9)-(11) has the explicit form

$$V = \frac{1}{2}\widetilde{x}(nT)^T\overline{P}((n+1)T)\widetilde{x}(nT) = \frac{1}{2}(x|c|z)^T\begin{bmatrix} K_x & K_{xc} & K_{xz} \\ K_{xc}^T & K_c & K_{cz} \\ K_{xz}^T & K_{cz}^T & K_z \end{bmatrix}\begin{pmatrix} x \\ c \\ z \end{pmatrix} \tag{23}$$

which can be expanded to yield, (Note: all K-expressions in Eqs. (23), (24) are evaluated at $t = (n+1)T$, whereas x,c,z are evaluated at $t = nT$).

$$V = \underbrace{\frac{1}{2}\left(x^T K_x x + c^T K_c c + 2x^T K_{xc} c\right)}_{\mathcal{F} = \text{Fixed Cost}} + \underbrace{\left(x^T K_{xz} + c^T K_{cz}\right)z}_{-\mathcal{A} = -\text{Assistance}} + \underbrace{\frac{1}{2}z^T K_z z}_{\mathcal{B} = \text{Burden}} \tag{24}$$

The role of the disturbance $w(t)$ in reducing the minimum possible value of $\widetilde{J}$ can now be clearly seen in Eq. (24). Namely, the impact of $w(t)$ on $V = $ min. $\widetilde{J}$ is reflected in the z-related terms in Eq. (24). If the collection

of terms labeled $\mathcal{a}$ ("assistance") is greater than the "burden" term $\mathcal{B}$,
then, and only then, will min. J be further reduced by the action of w(t).
Thus, following the ideas in [6] we define the "utility" $\mathcal{U}$ of the dis-
turbance w(t) as

$$\mathcal{U} = \text{Assistance} - \text{Burden} = -\left(x^T K_{xz} + c^T K_{cz}\right) z - \frac{1}{2} z^T K_z z \tag{25}$$

The condition $\mathcal{U} > 0$ indicates that the current behavior of w(t) is such that
it can help in reducing min. J. On the other hand, the condition $\mathcal{U} < 0$
indicates that the current behavior of w(t) is such that w(t) can only aggra-
vate (increase) the value of min. J. The collection of terms in Eq. (24)
which do not involve z is referred to as the "fixed-cost" $\mathcal{F}$ because that
contribution to V = min. J. is <u>invariant</u> with respect to the behavior of
disturbances w(t).

The disturbance utility function $\mathcal{U}$ defined by Eq. (25) can be studied in
the (x,c,z,t)-space to identify the domains of positive and negative utility;
the details are outlined in [6] and some specific examples, from continuous-
time disturbance-utilizing DAC theory, are presented in [7] and [9]. Note
that as time progresses, n = 0,1,2,..., the sign of $\mathcal{U}$ can change back and
forth.

THE EFFECTIVENESS $\mathcal{E}$ OF OPTIMAL DISTURBANCE-UTILIZING CONTROL

The linear-quadratic regulator theory is widely used to design feedback con-
trol laws of the form u($\cdot$) = $\mathbb{K}(\cdot)$ x($\cdot$). Traditionally, such applications
have ignored the presence of persistent disturbances w(t) and therefore,
when confronted with actual real-life disturbances in the field, such con-
trol laws do not yield "optimal" performance. Thus, it is interesting to
study how much better the disturbance-utilizing control law performs, com-
pared to the conventional linear-quadratic control law, when the two closed-
loop systems are subjected to the same typical realistic disturbances w(t).
To quantify such a comparison, Kelly [7] has proposed the concept of "effect-
iveness" $\mathcal{E}$ defined for the discrete-time case as

$$\mathcal{E} = \frac{\tilde{J}_{LQ} - \tilde{J}_{DUC}}{\tilde{J}_{LQ}} \times 100\% \tag{26}$$

where $\tilde{J}_{LQ}$ is the value of Eq. (9) obtained by using the conventional (undis-
turbed) discrete-time linear-quadratic control law, and $\tilde{J}_{DUC} = V$ is the
value Eq. (24) of Eq. (9) obtained by using the optimal disturbance-utilizing
control law Eq. (21) --- in <u>both</u> cases the plant Eq. (1a,b) is subjected to
the <u>same</u> disturbance w(t) [as generated by the assumed disturbance model
Eq. (1c,d)]. Thus, if the disturbance-utilizing controller Eq. (21) is a
better performer (as it should be) one should find that $\tilde{J}_{DUC}$ is <u>less</u> than $\tilde{J}_{LQ}$
and therefore $\mathcal{E}$ is <u>positive</u>. The maximum possible value of $\mathcal{E}$ is 100%
which would correspond to the (unlikely) case that $\tilde{J}_{DUC}$ = 0. Thus, the
closer $\mathcal{E}$ is to 100% the greater is the effectiveness of Eq. (21) compared to
the conventional linear-quadratic control law.

234

It is interesting to note that the conventional linear-quadratic control law used in such comparisons can be obtained directly from Eq. (21) by simply setting $z(nT) = 0$, $\forall n$, (and also $c(nT) = 0$, $\forall n$, if $\bar{y}_c(t) \equiv 0$ is the desired response). This observation shows that the disturbance-utilizing control law Eq. (21) automatically reduces to the conventional linear-quadratic control law whenever the disturbance $w(t)$ vanishes. In other words, the matrix $K_x(\cdot)$ in Eq. (21) and Eq. (22a) is precisely the <u>same</u> matrix used in the conventional (undisturbed) linear-quadratic regulator control law.

EXAMPLE DESIGN OF A DISCRETE-TIME DISTURBANCE-UTILIZING CONTROLLER

To demonstrate application of the controller design algorithm for discrete-time disturbance-utilization, we will consider a rather general version of a first-order plant with first-order disturbance. The plant discrete-time model Eqs. (1a, b) and disturbance discrete-time model Eqs. (1c,d) are expressed as

$$E\,x(nT) = \tilde{a}(nT)x(nT) + \tilde{b}(nT)u(nT) + \tilde{f}\tilde{h}(nT)z(nT) + \tilde{\gamma}(nT) \tag{27a}$$

$$y(nT) = c(nT)x(nT) \tag{27b}$$

$$E\,z(nT) = \tilde{d}(nT)z(nT) + \tilde{\sigma}(nT) \tag{27c}$$

where x = scalar, u = scalar, z = scalar. We will assume that the desired behavior is set-point regulation to $x(nT) = 0$ $\forall n$; therefore $\bar{y} = x$ in Eq. (4) and $\bar{y}_c \equiv 0$ in Eq. (5). Thus, we may set $G(t) \equiv 0$ in Eq. (5). The parameters $\tilde{a}$, $\tilde{b}$, $\tilde{f}\tilde{h}$, $\tilde{d}$ may be time-varying.

The discrete-time performance index $\tilde{J}$ in Eq. (9) is expressed as

$$\tilde{J} = \frac{1}{2}x^T(NT)\tilde{S}x(NT) + \frac{1}{2}\sum_0^{(N-1)}\left[x^T(nT)\tilde{q}x(nT) + u^T(nT)\tilde{R}u(nT)\right]\ ; \qquad \begin{array}{l} \tilde{S} > 0 \\ \tilde{q} > 0 \\ \tilde{R} > 0 \end{array} \tag{28}$$

where, in this example, $\tilde{s}$, $\tilde{q}$, $\tilde{R}$ are arbitrary positive scalars and $\varepsilon = -x$.

The optimal disturbance-utilizing control Eq. (21) for this example has the specific form

$$u^o(nT) = -\left[\frac{\tilde{b}}{\tilde{R} + \tilde{b}^2 k_x((n+1)T)}\right] \cdot \left[\tilde{a}k_x((n+1)T)x + \left[\tilde{f}\tilde{h}\,k_x((n+1)T) + \tilde{d}k_{xz}((n+1)T)\right]z\right] \tag{29}$$

where we have set $k_{xc} \equiv 0$ because $G(t) \equiv 0$ (set-point $\bar{y}_c$ is zero). The time-varying gains $k_x(\cdot)$, $k_{xz}(\cdot)$ associated with the control Eq. (29) are computed from the difference equations Eqs. (22a,c) which for this example reduce to

$$k_x(nT) = \frac{\tilde{R}\tilde{a}^2 k_x((n+1)T)}{\tilde{R} + \tilde{b}^2 k_x((n+1)T)} + \tilde{q}\ ; \qquad \begin{array}{l}\bar{c} = 1 \\ k_x(NT) = \tilde{s} > 0\end{array} \tag{30a}$$

$$k_{xz}(nT) = \left(\frac{\tilde{R}\,\tilde{a}}{\tilde{R} + \tilde{b}^2 k_x((n+1)T)} \right) \left[k_{xz}((n+1)T)\tilde{d} + k_x((n+1)T)\tilde{fh} \right]; \quad k_{xz}(NT) = 0. \tag{30b}$$

One can now compute the successive values of k_x, k_{xz} for $n = (N-1)$, $(N-2)$, $(N-3)$, ..., 2, 1, 0 using Eq. (30) and the indicated "starting" conditions at $t = t_0 + nT$. Those computed values are then stored and used later in the real-time computation of Eq. (29).

CONSIDERATION OF THE TIME-INVARIANT CASE OF THE EXAMPLE

If one assumes that the plant and disturbance models Eq. (27) came from a time-invariant continuous-time plant and disturbance model, the preceeding results Eqs. (29), (30) can be expressed in more explicit form. In particular, if Eqs. (27) are assumed to derive from the continuous-time models

$$\dot{x} = ax + bu + fw \tag{31a}$$

$$\dot{z} = dz + \sigma(t); \qquad w = hz \tag{31b}$$

where a, b, f, h, d are __constant scalars__, then

$$\tilde{a} = e^{aT}; \quad \tilde{b} = \int_0^T e^{a(T-\tau)} b\, d\tau = \frac{b}{a}(e^{aT}-1), \quad \left(= bT \text{ if } a = 0\right)$$

$$\tilde{fh} = \int_0^T e^{a(T-\tau)} fh\, e^{d\tau}\, d\tau = \left(\frac{f}{d-a}\right)\left[e^{dT} - e^{aT}\right], \quad \left(= fTe^{aT} \text{ if } a = d\right) \tag{32}$$

$$\tilde{d} = e^{dT}$$

Using Eq. (32) in Eqs. (29), (30) leads to the following explicit expressions (shown for the case $a \neq 0$, $d \neq a$). The control law Eq. (29) becomes

$$u^o(nT) = -\left[\frac{\frac{b}{a}(e^{aT}-1)}{\tilde{R} + \left(\frac{b}{a}\right)^2(e^{aT}-1)^2 k_x((n+1)T)} \right]\left[e^{aT}k_x((n+1)T)x + \left[\left(\frac{f}{d-a}\right)(e^{dT}-e^{aT})k_x((n+1)T) + e^{dT}k_{xz}((n+1)T)\right]z \right] \tag{33}$$

and Eqs. (30) for the gain matrices become

$$k_x(nT) = \frac{\tilde{R}e^{2aT}k_x((n+1)T)}{\tilde{R} + \left(\frac{b}{a}\right)^2(e^{aT}-1)^2 k_x((n+1)T)} + \tilde{q}; \qquad k_x(NT) = \tilde{s} \tag{34a}$$

$$k_{xz}(nT) = \left(\frac{\tilde{R}e^{aT}}{\tilde{R} + \left(\frac{b}{a}\right)^2(e^{aT}-1)^2 k_x((n+1)T)} \right)\left[e^{dT}k_{xz}((n+1)T) + \left(\frac{f}{d-a}\right)(e^{dT}-e^{aT})k_x((n+1)T) \right]; \quad k_{xz}(NT) = 0 \tag{34b}$$

RESULTS OF A SIMULATION STUDY OF THE EXAMPLE

The time-invariant case, Eqs. (31) - (34), of the example was studied by digital simulation techniques using the specific parameter values

236

$$a = +1; \quad b = +1; \quad f = +1; \quad h = +1; \quad d = 0; \quad w(0) = w(t) \equiv +1$$

$$t_0 = 0; \quad T_f = 10; \quad T = 1.0 \ (\therefore N = 10); \quad x(0) = +1 \tag{35}$$

Note that the open-loop plant is unstable, with open-loop pole at $+1$, and the disturbance w is constant with $\sigma(t) \equiv 0$. For this study, the following three sets of values of the weighting parameters $\tilde{s}$, $\tilde{q}$, $\tilde{R}$ in the performance index Eq. (28) were investigated

Case 1:	$\tilde{s} = 10$	$\tilde{q} = 1$	$\tilde{R} = 1$
Case 2:	$\tilde{s} = 1$	$\tilde{q} = 10$	$\tilde{R} = 1$
Case 3:	$\tilde{s} = 1$	$\tilde{q} = 1$	$\tilde{R} = 10$

$$\tag{36}$$

The resulting behavior of the optimal disturbance-utilizing control $u^o(t)$ and the plant state $x(t)$ are shown in Figure 1. The optimal trade-offs in the performance of $x(T_f)$, $x(t)$, and $u(nT)$, (corresponding to the relative magnitudes of the weighting parameters $\tilde{s}$, $\tilde{q}$, $\tilde{R}$ in Cases 1, 2, 3) are clearly evident in Figure 1.

REFERENCES CITED

1. C. D. Johnson, "Discrete-Time Disturbance-Accommodating Control Theory with Applications to Missile Digital Control," AIAA Jour. of Guidance Control, Vol. 4, No. 2, pp. 116-125, March 1981.

2. C. D. Johnson, "Accommodation of Disturbances in Linear Regulator and Servo-Mechanism Problems," IEEE Trans. on Automatic Control, (Special Issue on the "Linear-Quadratic Gaussian Problem"), Vol. AC-16, No. 6, December 1971.

3. C. D. Johnson, "Accommodation of Disturbances in Optimal Control Problems," International Journal of Control, Vol. 15, No. 2, pp. 209-231, 1972. Also Proc. Third Southeastern Symposium on System Theory, Atlanta, Ga., April 1971.

4. C. D. Johnson, "Theory of Disturbance Accommodating Controllers," Chapter 7 in the book: Advances in Control and Dynamics Systems, Vol. 12, Edited by C. T. Leondes, Academic Press, 1976.

5. C. D. Johnson and Skelton, R. E., "Optimal Desaturation of Momentum Exchange Control System," The 11th Joint Automatic Control Conference, Atlanta, Georgia, June 1970; Also, Journal of the AIAA, Vol. 9, No. 1, pp. 12-22, January 1971.

6. C. D. Johnson, "Utility of Disturbances in Disturbance-Accommodating Control Problems," Proceedings of the 15th Annual Meeting of the Society for Engineering Science; Gainesville, Fla., p. 347, December 1978.

7. W. C. Kelly, "Homing Missile Guidance with Disturbance-Utilizing Control," <u>Proceedings of the 12th Southeastern Symposium on System Theory</u>, Virginia Beach, Va., May 1980, p. 260.

8. P. Dorato and A. H. Levis, "Optimal Linear Regulators; The Discrete-Time Case," <u>IEEE Transactions on Automatic Control</u>, Vol. AC-16, No. 6, pp. 613-620, December 1971.

9. W. C. Kelly, "Theory of Disturbance-Utilizing Control with Applications to Missile Intercept Problems," Ph.D. Dissertation, 1979; The University of Alabama in Huntsville, Huntsville, Alabama.

FIGURE 1

Next page is blank.
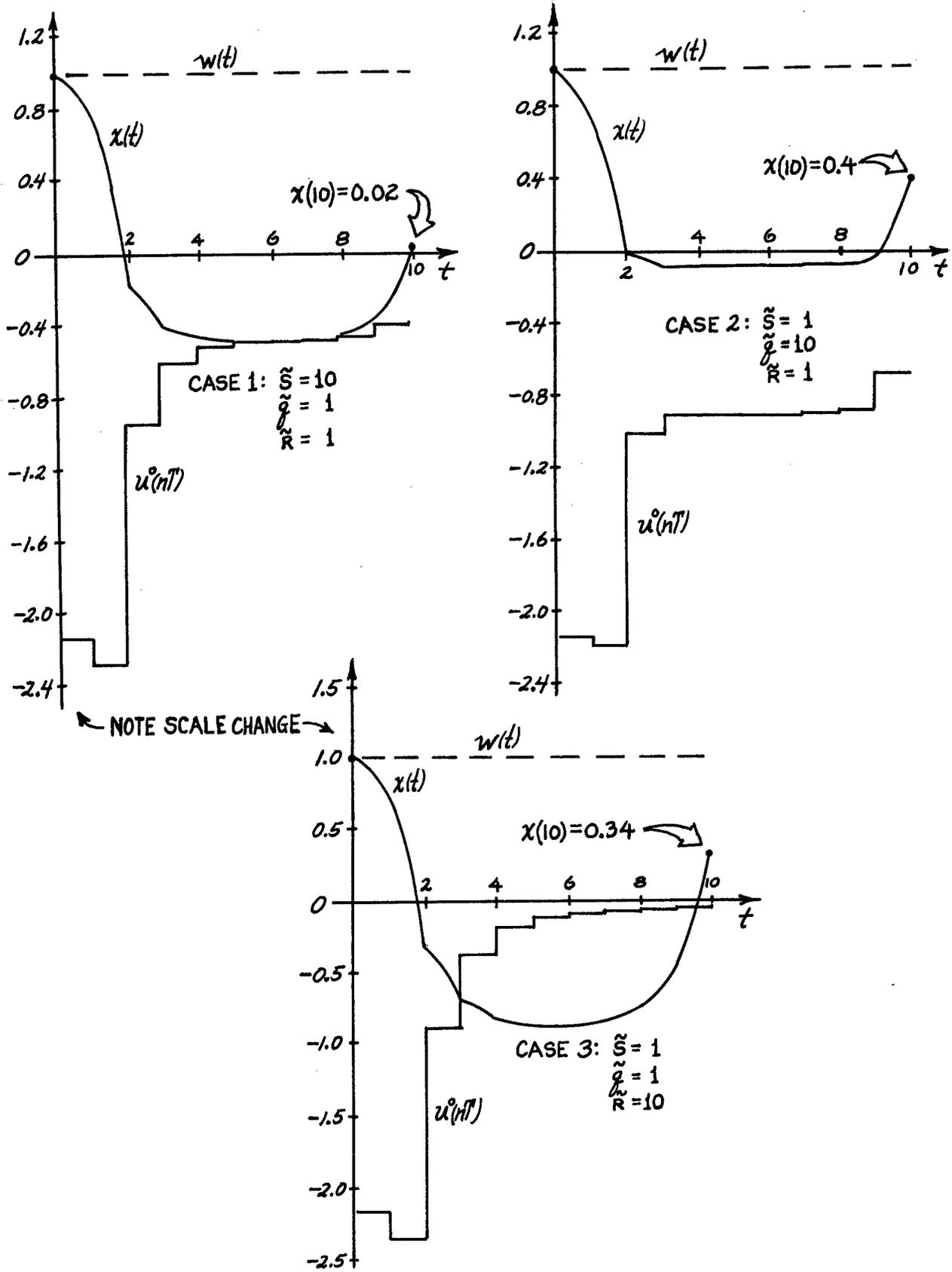
DISCRETE CONTROLLER DESIGN FOR GAUSSIAN AND WAVEFORM TYPE DISTURBANCES

Jerry Bosley
Computer Sciences Corporation

Dr. William C. Kelly
US Army Missile Laboratory
US Army Missile Command

ABSTRACT

This paper describes an application of newly-developed control theory relating to the design of discrete controllers which accommodate gaussian disturbances in addition to disturbances that possess "waveform structure". Previous work in this area applied linear-quadratic-gaussian theory to terminal homing missile problems with gaussian noise and, more recently, disturbance-utilizing control theory to terminal homing missile problems with "waveform-type" disturbances. This paper describes a new application which combines features of both approaches in terminal homing problems where both classes of disturbances may be present. The underlying theory of this combined approach is discussed and the operation of the discrete controller in a planar missile interceptor engagement model is illustrated with a numerical example.

INTRODUCTION

Algorithms for synthesizing disturbance-utilizing controllers were developed and applied by Johnson [1, 2, 3] several years ago to analog-type control problems where the uncertain external influences on the plant were "waveform type" disturbances. Just a year ago Johnson [4] reported the development and application of a design algorithm for synthesizing discrete-time disturbance-utilizing controllers. And now Johnson [5] has extended the discrete-time Disturbance-Utilizing Control (DUC) theory to include plant and sensor disturbances of the gaussian noise type with known mean and covariance.

The DUC theory is based on the fact that disturbances may sometimes produce effects which are beneficial to the primary control objectives. For instance, certain forms of wind gusts may actually help to steer a missile toward a specific target. Maximum utilization of a disturbance having waveform structure can be achieved by employing optimal control theory to design the controller. The key to obtaining maximum utilization of disturbances is to choose a performance index J so that, when J is minimized with respect to the control u(t), the primary control objective is accomplished and maximum use of the disturbance is achieved.

Uncontrolled inputs to control systems may be classified as either noise-type disturbances or disturbances with "waveform structure". Thermal noise in a radar receiver is an example of a noise-type disturbance, while gravity, wind gusts and electronic instrument drift are examples of waveform-type disturbances. While noise-type disturbances are characterized by their statistical properties (e.g., variance and mean), waveform-type disturbances can be modeled by determining a differential equation that the disturbances are known to satisfy.

If the uncertain external influences on the controlled process are waveform-type rather than noise-type disturbances, the well known stochastic control techniques [6,7] do not result in the most effective controller. On the other hand, if the uncertain external influences are noise-type rather than waveform-type disturbances, then Johnson's DUC theory is inadequate; the DUC controller does regulate the set point, however it uses large amounts of control energy trying to utilize the random noise.

In some practical applications, the disturbances acting on the plant consist of a combination of waveform-type disturbances and noise-type disturbances. Moreover, the sensor measurements are usually corrupted by additive noise which tends to obscure the output behavior information. Thus, Johnson extended the discrete-time DUC theory to include those cases where the plant may be subject to noise-type disturbances and where the plant output sampled measurements may be corrupted by additive noise. This extended theory is referred to as discrete-time Noisy DUC theory.

The discrete-time Noisy DUC theory is applied in this paper to the problem of utilizing disturbances in a homing missile guidance problem. While the conventional approach to handling disturbance effects is to attempt to eliminate them, the approach taken here is to formulate the optimal controller that accounts for the waveform properties of the disturbance. Numerical results are given to show the comparison between the performance of the noisy disturbance-utilizing controller and a conventional linear-quadratic-gaussian controller in the presence of both noise-type and waveform-type disturbances.

BACKGROUND

The Noisy DUC theory in [5] is developed for plants which can be modeled as linear dynamical systems, with respect to an appropriate operating point or regime. Specifically the plant is modeled by:

$$\dot{x} = A(t)x + B(t)u + F_d(t)w_d + F_{nl}(t)w_{nl} \qquad (1\text{-}a)$$

$$y = C(t)x + v_n \qquad (1\text{-}b)$$

242

where $x = (x_1, \ldots, x_n)$ is the plant state vector; $y = (y_1, \ldots, y_m)$ is the measurement vector; u is the control input; w_d is the vector of waveform-type disturbances; w_{n1} is the vector of noise-type disturbances and v_n is the vector of measurement noise which corrupts the data $C(t)x$ in the output measurement $y(t)$.

The vector noise terms w_{n1}, v_n in (1) are assumed to be white noise random processes with known means and covariances. Mathematical models for the gaussian random processes $\{w_{n1}\}$, $\{v_n\}$ are

$$\mathcal{E}[w_{n1}] = 0; \quad \mathcal{E}[v_n] = 0$$

$$\text{cov}[w_{n1}(t), w_{n1}(\tau)] = Q_{n1}(t)\delta(t - \tau)$$

$$\text{cov}[v_n(t), v_n(\tau)] = R_n(t)\delta(t - \tau)$$

$$\text{cov}[w_{n1}(t), v_n(\tau)] = 0$$

where $\mathcal{E}[\cdot]$ denotes the expectation (mean value) operator, $\text{cov}[\cdot,\cdot]$ denotes the covariance operator, and $Q_{n1}(t)$, $R_n(t)$ are, respectively, non-negative definite and positive definite symmetric matrices.

The vector of waveform-type disturbances $w_d(t)$ in (1) is modeled by

$$w_d = H(t)z \tag{2-a}$$

$$\dot{z} = D(t)z + \sigma(t) + F_{n2}(t) w_{n2} \tag{2-b}$$

where $z = (z_1, \ldots, z_p)$ is the disturbance state vector and w_{n2} denotes a vector white noise process with known mean and covariance. The mathematical model for $\{w_{n2}\}$ is

$$\mathcal{E}[w_{n2}] = 0$$

$$\text{cov}[w_{n2}(t), w_{n2}(\tau)] = Q_{n2}(t)\delta(t - \tau); \quad Q_{n2} \geq 0$$

$$\text{cov}[w_{n1}(t), w_{n2}(\tau)] = 0; \quad \text{cov}[w_{n2}(t), v_n(\tau)] = 0$$

The term $\sigma(t)$ denotes a sparse sequence of totally unknown impulses (unknown arrival times and unknown intensities).

The mathematical models (1), (2) are continuous-time models defined for all time t. However, to design a discrete-time digital controller it is convenient to have discrete-time versions of the models of (1), (2) which describe the behavior of $x(t)$ and $w_d(t)$

at discrete points in time $t = t_o$, $t_o + T$, $t_o + nT$, where T is the sampling period associated with the digital controller. The procedures for developing discrete-time versions of the mathematical models (1), (2) are described in detail in [8]. Application of those procedures to (1) and (2) leads to the following discrete-time models

$$Ex(nT) = \tilde{A}(nT)x(nT) + \tilde{B}(nT)u(nT) + \widetilde{F_dH}(nT)z(nT)$$

$$+ \tilde{F}_{n1}(nT)\tilde{w}_{n1}(nT) + \tilde{\tilde{\gamma}}(nT) \qquad (3\text{-}a)$$

$$Ez(nT) = \tilde{D}(nT)z(nT) + \tilde{\sigma}(nT) + \tilde{F}_{n2}(nT)\tilde{w}_{n2}(nT) \qquad (3\text{-}b)$$

$$y(nT) = C(nT)x(nT) + \tilde{v}_n(nT) \qquad (3\text{-}c)$$

where the matrices $\tilde{A}$, $\tilde{B}$, $\widetilde{F_dH}$, etc. are related to A, B, F_d, H, F_{n1}, D in (1), (2) by expressions given in [8] and E is the delay operator, $Ex(nT) = x((n+1)T)$. The terms $\tilde{w}_{n1}(nT)$, $\tilde{v}_n(nT)$, $\tilde{w}_{n2}(nT)$ in (3) represent discrete-time noise processes which are modeled as sequences of zero-mean, independent gaussian random variables with known covariances

$$\text{cov}[\tilde{w}_{n1}(nT), \tilde{w}_{n1}(jT)] = Q_{n1}\delta(n - j)$$

$$\text{cov}[\tilde{v}_n(nT), \tilde{v}_n(jT)] = R_n\delta(n - j)$$

$$\text{cov}[\tilde{w}_{n2}(nT), \tilde{w}_{n2}(jT)] = Q_{n2}\delta(n - j) \quad \text{for all } n, j$$

where $Q_{n1} \geq 0$, $R_n > 0$, $Q_{n2} \geq 0$ may vary with time.

The discrete-time models are consolidated into one composite model written as

$$E\tilde{x} = \left(\frac{Ex}{Ez}\right) = \bar{A}(nT)\tilde{x}(nT) + \bar{B}(nT)u(nT)$$

$$+ \bar{F}(nT)\tilde{w}_n(nT) + \bar{\delta}(nT) \qquad (4\text{-}a)$$

$$y(nT) = \bar{C}\tilde{x}(nT) + \tilde{v}_n(nT) \qquad (4\text{-}b)$$

where

$$\bar{A} = \left[\begin{array}{c|c} \tilde{A} & \widetilde{F_dH} \\ \hline 0 & \tilde{D} \end{array}\right] \quad ; \quad \bar{B} = \left[\frac{\tilde{B}}{0}\right] \quad ; \quad \bar{F} = \left[\begin{array}{c|c} \widetilde{F_{n1}} & 0 \\ \hline 0 & \widetilde{F_{n2}} \end{array}\right] \qquad (4\text{-}c)$$

$$\bar{C} = [C|0] \quad ; \quad \tilde{w}_n = \left[\frac{\tilde{w}_{n1}}{\tilde{w}_{n2}}\right] \quad ; \quad \bar{\delta} = \left[\frac{\tilde{\tilde{\gamma}}}{\tilde{\sigma}}\right] \qquad (4\text{-}d)$$

Since the plant motions $x(t)$ governed by (1) are random in nature (due to the presence of w_d) the expected value of the performance index $\tilde{J}$ is to be minimized. Thus, when $\mathcal{E}[\tilde{J}]$ is minimized with respect to the control $u(nT)$, the primary control objective is accomplished and maximum use of the disturbance w_d is achieved. $\mathcal{E}[\tilde{J}]$ is given in [5] in terms of $\tilde{x}$ as

$$\mathcal{E}[\tilde{J}] = \mathcal{E}\left\{\frac{1}{2}\tilde{x}^T(NT)\,\hat{\tilde{S}}\tilde{x}(NT) + \frac{T}{2}\sum_{n=0}^{n=(N-1)}[\tilde{x}^T(nT)\,\hat{\tilde{Q}}\tilde{x}(nT)\right.$$

$$\left. + u^T(nT)\,\tilde{R}u(nT)]\right\} \tag{5}$$

where

$$\hat{\tilde{S}} = \bar{C}^T\tilde{S}\bar{C}, \qquad \hat{\tilde{Q}} = \bar{C}^T\tilde{Q}\bar{C}$$

and the time interval of problem definition (t_o, T_f) has been divided into N equal segments of length T. The weighting matrices $\tilde{S}, \tilde{Q}, \tilde{R}$ are symmetric with $\tilde{S} \geq 0$, $\tilde{Q} \geq 0$, $\tilde{R} > 0$, and $\tilde{S} + \tilde{Q} > 0$.

The discrete-time Noisy DUC problem may be precisely described as follows. Given the composite plant model (4) find the control $u^o(nT)$ which minimizes (5) for all independent random initial conditions $\{x(t_o), z(t_o)\}$ satisfying

$$\text{mean } x(t_o) = \bar{x}(t_o); \quad \text{cov}[x(t_o)] = R_{xo}$$

$$\text{mean } z(t_o) = \bar{z}(t_o); \quad \text{cov}[z(t_o)] = R_{zo}$$

where $\bar{x}, \bar{z}, R_{xo}$ and R_{zo} are given. As is customary in the DUC theory, the sparse terms in $\bar{\delta}$ in (4) are neglected in deriving the control since they are completely unknown. This problem is of the form known as the "discrete-time linear-quadratic-gaussian optimal control problem" which has been extensively studied in the literature and its solution is described in [9]. When that known solution is applied, the optimal, discrete-time disturbance-utilizing control $u^o(nT)$ is given by

$$u^o(nT) = -\left[\tilde{R}(nT) + \bar{B}^T(nT)\bar{P}\big((n$$

$$+ 1)T\big)\bar{B}(nT)\right]^{-1}\left[\bar{B}^T(nT)\bar{P}\big((n$$

$$+ 1)T\big)\bar{A}(nT)\right]\hat{\tilde{x}}(nT) \tag{6-a}$$

where $\bar{P} = \bar{P}^T$ obeys

$$\bar{P}(nT) = \bar{A}^T(nT)\bar{P}\big((n+1)T\big)\bar{A}(nT) + \tilde{Q}$$

$$- \left[\bar{B}^T(nT)\bar{P}\big((n+1)T\big)\bar{A}(nT)\right]^T\left[\tilde{R}\right.$$

$$+ \bar{B}^T(nT)\bar{P}\big((n+1)T\big)\bar{B}(nT)\right]^{-1}\left[\bar{B}^T(nT)\bar{P}\big((n\right.$$

$$+1)T\big)\bar{A}(nT)\right] \quad ; \quad \bar{P}(NT) = \hat{\tilde{S}} \qquad (6\text{-}b)$$

where $\hat{\tilde{x}}(nT)$ denotes the estimate of $\tilde{x}(nT)$ obtained from a discrete-time Kalman filter. The essential difference between the noisy and non-noisy solutions for the optimal control is in the term $\tilde{x}(nT)$. In the non-noisy case, $\hat{\tilde{x}}$ is generated by an observer with rather arbitrary observer gains. In the noisy case, $\hat{\tilde{x}}(nT)$ is generated by a precisely described Kalman filter with specific time-varying gains. The Kalman filter is given by

$$E\hat{\tilde{x}} = \bar{A}(nT)\hat{\tilde{x}}(nT) + \bar{B}(nT)u(nT) + \bar{K}_f(nT)\left[y(nT)\right.$$

$$- \bar{C}(nT)\hat{\tilde{x}}(nT)\right]$$

$$\hat{\tilde{x}}(o) = \hat{\tilde{x}}(t_o) = \big(\bar{x}(t_o)\,|\,\bar{z}(t_o)\big) = \bar{\tilde{x}}(t_o) \qquad (7)$$

The Kalman gain matrix K_f is specified by

$$\bar{K}_f(nT) = \bar{A}(nT)\bar{P}_f(nT)\bar{C}^T(nT)\left[\bar{C}(nT)\bar{P}_f(nT)\bar{C}^T(nT)\right.$$

$$+ R_n(nT)\right]^{-1} \qquad (8\text{-}a)$$

where the symmetric matrix $\bar{P}_f$ is governed by the discrete-time Riccati matrix equation

$$\bar{P}_f\big((n+1)T\big) = \bar{A}(nT)\bar{P}_f(nT)\bar{A}^T(nT)$$

$$- \bar{A}(nT)\bar{P}_f(nT)\bar{C}^T(nT)\left[\bar{C}(nT)\bar{P}_f(nT)\bar{C}^T(nT)\right.$$

$$+ R_n(nT)\right]^{-1}\bar{C}(nT)\bar{P}_f(nT)\bar{A}^T(nT)$$

$$+ \bar{F}(nT)Q_n(nT)\bar{F}^T(nT) \qquad (8\text{-}b)$$

with initial condition

$$\bar{P}_f(o) = \text{cov}[\tilde{x}(t_o)] = \left[\begin{array}{c|c} R_{xo} & 0 \\ \hline 0 & R_{zo} \end{array}\right] \qquad (8\text{-}c)$$

and where

$$Q_n = \left[\begin{array}{c|c} Q_{n1} & 0 \\ \hline 0 & Q_{n2} \end{array}\right]$$

(8-d)

It is useful to examine the detailed structure of the individual equations associated with expressions (6) (7) (8). Set

$$\bar{P} = \left[\begin{array}{c|c} K_x & K_{xz} \\ \hline K_{xz}^T & K_z \end{array}\right]$$

(9)

Substitution of (9), (4-c) and (4-d) into (6-a) leads to the following

$$u^o(nT) = -\left[\tilde{R}(nT) + \tilde{B}^T(nT)K_x\left((n+1)T\right)\tilde{B}(nT)\right]^{-1}\tilde{B}^T(nT)\left[K_x\left((n+1)T\right)\tilde{A}(nT)\hat{x}(nT) + \left(K_x\left((n+1)T\right)\widetilde{F_dH}(nT) + K_{xz}\left((n+1)T\right)\tilde{D}(nT)\right)\hat{z}(nT)\right]$$

(10)

A set of three coupled matric difference equations which govern the matrices $K_x(nT)$, $K_{xz}(nT)$, $K_z(nT)$ is obtained by substituting (4-c), (4-d) and (9) into (6-b). That set of equations, which is lengthy, is documented in [4] and therefore will not be repeated here. Note that if $\hat{z}(nT)$ in (10) were set to zero the optimal disturbance-utilizing-control would become the conventional LQG control.

Detailed expressions for the Kalman filter are obtained by substituting (4-c) and (4-d) into (7) to obtain

$$E\hat{x} = \tilde{A}\hat{x} + \widetilde{F_dH}\hat{z} + \tilde{B}u + \bar{K}_{fx}(y - C\hat{x}); \quad \hat{x}(t_o) = \bar{x}(to)$$ (11-a)

$$E\hat{z} = \tilde{D}\hat{z} + \bar{K}_{fz}(y - C\hat{x}); \quad \hat{z}(t_o) = \bar{z}(t_o)$$ (11-b)

where

$$\bar{K}_f = \left[\begin{array}{c} \bar{K}_{fx} \\ \hline \bar{K}_{fz} \end{array}\right]$$

(12)

Detailed expressions for the Kalman gain matrices in (11) are obtained by substituting (4-c), (4-d), (12) and the expression

$$\bar{P}_f = \left[\begin{array}{c|c} \bar{P}_{xx} & \bar{P}_{zx}^T \\ \hline \bar{P}_{zx} & \bar{P}_{zz} \end{array}\right]$$

into (8-a) to obtain

$$\bar{K}_{fx} = (\tilde{A}\bar{P}_{xx} + \widetilde{F_d H}\bar{P}_{zx})C^T[C\bar{P}_{xx}C^T + R_n]^{-1} \qquad (13\text{-}a)$$

$$\bar{K}_{fz} = \tilde{D}\bar{P}_{zx}C^T[C\bar{P}_{xx}C^T + R_n]^{-1} \qquad (13\text{-}b)$$

In a like manner, the set of matric difference equations governing the blocks $\bar{P}_{xx}$, $\bar{P}_{zx}$, $\bar{P}_{zz}$ are obtained from (8-b) as

$$EP_{xx} = (\tilde{A}\bar{P}_{xx} + \widetilde{F_d H}\bar{P}_{zx})\tilde{A}^T + (A\bar{P}_{zx}^T + \widetilde{F_d H}\bar{P}_{zz})(\widetilde{F_d H})^T$$

$$- [\tilde{\alpha}][C\bar{P}_{xx}C^T + R_n]^{-1}[\tilde{\alpha}]^T$$

$$+ \tilde{F}_{n1}Q_{n1}\tilde{F}_{n1}^T; \quad \bar{P}_{xx}(o) = R_{xo} \qquad (14\text{-}a)$$

$$E\bar{P}_{zx} = \tilde{D}[\bar{P}_{zx}\tilde{A}^T + \bar{P}_{zz}(\widetilde{F_d H})^T]$$

$$- [\tilde{\beta}][C\bar{P}_{xx}C^T + R_n]^{-1}[\tilde{\alpha}]; \quad \bar{P}_{zx}(o) = 0 \qquad (14\text{-}b)$$

$$E\bar{P}_{zz} = \tilde{D}\bar{P}_{zz}\tilde{D}^T - [\tilde{\beta}][C\bar{P}_{xx}C^T + R_n]^{-1}[\tilde{\beta}]^T$$

$$+ \tilde{F}_{n2}Q_{n2}\tilde{F}_{n2}^T; \quad \bar{P}_{zz}(o) = R_{zo} \qquad (14\text{-}c)$$

where

$$[\tilde{\alpha}] = \tilde{A}\bar{P}_{zz}C^T + \widetilde{F_d H}\bar{P}_{zx}C^T$$

$$[\tilde{\beta}] = \tilde{D}\bar{P}_{zx}C^T$$

The matric equations (14) can be integrated in forward time since the initial values $\bar{P}_{xx}(o)$, $\bar{P}_{zx}(o)$, $\bar{P}_{zz}(o)$ are explicitly known. On the other hand, the matrices $K_x(nT)$, $K_{xz}(nT)$, $K_z(nT)$ must be obtained by backward-time integration of (6-b) since only the terminal values (t = NT) are known.

APPLICATION TO HOMING MISSILE GUIDANCE

MATHEMATICAL MODEL

As an illustration of the Noisy DUC theory the controller design algorithms developed by Johnson [5] are applied to a homing intercept problem. The missile is to be controlled during the final phase of its flight so that its position coincides with that of a target at a specified terminal time, even in the face of disturbances which may, or may not, be detrimental to the control objective.

The planar geometry for this problem is shown in Figure 1, where the origin is located at the moving target position and the position of the missile is defined by the coordinates (x_M, y_M), where X_M is horizontal and Y_M is vertical.
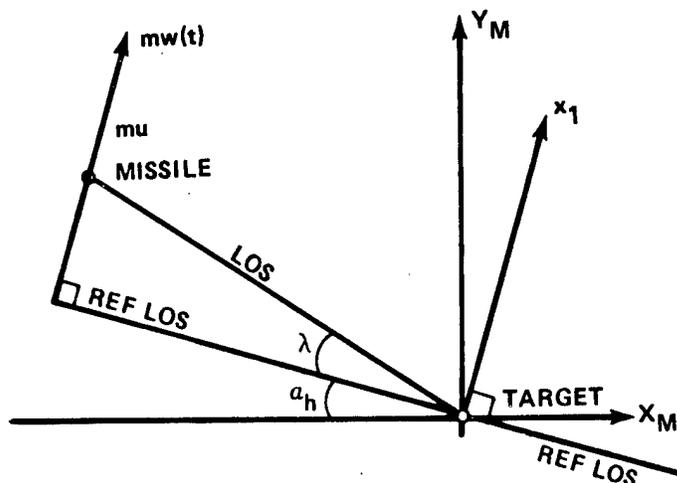

Figure 1. Relative intercept geometry.

It is convenient to consider a reference line-of-sight (REF LOS) passing through the target and oriented at a known angle α_h relative to the horizontal line X_M. The REF LOS is established a priori, and may correspond to a desired orientation of the line-of-sight. A coordinate x_1 is established normal to the REF LOS (Figure 1) and it is assumed that the missile begins the homing phase of the problem with a certain displacement $x_1(o)$ and velocity $x_2(o)$ (where $x_2 = \dot{x}_1$) normal to the REF LOS. It is assumed that a previous "midcourse" guidance phase has delivered the missile to the beginning of the homing phase at $t = t_o$; thus, non-zero values of $x_1(o)$ and $x_2(o)$ characterize the extent to which the midcourse phase has failed to enable the missile to start the homing phase under ideal conditions. The initial range to the target and the closing velocity are assumed given. The problem at hand uses the "small LOS" assumptions as in [10] and considers that the disturbance forces of primary interest are those acting normal to REF LOS. Errors in estimating time-to-go to intercept are not considered here.

The equations describing the motion of the missile normal to the REF LOS are

$$\dot{x}_1 = x_2 + w_{n1}(t)$$

$$\dot{x}_2 = u + w_d(t) + w_{n1}(t)$$

$$y = x_1 + v_n(t)$$

These equations may be written in the form

$$\dot{x} = A_x + Bu + F_d w_d + F_{n1} w_{n1} \qquad (15\text{-a})$$

$$y = Cx + v_n \qquad (15\text{-b})$$

where

$$A = \begin{bmatrix} 0 & 1 \\ 0 & 0 \end{bmatrix} ; \quad B = \begin{pmatrix} 0 \\ 1 \end{pmatrix} ; \quad F_d = \begin{pmatrix} 0 \\ 1 \end{pmatrix} ; \quad F_{n1} = \begin{pmatrix} 1 \\ 1 \end{pmatrix} ;$$

$$C = [1 \ 0] \qquad (15\text{-c})$$

It is assumed in the example to follow that the waveform-type disturbance consists of a linear combination of constant sequences and linear ramps:

$$w_d(t) = C_1 + C_2 t$$

where C_1 and C_2 are unknown constants. The disturbance process is written in state-variable form as

$$z_1 = w_d$$

$$\dot{z}_1 = z_2 + \sigma_1(t) + w_{n2}(t)$$

$$\dot{z}_2 = 0 + \sigma_2(t) + w_{n2}(t)$$

or in the form

$$\dot{z} = Dz + \sigma(t) + F_{n2} w_{n2} \qquad (16\text{-a})$$

$$w_d = Hz \qquad (16\text{-b})$$

where

$$D = \begin{bmatrix} 0 & 1 \\ 0 & 0 \end{bmatrix} ; \quad H = [1 \ 0] ; \quad F_{n2} = \begin{pmatrix} 1 \\ 1 \end{pmatrix} \qquad (16\text{-c})$$

and $\sigma(t) = [\sigma_1, \sigma_2]$ a sparse vector-impulse sequence occurring at unknown instants.

The corresponding discrete-time models are

$$Ex(nT) = \tilde{A}x(nT) + \tilde{B}u(nT) + \widetilde{F_d}Hz(nT) + F_{n1}\tilde{w}_{n1}(nT)$$
$$+ \tilde{j}(nT)$$

$$y(nT) = Cx(nT) + \tilde{v}_n(nT)$$

$$Ez(nT) = \tilde{D}z(nT) + \tilde{\sigma}(nT) + \tilde{F}_{n2}\tilde{w}_{n2}(nT)$$

$$w_d(nT) = H(nT)z(nT)$$

where

$$\tilde{A} = \begin{bmatrix} 1 & T \\ 0 & 1 \end{bmatrix} ; \quad \tilde{B} = \begin{pmatrix} T^2/2 \\ T \end{pmatrix} ; \quad \widetilde{F_dH} = \begin{bmatrix} T^2/2 & T^3/6 \\ T & T^2/2 \end{bmatrix}$$

$$\tilde{F}_{n1} = \begin{pmatrix} T + T^2/2 \\ T \end{pmatrix} ; \quad \tilde{F}_{n2} = \begin{pmatrix} T + T^2/2 \\ T \end{pmatrix} ; \quad \tilde{D} = \begin{bmatrix} 1 & T \\ 0 & 1 \end{bmatrix}$$

The waveform-type disturbances considered in this problem are gravity, wind and target maneuver [10]. The gravity component acting normal to the REF LOS is -32.2 cos α_h. The acceleration disturbance due to wind is modeled by the acceleration waveform of Figure 2, acting in a direction normal to the REF LOS. The target maneuver acting normal to the REF LOS has the waveform described in Figure 3 with a peak acceleration value of 128 ft/sec^2.
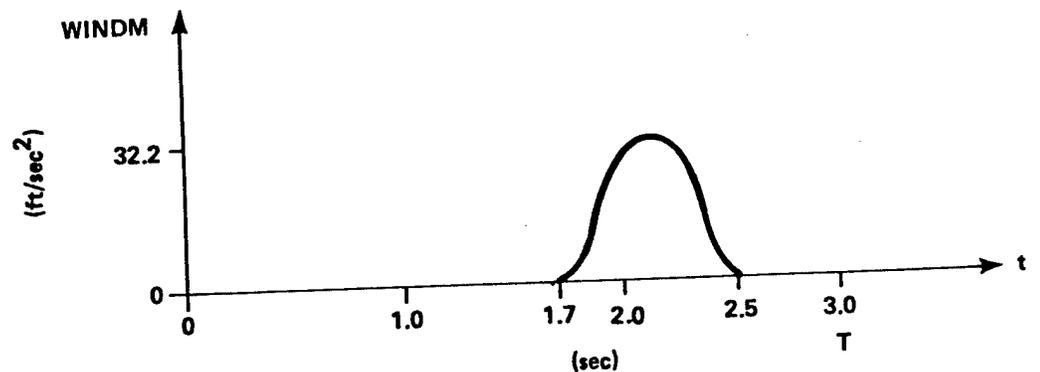

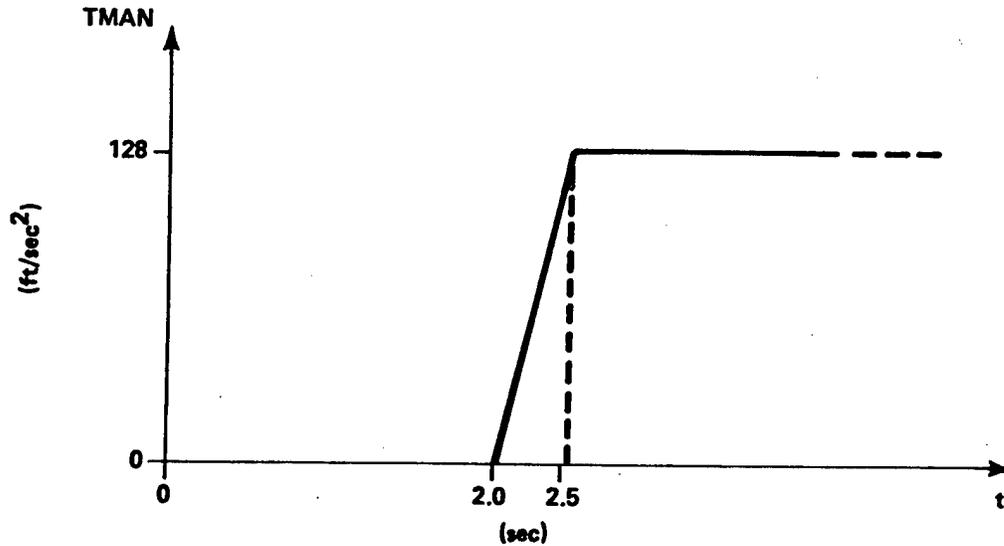Figure 2. Actual wind disturbance (WINDM) input.

251

Figure 3. Actual maneuver disturbance (TMAN) input.

The gaussian noise disturbances considered in this problem are w_{n1}, w_{n2}, v_n in (15) (16). They are assumed to have zero means and known covariances Q_{n1}, Q_{n2}, R_n, respectively.

CONTROL OBJECTIVE

The primary control objective is to drive the displacement of the missile (normal to the REF LOS) to zero at a specified terminal time T_f; that is, to regulate the state x_1 to zero at $t = T_f$. The value of x_1 at $t = T_f$ is defined as miss distance. The secondary objective is to achieve the primary objective while effectively utilizing the "free" energy of the disturbances. The control objectives are to be achieved by minimizing the expected value of the performance index

$$\varepsilon[\tilde{J}] = \varepsilon\left\{\frac{1}{2}x^T(nT)\hat{\tilde{S}}x(nT) + T/2 \sum_{n=0}^{n=N-1} [x^T(nT)\hat{\tilde{Q}}x(nT) + u^T(nT)\tilde{R}u(nT)]\right\}$$

subject to the plant equations (15) and the waveform disturbance process equations (16). The resulting optimal control $u^o(nT)$ is given by (10). The control energy consumption (CEC) is computed for analyses as follows:

$$CEC = T/2 \sum_{n=0}^{n=N-1} [u^T(nT)\tilde{R}u(nT)]$$

252

DISCUSSION OF RESULTS

The homing intercept problem is solved by applying the Noisy DUC theory. First the composite state vector $\tilde{x}$, the composite system (4), and the expected value of the performance index (5) are established. Then the optimal control is computed by (10) after the gains $K_x(nT)$, $K_{xz}(nT)$ are computed. The problem is solved on a CDC-6600 computer, using backward-time integration to find the initial conditions for K_x, K_{xz}, and K_z, although closed-form algorithms would typically be used to compute the gains K_x and K_{xz} in applications. Estimates of the states, x and z are obtained from the discrete-time Kalman filter (11).

A Monte Carlo approach was developed to generate the expected value of the performance index. This approach consists of executing a specified number of runs where normally-distributed random variables are generated each run for the initial conditions of the plant state and the REF LOS orientation angle. The resulting miss distance, performance index and control energy consumption from each run are used in the computation of means and standard deviations.

A sensitivity study was conducted using both deterministic and stochastic simulations to determine "best" values for $\tilde{S}$ and Q_{n2}. The following parameters were fixed for the study:

$$\bar{x}_1(o) = 300 \text{ ft;} \qquad\qquad \bar{x}_2(o) = 0.0 \text{ ft/sec}$$

$$\bar{z}_1(o) = -32.2 \text{ ft/sec}^2; \qquad\qquad \bar{z}_2(o) = 0.0 \text{ ft/sec}^3$$

$$R_{xo} = \begin{bmatrix} 225 & 0 \\ & \\ 0 & 4 \end{bmatrix}; \qquad R_{zo} = \begin{bmatrix} 1000 & 0 \\ & \\ 0 & 100 \end{bmatrix}$$

$$\tilde{R} = 1; \qquad \tilde{Q} = \begin{bmatrix} 0 & 0 \\ 0 & 0 \end{bmatrix}; \qquad \tilde{S} = \begin{bmatrix} \tilde{S}_{11} & 0 \\ 0 & 0 \end{bmatrix}$$

$$Q_{n1} = 1; \qquad R_n = 1$$

$$T = 0.05 \text{ sec;} \qquad \alpha_h = 30 \text{ deg}$$

Integration stepsize = 0.01; T_f = 4.5 sec. The missile closing velocity is 2000 ft/sec and at t_o, the missile distance from the target is 9000 ft.

For the first phase of the study, only deterministic runs were made to determine sensitivities. In this analysis of performance variation with $\tilde{S}$, all the waveform-type disturbances were simulated and the disturbance states were corrupted by the noise $\{w_{n2}\}$ which had the characteristics

$$\varepsilon[w_{n2}] = 0; \quad \text{cov}[w_{n2}] = Q_{n2} = 1$$

The variances of the simulated noise terms $\{w_{n1}\}$, $\{w_{n2}\}$ and $\{v_n\}$, computed each run, were always nearly 1.

The results of varying $\tilde{S}$ are plotted in Figure 4 for both the conventional linear-quadratic-gaussian (LQG) controller and the noisy disturbance-utilizing controller (NDUC). Since $\overline{C}^T \tilde{S} \overline{C} = \hat{S}_{11}$, $\hat{S}_{11}$ will be referred to as S.
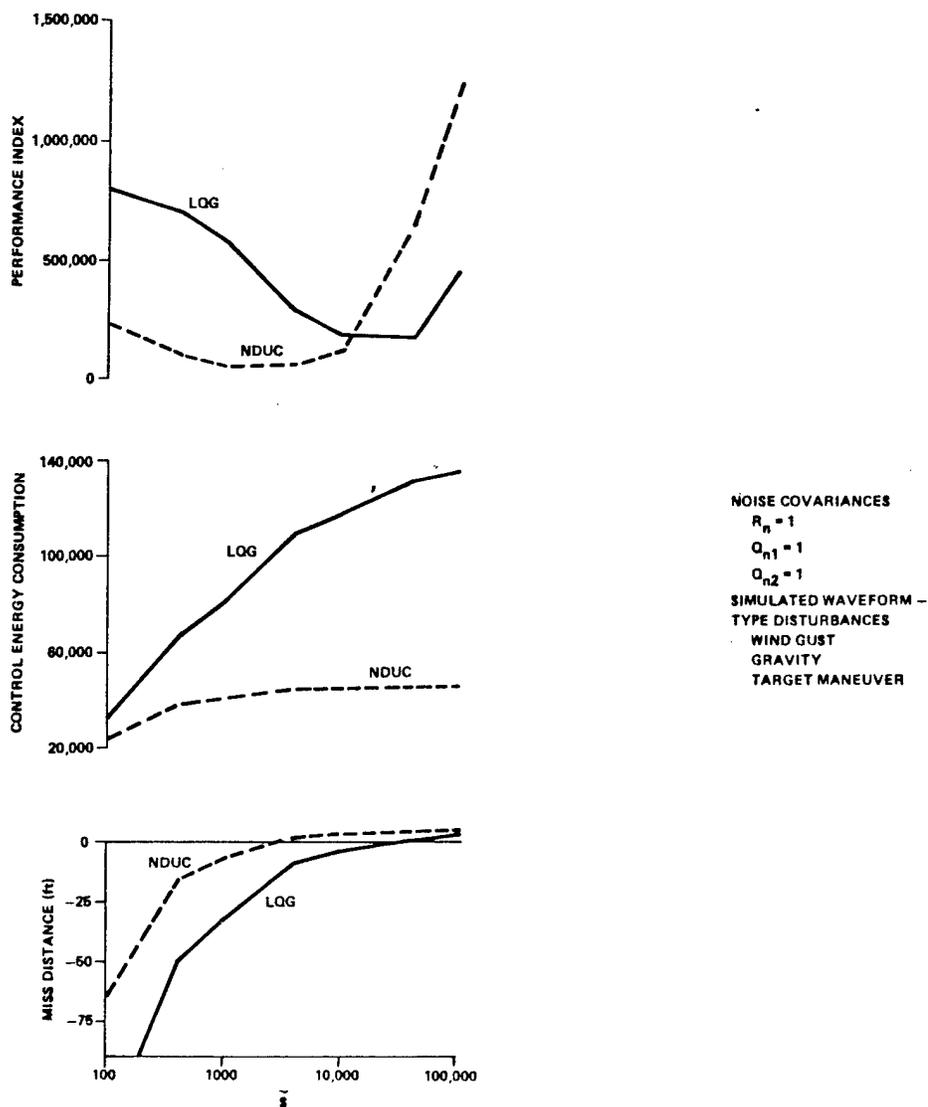

Figure 4. Performance as a function of terminal weighting $\tilde{S}$.

254

As $\tilde{S}$ increases the miss distance approaches a bias value rather than zero (later shown to be due to target maneuver). Figure 5 shows the missile altitude versus ground range for the LQG with $\tilde{S}$ set to 100. The missile hits in front of the target for all values of $\tilde{S}$ less than 100,000 for the LQG and for all values of $\tilde{S}$ less than 5000 for the NDUC.
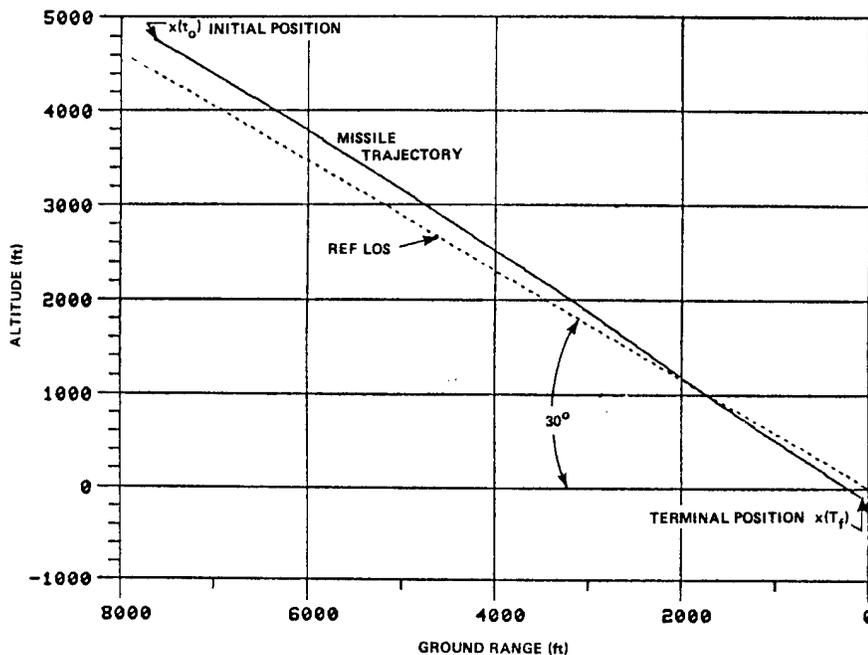

Figure 5. Missile trajectory with terminal weighting $\tilde{S}=100$.

An $\tilde{S}$ value which results in an acceptable miss distance can be picked for the LQG controller, however, the control energy consumption for the NDUC with the same $\tilde{S}$ is much lower.

The waveform-type disturbance states (continuous) and estimates (sampled) are plotted on Figure 6. Estimates of the wind and the target maneuver lag the actual disturbances because the weighting Q_{n2} on the new values input to the Kalman filter is low. However Q_{n2} can be increased to improve the estimate of the waveform-type disturbance. A value of 100 was chosen for $\tilde{S}$ and Q_{n2} was varied. The results, plotted on Figure 7, show that the minimum performance index is obtained for a value of Q_{n2} equal to 10,000. The lag in the target maneuver estimate is reduced as Q_{n2} is increased (see Figure 8). However, the increased Q_{n2} weighting causes the waveform estimate to fluctuate more which increases the control energy consumption. The performance improvement due to "better" estimates

255

is eventually offset by the control energy consumption so that a minimum performance index is obtained. It should be noted that the actual noise term $\{w_{n2}\}$ is simulated as random white noise with a measured variance of approximately 1.0.
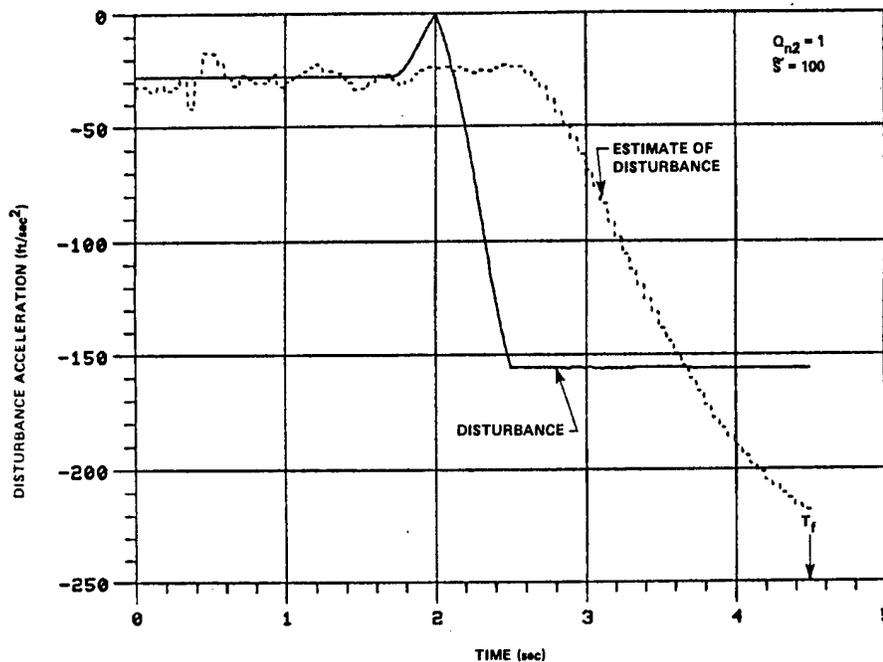

Figure 6. Disturbance estimate with $\tilde{S}=100$ and $Q_{n2} = 1$ (Q_{n2} chosen too low).

With the value of Q_{n2} set at 10,000, variation of $\tilde{S}$ is reexamined and the results are presented in Figure 9. Minimum performance index occurs for an $\tilde{S}$ value of 100. Further investigation of $\tilde{S}$ variation was conducted using a Monte Carlo simulation.

The Monte Carlo error sources were taken to be the initial conditions for the plant states and the REF LOS orientation angle. Normally distributed error source values are picked from the computer system library random number generator based on the specifications given in Table 1.

TABLE 1. MONTE CARLO PARAMETERS AND VALUES

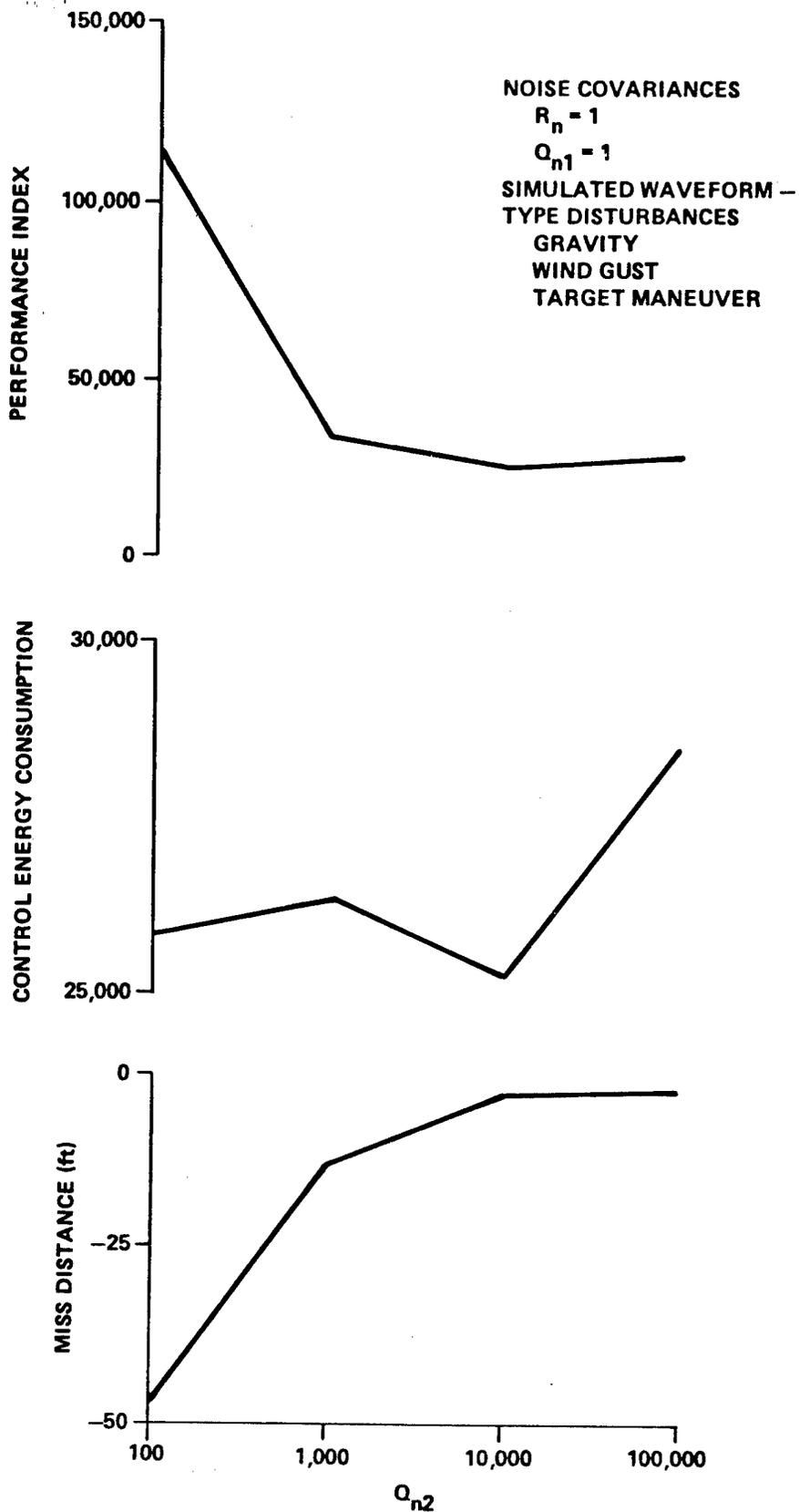| VARIABLE	MEAN	STANDARD DEVIATION
$X_1(o)$	300.0	15.0
$X_2(o)$	0.0	2.0
α_h	30.0	5.0

256

Figure 7. Noisy DUC performance versus choice of Q_{n2} ($\tilde{S} = 100$).
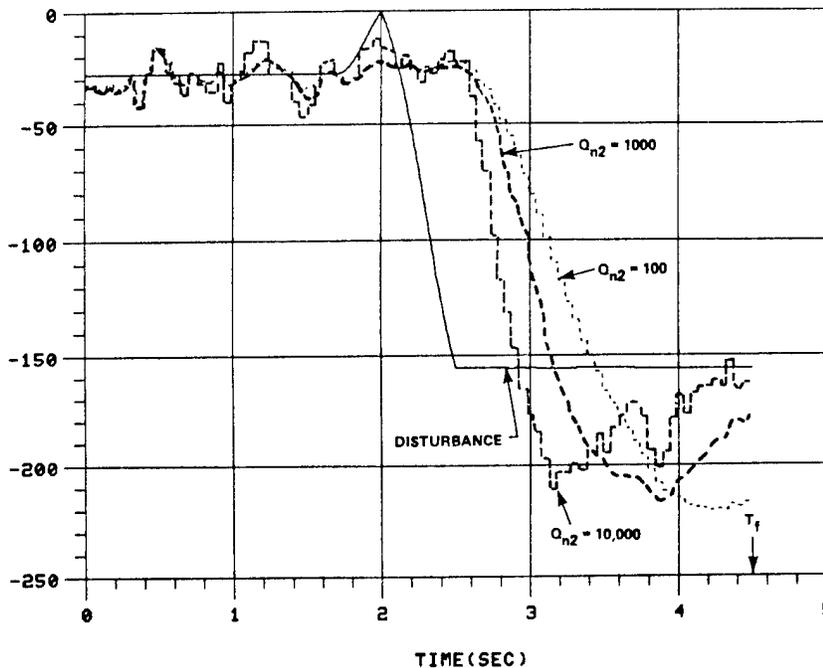
Figure 8. Effect of choice of Q_{n2} on lag in disturbance estimate $(\tilde{S}=100)$.

The controller performance as a function of $\tilde{S}$ for Monte Carlo 25-run sets is shown in Figure 10. Although the "best" mean values for miss distance and performance index occur for $\tilde{S}$ equal to 100, the miss distance approaches an offset value when $\tilde{S}$ is equal to 200 or 250.

Selecting $\tilde{S}$ as 250 and $\tilde{Q}_{n2}$ as 10,000 the disturbances were adjusted as shown in Table 2 to determine if the miss distance offset is caused by the noise or one or more of the waveform-type disturbances. As magnitude of the target maneuver increases from 0 to 128 ft^2/sec, the miss distance increases indicating that the target maneuver causes the offset. Note that the no gravity case has the highest values which clearly indicates the utilization of gravity to reduce control energy requirements.

Further Monte Carlo analysis of the miss distance offset as a function of $\tilde{S}$ was performed for the no-target-maneuver case. The results (see Figure 11) indicate that 250 is an appropriate value for $\tilde{S}$. The data (shown on Figure 10) generated for the noise and waveform-type disturbances also indicates that 250 is a "best" value for $\tilde{S}$.
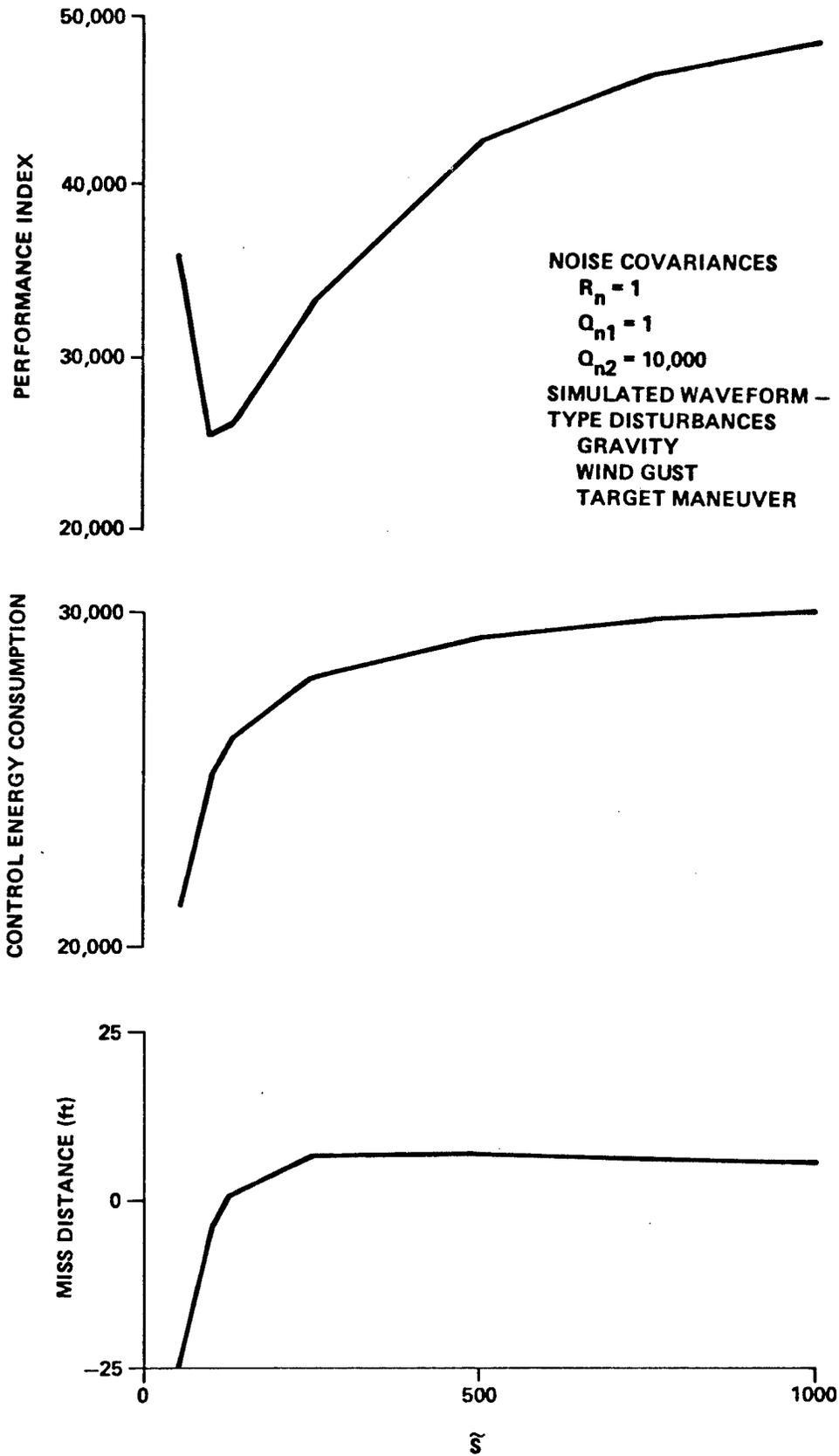
258

Figure 9. Noisy DUC performance versus terminal weighting $\tilde{S}$ with Q_{n2} = 10,000.
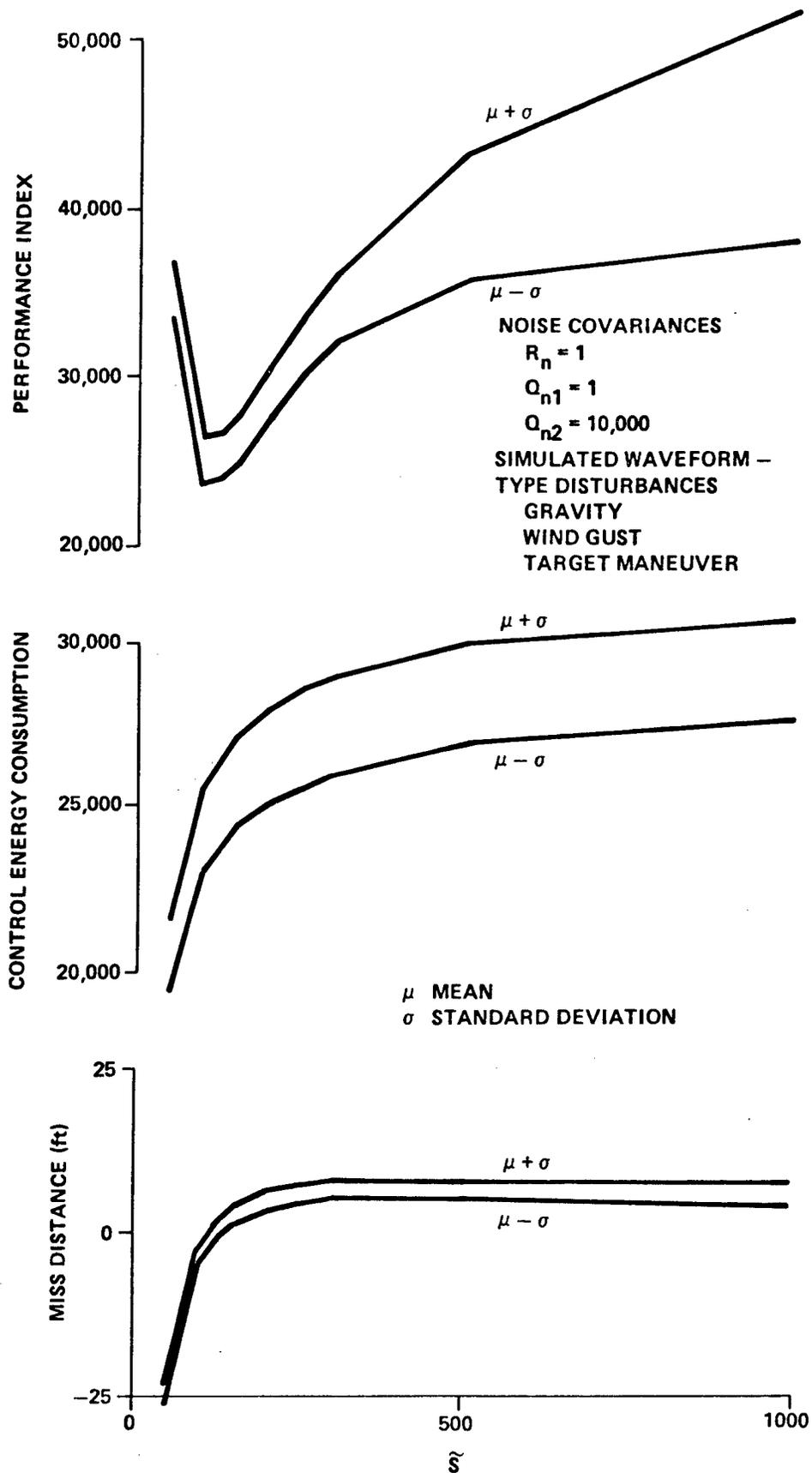
Figure 10. Monte Carlo bounds on noisy DUC performance versus terminal weighting.

A final comparison is made between the LQG and NDUC controllers for various cases. The 25-run set Monte Carlo results are listed in Table 3. This table shows the effects of deleting individual disturbance inputs. In general, the NDUC achieves lower misses when waveform-type disturbances (or waveform-type disturbances plus gaussian noise) are present.

TABLE 2. NOISY DUC MISS DISTANCE OFFSET FOR VARIOUS DISTURBANCE CONDITIONS

CONDITION	PERFORMANCE INDEX MEAN/STANDARD DEVIATION	MISS DISTANCE MEAN/STANDARD DEVIATION	CONTROL ENERGY CONSUMPTION MEAN/STANDARD DEVIATION
NO GRAVITY	31854/1884	6.7/1.1	26092/1471
NO WIND	28950/121	6.4/0.1	23825/200
NO TARGET MANEUVER	2323/512	-0.3/1.1	2178/528
QUARTER OF NORMAL TARGET MANEUVER	4287/655	1.3/1.1	3942/686
HALF OF NORMAL TARGET MANEUVER	9843/963	2.9/1.1	8685/929
ALL NOISE AND WAVEFORM DISTUR-BANCES	31732/1710	6.0/1.1	27106/1500
NO NOISE	31025/103	6.0/0.1	26477/178
NO WAVEFORM-TYPE DISTUR-BANCE	3119/160	0.9/0.1	3028/151

TABLE 3. PERFORMANCE OF NOISY NDUC VERSUS LQG FOR VARIOUS DISTURBANCE CONDITIONS

CONDITION	PERFORMANCE INDEX MEAN/STANDARD DEVIATION		MISS DISTANCE MEAN/STANDARD DEVIATION		CONTROL ENERGY MEAN/STANDARD DEVIATION	
	LQG	NDUC	LQG	NDUC	LQG	NDUC
NO NOISE	430841/10258	31025/103	-55.8/0.7	6.0/0.1	41307/1090	26477/178
NO GRAVITY	261412/413	31854/1884	-43.5/0.1	6.7/1.1	24396/26	26092/1471
NO WIND	440596/10397	28950/121	-56.4/0.7	6.4/0.1	42797/1132	23825/200
NO TARGET MANEUVER	15729/1881	2323/512	-10.5/0.7	-0.3/1.1	1997/203	2178/528
NO WAVEFORM-TYPE DISTURBANCE*	1691/161	1691/161	0.9/0.1	0.9/0.1	1583/151	1581/151

*THE INITIAL CONDITION ON $\hat{z}_1$, WHICH IS USED IN THE DUC CONTROL LAW, IS SET TO ZERO FOR THIS CASE ONLY.
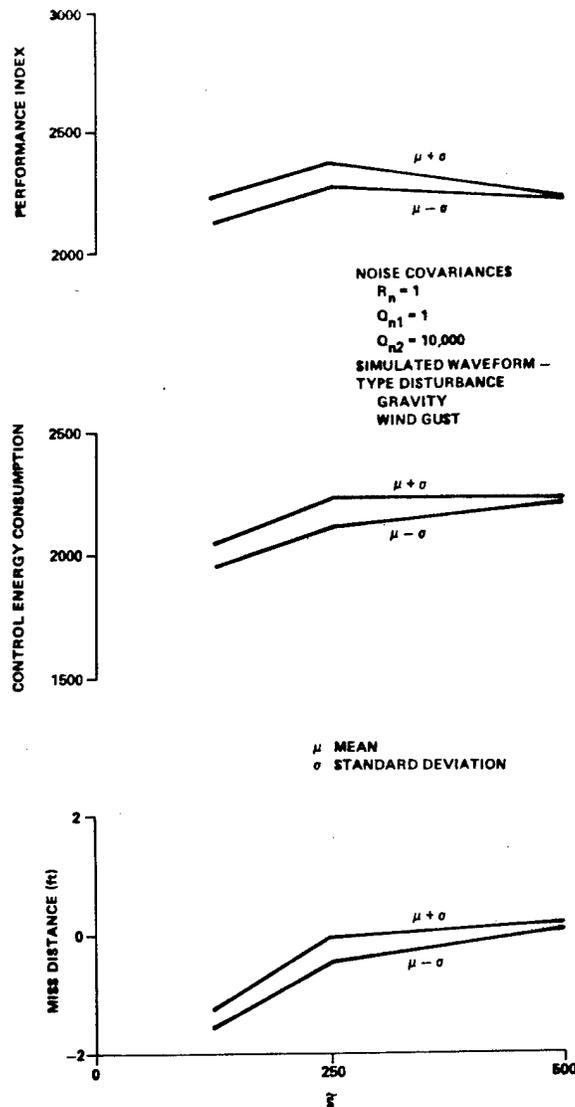
Figure 11. Monte Carlo performance bounds for noisy DUC non-maneuver case.

CONCLUSIONS

The results of this investigation show that the Noisy DUC controller provides improved performance, when compared with an LQG controller, in those cases in which both "waveform-type" disturbances and gaussian noise are present. Although the problem considered here is relatively simple, it demonstrates the potential of the Noisy DUC approach. In a following investigation this technique will be used to design a control law which will be implemented in a six degree-of-freedom air defense simulation.

REFERENCES

1. Johnson, C.D., "Accommodation of External Disturbances in Linear Regulator and Servomechanism Problems," IEEE Trans. on Automatic Control, Vol. AC-16, No. 6, pp. 635-644, December 1971.

2. Johnson, C.D., "Accommodation of Disturbances in Optimal Control Problems," International Journal of Control, Vol. 15, No. 2, pp. 209-231, 1972.

3. Johnson, C.D. and Skelton, R.E., "Optimal Desaturation of Momentum Exchange Control Systems," AIAA Journal, Vol. 9, No. 1, pp. 12-22, 1971.

4. Johnson, C.D., "Design of Discrete-Time Disturbance-Accommodating Controllers for the Disturbance-Utilization Mode," Dynamic Systems Research and Training Corporation Report, June 1980.

5. Johnson, C.D., "Design of Disturbance-Utilizing Controllers for Plants with Noisy Measurements and Disturbances," Dynamic Systems Research and Training Corporation Report, January 1981.

6. Meditch, J.S., Stochastic Optimal Linear Estimation and Control, McGraw-Hill Book Company, Inc., 1969.

7. Astrom, K.J., Introduction to Stochastic Control Theory, Academic Press, Inc., 1970.

8. Gambill, R.T., et. al., "Advanced Analysis for Future Missiles," U.S. Army Missile Command, Redstone Arsenal, Alabama, Tech. Report, No. RG80-8, November 1979.

9. Sage, A.P. and White, C.C., Optimum Systems Control, Prentice-Hall, Inc. Englewood Cliffs, New Jersey, 1977.

10. Kelly, W.C., "Theory of Disturbance-Utilizing Control with Application to Missile Intercept Problems," Tech. Report RG-80-11, U.S. Army Missile Command, Redstone Arsenal, Alabama, 12 December 1979.

Next page is blank.

STABILITY CONTROL OF LARGE INERTIA, DYNAMICAL, NONLINEAR SYSTEMS IN THE PRESENCE OF UNSTABILIZING DISTURBANCES

John E. Bennett and Haren Almaula
Electrical and Computer Engineering Department
Clemson University
Clemson, South Carolina   29631

ABSTRACT

This paper presents a generic study showing stability control of a large inertia, dynamical, nonlinear system such as a power system. The techniques of this study could be applied to a number of applications including both Slewing and Position of Fire Control Systems, and the stability of electrical generators in the presence of disturbances.

The stabilizing control is obtained by a generating, a priori, a sequence of stabilizing trajectories, which converges to a desired or "best" stabilizing trajectory. The initial control is chosen as an optimal one for the approximate linear case, and then an iterative procedure yields a sequence of trajectories and control schemes for the nonlinear system. The final controller is shown to be robust, and it stabilizes certain disturbances that in the uncontrolled case lead to unstable system behavior.

An example of stabilizing a faulted, 1000 MW, generator is shown. Unlike prior studies, a nonlinear model of the generator including magnetic saturation was used, and the results showed enhanced transient stability over previous techniques.

INTRODUCTION

Presently, large megawatt synchronous generators are disconnected from a power system when a major fault is detected at its terminals, and it could take several hours to reconnect the generator to the system. However, if the generator was disconnected from the system and the fault was allowed to clear, then the generator would accelerate for the time-period it has no load. When, after clearing the fault, the generator is reconnected to the system, the question now is whether the generator remains in synchronism or not. Posed in terms of control theory language, the question is whether or not a stable equilibrium state can be reached after the occurrence of a fault?

This paper presents the results of a generic study [1] using statefeedback in a suboptimal scheme for the stability control of a synchronous generator. The control action proposed from this study can be determined prior to a fault and is shown to stabilize disturbances that in the uncontrolled case lead to instability. Since the synchronous generator is a large inertia dynamical, nonlinear system it is felt that results of this study can be applied to similar problems in slewing and position of fire control systems.

PROBLEM DESCRIPTION

It is well recognized that the optimal control of nonlinear systems will often have to be obtained from an iterative scheme [2,3]. The closed-form analytical solution, while most desirable, is not known for nonlinear systems except for a few special cases. The transient stability problem of a power system is a nonlinear problem which is concerned with the development of a stabilizing control law for a large inertia, dynamical system where the system is subjected to a major disturbance and must be returned to an equilibrium state, the exact nature of which is not known a priori. Thus the structure of the problem is of the form: Given the dynamical system

$$\dot{\underline{X}} = f(\underline{x},\underline{u},t) \qquad\qquad (1)$$

determine a control $\underline{u}^*$, that transfers the system from the present state to an equilibrium state in a finite time interval, while minimizing a suitable performance index.

To solve this stabilization problem some researchers have devised 'optimal-aiming' strategies that attempt to aim the system at each point of its trajectory to a stable solution [4,5,6]. The trouble with such 'pointwise' control strategies is that stabilization of the nonlinear system is not guaranteed and in fact there exist controllable linear systems which will be destabilized by such strategies [7]! Clearly such a strategy is a poor choice for the problem at hand. Other researchers [8,9,10] have

265

suggested open-loop schemes for the transient stability control of the synchronous generator. But open-loop schemes do not take into account any changes in the system that could occur in the post-disturbance period. Rather the attempt is to return the system to exactly its pre-fault status, irrespective of whether this is an equilibrium state or not for the post-fault period. Such strategies can, in some circumstances, push the system into unstable regions and not aid transient stability at all. A feedback control strategy that continually obtains information on the states avoids this pitfall. In this study the control is applied as a state-dependent feedback control that attempts to force the system to a closer target trajectory leading to an equilibrium state. The problem is essentially the tracking problem described by Athans and Falb [11] except that the system is nonlinear and that a desired target set is not known exactly but must be specified by exercising engineering judgement.

In the study, the model of the synchronous generator used is not the conventional d-q-o axis model, but a direct-phase reference model. The details of the direct-phase model are given in [12]. It will suffice to state here that compared to the conventional model, this model gives system states that are conceptually more meaningful and physically measurable. After rearranging Kirchhoff's mesh equation and Newton's equation of motion for rotating bodies the nonlinear state vector equation is obtained as

$$\dot{\underline{X}}(t) = \underline{A}(\underline{X},t)\underline{X}(t) + \underline{B}(\underline{X},t)\underline{U}(t) + \underline{V}(t) \tag{2}$$

where

$\underline{X}$ is the state vector composed of the rotor-angle and currents of the generator,

$\underline{U}$ is the control vector consisting of the excitation voltage, and prime-mover torque,

and $\underline{V}$ is the vector that accounts for bus-voltage effects.

It is important to note that the matrices $\underline{A}$ and $\underline{B}$ have elements that are not only time-varying but also non-linear in the state $\underline{X}$. Further, it should be noted that since the system trajectory covers a wide range of states, linearization about a nominal steady-state will not yield meaningful results. For example, it makes little sense to linearize the synchronous generator parameters at a nominal excitation when excitation voltage is chosen as one of the control variables and is to be varied over its full range.

SUBOPTIMAL SYNTHESIS OF THE CONTROLLER

Stability of the synchronous generator is most easily depicted as the rotor angle behavior following a system fault. Figure 1 is an example of both stable and unstable behavior. In the unstable case, the rotor angle grows large without bound, while in the stable case, the response following a disturbance decays. The

The aim of a controller would be to make a system that has the unaugmented response of the unstable case to follow the response of that in the stable case, namely damped oscillations. Thus a damped oscillation of the rotor angle in the post disturbance interval is to be chosen as part of the target trajectory. Following the outline for the tracking problem [11], a suitable quadratic performance index in terms of the error from the target set is formulated as

$$J = \langle \underline{e}(t_f), \underline{F}\, \underline{e}(t_f) \rangle$$

$$+ \tfrac{1}{2} \int_{t_f}^{t_f} \langle \underline{e}(t), \underline{Q}(t)\underline{e}(t)\rangle + \langle \underline{U}(t), \underline{R}(t)\underline{U}(t)\rangle\, dt \qquad (3)$$

where

$$\langle , \rangle \qquad = \text{an inner product,}$$
$$[t_o, t_f] \qquad = \text{the time interval for control action,}$$
$$F \qquad = \text{a symmetric weighting matrix,}$$
$$\underline{Q}(t) \qquad = \text{a semipositive definite weighting matrix,}$$
$$\underline{R}(t) \qquad = \text{a positive definite weighting matrix,}$$
$$\underline{e}(t) \qquad = [\underline{Z}(t) - \underline{Y}(t)]$$
$$\qquad = [\underline{Z}(t) - \underline{C}(t)\underline{X}(t)] \text{ is the error,}$$

with $\underline{Z}(t)$ a target vector and $\underline{Y}(t) = \underline{C}(t)\underline{X}(t)$ the observation vector.

The optimal control for the linear control problem is known to be

$$\underline{U}^*(t) = \underline{R}^{-1}(t)\, \underline{B}^T(t)\, [\underline{G}(t) - \underline{K}(t)\, \underline{X}(t)] \text{ and} \qquad (4)$$

where $\underline{K}(t)$ is the solution of the matrix differential equaton

$$\underline{K}(t) = -\,\underline{K}(t)\underline{A}(t) - \underline{A}^T(t)\underline{K}(t)$$

$$+ \underline{K}(t)\underline{B}(t)\underline{R}^{-1}(t)\underline{B}^T(t)\underline{K}(t)$$

$$- \underline{C}^T(t)\underline{Q}(t)\underline{C}(t) \quad , \qquad (5)$$

with boundary condition

$$\underline{K}(t_f) = \underline{C}^T(t_f)\, \underline{F}\, C(t_f) \qquad (6)$$

the vector $\underline{G}(t)$ is the solution of the linear vector differential equation

$$\underline{G}(t) = \underline{K}(t)\underline{B}(t)\underline{R}^{-1}(t) - \underline{A}^T(t)\, \underline{G}(t)$$

$$+ \underline{K}(t)\underline{V}(t) - \underline{C}^T(t)\underline{Q}(t)\underline{Z}(t) \quad , \qquad (7)$$

with boundary condition

$$\underline{G}(t_f) = \underline{C}^T(t_f)\, \underline{F}\, \underline{Z}(t_f) \quad .$$

Since the backward-time solutions of Equations (5) and (7)
require knowledge of the system trajectory a 'seed' case must
first be obtained. The procedure for starting the iterative
scheme is then to obtain a system trajectory with no applied
control. This is shown in Figure 2 where the system was faulted
for six cycles before the fault was cleared. With this 6 cycle
fault, the system is stable in the sense that rotor swings do not
increase in amplitude. That the swings do not decay either is
due to the fact that sufficient damping was not included in the
synchronous generator model, making the results of the study
somewhat conservative. Whereas in the practical system, there is
viscous damping of the rotor that would enhance decay and
therefore the system would stabilize faster. The 'seed'
trajectory, $\underline{X}^o(t)$, is used to obtain solutions of Equations (5)
and (7) namely $\underline{K}^1(t)$ and $\underline{G}^1(t)$. These matrices can now be
used to construct the control of Equation (4), $\underline{U}^1(t)$. Since the
system is nonlinear $\underline{U}^1(t)$ may, in general, not be the optimal
control, and another trajectory $\underline{X}^1(t)$ is obtained. Equations
(5) and (7) are solved once again to obtain solutions $\underline{K}^2(t)$ and
$\underline{G}^2(t)$, and a control $\underline{U}^2(t)$ can now be constructed. The
iterative scheme is obvious and a sequence of controllers,
$\underline{U}^n(t)$, is constructed until a satisfactory system trajectory
$\underline{X}^n(t)$ is obtained.

Figure 3 shows that a satisfactory trajectory is obtained in just
two iterations, while Figure 4 shows the associated control.
Note that a disturbance of 15 cycle duration has been stabilized
in Figure 3. This disturbance destabilizes the trajectory shown
in Figure 2. The magnitude of either control variable in Figure
4, is not unacceptably large. The 60Hz component in the excita-
tion voltage is really a reflection of the imbalance in the
stator currents, not a control effort, and this component is seen
to be decaying.

To check for the robustness of the controller, it was used to
stabilize the system starting from a different initial condition
than that was used in constructing the original controller. The
results are shown in Figure 5, and it can be seen that successful
control action is obtained.

The important difference between this control scheme and other
ones reported by researchers earlier [6,8,9,10] is that this
control action is applied after the clearing of the fault and not
immediately upon the detection of the fault. The advantage being
that control action can be applied only to disturbances for which
it is known that stabilizing action will be successful. This
selective application is crucial, for in a power system, often
there are disturbances where it is better to sacrifice system
integrity and maintain system security (load shedding), than to
attempt to maintain system integrity and lose system security
(black-out). It is the state-dependent nature of the control
action that permits this selectivity and the feedback application
results in enhanced transient stability margins. Compared to

open-loop strategies, the advantage of the feedback scheme is that action can be applied only to those disturbances for which the system does not have inherent stability. Open-loop schemes apply control effort indiscriminately to every disturbance whether the system possesses inherent stability or not. For a power system where the effect of frequent stresses must be considered on the life cycle of very expensive equipment this is an important consideration in selecting a control strategy.

CONCLUSION

The applicability of the methods of linear optimal control to a nonlinear system has been demonstrated. The control scheme is obtained by an iterative procedure and is shown to both improve stability margin and stabilize major disturbances. A synthesis of the power systems and control systems approaches to the transient stability problem was achieved by allowing the generator and the external power system to have a common set of state variables. As mentioned previously, it might be possible to apply these same techniques to enhance the control of both slewing and position control of five control systems.

REFERENCES

1. Almaula, H. and Bennett, J. E., "State Feedback Transient Stability Control of Large Synchronous Generators" paper submitted for publication.

2. Vidyasagar, M., _Nonlinear Systems Analysis_, Englewood Cliffs, NJ: Prentice-Hall Inc., 1978.

3. Plant, J. B., _Some Iterative Solutions in Optimal Control_, Cambridge, MA: MIT Press, 1968.

4. Barnard R. D., "Optimal-aim Regulation and Tracking in Large-order Network, "_J. Networks_, vol. 5, pp. 307-329, Oct. 1975.

5. Barnard, R. D., "Continuous time Implementation of Optimal-aim Controls, "_IEEE Trans. Autom. Contr._, vol. AC-21, pp. 432-434, June 1976.

6. Thomas, R. J., Thorp, J. S. and Pottle, C., "A Model-Referenced Controller for Stabilizing Large Transient Swings in Power systems," _IEEE Trans. Autom. Control_, vol. AC-21, no. 5, pp. 746-750, Oct. 1976.

7. Barmish, B. R., Thomas, R. J. and Lin, Y. -H., "Convergence Properties of a Class of Pontwise Control Strategies," _IEEE Trans. Autom. Control_, vol AC-23, no. 5, pp. 954-956, Oct. 1978.

8. Reitan, D. K. and Rama Rao, N., "Optimal Control of Transients in a Power System," _Proc. IEEE_ (letter), vol. 57, no. 8, pp. 1448-1449, August 1969.

9. Kundur, P. and Bayne, J. R., "A Study of Early Valve Actuation using Detailed Prime-Mover and Power Systems Simulaton," _IEEE TRANS. Power Appar. Syst._, vol. PAS-94, no. 4, pp. 1275-1282, July/August 1975.

10. Balu, N. J., "Fast Turbine Valving and Independent Pole-Tripping Breaker Applications for Plant Stability," IEEE Conf. Paper A77-262-9, presented at 1977 IEEE PES Winter Meeting, New York, January 1977.

11. Athans, M. and Falb, P. L., _Optimal Control An Introduction to the Theory and It's Applications_, New York: McGraw-Hill Book Co., 1966.

12. Almaula, H. and Bennett, J. E., "Simulation of the Transient Behavior of a Synchronous Machine using Standard Data," Proc. of Thirteenth Annual Symposium on System Theory, Clemson, S.C., March 1979.
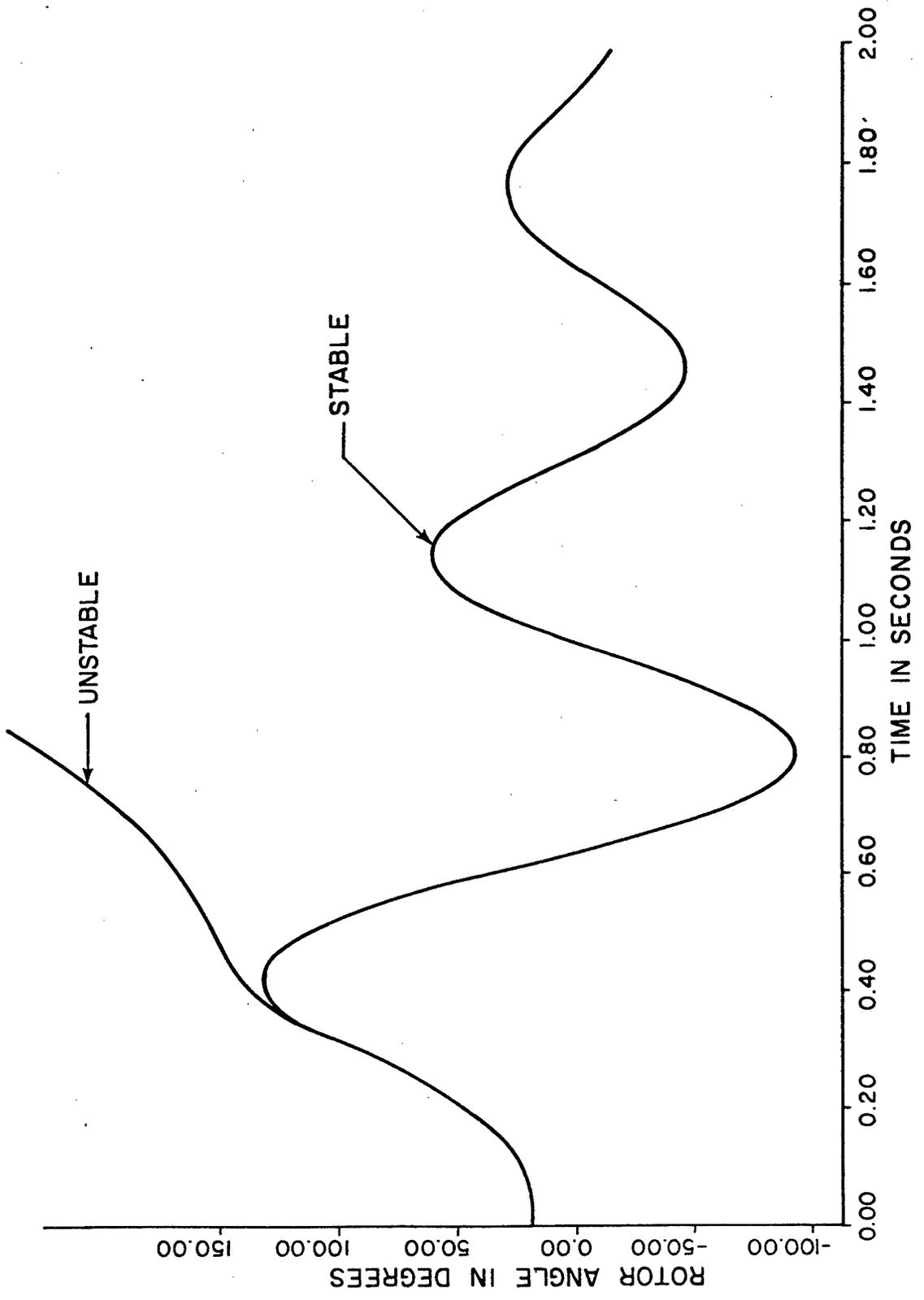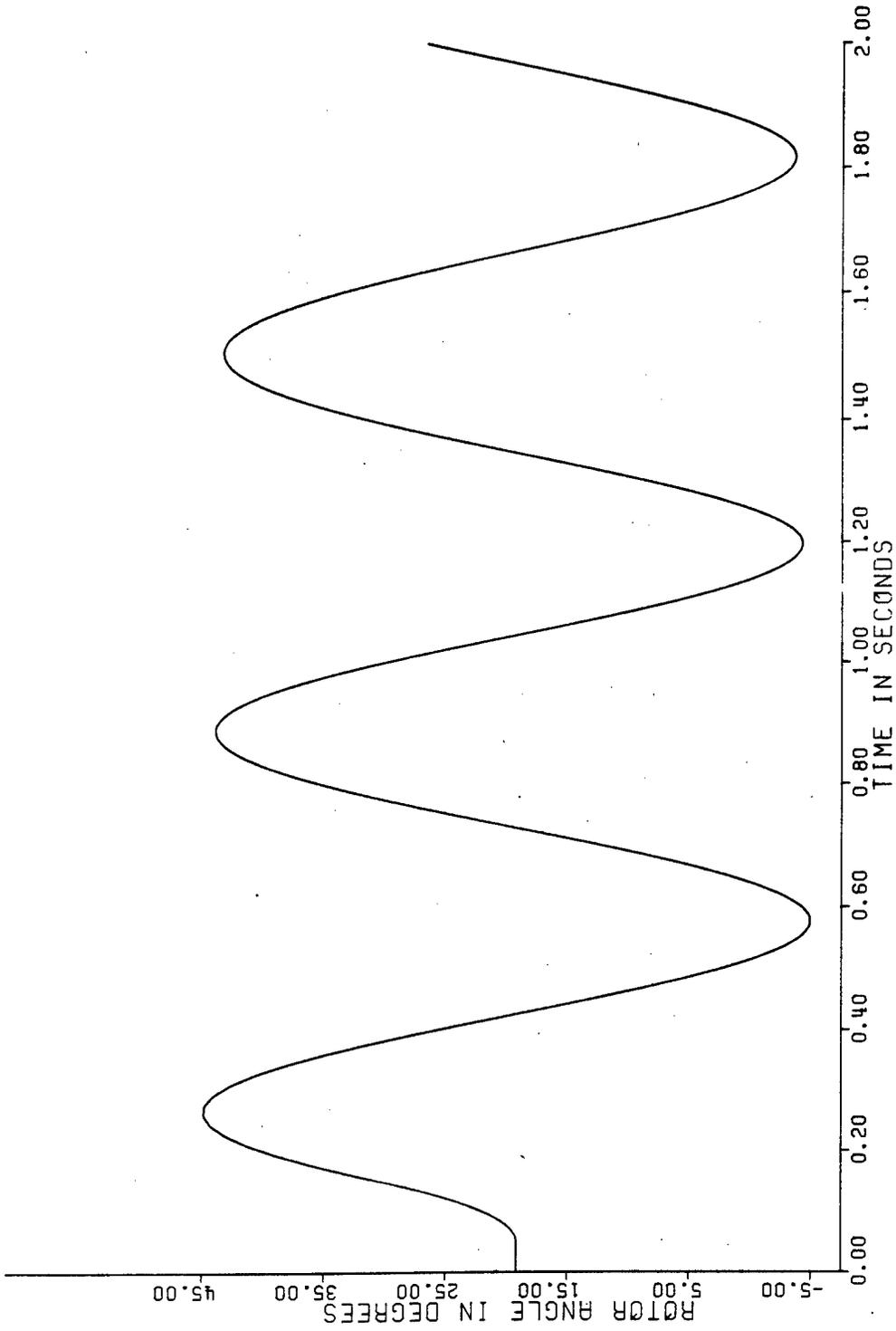
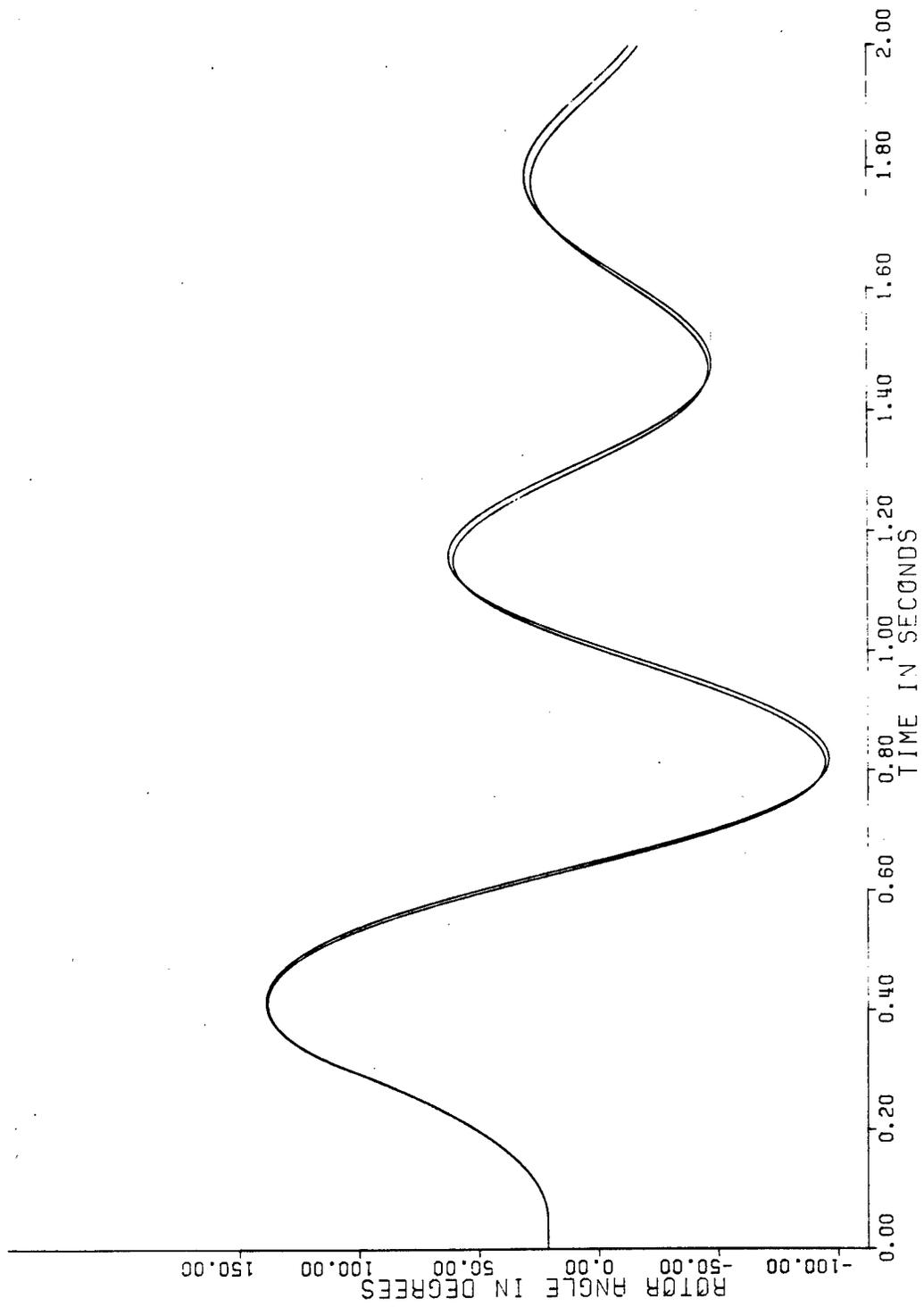FIGURE 1 ROTOR POSITION

FIGURE 2   SEED CASE FOR ROTOR TRAJECTORY

272

FIGURE 3 STABILIZED TRAJECTORY

273
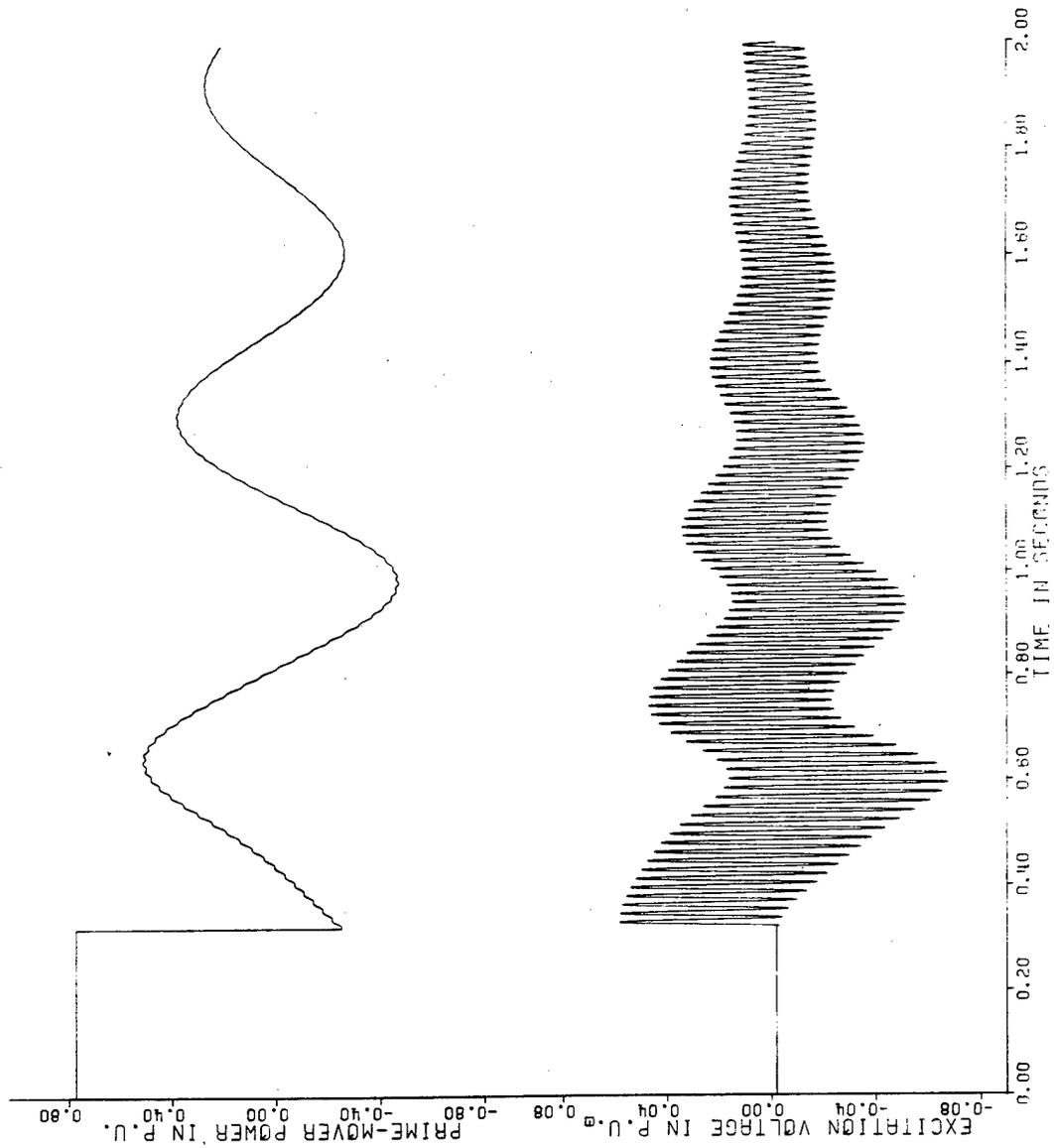
FIGURE 4 CONTROLLER BEHAVIOR
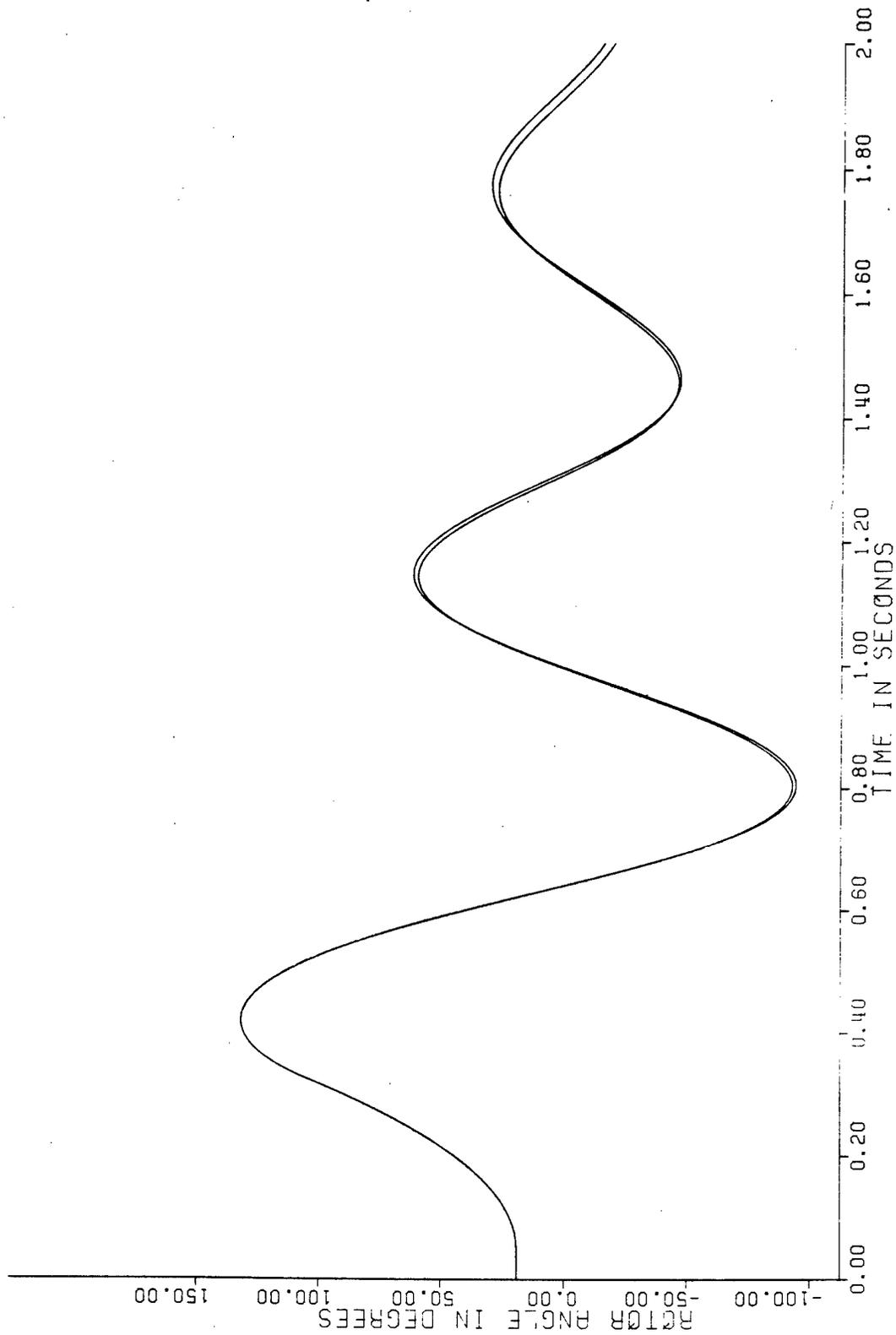
FIGURE 5 EXAMPLE OF ROBUST CONTROL

Next page is blank.

DISTRIBUTION LIST

NO. OF COPIES	ORGANIZATION
12	Commander Defense Technical Information Center ATTN: TCA Cameron Station Alexandria, VA 22314
6	Commander US Army Materiel Development & Readiness Command ATTN: DRCCP DRCPA-S DRCDE-R DRCDE-D DRCBSI-L DRCBSI-D 5001 Eisenhower Avenue Alexandria, VA 22333
2	Commander US Army Armament Research & Development Command ATTN: DRDAR-SEA Technical Library
1 1 1 1 1 1 1 1 1 1	ATTN: DRDAR-SCF-DD (W. J. Dzwiak) (S. A. Goodman) DRDAR-SCF-CC (J. Schmitz) DRDAR-SEA (Richard Moore) DRDAR-SCF-C (Dr. Norman Coleman) (Edward Carroll) (Ronald Johnson) DRDAR-SCS-M (Dr. T. Hutchings) DRDAR-SCF-C (Mr. Pak T. Yip) (B. L. Schulman) Dover, NJ 07801
1	Commander Rock Island Arsenal ATTN: Tech Lib Rock Island, IL 61299
1	Commander Harry Diamond Laboratories ATTN: DELHD-SAB 2800 Powder Mill Road Adelphi, MD 20783

NO. OF COPIES	ORGANIZATION
1	Director US Army TRADOC Systems Analysis Activity ATTN: ATAA-SL ATTA-T White Sands Missile Range, NM 88002
1	Commander US Army Mobility Equipment R&D Command ATTN: DRDME-US (L. Medler) Ft Belvoir, VA 22060
1	Dr. Daniel O. Molnar Guidance & Navigation Tech, M/S 88-39 Boeing Aerospace Company P.O. Box 3999 Seattle, Washington 98124
1	Dr. Sol Gully ALPHATECH Inc. 3 New England Executive Park Burlington, MA 01803
1	Dr. Johnathan Korn ALPHATECH Inc. 3 New England Executive Park Burlington, MA 01803
1	Dr. Sam Bose Litton Guidance and Control Systems 5500 Canoga Ave Woodland Hills, CA 91365
1	Professor Max Mintz Department of Systems Engineering University of Pennsylvania Philadelphia, PA 19104
1	E. R. Pate Department of Systems Engineering University of Pennsylvania Philadelphia, PA 19104
1	Professor Naim A. Kheir University of Alabama in Huntsville Department of Electrical Engineering Huntsville, AL 35899
1	Commander US Naval Surface Weapon Center ATTN: Code G42 (Harry Nikirk) Silver Spring, MD 20910

NO. OF COPIES	ORGANIZATION
1	Commander US Army Troop Support & Aviation Materiel Readiness Command ATTN: DRSTS-BA 4300 Goodfellow Blvd St Louis, MO 63120

4	Commander
	US Army Tank-Automotive Research & Development Command
	ATTN: DRDTA-UL (Tech Lib)
	      DRDTA-V
	      DRDTA-ZSA (Dr. Ronald R. Beck)
	      DRDTA-RCKS (Dr. Richard Lee)

1	Commander US Army Mobility Equipment R&D Command ATTN: DRDME-O Fort Belvoir, VA 22060
1	Commander US Army Natick R&D Command ATTN: DRDNA-O Natick, MA 01760
1	Chief Defense Logistics Studies Information Exchange US Army Logistics Management Center ATTN: DRXMC-D Fort Lee, VA 23801
2	Commander US Army Tank-Automotive Research & Development Command ATTN: DRDTA-RCKS (1LT Dana S. Charles) (Johnthan F. Kring)
4	Commander US Naval Weapons Center ATTN: Code 3911 (T. L. Moran), (Dr. Robert D. Smith) China Lake, CA 93555 (Gary Hewer) (Michael L. Munford)

8	Commander
	US Army Armament Research & Development Command
	ATTN: DRDAR-LC-E (Raymond Goldstein)
	      DRDAR-SCP (Thomas Hutchings
	      DRDAR-SCP (Yick Cheong Woo, Arnold Klausner,
	              Gim Chin)
	      DRDAR-SEA (Ray Weir)
	      DRDAR-LCA (M. Nowak), (Henry Hudgins)
	Dover, NJ 07801

NO. OF COPIES	ORGANIZATION
1	Commander US Army Test & Evaluation Command ATTN: STEDP-MT-L Dugway Proving Ground, UT 80222
1	Commander US Army Aviation R&D Command ATTN: DRDAV-BC PO Box 209 St. Louis, MO 63166
1	Commander US Army Concepts Analysis Agency 8120 Woodmonth Avenue Bethesda, MD 20014
2	Commander David W. Taylor Ship R&D Center ATTN: Code 1576 (Mr. William E. Smith) Code 1576 (Mr. T. L. Moran) Bethesda, MD 20084
1	Reliability Analysis Center ATTN: Mr. I. L. Krulac Griffiss AFB, NY 13441
1	Commander Applied Technology Laboratory US Army Research & Technology Laboratories ATTN: DAVDL-ATL-ATA (Dr. C. E. Hammond) Ft Eustis, VA 23604
2	Commander US Air Force Armament Laboratory (AFSC) ATTN: DLM (1LT McClendon, 1LT P. L. Verges) Eglin Air Force Base, Florida 32542
1	Commander US Air Force Wright Aeronautical Laboratories (AFSC) ATTN: FIGC (Dr. David K. Bowser) Wright-Patterson AFB, Ohio 45433
2	Commander US Naval Surface Weapons Center ATTN: Code F14 (Kenneth J. Hintz) Code F14 (Richard A. Holden) Dahlgren, VA 22448

NO. OF COPIES	ORGANIZATION
1	Commander US Naval Research Laboratory ATTN: Code 7931 (Dr. Warren William) Washington, DC 20375
1	Commander US Naval Weapons Center ATTN: Code 3911 (Dr. Robert D. Smith) China Lake, CA 93555
1	President USAARENBD ATTN: ATZK-AE-CV (Mr. William West) Ft Knox, KY 42101
1	General Electric Company Ordnance Engineering ATTN: Paul Cushman 100 Plastics Ave Pittsfield, Mass 01201
1	Commander US Army Electronics R&D Command ATTN: DRDEL-SA Fort Monmouth, NJ 07703
1	Commander US Army Communications R&D Command ATTN: DRDCO-TCS-BS (Dr. Leon Kotin) Fort Monmouth, NJ 07703
1	Commander US Army Electronics R&D Command ATTN: DRDEL-AP-OA 2800 Powder Mill Road Adelphi, MD 20783

23

Commander
US Army Missile Command

ATTN:	ATTN:
DRSMI-C (R&D)	DRSMI-V
DRSMI-RGN (Dr. William C. Kelly)	DRSMI-XG
DRSMI-RD (Ernst Evers)	DRSMI-XB
DRSMI-RDD (R. E. Dickson)	DRSMI-T
DRSMI-R	DRSMI-T
DRSMI-RS	DRSMI-RH
DRSMI-RG	DRSMI-CF
DRSMI-RE (Waite Todd)	DRSMI-RS
DRSMI-RR	DRSMI-HA
DRSMI-D	DRSMI-HEL
DRSMI-O	DRSMI-LC
Redstone Arsenal, AL 35809	DRSMI-PE

NO. OF COPIES	ORGANIZATION
1	Mr. Donald P. Glasson The Analytic Science Corporation Reading, Mass 01867
1	Mr. Joseph N. Craig Adaptronics, Inc. 1750 Old Meadow Road McLean, VA 22102
1	Dr. C. D. Johnson Department of Electrical Engineering The University of Alabama in Huntsville Huntsville, AL 35899
1	Dr. Harold Patrick Control Dynamics Inc. 221 East Side Square Suite 1B Huntsville, AL 35801
1	Dr. George B. Doane III Control Dynamics Inc. 221 East Side Square Suite 1B Huntsville, AL 35801
1	CPT Tom L. Riggs, USAF Department of Astronautics and Computer Science United States Air Force Academy, Colorado 80840
1	Professor John E. Bennett Electrical & Computer Engineering Department Clemson University Clemson, SC 29631
1	Mr. Haren Almaula Electrical & Computer Engineering Department Clemson University Clemson, SC 29631
1	N. K. Loh Center for Robotics & Advanced Automation School of Engineering Oakland University Rochester, Michigan 48063

282

NO. OF COPIES	ORGANIZATION
1	K. C. Cheok Center for Robotics & Advanced Automation School of Engineering Oakland University Rochester, Michigan 48063
1	Dr. John Hsing COMSAT Laboratory 22300 Comsat Drive Clarksburg, MD 20734
1	Mr. James McPartland Naval Air Development Center Code 6012 Warminister, PA 18974
1	Mr. Gerlad Grube Bell Telephone Labs Rm 4C250B Whippany, NJ 07981
1	Mr. Paul A. Murad Bendix Corporation Guidance Systems Div Teterboro, NJ 07608
1	Mr. Harris C. Rawicz Lockheed Electronics Co., Inc. Products & Systems Div Plainfield, NJ 07061
1	Mr. William J. Bigley Lockheed Electronics Co., Inc. Systems Division Plainfield, NJ 07061
1	Min-I.J. Chang Goodyear Aerospace Corporation Akron, Ohio 44315
1	Mr. Al Bills TASC 24 Hollywood Blvd, W. Suite #1 Fort Walton Beach, FL 32548
1	Mr. Jerry Bosley Computer Science Corporation 200 Sparkman Drive Huntsville, AL 35805

NO. OF COPIES	ORGANIZATION
1	Mr. Wayne Kenrick Computer Science Coproration 200 Sparkman Drive Huntsville, AL 35805
1	Program Manager Mr. C. W. Smoots GACIAC, IIT Research Institute, Div E 10 West 35th Street Chicago, IL 60616
1	Dr. Joe Bram AFOSR/NM Bldg 410 Bolling AF Base Washington, D.C. 20332
1	Dr. Stuart Brodsky Code 411MA 800 N. Quincy St. Arlington, VA 22217
1	Dr. Peter S. Maybeck Dept of Electrical Engineering Air Force Institute of Technology Wright Patterson Air Force Base, OH 45433
1 1 1 1 1 1 1	HQDA (DAMA-WSZ-C (Dr. R. J. Heatson) (DAMA-WSM) (DAMA-WSW (DAMA-ARZ-A (DAMA-ARZ-E (DAMA-ARZ-C (DAMA-ARZ-D WASH, DC 20310
2	Commander US Army Tank-Atuomotive Materiel Readiness Command ATTN: DRSTA-SA (Arnold Solomon) (Daniel Meng) Warren, Michigan 48090

Aberdeen Proving Ground

3	Cdr, USATECOM ATTN: Huber Cole DRSTE DRSTE-CS-A Bldg 314

NO.OF COPIES	ORGANIZATION
3	Dir, HEL ATTN: DRDAR-TSB-S (STINFO BRANCH) Monica Glumm DRXHE-AM (Seymour Steinberg)
1 1	Dir, USAMSAA ATTN: DRXSY-MP (Herbert E. Cohen) DRXSY-A (Mr. D. O'Neill) DRXSY-A(D.Nuzman) DRXSY-C (Mr. A. Reid) DRXSY-CS(Toney Perkins) DRXSY-CS (Patrick E. Cororan) DRXSY-G (Mr. J. Kramer) DRXSY-G (John Groff) DRXSY-F (Dr. W. Copes DRXSY-A (John Meredith DRXSY-A (Joseph Wald) DRXSY-DA (Dr. Atzinger) DRXSY-J (Mr. J. Blomquist) DRXSY-F (Harry Harris) DRXSY-G (Bob Conroy)
1	Dr. James F. Leathrum Dept of Electrical & Computer Engineering Clemson University Clemson, SC 29631
1	Mr. D. H. Chyung Division of Information Engineering University of Iowa Iowa City, Iowa 52242